MODELLING OF EXTREME INDIVIDUAL OVERTOPPING EVENTS AT VERTICAL SEAWALLS

Thomas Davey

Doctor of Philosophy

The University of Edinburgh

2010

Abstract

Wave overtopping at coastal structures occurs as a sequence of discrete events. This phenomenon is, however, commonly characterised as a continuous process. This mean discharge measurement is not always the most appropriate measure of the hazard at a coastal structure. It is often the case that the event with the maximum individual overtopping volume poses the greatest risk to personnel and property. In cases where recreational and transport infrastructure may be a secondary "user" of the structure, quantifying this hazard becomes particularly important.

An obstacle to the accurate quantification of individual overtopping events obtained from random wave models, both physical and numerical, is the small number of large events obtained from tests. Individual overtopping is analysed probabilistically. The tendency for the extremes of the distributions to be poorly described leads to significant errors when predicting the extreme events. This is complicated further by the existence of distinctive regimes of the overtopping response - waves may overtop in a "green-water" manner or impulsively break onto the structure resulting in a violent overtopping event. The aim of this research is to develop and validate a method focussed on giving the best-possible quantification of maximum overtopping within the fixed constraint of laboratory testing time.

Specifically, the approach taken here is to apply statistical tools to increase the occurrence frequency of the most extreme individual overtopping events for a given sea state. In basic terms, seas more extreme than the standard design conditions are used for testing purposes. The overtopping measurements from these extreme tests are analysed using the probability distributions of the design sea parameters. This process ensures the extreme sea tests produce results representative of the design sea case, but with the response distribution shifted to describe better the extreme region. In effect, this procedure replicates several repeat tests of the design sea with a single test run.

The strength of this method is that it makes no strong assumptions on the factors influencing the overtopping response. In doing so, the advantages of random wave modelling are retained. It is also ideally suited to shallow water applications as no wave transformation effects need be modelled. All the statistical processes are based upon measurements taken after transformation of the sea. This thesis develops and examines the application of this method to vertical seawall overtopping and offers guidance on the optimum usage of the technique. The technique, as demonstrated, shows a reduction in test length by a factor of 2-4 to be feasible. Overtopping measurements from physical model tests using extreme sea tests were similar to those obtained from conventional design sea testing.

Declaration

This thesis has been composed by myself and, except where stated, the work contained is my own. Furthermore, the work contained has not been submitted for any other degree or professional qualification.

.....

Thomas Davey

August 2009

Contents

1 Introduction

1.1 Background & Research Drivers

Engineering problems are often concerned with the extreme behaviour of a particular system. This may be the extreme values of a quantifiable response or a unique infrequent event. In some circumstances these events may be relatively straightforward to analyse. A simple structural element may be subjected to an ever increasing load. The extreme deflections may be measured and the force associated with the eventual failure may be recorded. The fact that there is a direct correlation between a single parameter (i.e. force) and the response is well understood. In more complex problems the cause and effect relationships are less clear. The causal parameters governing the extreme behaviour may not be well understood. Indeed, in the case failure mode analysis the extreme response may not be fully defined. Many marine engineering environment situations are subject to these problems.

Oceans are observed as random processes measured in terms of global values and summary statistics. Many characteristics of a system can be inferred from these values and parameters. A coastal engineer may be able to reproduce a particular sea and examine the rate at which waves overtop a seawall. A study on a Wave Energy Converter (WEC) may reveal the operational characteristics in a particular environment. These are both essentially mean responses. The examination of the extreme behaviour is more complex. In the seawall example this is the largest single overtopping event. In the WEC this may represent the failure of the device. Understanding these extremes is often extremely important. The largest overtopping volume is often associated with the greatest

risk to personnel or property. The failure of a WEC represents lost investment and confidence. The factors influencing these extreme events may differ significantly from those relating to the "mean" response. If these infrequent events are to be well understood long simulations of various sea states are required. This is inefficient and potentially expensive. The feasibility of methods for reducing the lengths of these tests is explored in this research.

1.2 Outline of this Research

1.2.1 Objectives and Thesis Structure

The broad aim of this project was to examine methods to improve efficiency and increase modelling confidence in the quantification of extreme values for marine modelling problems, the motivation for which is discussed above (§1.1). In order to investigate a given technique the following objectives were set:

1. Select a marine response suitable for benchmarking new tools and methods.
2. Quantify the uncertainty and error associated with the extreme response using conventional modelling tools.
3. Develop and optimise new methods for extreme response analysis.
4. Benchmark the magnitude of the response obtained using the new analysis methods with the benchmark values.
    a. Quantify the accuracy of the "mean" extreme response. Do the new methods produce an acceptably accurate estimate of the response?
    b. Compare the uncertainty in the estimated values produced using the new method. Do the new methods improve efficiency when compared to conventional testing?

The above objectives are necessarily broad, being based upon a generic response and an undefined modelling method. The structure of this thesis does, however, follow the path laid out by these objectives.

Individual wave overtopping volumes at vertical seawalls were chosen as the benchmark study case (Objective 1; §2-4). Overtopping presents an interesting challenge as the response is potentially non-linear and non-monotonic. These factors, combined with typically small sample sizes, tend to result in large degree of uncertainty in the estimated response magnitude. The choice of a shallow-water coastal response also introduces the challenges of incorporating wave transformation effects. In some senses this increases the complexity of the research, but it also plays to the strengths of statistical techniques that might not otherwise be of primary interest. Specifically, it was determined that a coastal engineering problem would be ideal for applying the Importance Sampling technique that forms the backbone of this research.

It should be noted that this work is not intended to be an "overtopping thesis". The study of overtopping has been conducted as part of a wider study into techniques for shortening test lengths. The overtopping behaviour has not been characterised using a wide ranging set of variables. Attention has instead been devoted to quantifying the uncertainty over a narrow range of sea-states and structural configurations (Objective 2; §3-4). Studies at this level of detail are rarely feasible in a commercial context in the coastal engineering field. The context and relevance of this work is outlined below (§1.2.2).

The modelling technique studied in detail in this thesis is an adaptation of the Importance Sampling methodology employed in the field of Monte Carlo statistics. The Importance Sampling technique was chosen for study as it potentially reduces test sequence lengths while largely maintaining the benefits of random wave modelling. Its non-deterministic nature also makes it a promising candidate for shallow water applications as wave transformation effects need not be modelled. This technique has been developed (Objective 3; §5) and compared to conventional modelling results (Objective 4; §6-7) in the course of this research. A brief overview of the technique is given below (§1.2.3).

1.2.2 Overtopping Research Context

It is noted above that this research is not intended to characterise overtopping behaviour over a wide range of conditions. This has already been examined in detail in several studies, the results of which are encapsulated in the European Overtopping Manual (EurOtop, 2007). This research takes a small "slice" of the conditions covered in these larger studies and attempts to quantify the uncertainty involved in the modelling process.

The specifics of overtopping behaviour are addressed in detail within the main body of this thesis. In brief, vertical seawall overtopping has several interesting properties which are relevant to examining the quantification of extreme responses:

- Several different overtopping modes are possible. In broad terms, waves may overtop in a non-breaking (green-water/pulsating) or breaking (violent/impulsive) manner. This contributes to non-linear and non-monotonic nature of the response (described below).
- The response is non-linear when measured against a number of parameters. This is particularly evident when examining overtopping measurements against freeboard height. Waves which are below a certain threshold relative to the freeboard will exhibit no overtopping. Beyond this threshold the volumes will increase exponentially, with the caveat that the behaviour may also be non-monotonic.
- Mean and individual overtopping volumes may be non-monotonic when assessed against parameters such as wave height. In essence, the largest waves may not produce the largest overtopping response. The interactions with the seawall are complex and are difficult to characterise.
- Seawall (and breakwater) overtopping is a coastal phenomena measured in shallow water. The wave transformations involved in moving from deep-water are non-trivial to quantify accurately, particularly if required at the level of individual waves.

- Many coastal design scenarios require low-admissible overtopping rates. That is, only a very low number of overtopping waves is acceptable. The sampling error involved in quantifying the extreme response from model tests will be large in these situations.

The uncertainty in quantifying overtopping responses is large, a fact widely recognised by those working in the field. A "factor of two" is often given as a rule-of-thumb for the expected variation from a given mean value. This large uncertainty provides a good opportunity for developing and evaluating error reducing techniques.

1.2.3 Importance Sampling Methodology

The broad aim of this research is to improve the efficiency of random wave modelling when examining extreme values of a given response (e.g. vertical sea wall overtopping). In essence this requires that test lengths are shortened while maintaining the same level of accuracy as would be achieved with a conventional modelling approach. Alternatively, longer tests lengths may be used but with the response quantified with greater confidence.

In order to achieve this aim a technique, referred to here as "Importance Sampling", has been explored and developed. Importance Sampling, in its original form, is a variance reduction method employed in the field of Monte Carlo modelling. In basic terms the magnitude of the response in one distribution (the design condition) is inferred from a second, more extreme, distribution (this is explained in more detail in §2.6). This more extreme distribution will contain a greater proportion of large magnitude events (e.g. individual overtopping volumes) and therefore increases the efficiency of the modelling process by avoiding the generation, or measurement, of many smaller inconsequential events. In the context of this research this more extreme distribution relates to measurements obtained with an Extreme Sea. This Extreme Sea is a sea state more energetic than the conventionally modelled Design Sea state. The design waves (or wave groups) associated with the maximum response in the Design Sea will occur more frequently in the Extreme

Sea. In effect, results equivalent to several repeat tests (of a standard fixed length) may be obtained with a single Extreme Sea test.

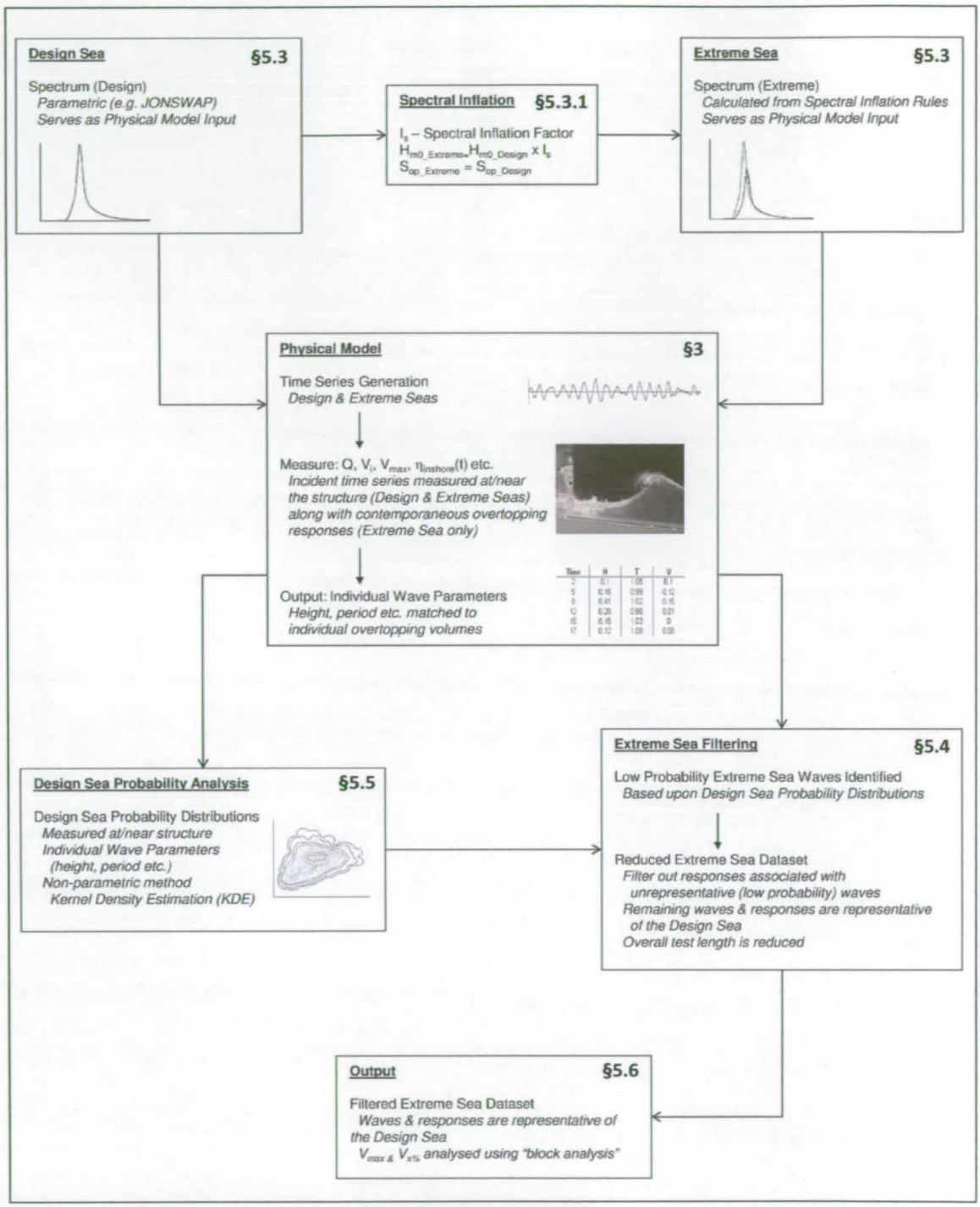

Figure 1.1 Outline of Importance Sampling Methodology

The Importance Sampling methodology explored is outlined by the flowchart illustrated in Figure 1.1. Information relating to the separate processes are marked by bold text in the following description of the technique.

The challenge with the Importance Sampling approach is to relate the waves in the **Extreme Sea** to the **Design Sea** conditions. The Extreme Sea spectrum is calculated through a process referred to here as **Spectral Inflation** by which the Design Sea spectrum is scaled both in term of elevation (by H_{m0}) and time (by T_p). The generated spectra serve as the inputs to the modelling system (**Physical Model**). For this application, this takes the form of a small scale vertical seawall installed in a two-dimensional wave flume. Elevation time series measurements are taken in shallow water at, or near, the structure. This is an important feature of the Importance Sampling method as it avoids the need to model complex transformations as the waves propagate up the beach from deep to intermediate or shallow water depth. The Design Sea must therefore be generated in the flume to provide a description of the design sea state in the vicinity of the structure[1]. It is this shallow water data that is used in the Extreme Sea filtering process described below. The Extreme Sea is used to collect the overtopping time series data (individual volumes with time stamps). The ability to record the response along with the contemporaneous sea state is a requirement of the Importance Sampling method.

The measured elevation time series is analysed to produce a number of time series parameters (e.g. wave heights and periods). The Extreme Sea individual overtopping events are paired with appropriate individual waves based upon their respective time stamps. These data matrices are used to filter the overly-extreme waves from the Extreme Sea dataset. If this process is effective the resulting filtered dataset will contain only waves representative of the Design Sea.

The filtering process is conducted by producing joint probability distributions describing the individual wave parameters in the Design Sea (**Design Sea Probability Analysis**). These distributions are produced using Kernel Density Estimation (KDE), a non-parametric method that requires relatively few assumptions regarding the underlying nature of the data. Low probability

[1] In the course of this research the overtopping volumes associated with the Design Sea state

waves are removed from the Extreme Sea dataset, along with their associated overtopping events, based upon these Design Sea distributions (**Extreme Sea Filtering**).

The resulting filtered Extreme Sea dataset must be further analysed to quantify the extreme individual overtopping parameters (**Output**). The parameters in question are the maximum individual volume (V_{max}) or a particular exceedance value (e.g. $V_{1\%}$). This is achieved through a processed referred to here as "Block Analysis". This involves dividing the Extreme Sea dataset (in the form of a time series of individual wave measures and overtopping volumes) into a number of equal duration blocks. Each block is intended to be representative of an individual Design Sea test (of e.g. 1000 waves) but with a shorter duration (in line with the efficiency improvement aims of the Importance Sampling method). Each block is then analysed (in terms of V_{max} and $V_{x\%}$) as if the results were obtained from a conventional random sea test.

The background of the Importance Sampling method is described in §2.6. The experimental programme (physical model), overtopping measurements and associated measurements are discussed in §3 and §4. The detailed methodology of the Importance Sampling method is described in §5. Also detailed here are the methods used in the estimation of the Design Sea joint probability distributions and the Block Analysis method used to investigate the filtered Extreme Sea dataset. The application of the Importance Sampling method using the measurements obtained in the experimental programme is described in §6. The choice of filtering parameters and the optimisation of the joint probability distribution fitting procedure is also discussed.

1.2.4 Terminology and Conventions

The provided glossary outlines the notation used throughout this thesis. The terminology used within the marine and coastal engineering community is often specific to a particular research/engineering niche, and meanings can differ.

"Response"

The term "response" describes a particular behaviour induced by the sea. In this research it primarily refers to waves overtopping a coastal structure. In other fields it may refer to dynamic behaviour observed in Wave Energy Converter (WEC), or a force exerted on fixed structure.

Sea State Characterisation

Sea state parameters may be defined using either frequency-domain or time-domain analysis. This research has used frequency domain parameters for the characterisation of sea states, unless otherwise stated. The term "significant wave height" has been taken to refer to H_{m0}.

Individual Wave Characterisation

Individual wave parameters, such as height and period, have been derived using zero downcrossing analysis, unless otherwise stated. The rationale for this methodology is explained in the main body of the thesis.

"Extreme" waves and events

The term "extreme" is used to refer to the largest event, or expected event, in a particular record. Thus the "extreme wave height" is simply the largest measured wave height. This is a near universal definition, but the term has also been used as synonym for "rogue" or "freak" waves in various publications.

An "extreme event" is the largest measured response (overtopping volume) in a given record. In order to avoid confusion with the "Extreme Seas" used in the Importance Sampling method, the term **"Maximum Individual Overtopping Volume"** has been used to describe these largest events.

"Importance Sampling"

The Importance Sampling method detailed here may differ from more conventional applications. Unless otherwise stated, "Importance Sampling" refers to the method described within the main body of this thesis.

2 Literature Review

2.1 Introduction

A significant volume of literature exists describing overtopping at coastal structures. The published research and guidance covers topics including overtopping mechanisms (i.e. the actual nature of the overtopping response), overtopping hazards and measurement uncertainties. The most relevant elements of this research are examined below. In broad terms the literature detailed here may be divided into two broad categories. Firstly, the nature of the overtopping response and its associated uncertainties are examined. This includes a discussion of the motivation for examining overtopping behaviour (e.g. understanding the hazard to properties and personnel). Particular attention is paid to the quantification of individual overtopping events, as opposed to mean discharge. Secondly the improvement of modelling efficiency is explored. Traditional irregular wave modelling techniques tend to be inefficient in terms of the test length when examining extreme responses. Ongoing research and prospective techniques for addressing this issue are discussed.

2.2 Hazard Assessment – Mean and Individual Responses

2.2.1 The Need to Quantify Overtopping Response

Figure 2.1 Wave overtopping at a monolithic breakwater (© Gerard Fournier / Editions Jos le Doare)

The need to quantify the overtopping volume at a seawall or breakwater is largely borne out of the requirement to assess the hazard at the structure. This hazard may be assessed in terms of the threat to the users of the structure, or the dangers faced by the structure itself. The critical "design" hazard will depend very much on the function and nature of the coastal structure.

Coastal defence structures vary in their primary purpose and may have several secondary uses. The most obvious purpose of a coastal structure is to protect property, with the design parameters depending very much on the nature of this property. Port infrastructure, for example, will likely have different requirements compared to an ocean-side residential housing development. The hazard posed may come directly from wave impact or from flooding. Identifying the nature of the hazard will drive the methodology used in quantifying overtopping events.

Figure 2.2 Overtopping damage to railway infrastructure in Port Elizabeth, South Africa

Transport infrastructure, usually in the form of roads and railways, is often incorporated closely with coastal defences as a primary or secondary user. Promenades consisting of roadways, with pedestrian access, may also be observed in many coastal towns. The issue of pedestrian access is an important one. Coastal structures may act as recreational areas for activities such as fishing, water sports or as a general amenity space. It would be wrong to assume that the public will always remove themselves from danger when faced with overtopping at a seawall or breakwater. In fact, people may gather at the crest of the structure to "enjoy" the overtopping. This is perhaps based on the attitude that the seawall will protect them, with the overtopping being little more than superficial spray. This perception belies the fact that at least 12 people have died due to wave overtopping in UK between 1999 and 2002 (Allsop *et al.*, 2003). The media reporting of these events also tends to give the impression that this events are due to "freak" waves or circumstances. The overtopping limits for pedestrian access will tend to be more restrictive than the requirements required for structural safety (Franco *et al.*, 1994).

Breakwaters may have similar overtopping limit requirements to seawalls in many respects, such as structural safety and user protection. An additional factor that may be significant is the need to minimise "wave transmission". Wave transmission at a monolithic structure occurs when the overtopping mass of water creates waves behind the breakwater. Mechanisms other than overtopping may be responsible for wave transmission. In porous structures such as rubble mound breakwaters waves may be transmitted directly through the structure.

In the vast majority of design cases it is desirable to reduce wave overtopping, all other factors being equal. There are, however, a few notable exceptions to this rule. In the case of breakwater design some wave transmission may be desirable to facilitate the formation of salients for beach protection purposes (Goda, 2000). A more recent development is a desire to capture the power of overtopping for energy generation purposes. The most prominent example of this is probably "Wave Dragon" as originally designed by Aalborg University, Denmark and now being developed by Wave Dragon ApS. Wave Dragon is a floating Wave Energy Converter (WEC) consisting of a reservoir replenished by overtopping waves (Tedd, 2007). The overtopping waves generate a head difference between the reservoir and ocean surface, allowing the water to be returned to the sea through turbines.

It should be noted that coastal structures may have rather high permissible overtopping levels. Low crested breakwaters can offer cost effective solutions where access is not required at all times. In these cases quantifying the overtopping behaviour may be of low importance in the design process.

Regardless of whether overtopping is a parameter to be minimised or maximised, it is important that the behaviour is properly understood. Efficient design relies on the definition of the constraints for a particular application. At a seawall or breakwater it is unlikely to be acceptable to simply "build it high" in order to minimise overtopping. The cost of extreme over-specification is unacceptable in most instances, especially as coastal defences are often

constructed using public funds. Accurate estimation of overtopping response allows engineers to design structures more closely to specification with less need for expensive margins of error.

2.2.2 Tolerable Mean and Individual Overtopping Response

When examining overtopping we are usually concerned with characterising the behaviour associated with a particular sea state. The choice of parameters used to measure overtopping is dependent on the nature of the hazard and the quality of the prediction and modelling tools available. In this research overtopping is quantified in terms of the volume of water deposited landward of the structure. Other measures of overtopping include the water throw velocity (Bruce *et al.*, 2001) and post-overtopping forces (Ingram *et al.*, 2008).

Overtopping at a structure occurs as a series of discrete events (individual overtopping volumes). In many cases it may be desirable or necessary to characterise overtopping as a continuous process. In this case the overtopping is measured as a volume flow rate per unit length of structure. It is usual to refer to this mean measurement as the "overtopping discharge". It should, however, be noted that this expression is occasionally used to refer to overtopping in a more general sense. The relationship between individual overtopping volumes (V_i) and the overtopping discharge (q) is given by the expression

$$q = \frac{1}{t_{max}} \sum_{i=1}^{N_{ow}} V_i \qquad (1)$$

where N_{ow} is the number of overtopping waves and t_{max} represents the duration of the measurement window.

Treating overtopping as a continuous process measured by the mean discharge has practical advantages. Experimentally, whether in the lab or the field, it is relatively easy to measure. The total volume of water collected over a length of structure is simply divided by the collection time (t_{max}). Measurement of individual volumes requires real-time data-logging in order that the discrete events may be quantified.

Type	Surface Armouring	Mean Discharge q (l/s/m)
Coastal dyke	Concrete on front slope, with soil on crown and back slope	< 5
	Concrete on front slope and crown, with soil on back slope	20
	Concrete on front slope, crown and back slope	50
Revetment	No pavement on ground	50
	Pavement on ground	200

Table 2.1 Tolerable discharge for structural safety (Goda, 2000)

Tolerable overtopping limits are often given in terms of the mean discharge. Goda (2000) published structural safety guidance originally determined from studies carried out in the late 1960s. The tolerable discharge limits were based on damage observed at the structures in Japan after exposure to typhoons. Goda's results are reproduced in Table 2.1 with notation and units updated for uniformity. These figures now form part of the guidance in EurOtop manual (Pullen *et al.*, 2007).

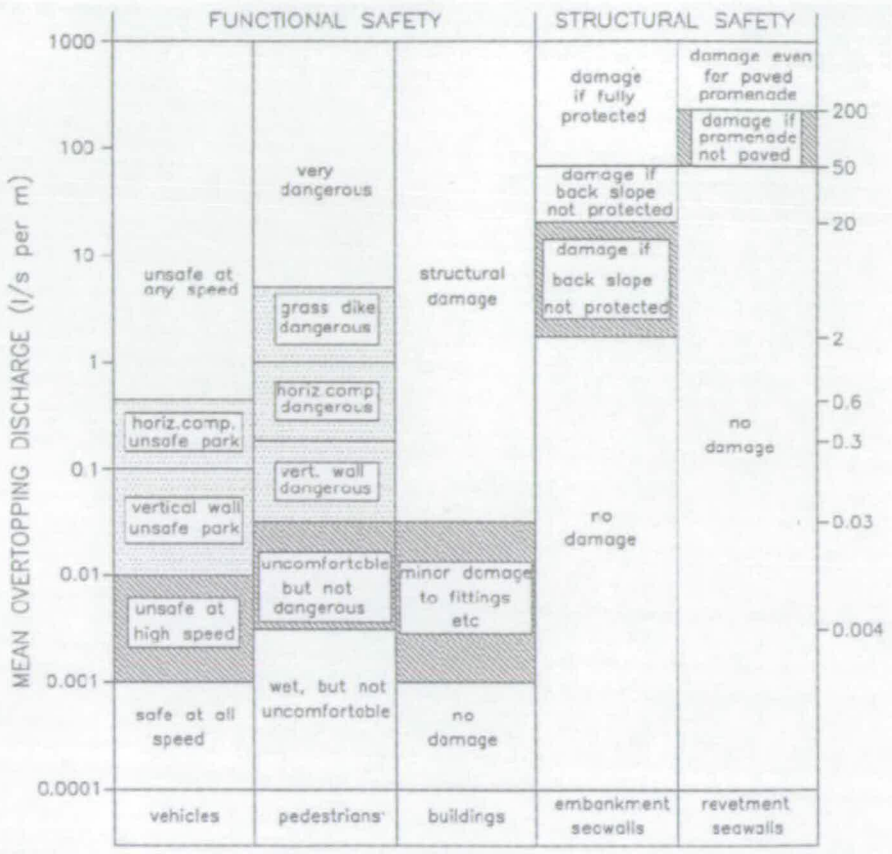

Figure 2.3 Permissible Mean Overtopping Discharges (Franco et al., 2004)

While the structural safety of the seawall or breakwater is obviously important, it may not be the critical consideration when determining the tolerable discharge. The limits for utilisation tend to be more stringent than structural requirements. These "functional safety" limits take into account pedestrian and vehicle access. It may also take into account damage to buildings, although this might be seen as more akin to structural safety. Franco *et al.* (1994) expanded on Goda's guidelines to produce discharge guidance for a number of scenarios (Figure 2.3). The pedestrian and vehicular limits were determined through laboratory measurements at full and reduced (1:20) scale. The full scale testing was conducted by directing a known volume of water at a representative velocity at the subject. The "subject" consisted of both ballasted mannequin dummies and volunteers (the paper's lead author). The dummy had to be ballasted up to double the man's actual weight to have the same falling response. It can perhaps be tentatively concluded that testing with inanimate

models tends to produce a conservative estimate of a person's response to an overtopping wave.

Endoh & Takahashi (1994) investigated the dangers faced by pedestrians on breakwaters. This research was prompted by the recognition that breakwaters in Japan were increasingly serving as public recreation areas. This research experimentally and numerically investigated the dangers faced by a person hit by an overtopping wave. This included both the falling response and the danger of being swept off the structure. The authors found that a discharge rate of 0.04 l/s/m would knock a person over, with a flow of 6 l/s/m carrying them into the sea. These figures closely agree with the guidance of Franco *et al.* (1994).

Overtopping measurements from field studies, laboratory tests and numerical models were examined in the course of the CLASH[2] project. In the course of this project Allsop (2005) collated and updated the tolerable overtopping levels from the sources stated above (Table 2.2). These limits were later incorporated in the EurOtop guidance outlined below.

User	Hazard type and reason	Mean Discharge q (l/s/m)	Max Volume V_{max} (l/m)
Pedestrians	Trained staff, well shod and protected.	1-10	500 at low level
	Aware pedestrian, able to tolerate getting wet, wider walkway.	0.1	20-50 at high level or velocity
Vehicles	Driving at low speed, overtopping by pulsating flows at low flow depths.	10-50	100-1000
	Driving at moderate or high speed, impulsive overtopping.	0.01-0.05	5-50

Table 2.2 EurOtop tolerable overtopping limits

[2] Crest Level Assessment of coastal Structures by full scale monitoring, neural network prediction and Hazard analysis on permissible wave overtopping

The current "state of the art" overtopping guidance is contained within the European Overtopping Assessment Manual (EurOtop). EurOtop's guidance contains Goda's (2000) structural limits (Table 2.1) as well incorporating functional limits from the CLASH project. The limits relating to pedestrian and vehicle access are reproduced in Table 2.2. The guidance incorporates findings from the CLASH project in noting a range of discharges acceptable to people on the structure. It is noted by CLASH and EurOtop that an individual's understanding and perception of overtopping processes will affect vulnerability when on a coastal structure. The overtopping limits recognise that trained staff members are deemed to be able to cope with a higher mean discharge than the general public. This higher limit does however require that there is no overtopping jet falling on the personnel and that there is a low danger of falling from the walkway. EurOtop also contains the proviso that a low discharge limit of 0.03 l/s/m might be more suitable for particularly hazardous structures, such as those with narrow walkways or no clear view of the sea.

The vast majority of published overtopping limit guidance relates hazard to mean discharge rather than maximum individual volumes. The mean discharge may not, however, be the best measure of the most extreme hazard. The mean discharge does not distinguish between a long series of moderately sized events and a few large overtopping volumes. This maximum individual event volume (V_{max}) is not closely related to the mean discharge (Smith *et al.*, 1994), although large individual volumes will tend to be observed in seas with large discharge rates. Franco *et al.'s* (1994) experiments suggest an individual overtopping volume of 50 l/m could knock a person over when striking their upper body. Overtopping flows at low level may be considerably higher and the EurOtop manual suggests up to 2000 l/m is acceptable for trained staff subjected to low level flows on a dike. At a vertical seawall this limit is reduced to 100 l/m. Maximum volumes for other scenarios and situations are given in Table 2.2.

2.2.3 Nature of the Overtopping Response

The behaviour of waves at seawalls is complex with a number of factors influencing the nature of the overtopping response. Understanding these response modes is important when attempting to predict overtopping volumes (and forces) or when analysing model measurements.

A wave train propagating along a beach will undergo transformations as the water depth reduces. These transformations are primarily due to refraction, shoaling and wave breaking (Goda, 2000). Wave diffraction due to structures and geographic features may also occur.

Wave refraction occurs in shallow water (depth less than approximately one half the wavelength) when the beach surface starts to exert a significant influence on the wave kinematics. The effect is that the wave fronts tend to transform to the contours of the bottom topography. In the case of a planar beach the waves will become aligned with the shoreline. This is clearly a three-dimensional phenomenon and does not influence the two-dimensional experiments conducted as part of this research. The other three-dimensional transformation of note is wave diffraction. Diffraction is a process by which wave direction changes due to the presence of obstacles such as breakwaters or islands. The waves will tend to pivot around the extremity of the structure. While these processes are not directly relevant to the overtopping experiments detailed here, it is important to acknowledge their influence should the developed techniques be applied to three-dimensional modelling in the future.

Wave shoaling is the process by which the wave height changes as the velocity of the waves (wave celerity) is reduced by the decreasing water depth. The reduction in celerity is accompanied by a reduction in wavelength. If no energy dissipation occurs, the constant energy flux will result in an increase in wave height (see e.g. Goda, 2000 and Oumeraci *et al.*, 2001). This clearly results in an increase in wave steepness (H/L) and thereby influences the onset of wave breaking.

Wave breaking is a process which is very significant to the overtopping response observed at seawalls and breakwaters. Wave breaking irreversibly dissipates energy and results in a reduction in wave height. The exact process that results in a wave breaking is complex, but may be treated as a function of the wave steepness and relative water depth. The wave shoaling and breaking relationship for $H_{1/3}$ ($\approx H_{m0}$) is represented graphically by Goda (2000) for a number of beach gradients. The relationship for a 1/30 beach is illustrated in Figure 2.4.

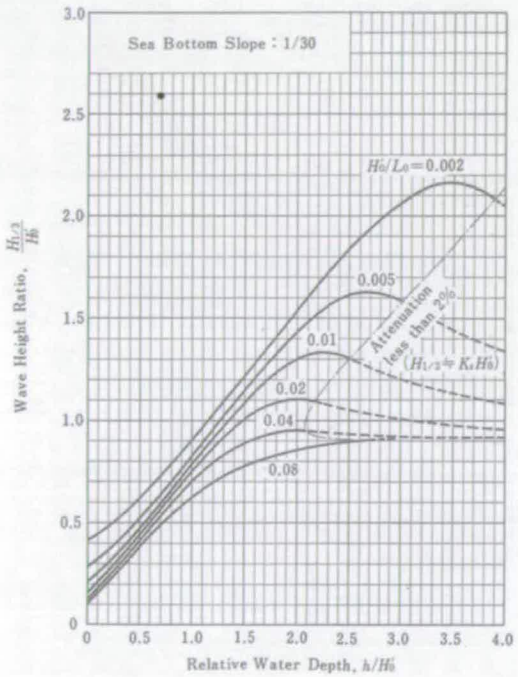

Figure 2.4 Estimates of wave heights in the surf zone (Goda, 2000)

The influence of the wave transformation behaviour becomes clear when examining the mechanism of individual overtopping events. Historically, overtopping has been treated as monotonic process dependent on a fixed set of parameters (see §2.3). Individual overtopping events were assumed to vary by degree, but were treated as essentially similar in the nature of the response. Qualitative observations, however, revealed this to be false. The violence of wave overtopping events would vary considerably. This behaviour was formally characterised by Allsop *et al.* (1995) and Oumeraci *et al.* (2001). The

overtopping behaviour can be separated into three broad categories: pulsating overtopping; impulsive overtopping; and broken-wave overtopping.

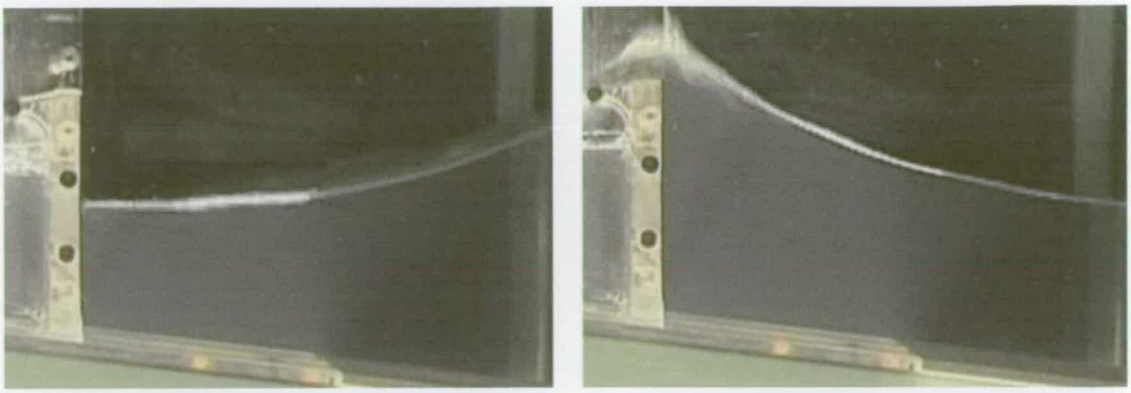

Figure 2.5 Pulsating ("green-water") overtopping at a vertical seawall at model scale

Pulsating overtopping tends to occur in deeper water with waves of lower steepness. This response is also referred to as "green-water" and reflecting wave overtopping. The overtopping wave in this scenario will runup the structure before passing over the seawall crest, as illustrated in the physical modelling images in Figure 2.5.

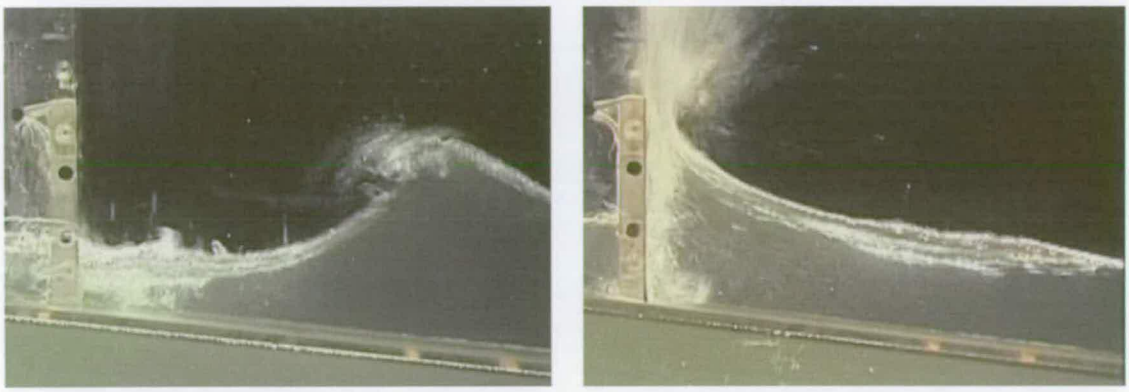

Figure 2.6 Impulsive ("violent") overtopping a vertical seawall at model scale

Impulsive overtopping tends to occur in shallower water with waves of higher steepness. If the wave breaks immediately in front of the structure it may violently impact the structure producing a highly aerated, high velocity overtopping jet. This process is clearly illustrated in the physical modelling images in Figure 2.6.

Broken-wave overtopping occurs when waves break some distance prior to impact with the structure. In general terms, this type of overtopping response may be treated as a less severe version of impulsive overtopping due to the energy dissipation of the breaking process.

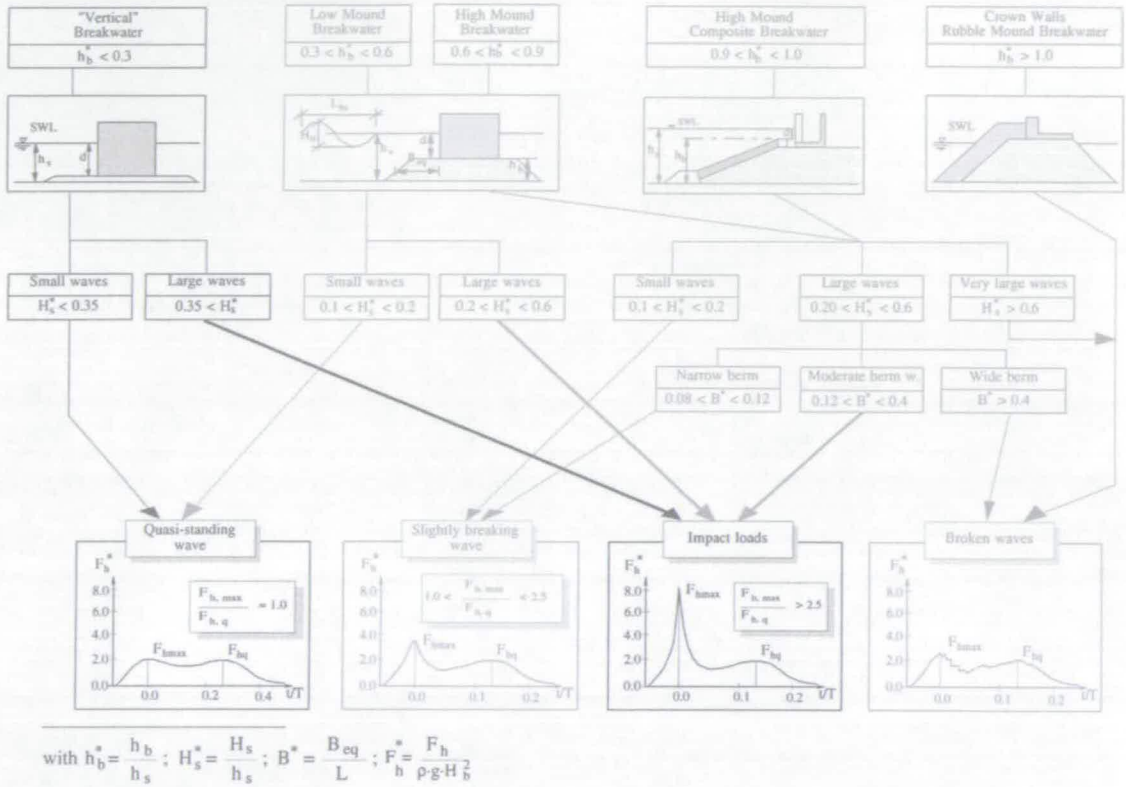

Figure 2.7 PROVERBS (Oumeraci *et al.*, 2001) response parameter map with vertical wall guidance highlighted.

The PROVERBS project (Oumeraci *et al.*, 2001) used the relative wave height at the structure (H_{m0} / h_s) to determine the wave behaviour. When taken into consideration with the structure type (e.g. vertical seawall, rubble mound breakwater etc.) the wave regime at the structure may be predicted. This procedure is illustrated by the "parameter map" in Figure 2.7. At a vertical structure "impact loads" (impulsive overtopping) are expected for relative wave height values greater than 0.35. PROVERBS does not offer extensive guidance on wave overtopping volumes and the map reproduced here is intended for the prediction of wave forces on structures.

Allsop *et al.* (1995) developed the empirical h_* parameter for prediction of the overtopping regime at the structure:

$$h_* = \frac{h_s}{H_{m0}} \cdot \frac{2 \cdot \pi \cdot h_s}{g \cdot T_m^2}. \tag{2}$$

The h_* parameter significantly differs from the relative water depth with the inclusion of the wave period, thereby accounting for average steepness of the waves impacting the structure. Laboratory tests showed impulsive overtopping events predominated for seas with $h_* < 0.3$. The h_* parameter is the method recommended both by the EA-Manual and EurOtop for identification of the overtopping regime.

2.3 Mean Overtopping Volumes

This thesis is primarily devoted to understanding the nature of individual overtopping responses. The majority of published guidance is, however, based upon predicting the mean overtopping rate. While these prediction methods are not used extensively in this research, it is worthwhile examining the basis behind them.

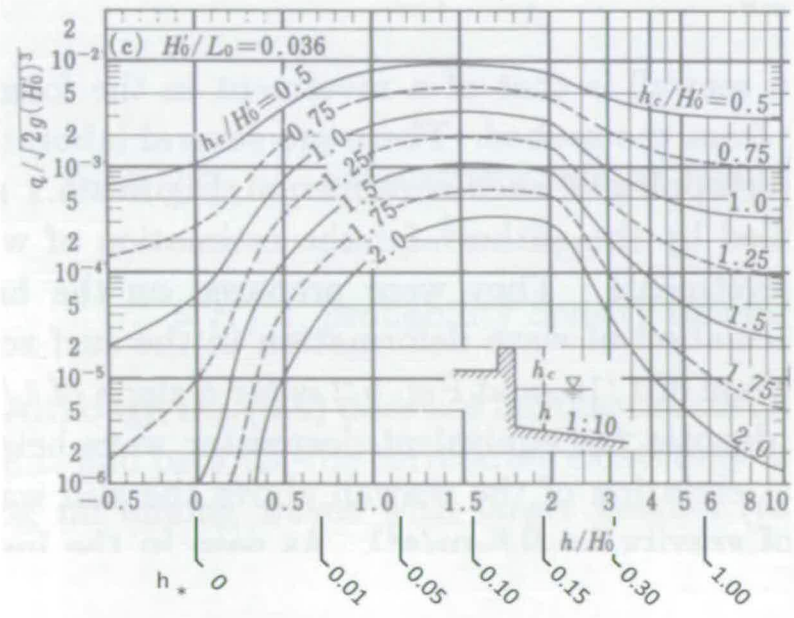

Figure 2.8 Overtopping rate prediction chart for 1:10 bottom slope and offshore steepness of 0.036 (Goda, 2000). Labels have been added to Goda's original diagram denoting a range of h_* values.

Goda (2000) produced design diagrams predicting the overtopping rate for vertical revetments for a range of bathymetry gradients (1:10 and 1:30), as shown in the example in Figure 2.8. These empirical charts, originally published in the 1970s, were produced from laboratory tests using irregular (random) seas. The discharge prediction for a particular bathymetry and offshore steepness is a function of the relative water depth (h/H_{m0}) and the relative crest freeboard (R_C/H_{m0}). It should be noted that Goda's terminology and notation differs in some respects from convention. In particular Goda uses a measure of wave height denoted as the "equivalent deepwater wave height" (H_0'). This term describes the wave height after refraction and diffraction effects, but before transformation due to shoaling and breaking. In the context of a two-dimensional example H_0' is equivalent to the offshore significant wave height ($H_{m0\_offshore}$).

Goda's charts, as is intuitively expected, predict that a reduction in relative freeboard results in an increase in the overtopping discharge for a given relative water depth. The trend with changing relative depth, however, is not consistent. The outer extremes of the chart (i.e. shallow and deep water) show the lowest overtopping rates with the maximum occurring in the relative depth range of approximately 1.0 to 2.0. Considering the observations relating to wave behaviour at the structure (2.2.3) it is expected that a range of overtopping behaviours, from pulsating to impulsive to broken waves, will be observed as the water depth reduces. It is these changes in overtopping regime that result in the non-linear variation in overtopping response at the structure that Goda's chart clearly illustrates.

The overtopping regime changes in Figure 2.8 may be more clearly understood by use of the wave breaking parameter (h_*) as described above (2.2.3). Rewriting h_* in terms of wavelength gives

$$h_* = \frac{h^2}{H_{m0\_inshore} \cdot L_m} \tag{3}$$

where

$$L_m = \frac{g \cdot T_m^2}{2\pi}. \tag{4}$$

If the wave steepness and the relative water depths are known, as they are in this case, h* may be expressed as:

$$\begin{aligned} h_* &= \frac{h^2}{H_{m0,i} \cdot L} \\ &= \frac{h^2}{k_s \cdot H_{m0,o} \cdot L} = \frac{1}{k_s} \cdot \left(\frac{h}{H_{m0,o}}\right)^2 \cdot \frac{H_{m0,o}}{L} \\ &= \frac{1}{\text{Shoaling Coefficient}} \times \text{Relative Depth}^2 \times \text{Wave Steepness}. \end{aligned} \tag{5}$$

The offshore wave height must be translated to give the inshore wave height through use of a shoaling coefficient (k_s). The value of k_s for a given wave steepness, bottom slope and relative water depth may be determined using Shuto's method as described by Goda (2000). Given that these values are known, values of h* may be incorporated into Goda's prediction chart (Figure 2.8).

Modifying the relative depth axis in Figure 2.8 to include the associated h* values gives a clearer understanding of the overtopping processes involved. Seas with values of h* below 0.3 are expected to result in predominately impulsive (breaking) waves at the structure. Strongly impulsive conditions are expected to be observed for h* values below 0.2 (Allsop *et al.*, 2005). It is within this strongly impulsive region that the largest overtopping discharges are observed. It is clear, therefore, that a change in overtopping regime is an important factor that must be accounted for when designing or assessing a vertical coastal structure. In this particular chart, a reduction in relative depth from a ratio of 3 to 2 may increase the overtopping discharge by an order of magnitude for some relative freeboard configurations. Further reducing the relative depth will eventually result in the overtopping discharge tending towards zero. At these very low relative depths the wave regime has shifted to

broken wave conditions, with much of the energy dissipated prior to impacting the structure.

While it is clear from examination of the chart in Figure 2.8 that the overtopping regime influences the discharge rate, this was not explicitly commentated upon in Goda's guidance. The non-monotonic behaviour at the seawall complicated attempts to provide formulaic, empirical predictions of the overtopping discharge. Franco *et al.* (1994) gave the following equation based upon two-dimensional scale model testing:

$$\frac{q}{\sqrt{g \cdot H_{m0}^3}} = 0.2 \cdot \exp\left(-4.3 \frac{R_C}{H_{m0}}\right) \tag{6}$$

While not explicitly stated by Franco *et al.*, Equation (6) may be considered valid for approximately $0.7 < R_c/H_{m0} < 2.8$ based on the fitted data. Allsop *et al.* (1995) modified this equation based upon physical model tests in deep and shallow water,

$$\frac{q}{\sqrt{g \cdot H_{m0}^3}} = 0.03 \cdot \exp\left(-2.05 \frac{R_C}{H_{m0}}\right), \tag{7}$$

valid for $0.03 < R_c/H_{m0} < 3.2$. This range of relative freeboard is significantly wider than both Franco *et al.'s* formula and Goda's design chart (Figure 2.8). There is no attempt, however, to account for the effects of the relative water depth at the structure. There is therefore no consideration of any relationship between the wave regime at the structure and the overtopping volume.

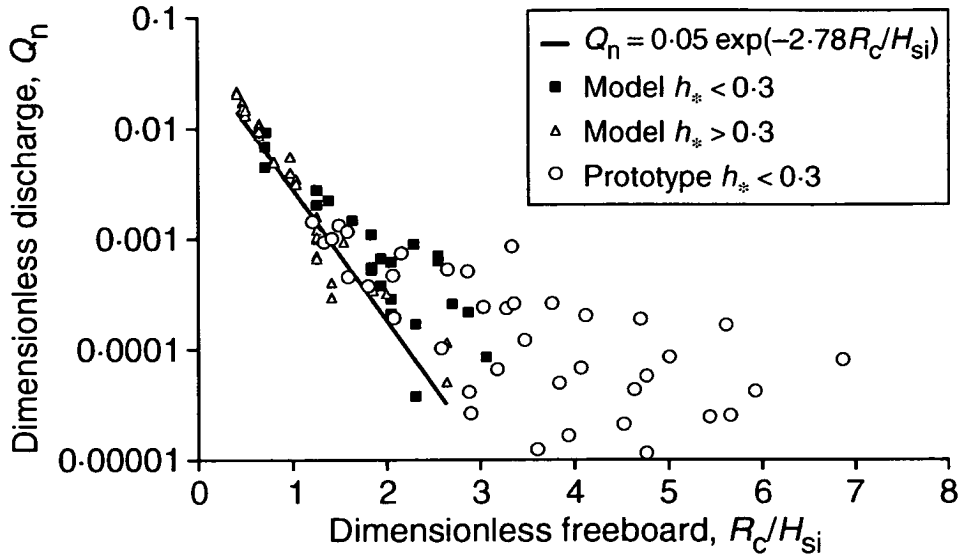

Figure 2.9 Overtopping discharges compared with the empirical equation of Franco *et al.* (1994) as modified by Besley *et al.* (1998). $Q_n = q/(g \cdot H_{mo}^3)^{1/2}$. Plot reproduced from Allsop *et al.* (2005).

Allsop *et al.'s* (1995) development of the h_* parameter allowed for a more refined and representative description of the overtopping discharge. Rather than using a single empirical equation, pulsating (predominately non-breaking waves) and impulsive (predominately breaking waves) sea conditions were treated as two separate cases. This revised approach is incorporated in the UK's Environment Agency's "Wave Overtopping at Seawalls – Design and Assessment Manual" (Besley, 1999) and is also described by Besley *et al.* (1998). The prediction for pulsating wave conditions ($h_* > 0.3$, see §2.2.3) is essentially a modified version of Franco *et al.'s* (1994) equation, taking the form

$$\frac{q}{\sqrt{g \cdot H_{m0}^3}} = 0.05 \cdot \exp\left(-2.78 \frac{R_C}{H_{m0}}\right), \qquad (8)$$

valid for $0.03 < R_c/H_{m0} < 3.2$. This equation is compared with full scale and model data in Figure 2.9. Good agreement between the data with $h_* > 0.3$ (predicted pulsating) and the formula is evident with relatively little scatter. It is clear, however, that the data regarded as impulsive according to h_* do not show a good fit with Franco *et al.'s* exponential formula.

In order to account for the differing behaviour of impulsive seas ($h_* \leq 0.3$) a different formula taking account of h_* star is used, taking the form

$$Q_h = 1.37 \times 10^{-4} \cdot R_h^{-3.24}, \tag{9}$$

valid for $0.05 < R_h < 1.0$. This formula is given in terms of the "dimensionless crest freeboard", notated as R_h and defined as

$$R_h = \frac{R_C}{H_{m0}} \cdot h_*. \tag{10}$$

The dimensionless discharge for impulsive sea conditions (Q_h) is given by

$$Q_h = \frac{Q}{h_*^2 \sqrt{g \cdot h^3}} \tag{11}$$

The impulsive wave equation (9) was revised by Bruce *et al.* (2001) following small scale model tests. This revised equation takes the form

$$Q_h = 1.92 \times 10^{-4} \cdot R_h^{-2.92}, \tag{12}$$

with the valid dimensionless crest freeboard (R_h) range being unchanged. This revised equation is incorporated in the European Overtopping Manual (Pullen *et al.*, 2007) which represents the current "state-of-the-art" in overtopping prediction. The manual's guidance for pulsating sea conditions (Equation (8)) remains unchanged.

The treatment of the overtopping discharge in two separate equations clearly indicates an attempt to account for the non-monotonic nature of the overtopping response. In the main this approach has been successful, and has proved more effective than a "one size fits all" approach, with the scatter in the predicted discharges significantly reduced (Allsop *et al.*, 2005). It should be noted, however, that the treatment of seas as simply impulsive or pulsating is a simplification of the processes involved. The collection of discrete overtopping events which produce the overtopping discharge may not be uniform in their behaviour. The h_* parameter gives guidance on the expected predominant behaviour but does not necessarily describe the overtopping action of every

event in the sea. Examination of Figure 2.9 shows that while Franco *et al.'s* exponential formula poorly predicts the discharge of the h_* predicted impulsive seas as a whole, several of these impulsive results do show good agreement with the pulsating equation. It may be that the h_* parameter did not successfully predict the predominant behaviour for these tests, or the impulsive waves were not dominant in their contribution to the total overtopping volume. In either case it is clear that care must be taken if individual wave behaviour is to be characterised using the h_* parameter or similar method.

2.4 Individual Overtopping Volumes

2.4.1 Studies and Prediction Methods

Guidance relating to tolerable overtopping limits has suggested that individual overtopping volumes may be a more accurate measure of hazard than the mean discharge (see §2.2.2). There has, however, been relatively little research conducted into characterising individual overtopping events. The little guidance that has been published has concentrated on describing the overtopping volumes through use of the Weibull distribution.

Franco *et al.* (1994) examined the distribution of individual overtopping volumes obtained from small scale model tests. A three-parameter Weibull distribution was fitted to the test results:

$$P(V_i \geq v) = \exp\left(-\frac{v-c}{a}\right)^b \qquad (13)$$

where $P(V_i \geq v)$ is the probability that an individual event volume (V_i) exceeds a given a given value (v) and a, b and c are respectively the shape, scale and location parameters. In this case the distribution describes the individual volume exceedance probability. More commonly the distribution is expressed as a non-exceedance probability, i.e. the probability that an individual volume will not exceed a given value. While this distinction makes little practical difference, the non-exceedance probability has become the conventional measure and will be used as the basis of the distributions in this thesis. Franco *et al.* also fitted the

distribution to all the waves in the test (N_w) rather than just the overtopping waves (N_{ow}). As the non-overtopping waves will obviously be assigned an overtopping volume of zero the use of three-parameter distribution incorporating a location parameter is necessitated. If the distribution is used to describe only the overtopping waves the location parameter may be neglected ($P(V_i>0)=1$). Using a two-parameter Weibull distribution written in terms of non-exceedance the overtopping volume distribution may be described as:

$$P(V_i \leq v) = 1 - \exp\left(-\frac{v}{a}\right)^b. \tag{14}$$

Franco *et al.'s* (1994) model tests yielded shape parameter (b) value of 0.75, which it is claimed showed little variability. The scale parameter was found to be a function of the average individual overtopping volume ($\overline{V}$) with the relationship

$$a = 0.84 \cdot \bar{V} = 0.84 \cdot \frac{T_m \cdot Q}{\frac{N_{ow}}{N_w}}. \tag{15}$$

Franco *et al.* also offer a formula for the prediction of the proportion of overtopping waves:

$$\frac{N_{ow}}{N_w} = \exp\left(-\frac{1}{0.91}\frac{R_c}{H_{m0}}\right)^2. \tag{16}$$

This relationship is based on the assumption that the proportion of overtopping waves is Rayleigh distributed and related to the relative freeboard. This relationship appears to be supported by Franco *et al.'s* experimental results. This equation is also reproduced in the EA-Manual (Besley, 1999) with the proviso that it is valid only for pulsating seas for relative freeboards $0.03 < R_c/H_{m0} < 3.2$. Franco *et al.'s* tests were conducted in relatively deep water and can not be considered valid for cases where impulsive (breaking) waves may dominate.

The EA-Manual recommends that for impulsive seas ($h_* < 0.3$) the following equation is used to describe the proportion of overtopping waves:

$$\frac{N_{ow}}{N_w} = 0.031 \cdot R_h^{-0.99} \quad (17)$$

valid for $0.05 < R_h < 1.0$, where R_h is dimensionless crest freeboard as defined in Equation (10).

Regime	s_{op}	Scale Parameter (a)	Shape Parameter (b)
Pulsating	0.02	$0.74 \cdot \overline{V}$	0.66
	0.04	$0.90 \cdot \overline{V}$	0.82
Impulsive	-	$0.92 \cdot \overline{V}$	0.85

Table 2.3 Weibull distribution scale and shape parameters as given in the Wave Overtopping of Seawalls – Design and Assessment Manual (Besley, 1999)

The EA-Manual uses the two parameter Weibull distribution (Equation (1)) to describe individual overtopping volumes. Unlike Franco *et al.* (1994), the shape and scale distributions are chosen based on the predominant sea state (pulsating or impulsive). This guidance is reproduced here in Table 2.3. In the case of pulsating seas the distribution scale and shape is influenced by the offshore steepness (s_{op}). It is noted by Besley (1999) that model tests confirmed Franco *et al.'s* (1994) estimation of the shape parameter ($b = 0.75$) as generally accurate for pulsating seas. Tests had also revealed, however, that the shape parameter took a lower value for long-crested waves, hence the dependency on s_{op} observed in Table 2.3. Besley also notes that a "conservative approach" was taken when specifying the shape parameter. This essentially means that the predicted shape parameter may be expected to be lower than is observed in practice, thus extending the tail of distribution. No such dependence on wave steepness was seen in the impulsive tests.

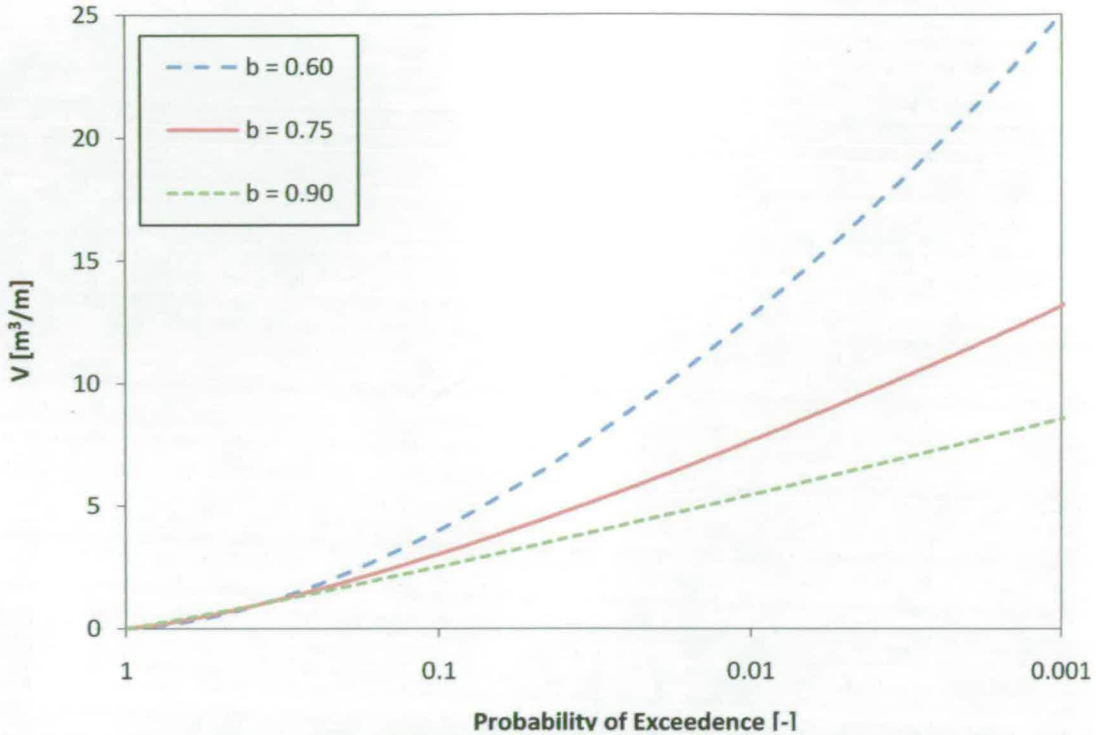

Figure 2.10 Weibull probability distributions of individual wave overtopping with various shape (b) values and scale value (a) of 1.0.

The European Overtopping Manual (EurOtop - Pullen *et al.*, 2007) effectively reverts to the guidance of Franco *et al.* (1994) as described above. This is justified by authors on the basis that the shape parameters given in the EA-Manual are mostly within the range 0.6 to 0.9. A shape parameter value of 0.75, as given by Franco *et al.* (1994), represents the average of this range of values. In turn, the reasoning given for this simplification is the observation that the distribution shape varies little over this shape parameter range. The distribution shapes are illustrated here in Figure 2.10, with the scale parameter set to a value of 1.0. While the distributions are similar in form, they show a notable deviation at the low probability extreme. The 0.1% exceedance probability volume shows a disagreement of approximately 30%. The justification for this simplification, compared to the EA-Manual, may be that the small datasets used to deduce the steepness-dependent shape parameters may only create the illusion of increased accuracy.

Given the distribution of individual overtopping events it is possible to estimate the maximum overtopping volume (V_{max}) if the total number of overtopping events is known. Franco *et al.* (1994), Besley (1998) and Pullen *et al.* (2007) use the following relationship to describe the probability of an overtopping event exceeding V_{max}:

$$P(V_i \geq V_{max}) = \frac{1}{N_{ow}}. \tag{18}$$

Given that N_{ow} is known, or can be predicted, for a particular test the expected value of V_{max} may be calculated based upon the Weibull distribution

$$V_{max} = a \cdot (\ln(N_{ow}))^{1/b}. \tag{19}$$

where a and b are the scale and shape parameters respectively. This relationship is common to the guidance of Franco *et al.* (1994), the EA-Manual (Besley, 1999) and EurOtop (Pullen *et al.*, 2007). The suitability of this method to describe the extreme of a distribution is discussed in depth in this thesis.

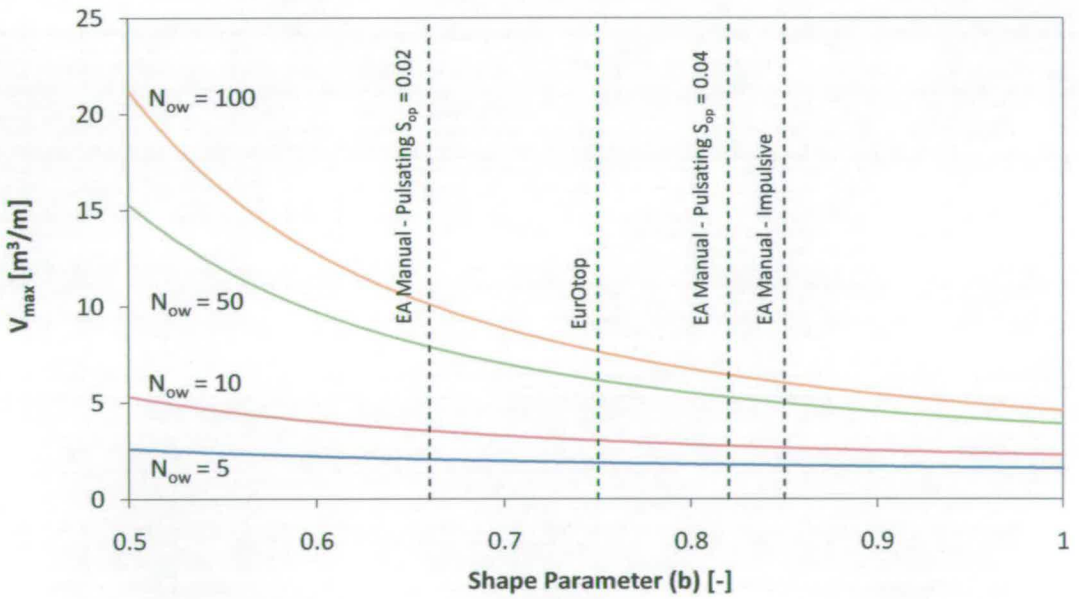

Figure 2.11 Predicted values for V_{max} as given by the EA-Manual (Besley, 1999) and EurOtop (Pullen *et al.*, 2007) for a nominal shape parameter (a = 1).

It is detailed above that the EurOtop manual uses a single shape parameter in contrast to the multiple steepness dependent b values given in the earlier EA-

Manual. Using the V_{max} prediction formula (Equation (19)) it is possible to examine the influence of the shape parameter. Figure 2.11 illustrates the variation of V_{max} with shape parameter for a range of N_{ow} values. It is notable that the use of single shape parameter may produce a non-conservative estimate of the maximum overtopping volume. The multiple shape parameters of the EA-Manual were abandoned, however, due to the inherent uncertainty present in the estimation of the shape parameter. The variation in shape parameter is examined in the course of this research.

Despite the near universal use of the Weibull distribution to describe individual overtopping volumes there is little published detailed justification for this. Franco *et al.* (1994) and the EA-Manual claim the distribution offers a good fit to the individual overtopping data but do not publish any justification beyond qualitative goodness-of-fit observations. It should be noted, however, that there is little evidence to suggest that the Weibull distribution does not offer a good fit to the overtopping volumes.

2.4.2 Error and Uncertainty

There have been few published studies examining systematically the errors associated with predicting and measuring the largest overtopping events. Much of the recognition that significant uncertainty is present is either based upon experience or an intuitive understanding of the prediction methods.

Two broad sources of uncertainty are present in the measurement of V_{max} from model testing. The first is simply the error associated with the measurement system. The second is the inherent variability present in the measurement of a single value from a stochastic process. Pearson *et al.* (2001) examined these uncertainties as part of the VOWS project. The error in the overtopping volume measurement system, similar to that used in this research (§3.3.2 and §3.3.3), was determined to be negligible. The greater uncertainty was present in the scatter of the results obtained from repeat tests with the same sea state. It should be noted that the scope of this study was quite small. Relatively little analysis was conducted into the uncertainty associated with repeat tests using

different realisations of the elevation time series (produced from the same spectrum).

The term "same sea state" is used here to describe tests carried out with the same inputted wave energy spectrum. Repeat tests may consist of simple nominally identical test runs (see §3.5.3 for information) or different time-domain realisations of the spectrum. While there are several methods for producing linear elevation time series from the spectrum, the most commonly used in wave tank facilities is the concept of sinusoidal superposition with pseudo-random phase angles. These phase angles are uniformly distributed between 0 and 2π and are produced using a random number generating algorithm[3]. These algorithms take a single seed number to produce a vector of values, hence taking the form of pseudo-random system.

Repeat tests carried out by Pearson *et al.* (2001) with nominally identical elevation-time histories (i.e. same seed number) showed the lowest variability in V_{max} with errors typically in the range of 5 – 8%. Altering the seed number increased the variability, with the typical scatter increasing to 15 - 20%. This relationship is intuitively expected to be true. In a perfectly repeatable system the error in V_{max} would be zero for tests with the same seed number. V_{max} will, however, always vary with different realisations of the spectrum. V_{max} is a measurement of a single event, and the wave, or wave group, producing that single event is unlikely to be reproduced exactly in different realisations of the elevation-time history.

Pearson *et al.* (2001) examined the influence of test length on the overtopping measurements. The mean discharge was shown to be a stationary process, with the variability reducing as the test length increased from ~100 to ~1000 waves. The results obtained appear to support the established use of 1000 wave tests when quantifying the mean response.

[3] A suitable random number generating algorithm is outline by Goda (2000). Various standard routines also exist in packages such as MATLAB.

The influence of test length on the value of V_{max} shows a different relationship than observed with the mean response. Longer test lengths resulted in an increased average value of V_{max}. This is the expected behaviour, based on the probabilistic relationship between the number of events and the expected extreme of a distribution (Equation (19)). Interestingly, the V_{max} results obtained by Pearson *et al.* (2001) show little change in the magnitude of the standard deviation with increasing test length.

Empirical prediction methods for V_{max} (§2.4.1) are based upon various parameters describing the sea state and structure configuration. These parameters are incorporated into the prediction formula in the form of the Weibull scale (a) and shape (b) parameters. Napp (2004) examined shape and scale parameters fitted to distributions of overtopping data obtained from physical modelling testing under impulsive conditions. The mean value of the "dimensionless scale parameter" ($a/\overline{V}$) was found to be distributed around 1.0·, similar to the EA-Manual value of 0.92 (Table 2.3). The scatter observed in the shape parameter was quite large, with values distributed between ~0.7 and ~1.3. The mean of the measured shape parameter was 0.96, close to the EA-Manual value of 0.85. As with the scale parameter, significant scatter was observed, with shape parameter values varying between ~0.6 and ~1.5. Relatively small errors in the estimation of the shape parameter may result in large variations in the estimation of V_{max}, as previously illustrated in Figure 2.10.

Napp (2004) found, based upon three-dimensional testing, that the values of V_{max} were overestimated by the EA-Manual impulsive formulae by an average factor of approximately 1.25. Attempts to fit new scale and shape parameters as a function of h_* (Equation (3)) produced little improvement in the accuracy of the estimation. It was suggested that this lack of improvement was largely due to the level of scatter in the scale and shape parameters.

A clear source of error in the estimation of V_{max} lies in determining the number of overtopping waves (N_{ow}). Napp (2004) showed the measured value of N_{ow}

(from three-dimensional tests) predicted by the EA-Manual may vary by up to an order of magnitude compared to the experiments in extreme cases, although more normally it fell within a factor of 5. The validity of these measurements assumes that the experimental equipment is capable of accurately recording individual overtopping events. This may not necessarily be the case. The practicalities of overtopping detection are discussed in §3.3. In brief, very small overtopping events are often indistinguishable from the background noise of the measurement system. This necessitates the use of a threshold system to identify the overtopping waves. Adjusting this threshold will yield varying values of N_{ow}. Given this potential source of uncertainty, attention was paid in this research to improving the effectiveness of the overtopping detection system. This is an area of overtopping research which is fraught with difficulty. Overtopping is a chaotic process and many events are difficult to define both qualitatively (e.g. through observation) or quantitatively, using measurement and detection apparatus.

2.5 NewWave and Related Approaches

2.5.1 Deterministic Wave Groups – "NewWave"

A feature of random wave modelling is that individual tests will tend to have rather long durations. Extending the test run will produce a more representative sample of waves for a particular sea state. Practical concerns will, however, tend to hinder any desire to carry out very long duration tests.

In cases where only the maximum response is of interest only a handful of waves in the random sea will produce results of interest. For this type of modelling situation deterministic techniques potentially offer wave descriptions equivalent to an infinite number of random wave model tests. This clearly makes this type of technique very attractive in terms of accuracy and efficiency.

The "NewWave" wave group as described by Tromans *et al.* (1991) produces a probabilistic description of the extreme wave (defined as the maximum crest elevation) for a particular sea frequency spectrum. The NewWave group

effectively describes the average shape surrounding the extreme crest as obtained from an infinite number of random seas. On the face of it, this property suggests a potential for the NewWave theory to produce maximum response results comparable to random wave model testing without the associated efficiency penalties.

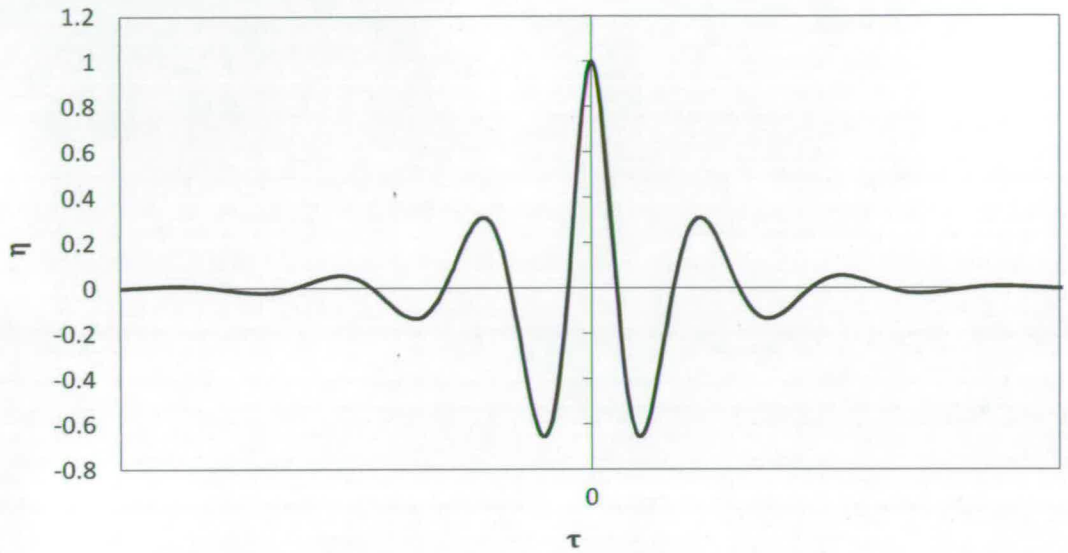

Figure 2.12 NewWave time history with nominal crest elevation. Based on JONSWAP spectrum with γ = 3.3.

An example of a typical NewWave elevation-time history is illustrated in Figure 2.12. This particular example is derived from a JONSWAP spectrum with a peak amplification factor (γ) of 3.3.

Tromans *et al.* suppose that the expected surface elevation (η^*) surrounding a crest (measured at time t_1) may be described as a function of time by the expression

$$\eta^*(\tau) = \alpha \cdot \rho(\tau) + g(\tau) \tag{20}$$

where $\tau = t - t_1$ and α is the crest elevation. The expression consists of deterministic ($\rho(\tau)$) and random ($g(\tau)$) part. The Gaussian (random) part has a value of zero at the crest. Taking the deterministic part only,

$$\eta_d^*(\tau) = \alpha \cdot \rho(\tau), \tag{21}$$

the most probable elevation surrounding the crest is described. As such, the deterministic expression $\rho(\tau)$ relates to the autocorrelation function of the surface elevation, with a value of 1 at the crest ($\tau = 0$). This function is described by the Fourier transform of the frequency spectrum, with zero phase angles:

$$\rho(\tau) = \frac{1}{\sigma^2}\sum_{n}^{N} d_n \cos(\varpi_n \tau) \tag{22}$$

where

$$d_n = S(\varpi_n)\Delta\varpi_n \tag{23}$$

and σ is the surface-elevation standard deviation of the underlying random sea. It can be shown by linear wave theory (see e.g. Krogstad & Arntsen. 2000) that the surface elevation variance is given by the expression

$$Var(\eta) = \sigma^2 = \sum_{n}^{N} d_n. \tag{24}$$

It may be observed from equations (22) and (24) that $\rho(\tau = 0) = 1$. Essentially, the expression $\rho(\tau)$ describes the most probable shape surrounding the wave crest for a particular spectrum. This shape is then scaled for a particular crest elevation to give the most probable surface elevation surrounding the crest (η_d^*) as expressed in equation (21). Including spatial dependence (X) gives the final NewWave expression

$$\eta_d^* = \frac{\alpha}{\sigma^2}\sum_{n}^{N} d_n \cos(k_n X - \varpi_n \tau), \tag{25}$$

where k is the wavenumber, related to the wavelength (L) by

$$k_n = \frac{2\pi}{L_n}. \tag{26}$$

The NewWave theory has been primarily applied using numerical modelling tools to investigate deep-water engineering problems. In particular, the method has been used to investigate forces on fixed offshore platforms. Rozario *et al.*

(1993) examined shear forces acted at the base of the North Sea Tern platform. Field data describing the forces exerted on the platform was provided by strain-gauge instrumentation. Wave kinematics derived from the NewWave theory were used to predict the base shear force using a hydrodynamic model of the structure. The NewWave values agreed both with the field measurements and similarly derived predictions using synthesised linear random elevation-time histories.

2.5.2 Combined Deterministic and Random Seas

The prime benefit of the NewWave theory is the more realistic description of the wave shape and kinematics *immediately* surrounding the extreme wave crest when compared to regular waves (Tromans *et al*, 1991). The adjacent waves (see Figure 2.12) do not represent the average shape of the waves adjacent to the extreme wave. This is not relevant in structures or devices where there is little or no dynamic response, such as the Tern platform examined by Rozario *et al.* (1993). In the case of floating vessels/devices and dynamically responding fixed structures the waves preceding and succeeding the extreme waves may also influence the response. These dynamic responses are usually examined using randomly generated waves, with associated uncertainty in the magnitude and shape of the largest wave. An attempt to combine the efficiency advantages of deterministic modelling with the variable load histories of a random wave model has been made by Cassidy *et al.* (2001) in the form of the Constrained NewWave theory. This technique involves embedding a NewWave group within a conventionally generated elevation-time history. In doing so control is exerted over the elevation and shape of the largest crest while the preceding and successive waves are representative of a real sea. Several NewWave groups may be embedded within the random wave train.

At present the principles of the Constrained NewWave method have not been applied to the field of coastal engineering. While coastal structures do not, in general, exhibit dynamic response mode there remains a possible influence of wave grouping on the measured response. An example is the influence of wave

setup at sloping and permeable structures, where waves preceding the overtopping wave cause a rise in the local mean water level, influencing the runup and overtopping response. A deterministic wave group embedded within a random sea may offer some insight into these behaviours. It would need to be proven, however, that the embedded deterministic group (e.g. NewWave) described the wave shape associated with the extreme response (i.e. the design wave).

2.5.3 Coastal Engineering Applications

The use of NewWave and similar deterministic techniques is not, as yet, well established for shallow water applications. The kinematics of focused wave groups propagating into shallow water was examined by Hunt *et al.* (2003). Wave interactions with a structure (e.g. overtopping or similar) were not examined in this research.

Recent research has extended the use of focused wave groups to examination of individual overtopping volumes at vertical seawalls. Jayaratne *et al.* (2008) examined violent overtopping behaviour using this technique. The breaking properties of the wave were adjusted by shifting the focus location and amplitude. The focused wave groups were generated using JONSWAP and square "top-hat" spectra. The aim of the experimental programme was to gain insight into the overtopping process rather than to quantify a particular design scenario. The measured overtopping volumes were not compared to measurements obtained using conventional random sea tests.

Examination of the overtopping results obtained by Jayaratne *et al.* (2008) illustrates the potential benefits of the deterministic approach. A series of ten repeat tests showed a variability of only ±6% in the overtopping volume for "low-aeration" events. More aerated violent events showed greater variation, although this is not specifically quantified in the published results. Nevertheless, this high level of repeatability suggests that focused wave groups may be useful tool for the physical modeller. The "missing link" in this area of research (if NewWave, and similar techniques, are to be used as an engineering design tool)

would appear to be the lack of cross-comparison with conventional modelling techniques.

2.6 Importance Sampling

Importance Sampling is a variance reducing technique employed in the application of Monte Carlo modelling. In particular it has been demonstrated in the field of structural engineering (e.g. Melchers, 1989). Monte Carlo simulations of structural failure are concerned with low-probability failure modes. Importance Sampling involves increasing the "severity" of the load distribution, compared to the design case, to better describe the failure regime of the system.

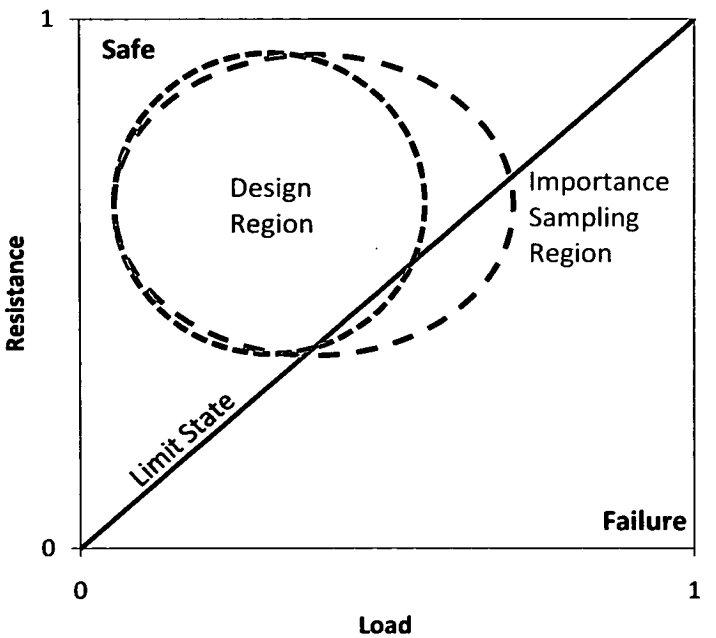

Figure 2.13 Basic Importance Sampling schematic illustrating the design region (some low probability contour) explored by conventional modelling compared to the Importance Sampling region.

An example of how the system may be applied in a structural modelling system is described diagrammatically in Figure 2.13. A range of loads and resistances (corresponding to different structural configurations) are simulated in the model. If the load stress is greater than the resistance stress (i.e. the strength) failure will occur. It is observed that few simulations will result in failure. The

Importance Sampling technique stretches the modelling region to provide more failure test cases. Low probability failure modes, where the design probability contour crosses the limit state line, are described better by the Importance Sampling model inputs.

The Importance Sampling technique was recognised as potentially having applications in field of overtopping modelling (Wolfram *et al.*, 2004). Quantifying the extreme overtopping behaviour for a particular sea state is hampered by low sample sizes. The complex nature of the overtopping response (§1.2.2) also presents further sources of uncertainty.

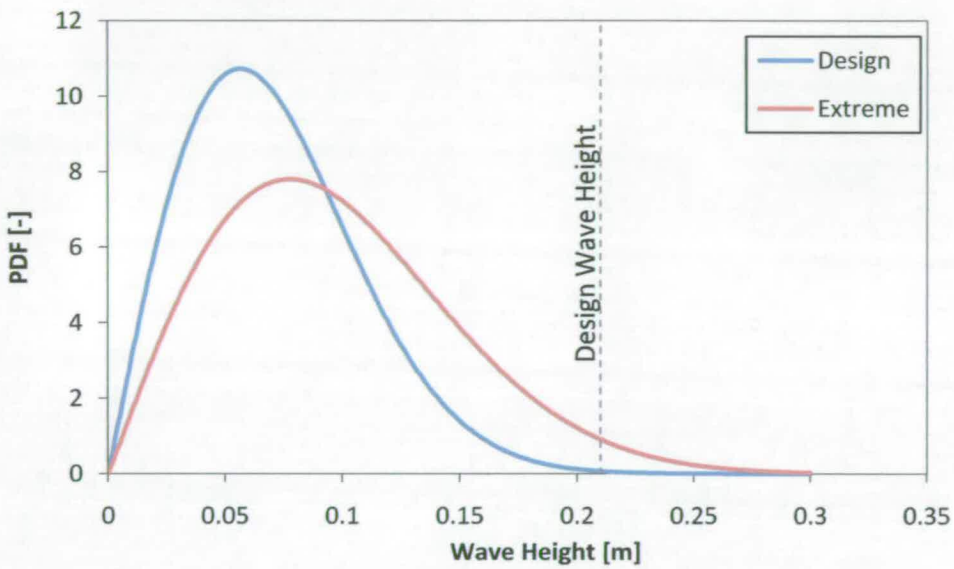

Figure 2.14 Hypothetical wave height probability distributions for Design and Extreme Seas showing the maximum wave height.

The Importance Sampling technique is applied in a marine modelling scenario by moving from a design (random) sea condition to a larger, more extreme sea. This is illustrated, in terms of wave height, by the distributions in Figure 2.14. Many more measurements may be made for the design wave height, reducing the sampling error. The advantage with this approach is that it is non-deterministic. There is no requirement to model the wave transformations involved in moving from deep to shallow water.

The process illustrated above is, however, a simplification of the processes involved in overtopping. In reality it is unlikely to be possible to define a design

wave height. Overtopping is a non-linear and potentially non-monotonic process influenced by a number of wave characteristics. Knowledge on the detailed behaviour of overtopping waves is often limited. Indeed, if the technique is to be employed beyond the field of overtopping it must be assumed that detailed wave interaction knowledge will be limited.

The concept of a limit state function does not translate well to the overtopping application, at least not as defined here. This research is concerned with maximum overtopping volumes, rather than failure modes.

This research has concentrated on developing an adaptation of the Importance Sampling technique for use in quantifying extreme responses in the marine environment. This has concentrated on applying the concept of the "extreme sea". While the "Importance Sampling" terminology has been retained, the methods detailed here differ significantly from the traditional application.

2.7 Summary

The majority of overtopping research has concerned the examination of mean overtopping discharge. While there is useful and high quality published guidance on individual overtopping events it is noted that there is limited information concerning the errors and uncertainties associated with these measurements. The experimental programme detailed in §3 was conducted, in part, to quantify these uncertainties, as presented in §4.

Two approaches are identified for the improvement of efficiency in random wave testing. The majority of recent and ongoing work concentrates on deterministic methods (e.g. NewWave). The alternative approach is a probabilistic approach which aims to reduce test lengths by removing "unimportant" waves from the sea state. This Importance Sampling technique is briefly outlined in §1 and explored in detail in the following chapters (§5 and §6). The experimental programme (§3) was conducted, in part, to provide data for the application of the Importance Sampling technique.

3 Experimental Programme

3.1 Introduction

The experimental programme conducted during this research examines overtopping at vertical seawalls. All testing was conducted in the University of Edinburgh's two-dimensional wave tank. This test programme was designed to examine both the inherent uncertainty present in overtopping measurements, and to produce data for use in the Importance Sampling technique outlined in §1.2.3 and described in detail in §5. This chapter outlines both the apparatus and the analysis methods used to extract the overtopping volumes from the raw measurements. The test programme is also explained in detail.

3.2 Experimental Facilities

3.2.1 Two-Dimensional Wave Tank

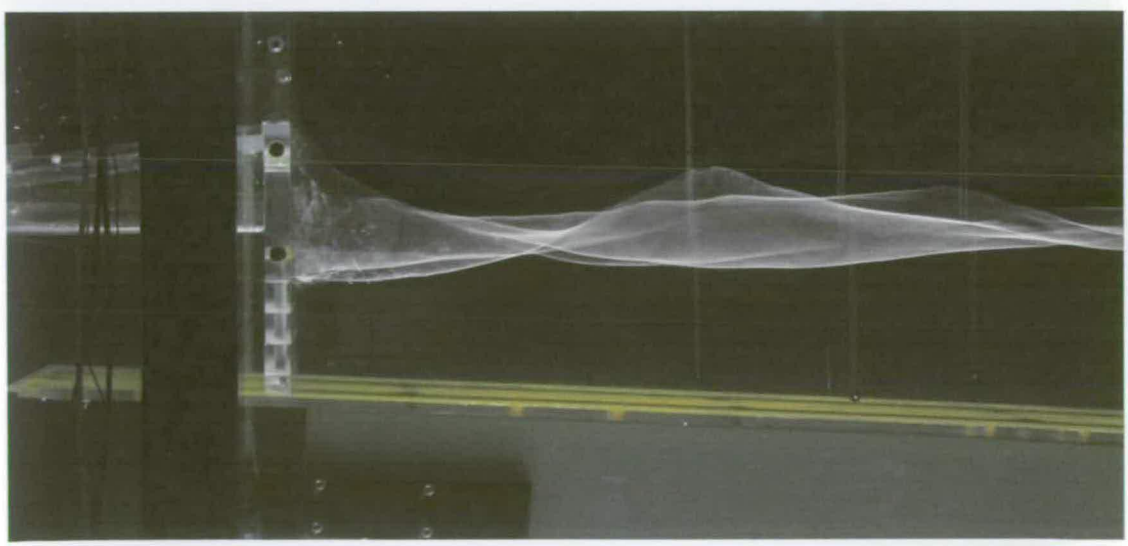

Figure 3.1 Seawall model installed in the wave flume with the adjustable beach visible.

The experimental testing that formed the backbone of this research was conducted in the two-dimensional "blue" tank located at The University of Edinburgh (Figure 3.1). This facility has been used in several coastal engineering studies, including the Violent Overtopping Waves at Seawalls (VOWS) project.

The flume has a working length of approximately 20m, a nominal width of 0.4m and a fixed water depth of 0.7m. The tank is of a modular construction, with each section 3.3m in length. The tank is raised approximately 1m from the ground and the bottom and both sides are glazed.

Waves are generated by a single flap-type wavemaker designed and manufactured by Edinburgh Designs Ltd. The wavemaker actively absorbs reflected waves through the use of a force feedback system. Control is applied using Edinburgh Designs' proprietary software, capable of producing regular and irregular seas based upon standard spectra.

Irregular waves are generated through the input of standard spectra. These are defined using the real peak frequency (f_p) and a nominal gain function. In the case of the JONSWAP spectrum the peak amplification factor (γ) is also specified. This spectrum is converted to a time-series within the WAVE software after specification of a seed-number to determine the sinusoidal component start phases. The ability to set the seed number (1-100) allows many unique time-domain realisations of the same spectrum to be generated.

The water surface-elevation is measured using water-piercing resistance-type wave gauges. These gauges consist of two parallel vertical metallic prongs. The voltage measured across these elements is directly proportional to the water elevation. The input unit to the data logging computer allows the voltage offset and amplification (gain) to be adjusted for each gauge. A gain value of 0.5 Volts / 1 cm was used. Given that the data acquisition card has a limit for each channel of ± 10 Volts, this allows the measurement of wave amplitudes up to ± 200 mm. In very extreme cases amplitudes up to approximately 150 mm may be

generated in the flume. There is therefore little chance of crests or troughs being "clipped" by the data logging system.

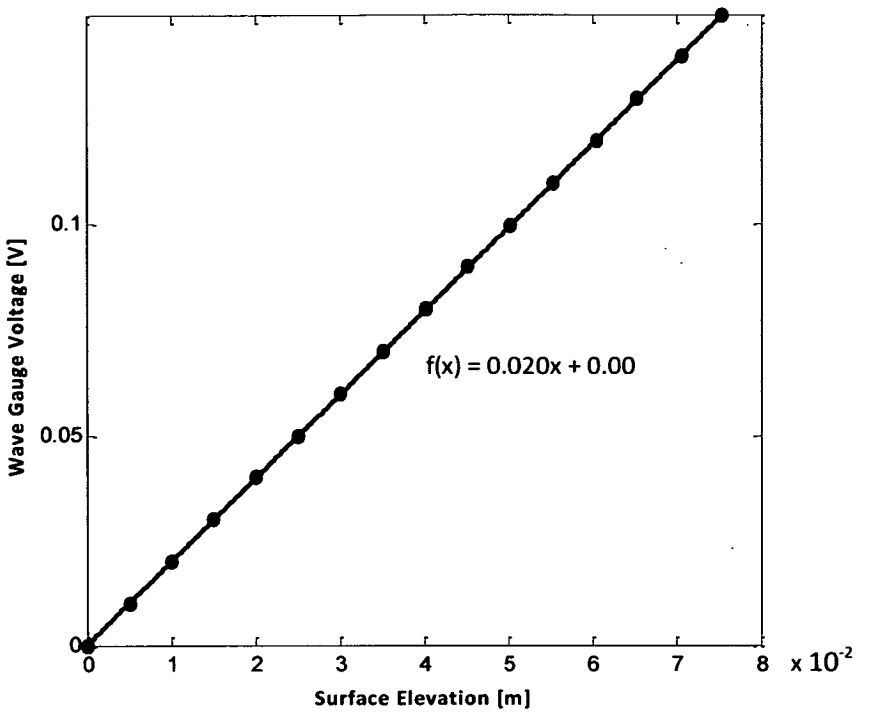

Figure 3.2 Wave gauge calibration chart with linear fitted calibration curve

The wave gauges are calibrated by being moved through a fixed distance of 100 mm, with the offset adjusted such that the voltage output is zero at the still water level. Given that the voltage and surface elevation are linearly related, the gauges may be calibrated based upon two measurements. This linear relationship was confirmed by the measurements illustrated in Figure 3.2.

The beach, partially visible in Figure 3.1, is fitted in sections corresponding to the modular design of the wave tank. The beach must therefore be terminated at one of these tank section joints. In practice, the seawall model must also be positioned at one of these section joins as the beach behind the structure must be removed to allow installation of the overtopping collection system (§3.3.1). The gradient of each section is infinitely adjustable. Water-piercing constant gradient beaches of steepness 1:10 to 1:30 may be accommodated. Shallower beaches require a "dog-leg" gradient, with a steep section at the seaward end, if they are to extend beyond the still water level.

3.2.2 Vertical Seawall Model

Two vertical seawall models were used for this research. Early tests were carried out using an existing model of total height 200 mm with an optional 30mm extension. This model consisted of a transparent acrylic seawall and frame incorporating a chute leading to a loadcell equipped collection tank (see §3.3.1 for more detail). The seawall crest was fitted with two metallic strips for overtopping event detection purposes.

While this existing model was adequate for initial testing, it was fairly limited in terms of configuration options. The design of the frame and overtopping collection chute prevented the seawall being easily modified for different seawall heights. Adjustment of the freeboard to depth ratio was also limited to finite steps. A new model was designed and constructed to allow greater testing flexibility (Figure 3.3).

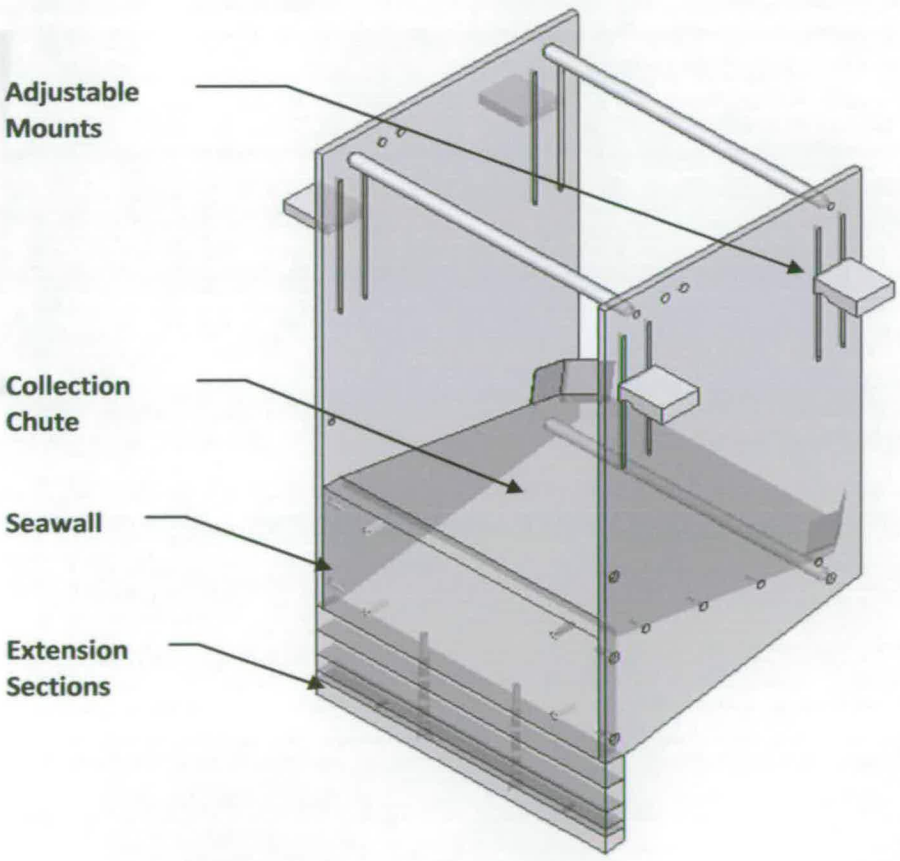

Figure 3.3 Seawall model with water collection chute and extension sections (metallic overtopping detection strips not shown)

The seawall model has an effective crest width (excluding frame sides) of 375 mm. The seawall height may be adjusted in 10 mm increments by use of extension sections bolted to the underside of the main seawall (Figure 3.3). The lowermost of these sections is profiled to ensure a close fit with the beach. The brackets supporting the seawall in the tank are fitted through slots in the frame, allowing for a continuously adjustable freeboard to depth ratio.

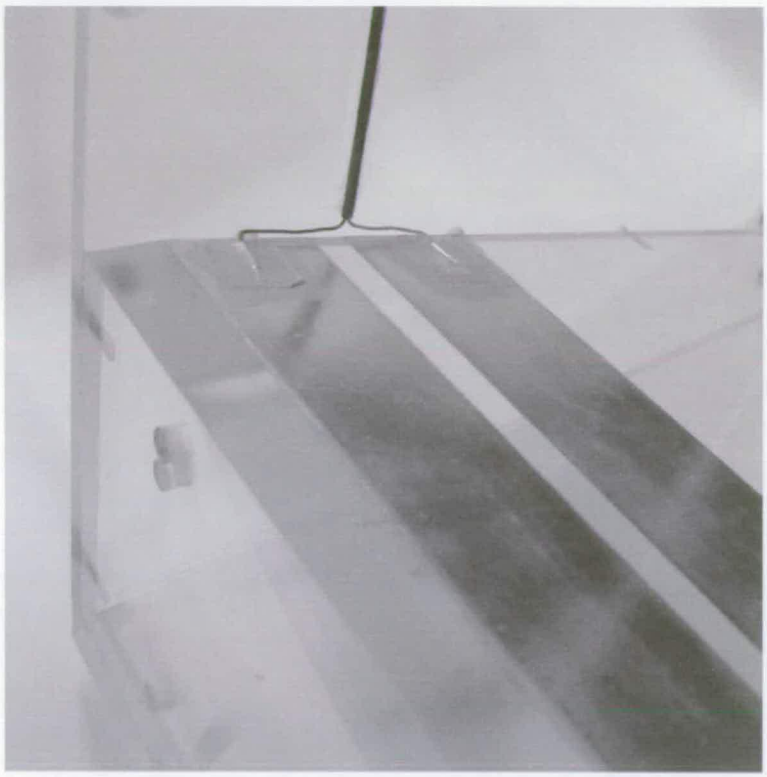

Figure 3.4 Metallic overtopping detection strips as fitted to model seawall

The seawall model incorporates metallic strips for the detection of individual overtopping events (Figure 3.4). These strips consist of sections of aluminium tape, commonly used in the repair of printed circuit boards and other applications where a thin conductive surface is required. A 9 Volt supply was connected between the strips, with the overtopping water completing the circuit. Silicone grease was applied to the gap between the strips to reduce water pooling. The voltage across the strips was logged, an overtopping event showing up as a spike in the signal. A precise timecode may then be applied to the overtopping event which, combined with the loadcell readings from the

collection tank, may be used to determine the individual overtopping values. This procedure is detailed in §3.3.2 and §3.3.3.

The discharge from overtopping waves is directed into the collection tank via a chute integral to seawall model structure, as illustrated in Figure 3.3. The measurement of the overtopping discharge is detailed in §3.3.1.

3.2.3 Data Acquisition and Data Handling

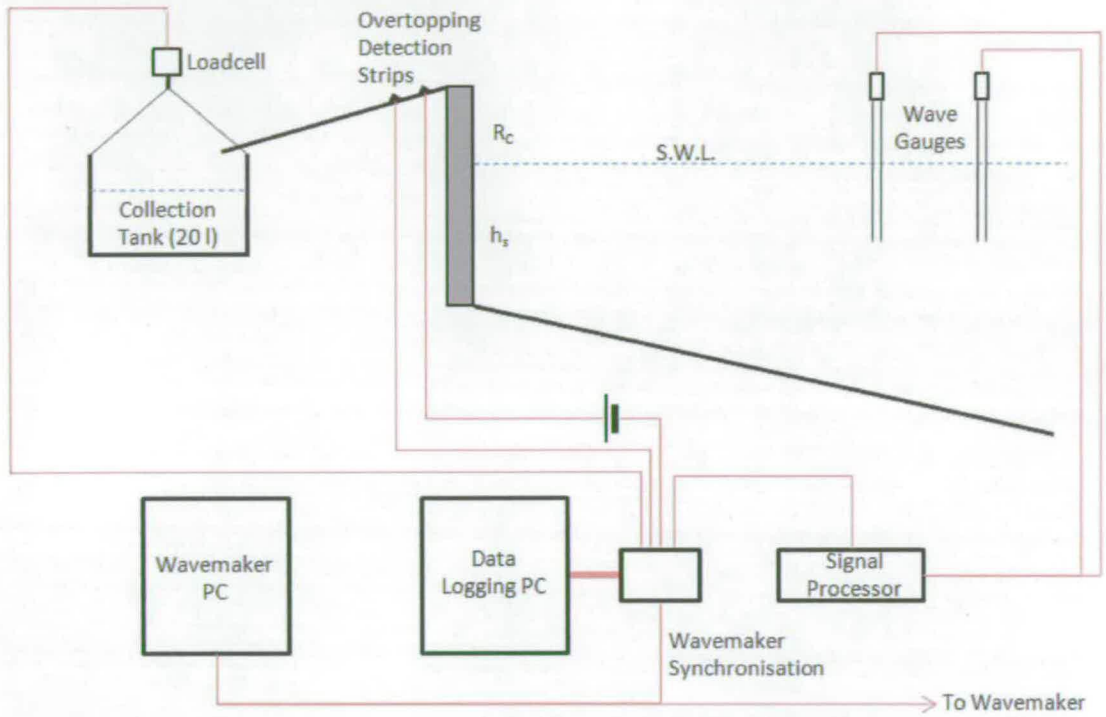

Figure 3.5 Wave-flume systems and data-acquisition schematic diagram

The data logging system is separate to the wave generation hardware (Figure 3.5). The synchronisation of these systems is discussed in §3.4.2. Several data logging and analysis systems have been used during the course of this research. Early testing was carried out using logging and analysis programmes running in HP-VEE and FORTRAN. In order to expand the flexibility and capability of the facility the software was later updated to a combination of Aalborg University's *WaveLab 2* software and custom-written MATLAB code.

In the course of this testing several long test programmes were undertaken. Testing of this nature is always prone to "human-error". This could simply be

the wrong spectral values entered into the sea input file or an incorrectly transcribed wave-gauge calibration function. While great care may be taken when setting up individual tests, this type of error is often difficult to detect and diagnose. Given that this research is concerned with assessing, and reducing, uncertainty in model testing, it was considered especially important to minimise these experimental errors. The following test procedures were therefore rigorously followed to minimise the risk of these errors, and allow easy examination of the wave generation and logging parameters post-testing.

- All sea input files are written and checked prior to testing commencing. The input files are not edited on a test-by-test basis to allow full traceability of input conditions. .
- The set-up parameters of each individual test were stored alongside the logged data. A clearly defined reference system was also used.
- All data channels were logged in the form of raw voltage inputs. The nature of the logging system allows the calibration functions to be stored within the same file for easy translation to the correct units. Should a calibration error be detected the function may be altered easily.

The logged data was analysed in the main using a combination of WaveLab and MATLAB routines (see §3.4). A custom function is used to import the data files into MATLAB, applying the calibration functions to the raw data in the process. This script is incorporated into a larger programme which archives the data in a form (MAT files) which is easily and efficiently accessed by other MATLAB routines. The data handling procedures used are intended to minimise the need for manual data entry (with the associated risk of error). Data files belonging to common test series are combined to form a single data structure that may be loaded into MATLAB programmes as a single entity.

3.3 Overtopping Measurement

3.3.1 Overtopping Collection and Measurement

The overtopping water is collected in a loadcell equipped tank mounted beneath the chute of the seawall model assembly, as illustrated schematically in Figure 3.2. This equipment has been in use for some time and is well proven. The assembly consists of two major elements, a watertight outer shell which provides a dry bay and the collection tank itself. The collection tank is suspended from the loadcell and hangs freely inside the outer shell. The collection tank has a maximum capacity of 20 litres.

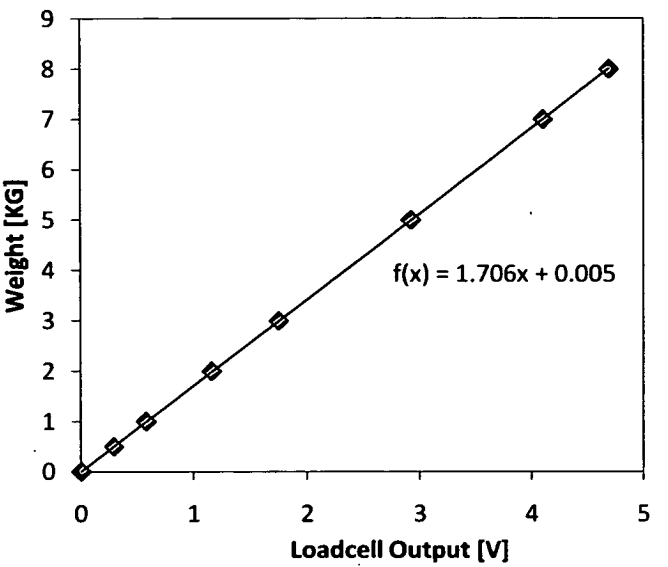

Figure 3.6 Loadcell calibration chart with linear fitted calibration line

The output from the loadcell is logged using the data acquisition system (§3.2.3) allowing for the measurement of individual overtopping volumes. The gain and offset of the signal is adjustable through an operational amplifier. The loadcell signal voltage was adjusted to give a value close to zero when the tank was empty, although this is not essential as the analysis software measures change in volume[4], not absolute values. The gain was set such that the Voltage when the tank was full would not exceed 10 Volts (the limit of the data acquisition

[4] While the loadcell obviously measures weight, the output will hereforth be referred to in terms of volume (1 kg = 1 litre), in line with the conventional measurement of individual overtopping events.

system). A calibration chart for the loadcell is shown in Figure 3.6 illustrating the linear behaviour of the measurement system. This loadcell calibration proved to be very stable, and no significant variation in calibration function was noted throughout the experimental programme.

3.3.2 Overtopping Event Detection and Measurement – Legacy System

Individual overtopping volumes are produced based on the signals logged from the overtopping detection (metallic strips) and overtopping measurement (loadcell) channels. This allows for increased accuracy compared to monitoring the measurement channel alone. The overtopping detection channel allows for precise timecode to be assigned to an overtopping event, which is particularly important in this research.

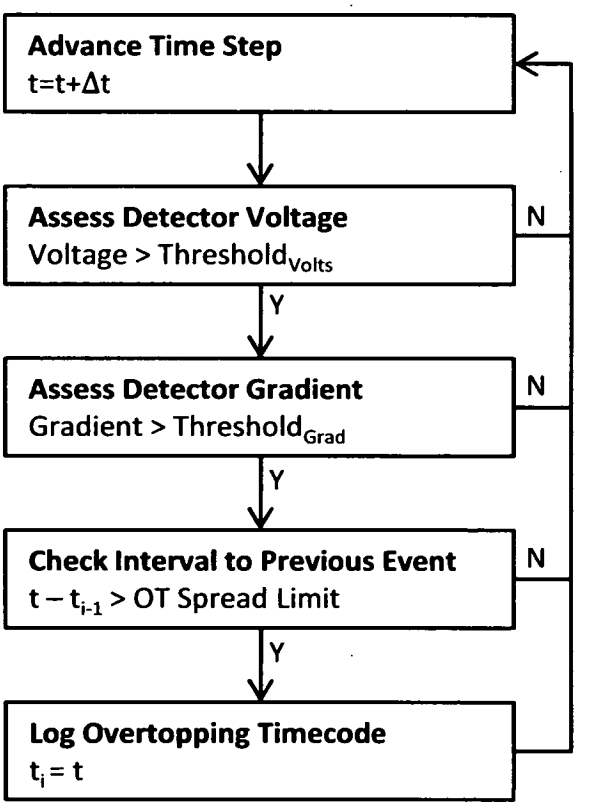

Figure 3.7 Overtopping detection logic flow chart – legacy system

The analysis procedure outlined here describes the original FORTRAN code[5], later transferred to MATLAB. This system was used for early testing and was later testing changed to a new implementation, described in §3.3.3.

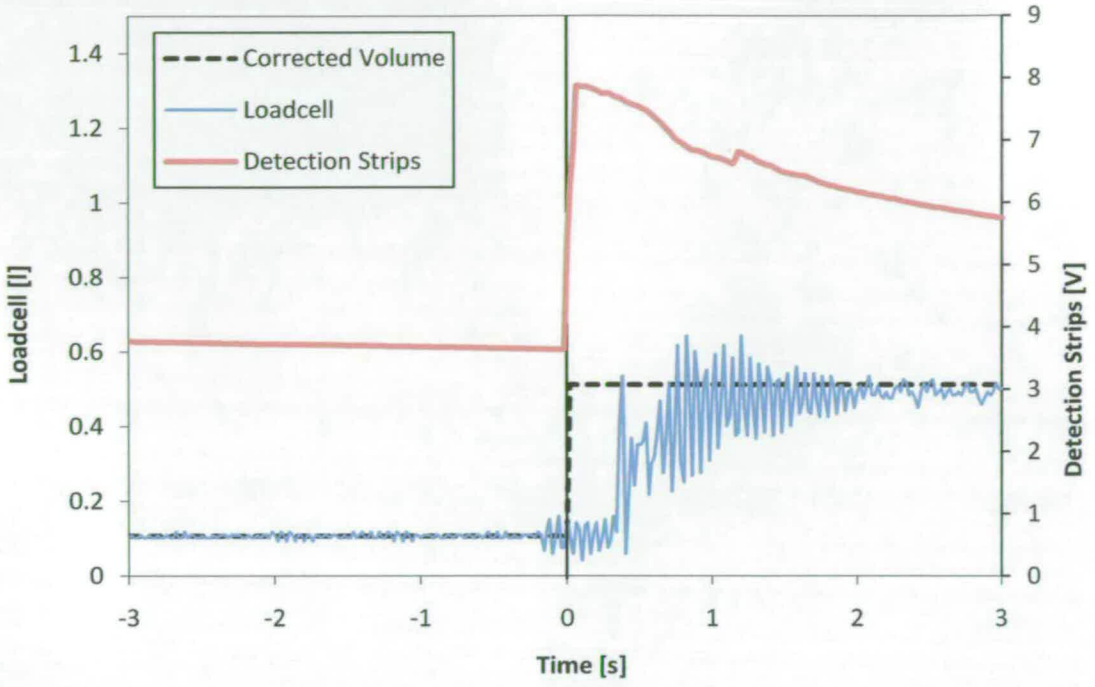

Figure 3.8 Overtopping event measurement with detection strip signal alongside raw and processed loadcell measurements

The analysis logic is illustrated by the chart in Figure 3.7. Individual overtopping events are identified by voltage spikes in the detection channel (Figure 3.8). These spikes are identified by their steep positive gradient. If and when a spike is detected which exceeds the chosen threshold it must also exceed a set minimum voltage. This prevents low voltage noise caused by small drops of water and other interference from registering an overtopping event. An overtopping wave may not result in a clean single spike. Voltage spikes very close together are therefore treated as a single event. The overtopping detection parameter values are given in Appendix 1.

[5] The FORTRAN overtopping analysis software was produce by Dr Jonathan Pearson, then of the University of Edinburgh.

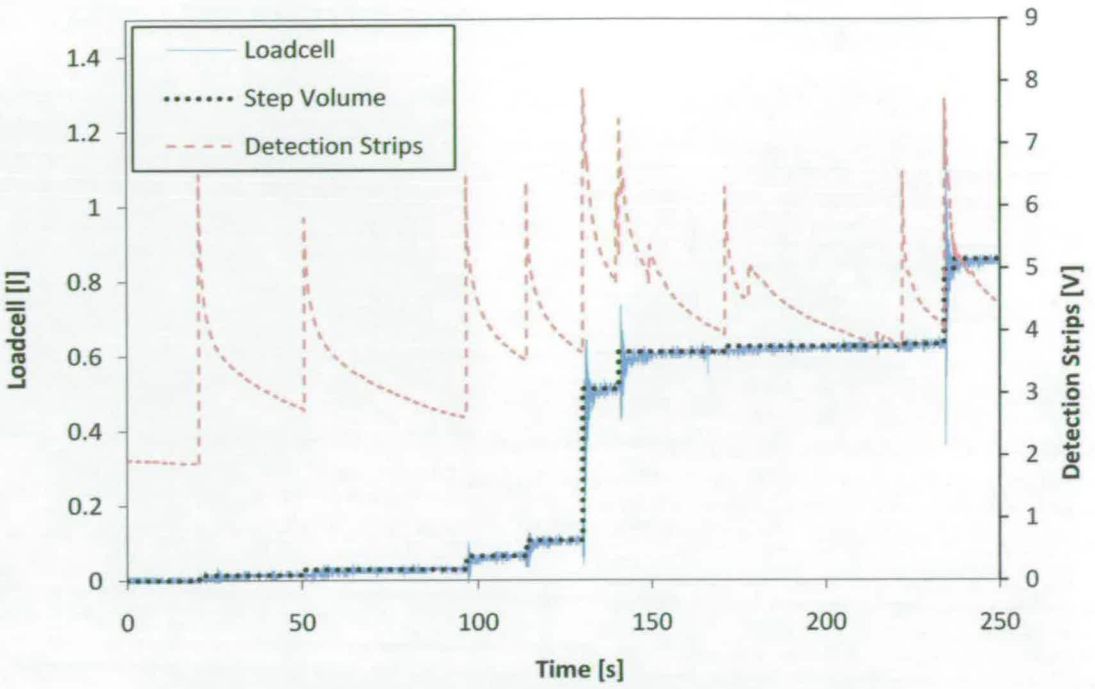

Figure 3.9 Overtopping record with multiple overtopping events

Once the individual overtopping event timecodes have been determined, the individual overtopping volumes may be analysed. Significant oscillations may be observed in the loadcell data, particularly when the volumes of water deposited in the collection tank are large. It is necessary therefore to use an averaged value based on the loadcell measurements between the detected overtopping events. As there is a small time delay between the overtopping wave passing over the detection strips and arriving in the collection tank, this average should not be taken over the entire time between overtopping timecodes. The solution is to use the average volume over the second-half of the interval between events. The collection tank volume may then be represented as stepped output, as illustrated in Figure 3.9. This output may be easily translated into a time-stamped list of individual overtopping volumes.

3.3.3 Overtopping Event Detection and Measurement – New Implementation

While the original ("legacy") overtopping code generally worked well, some limitations and discrepancies were noted in its output. The overtopping code described here works on the same basic principle as the legacy system, using the spikes in the overtopping detection channel to identify overtopping waves.

The code primarily differs in the logic used to identify an event and the method used to deduce the volume from the loadcell.

The problem of defining an overtopping wave is perhaps more difficult than it appears on initial inspection. In a distribution curve of volumes obtained from a hypothetical infinitely long test, the volumes will vary from zero up to the large (extreme) values. This effectively means that overtopping volumes may be infinitely small.

In practice, a wave may deposit only a very small volume of water over the crest of the seawall. These low extremes may appear initially insignificant, but if the overtopping response is to be correctly characterised it is important to understand the range of values obtained. Understanding the total number of overtopping waves is also important, as it is an input into the probability theory used to predict the maximum overtopping volume (V_{max}).

Experience with the legacy code demonstrated that it was often difficult to find an optimum sensitivity for the overtopping detection system. A highly sensitive system would appear to pick up all genuine overtopping events, but would also detect many apparently spurious events. A number of causes are hypothesised for this behaviour. Water may pool at the crest or on the tank/frame sides, creating false spikes when it runs across the strips. Interference from other equipment sharing the laboratory may also be picked up on the metallic strips and associated wiring. The nature of the overtopping events is also not entirely consistent. If the overtopping event produces a wide sheet of water a large, easily identifiable spike will be apparent on the detection readings. If the wave should produce only a small rivulet of water, the spike may be less obvious.

Overly low detection sensitivity will clearly result in overtopping events being erroneously ignored. This will have the secondary effect of the overtopping volumes being wrongly assigned to other detected events, reducing confidence in the measured individual volumes.

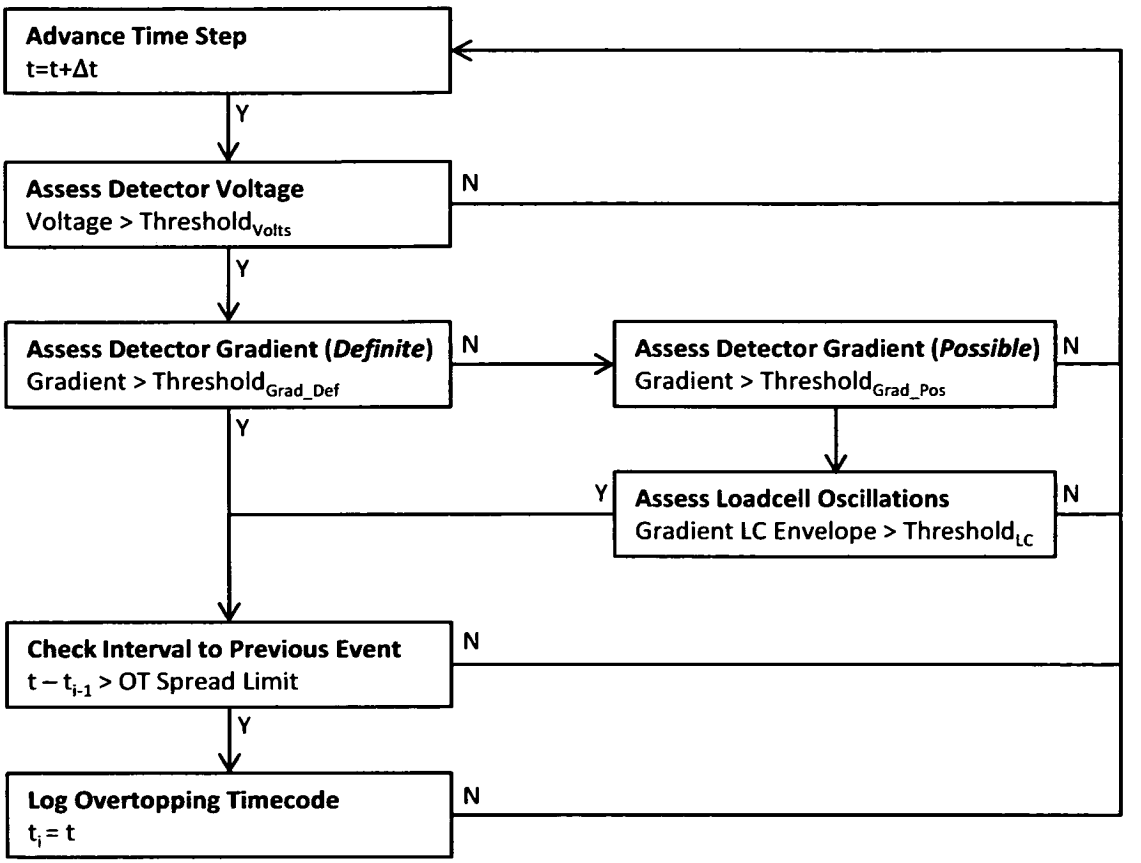

Figure 3.10 Overtopping detection logic flowchart – new implementation

In order to ensure the small overtopping volumes were detected without the side-effect of spurious events, a secondary detection logic was added to the system (Figure 3.10). In this new implementation, spikes in the detection channel are assessed as *Definite* or *Possible* events.

Definite events are defined by the Voltage gradient in the overtopping spike passing an upper threshold. This is identical in principle to the legacy detection code. Events identified as *Definite* are logged without any further checking.

Possible events are defined by the Voltage gradient in the overtopping spike passing a lower threshold. This high sensitivity criterion will likely log many spurious events. A secondary check is therefore necessary to determine which spikes should be disregarded. This is carried out through examination of the loadcell channel.

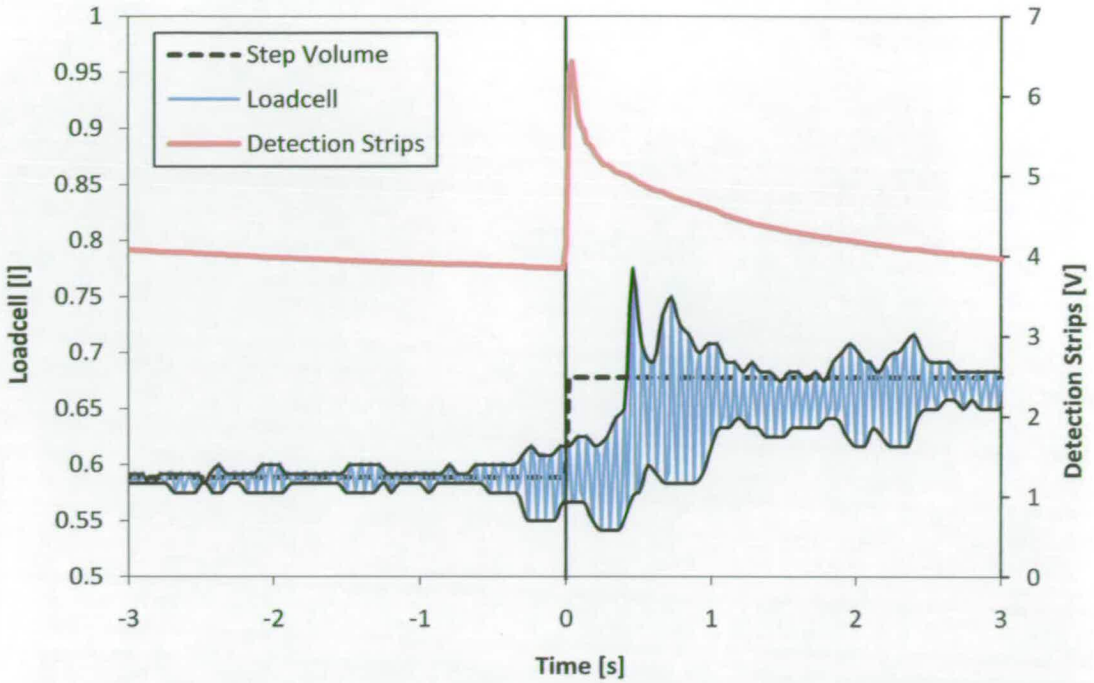

Figure 3.11 Overtopping detection strip measurement (*Possible* event) with loadcell measurement and fitted envelope.

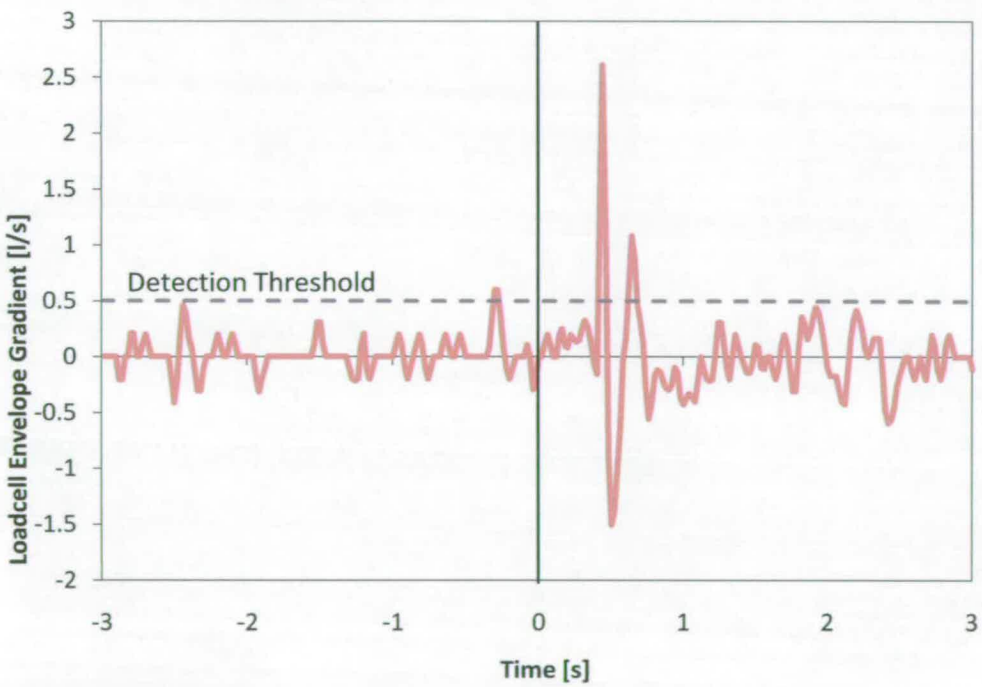

Figure 3.12 Rate of change of fitted loadcell envelope illustrated in Figure 3.11. Detection threshold for *Possible* events indicated.

It was noted when examining the logged overtopping data that even small volumes result in an oscillation in the loadcell signal due to the negligible

damping in the suspended collection tank. The presence of this oscillation is used as the secondary check to confirm the validity of *Possible* overtopping events. The procedure for identifying this oscillation is thus:

1. Carry out envelope fitting to the loadcell channel, as illustrated in Figure 3.11.
2. Differentiate the envelope amplitude (width) in order to identify sudden expansions associated with overtopping induced oscillations.
3. If the differential of the amplitude exceeds a set threshold (Figure 3.12), and occurs with a defined window following a *Possible* spike in the detection channel, confirm the overtopping event.

It should be noted that many small volume events are identified as *Definite*, with the inverse also occurring. This system is designed such that an overtopping event is unlikely to be missed, while spurious measurements are reduced. Very small overtopping volumes may be vulnerable to being missed by the secondary check in the *Possible* identification logic, but no more, and probably less, than was the case using the legacy system.

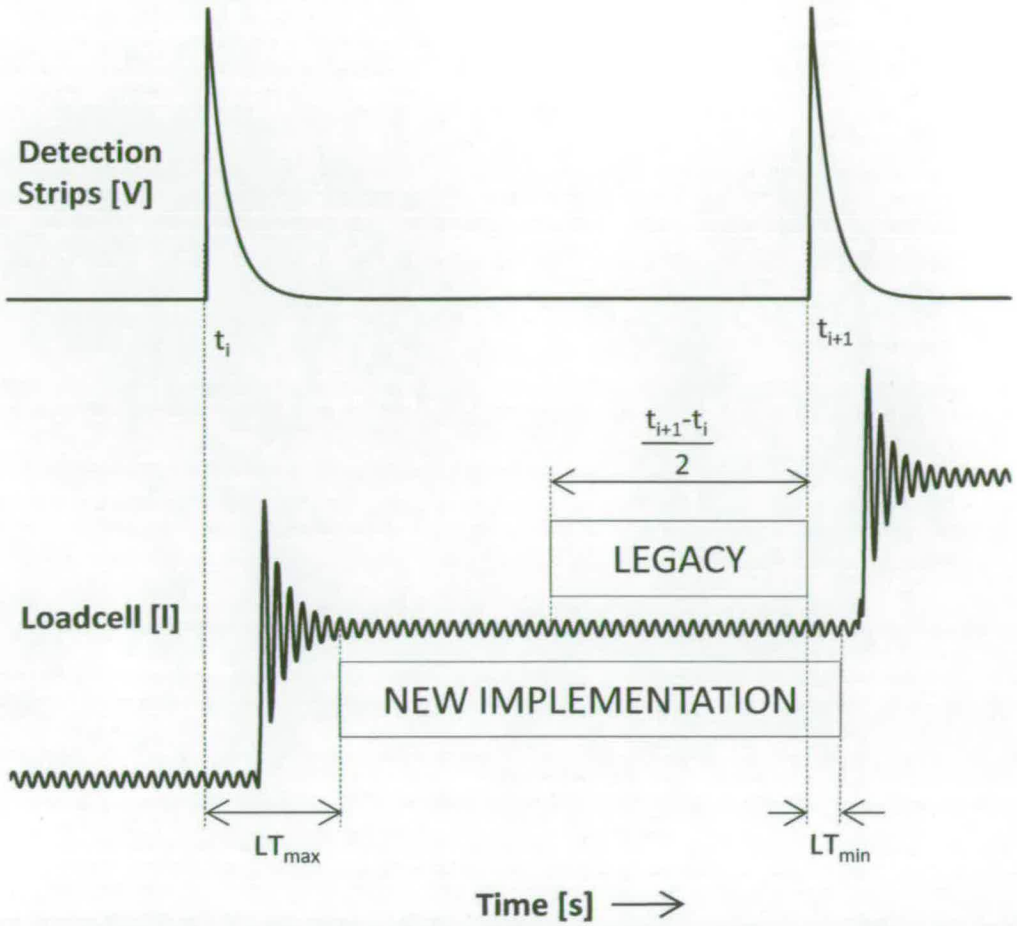

Figure 3.13 Schematic representation of loadcell averaging period between two overtopping events

The method used for extracting the individual volumes from the loadcell data was altered from the legacy software. A representation of the two methods is illustrated in Figure 3.13. Individual volumes are determined based on the volume of water in the tank between overtopping events. It is not desirable to calculate this volume based on a straightforward average due to the finite length of time required for the overtopping water to travel from the seawall crest to the tank. Examination of overtopping data yielded minimum (LT_{min}) and maximum (LT_{max}) values for this lag. Taking these lag values into account allows the averaging time to be maximised. It also prevents a potential problem where the legacy system would include a proportion of this lag time in the averaging calculation when the time between events was very short. This would result in the volumes being wrongly assigned between the two events.

A quality control measure employed in the overtopping system is the setting of an overtopping threshold. This minimum value, set to zero for this research, prevents the noise and oscillation in the system from identifying unrealistic negative overtopping volumes. This type of output may occur when measuring very small overtopping volumes, especially when preceded by a significantly larger volume. A similar check measure was employed in the legacy overtopping code.

Values for the overtopping analysis parameters are given in Appendix 1.

3.4 Software Tools

3.4.1 Sea State and Wave Analysis Tools

Several routines were used to produce time-domain and frequency-domain statistics for the elevation-time histories measured in the tank. Much of the analysis software/code was produced by third-parties and brief details of these tools are given below. Where necessary, new routines were written, in particular for time-domain analysis of individual waves and these are also outlined.

The calculation of the global sea statistics (e.g. H_{m0}, T_m etc.) was primarily carried out using the WaveLab 2 package, produced by Aalborg University, Denmark. This programme analyses time-series in both the frequency and time domain. While WaveLab is a powerful, proven and user-friendly package it does have some limitations. Primary among these is the inability to integrate the programme with custom routines (e.g. running in MATLAB).

Several functions contained in the Wave Analysis for Fatigue and Oceanography (WAFO) MATLAB toolbox produced by Lund University, Sweden were used during the course of this research. The use of these tools is detailed where relevant.

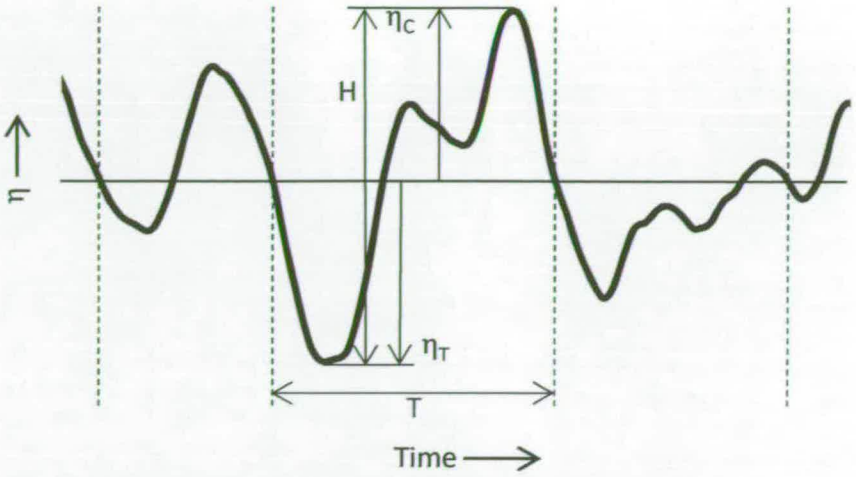

Figure 3.14 Zero downcrossing analysis of an elevation time series

Characterisation of waves is a necessary input to many of the analysis techniques employed in this research. The elevations of the crest and trough, as well as the wave period, are measured using zero-downcrossing analysis (Figure 3.14). The convention employed here is to refer to the trough elevation as positive in the downwards direction.

The simplest form of analysis is to base the zero-crossing and turning points (crest and trough) on the nearest logged data point. However, this clearly introduces a level of inaccuracy, and will result in the underestimation of the crest and trough heights. To reduce this error interpolation functions are used to describe better the regions between the discrete data points. The zero-crossing points are found using linear interpolation between the measurements above and below the still water level. The crest and trough values are estimated through a parabolic fitting technique, as suggested by Goda (2000). The elevations are given by the relationship:

$$\eta_{max/min} = C - \frac{B^2}{4 \cdot A} \tag{27}$$

where

$$A = \frac{1}{2}(\eta_{i-1} - 2 \cdot \eta_i + \eta_{i+1}), \tag{28}$$

$$B = \frac{1}{2}(\eta_{i+1} - \eta_{i-1}), \tag{29}$$

and

$$C = \eta_i. \tag{30}$$

The "i" subscript relates to the data point with the largest positive or negative value (for crest and trough respectively) lying between two-crossing points. The parabolic relationship may also be used to estimate the crest/trough time:

$$t_{max} = t_i - \Delta t \frac{B}{2 \cdot A} \tag{31}$$

where Δt is the sampling interval (assumed to be constant).

The wavelength (L) is, unless otherwise stated, calculated from the period (T) and water depth (h) as

$$L = \frac{g}{2 \cdot \pi} \cdot T^2 \cdot \tanh \frac{2 \cdot \pi \cdot h}{L}. \tag{32}$$

This expression must be solved numerically. In this research this was achieved using the Newton-Raphson iteration method.

3.4.2 Sea Synchronisation and Initialisation

It was noted in §3.2.3 that the data logging computer system is physically separate from the wave generation hardware. While this is not necessarily a significant drawback when dealing with single tests, it makes repeat tests with identical seas difficult to compare. This is particularly true when the matching of waves and events between identical repeat seas is critical. To overcome this a robust method of synchronising and initialising logged time-series data was implemented.

The solution was to record the analogue input to the wavemaker on the data logging computer (Figure 3.5). This channel is effectively treated as a wave gauge input. This analogue input allows the start-time of the wavemaker to be identified, assuming that data acquisition is initiated prior to activating the wavemaker.

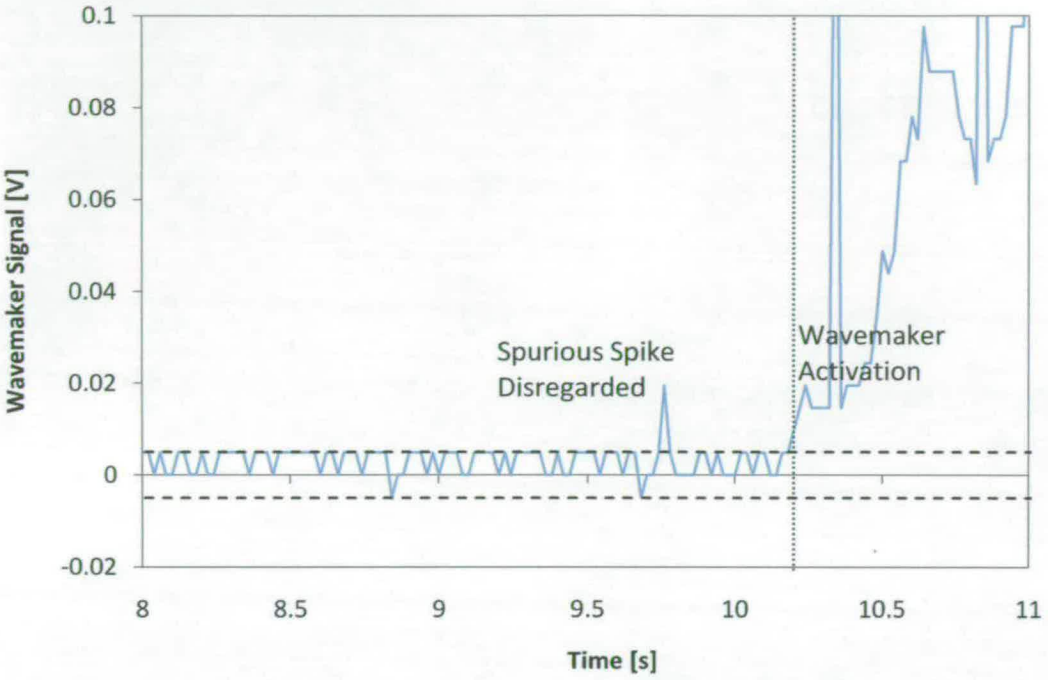

Figure 3.15 Wavemaker signal with activation time identified by exceedance of a set threshold (dashed lines)

The post-processing of the data file is carried out in MATLAB, and is incorporated into the data import routines described in §3.2.3. The start-point of wave generation is identified by the wavemaker signal exceeding a set threshold, as shown in Figure 3.15. This threshold is set high enough so that low-level noise does not erroneously set the initialisation point[6]. Spurious spikes in the data are also identified and removed. Once the start point of wave generation is identified a wave propagation margin is added. This allows the sea to become established and avoids the logging of still water at the start of the experiment. A margin of 20 seconds was used for the testing carried out in this

[6] The data acquisition is capable of resolving the logged signal to intervals of 0.00488 Volts (20 Volts range with 12 bit resolution). The initialisation threshold was set to 0.005 Volts - slightly above the lowest non-zero measurement.

research. The end point is determined by the desired duration of the test and is simply measured from the start point. The recorded timecodes are corrected to account for the removed data.

While the above method was generally effective, it was observed to demonstrate some slight variability. Noise in the recorded wavemaker signal would cause nominally identical tests to initialise at slightly different times, usually in the order of 0.5 seconds. It should be noted that this noise was only apparent in the logged duplicate wavemaker signal and was not present in the primary signal transmitted to the wavemaker.

In order to provide close synchronisation between tests with identical seas (as required for the calibration seas) a cross-correlation method was used. The first sea in the sequence was processed using the threshold exceedance procedure described above. The wavemaker signal from subsequent tests was compared to this first test using a cross correlation function incorporated within MATLAB. The lag between the tests was identified based upon the maximum correlation value. The start point of the second sea was then set based upon this lag. The value of the cross-correlation coefficient also provides a useful quality check function should an incorrect, supposedly identical signal be inputted to the wavemaker.

3.5 Test Procedures

3.5.1 Wave Tank Calibration

The techniques used in this research rely primarily on sea parameters measured at or near the model. Producing the correct sea in the tank is not necessarily a straightforward procedure. For a given spectrum (e.g. JONSWAP with $\gamma = 3.3$) the tank input is given as a real peak frequency input and a non-dimensional gain value (§3.2.1). The results of previous testing allow this gain value to be determined fairly easily for deep water. The resulting shallow water conditions, however, are dependent on the beach bathymetry and depth at the structure. Due to the number of variables it is not generally possible to examine

previous tests in order to determine the correct wave flume inputs. It should be noted that the "offshore" conditions in the wave flume may often more correctly be referred to as intermediate depth conditions, rather than true deep water.

The approach initially attempted was to translate the target shallow water sea parameters to deep water through use of a shoaling model. The model used was that of Shuto (1974) as described by Goda (2000). This method calculates the transformation through use of a shoaling coefficient (K_S), which relates to ratio of shallow and deep water wave heights:

$$K_S = \frac{H_{m0(inshore)}}{H_{m0(offshore)}}. \tag{33}$$

Shuto's method for the calculation of the shoaling coefficient is represented graphically, but may also be determined numerically. This procedure is described by Goda (2000).

The experience from this experiment is that the shoaling coefficients measured in the wave tank do not compare well to Shuto's predictions. A possible reason for this is the relatively close location of the deep water wave gauges to the wavemaker due to the long installed beach. The "deep" water measurements may also more accurately be referred to as intermediate depth, perhaps impairing the accuracy of the shoaling estimation. Wave conditions were therefore manually and iteratively adjusted based on the observed shoaling coefficient to achieve the target wave conditions. It should be noted again that this procedure only applied to the spectrum gain factor. The target peak frequency, entered as an input to the wavemaker software, was accurately reproduced in the flume.

3.5.2 Calibration Seas

When conducting physical model testing in a wave tank, accurately measuring the sea state is often complicated by the presence of the model. It may be the case that the model physically interferes with the placement of the

measurement equipment. This may be particularly true for floating models covering a relatively large area.

In coastal engineering modelling it tends to be physically impossible to position the wave gauges close to the structure. A more significant problem is the influence the model has on the wave climate. Waves will reflect off the structure, influencing the instantaneous surface-elevation in the tank. This effect is not limited to coastal engineering. These reflections and radiated waves may be observed when testing, for example, wave energy converters (WECs). The reflections are particularly strong when modelling monolithic structures such as the vertical seawalls used in this research. In order to accurately measure the incident elevation time series in the absence of strong reflections tests were conducted using "calibration seas".

Tests using a calibration sea are conducted with the seawall model (in this instance) absent. The beach bathymetry is unchanged, except that it is extended to pierce the still water level. A wave gauge positioned at the intended model location records the incident waves without the superposition of the strongest reflected components. This elevation time history will record any transformation effects induced by the beach, but the reflections and local wave deformations due to the structure will not be present. A separate test, using an identical generated time-series, is carried out to measure the response of the model. The synchronisation procedure described in §3.4.2 is used to match waves from the calibration tests to the response measurement tests.

While this technique doubles the number of tests required for each unique sea, it was felt that it was the most robust sea characterisation technique available. The alternative approach is the application of reflection analysis techniques (e.g. Mansard & Funke, 1987). These techniques use measurements from an array of wave gauges (typically three measurements for long crested seas) to separate the incident and reflected seas. This process is carried out in the frequency domain. Elevation time series, as required in this research, must be "reconstructed" using inverse Fourier transforms (IFFT) methods with the

values translated from the measurement point to the structure location. There are also doubts over the reliability of measurements taken near the structure. The sea state near the vertical seawall was observed to be frequently "chaotic", particularly when impulsive overtopping events occurred. In this case aeration of the water may be evident, potentially reducing the accuracy of the resistance-type wave gauges.

3.5.3 Identical Sea Repeatability

The use of calibration seas, described above, requires a high degree of repeatability from the wave tank. In order to check the repeatability of the wave tank, a series of tests was undertaken. Three nominally identical repeat tests were conducted, with an H_{m0} value of 0.06 m and a peak frequency of 0.85 Hz ($T_p \approx 1.18$ s). A JONSWAP spectrum was used with a peak amplification value (γ) of 3.3. The agreement between sea measurements from the repeat tests was examined in both the frequency and time domains. The tests were carried out with a constant plane beach installed (gradient of 1:17). Two wave gauges were used for each test, one in deep water prior to the beach, and the other in a depth of 140 mm. These test parameters represent a fairly typical experimental configuration for overtopping modelling.

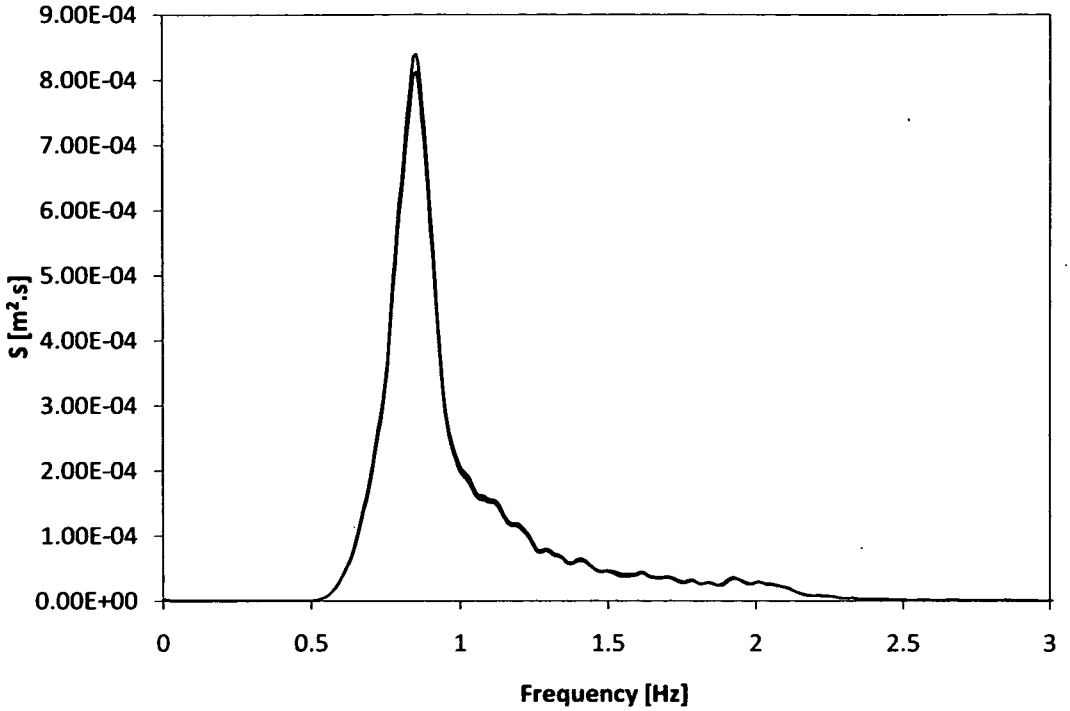

Figure 3.16 Deep water spectra measured from three nominally identical repeat wave flume tests

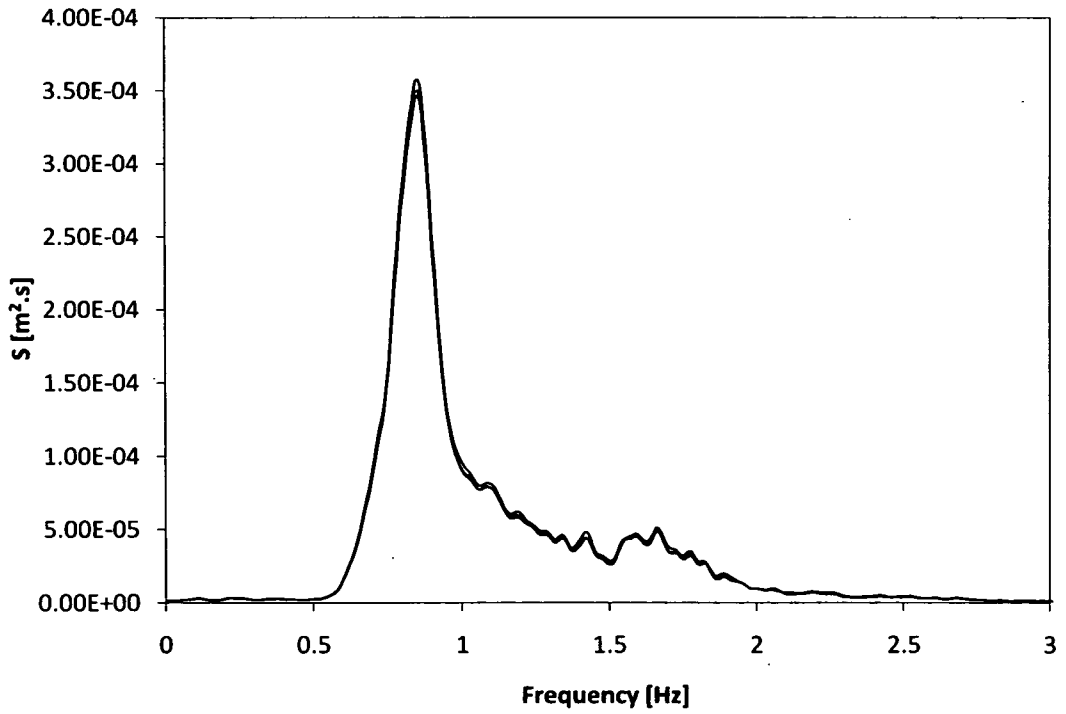

Figure 3.17 Shallow water spectra (h = 0.14 m) measured from three nominally identical repeat wave flume tests

Sea Parameter	Sea 1	Sea 2	Sea 3	Mean
Deep Water (h = 0.7 m)				
H_{m0} [m]	0.0601	0.0601	0.0612	0.0605 ± 1.2%
T_p [s]	1.18	1.18	1.18	1.18 ± 0.0%
$T_{-1,0}$ [s]	1.09	1.09	1.09	1.09 ± 0.0%
T_m [s]	0.977	0.973	0.970	0.973 ± 0.3%
H_{max} [m]	0.113	0.110	0.113	0.112 ± 1.8%
Shallow Water (h = 0.14 m)				
H_{m0} [m]	0.0430	0.0429	0.0437	0.0433 ± 1.5%
T_p [s]	1.18	1.18	1.18	1.18 ± 0.0%
$T_{-1,0}$ [s]	1.07	1.08	1.07	1.07 ± 0.6%
T_m [s]	0.970	0.960	0.950	0.960 ± 1.0%
H_{max} [m]	0.083	0.085	0.086	0.0847 ± 1.97%

Table 3.1 Comparison of deep and shallow water sea parameters from three nominally identical repeat tests.

The spectra for both deep and shallow water were analysed for both deep water (Figure 3.16) and shallow water (Figure 3.17) measurements. Visual inspection of the spectra indicates very good agreement between the repeat tests. This is borne out by the sea parameters, measured both in the frequency and time domains (Table 3.1). Wave height parameters (H_{m0} and H_{max}) agree to within 2% in both shallow and deep water. Measurements of wave periods showed typical errors of less than 1%. The greater error shown by the wave height parameters may be due, at least in part, to wave gauge calibration drift. During all experimental test runs the wave gauges were periodically recalibrated to minimise this source of error.

Deep	Sea 1	Sea 2	Sea 3
Sea 1	1	0.991	0.984
Sea 2	0.991	1	0.984
Sea 3	0.984	0.984	1

Shallow	Sea 1	Sea 2	Sea 3
Sea 1	1	0.975	0.977
Sea 2	0.975	1	0.970
Sea 3	0.977	0.970	1

Table 3.2 Elevation-time history correlation matrix for deep and shallow water measurements.

The ability to replicate accurately individual waves in an elevation time series is highly important for this research (§3.5.2). In order to establish the degree of repeatability, the correlations of the measured elevation time series were calculated (Table 3.2). The average deep water cross-correlation value was 0.99, dropping slightly to 0.97 for the shallow water measurements. These high correlations would appear to support the low variability observed in the parameters detailed in Table 3.1.

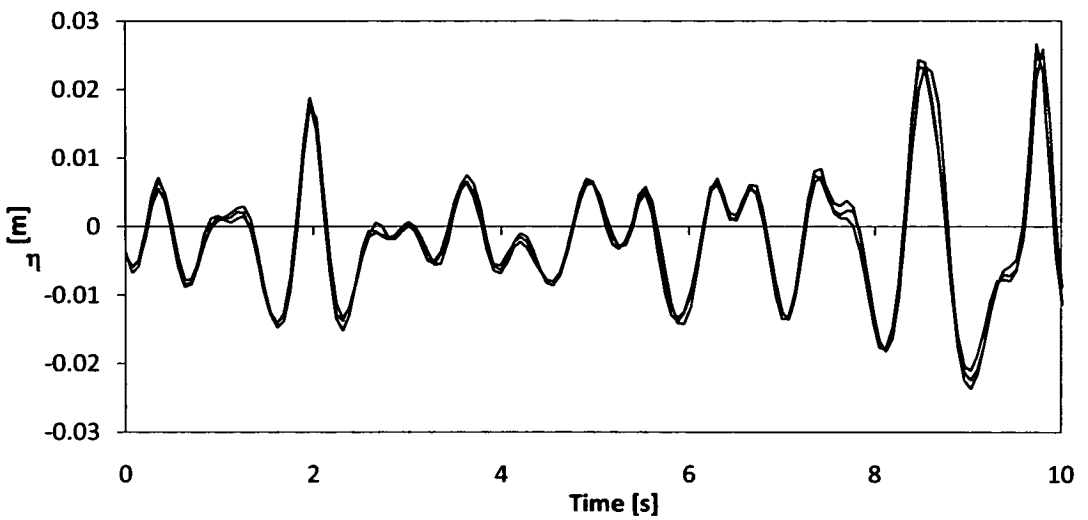

Figure 3.18 Shallow-water elevation time histories measured from three repeat tests.

A representative sample of the measured elevation time series is illustrated in Figure 3.18. The agreement between the three tests appears to be good with few deviations.

3.6 Test Programme

3.6.1 Test Series Setup

Several test series were conducted during the course of this research aimed at quantifying the overtopping volume uncertainty (§4), and in applying the Importance Sampling method (§5). The rationale for the design of these experiments is given below, along with more detailed explanations in the respective chapters where appropriate.

The test series are defined primarily by their input spectrum, the bathymetry and the configuration of the seawall. The tests were designed to deliver a particular overtopping regime (§2.2.3), overtopping ratio (N_{ow}/N_w) and wave steepness (s_{op}). The guidance contained within the EA-Manual was used to define the sea state and seawall configuration. The relative depth was chosen to give the correct overtopping regime, using the h_* formula (Equation (2)). The relative freeboard was set to give the target overtopping rate. These dimensionless parameters were then converted to real measurements through selection of H_{m0}. The scale was chosen such that the total overtopping volume was manageable, in that very small volumes introduce measurement errors while large volumes require recourse to a siphoning system to prevent overflowing of the overtopping collection tank. Finally, short "pilot" tests were conducted to check the agreement with the prediction formulae. If necessary the seawall geometry or sea-state was adjusted to give the target values. It should be noted that the purpose of these tests was not to check the accuracy of the EA-Manual or EurOtop formulae, hence the iterative adjustment of the test configuration.

3.6.2 Summary of Test Series

Configuration Code	Beach Gradient	h_s [mm]	R_c [mm]	Seawall Model §3.2.2	Overtopping Code §3.3
X	1:30	140	60	Old	Legacy
Y	1:30	160	100	New	New-Implementation

Table 3.3 Model and wave-tank configurations

Reference	# Tests	N_{ow}/N_w	s_{op}	$H_{m0\_inshore}$ [m]	$H_{m0\_offshore}$ [m]
X Configuration Tests					
2X	8 x 500s	460/4200	0.024	0.037	0.068
4AX	9 x 1000s	790/10500	0.042	0.042	0.072
4BX	2 x 1000s	390/2000	0.043	0.052	0.096
Y Configuration Tests ($s_{op} \approx 0.02$)					
2AY	10 x 1000s	220/8600	0.020	0.046	0.066
2BY	6 x 1000s	260/4900	0.019	0.050	0.072
2CY	4 x 1000s	370/3100	0.020	0.055	0.078
2DY	4 x 500s	250/1600	0.020	0.061	0.086
Y Configuration Tests ($s_{op} \approx 0.04$)					
4AY	10 x 1000s	450/11500	0.042	0.046	0.066
4BY	6 x 1000s	440/6500	0.042	0.050	0.072
4CY	5 x 1000s	540/5200	0.042	0.054	0.080
4DY	3 x 1000s	520/3000	0.042	0.060	0.088

Table 3.4 Summary of test series (detailed list of all tests provided in Appendix 2)

The wave tank configurations of the two test configurations presented in this research are outlined in Table 3.3. The sea-states and overtopping summaries for the tests conducted with these configurations are detailed in Table 3.4.

The X-configuration tests consist of three test series. Two of these series (2X and 4AX) consisted of multiple repeat tests with s_{op} values of 0.02 and 0.04

respectively. These tests were designed to allow the evaluation of repeat test uncertainty. The third X-configuration test series (4BX) consisted of two 1000 second repeat tests. This test series was originally conducted as an "Extreme Sea" for appraisal of the Importance Sampling method (§5).

The Y-configuration tests series represent a more through attempt to appraise the Importance Sampling concept. As with the X-configuration tests, several repeat tests (2AY and 4AY) were conducted to establish the underlying uncertainty and establish baseline overtopping volumes for assessment of the Importance Sampling method. Several Extreme Seas, with increasing overtopping rates, were then produced for s_{op} = 0.02 (2Y) and s_{op} = 0.04 (4Y). The number of repeat tests in these test series was determined by the requirement to produce a similar number of overtopping events to the baseline datasets (2AY and 4AY). The rationale for this is explained in detail in §5.

3.7 Summary

The experimental programme produced detailed measurements of individual overtopping volumes for several sea states through a number of repeat tests. This differs from the conventional approach to random wave modelling where the response to a certain test configuration or sea state is typically characterised using a single 1000 wave elevation time series. The larger datasets employed here allow the uncertainties associated with the extreme response to be examined in more detail, as detailed in §4.

These large "baseline" datasets also serve as the Design Seas for use in the application of the Importance Sampling method, explained in detail in §5. Several Extreme Sea datasets were also produced as part of the experimental programme. The Importance Sampling results obtained using these Design and Extreme Sea datasets are detailed in §6.

4 Individual Overtopping Distributions

4.1 Introduction

The prime goal of this research is the reduction of uncertainty in marine modelling applications. The role and importance of uncertainty may not, however, always be recognised. The majority of testing or modelling is not conducted with the express aim of quantifying the largest values. In the case of wave overtopping, a particular sea state and structure configuration may be characterised by single test run with a typical 1000 wave random sea. This test will give a value for the mean response (e.g. q or $\overline{V}$) and a value for the extreme response (e.g. V_{max} or $V_{1\%}$). It is tempting to effectively treat these values as absolute, without paying proper regard to the level of associated uncertainty. The practicalities and expense involved in conducting long test programmes will tend to preclude quantification of these uncertainties. In order to address this issue the expected uncertainties (for V_{max} in particular) have been studied and compared to the measured values obtained from the experimental programme (§3).

4.2 Distribution Fitting Method and Choice

4.2.1 Application of the Weibull Distribution

The Weibull distribution is well established as a method for the description of individual overtopping volumes. It is the distribution used by Franco *et al.* (1994), the EA-Manual (Besley, 1999) and EurOtop (Pullen *et al.*, 2007). The reasoning driving the use of this distribution is not always clear, although that is not to say it is the wrong choice.

The measurement of individual overtopping volumes is a relatively recent introduction to coastal engineering practice. Franco *et al.* (1994) initially attempted to fit the volumes obtained from non-impulsive overtopping tests (§2.2.3) using a Rayleigh distribution (exactly equivalent to a Weibull distribution with a shape parameter set to 2.0). Qualitative review of the goodness of fit demonstrated that the extreme values showed a poor fit with this distribution. The Weibull distribution appeared to show a closer agreement to the dataset. The Weibull distribution has continued to be the recommended method for describing individual overtopping volumes and is incorporated in the EA and EurOtop manuals (§2.4.1).

The choice of distribution family must be based upon the observed goodness-of-fit to collected data. Given the complex interaction of processes that may be involved in a single overtopping event there is little theoretical basis to inform the choice of distribution family.

4.2.2 Weibull Distribution Fitting Methodology

The Weibull distribution is described by up to three parameters: scale (a), shape (b) and location (c). The location parameter is useful for offsetting the distribution where some threshold exists below which data is not recorded. The EA-Manual Project Report (Besley *et al.*, 1999b) notes that this value is very small and therefore recommends the use of two-parameter distribution (with c = 0). The two parameter Weibull distribution (Equation (14)) is also used in the EurOtop manual.

Besley *et al.* (1999b) fitted two-parameter Weibull distributions to individual overtopping measurements taken at a vertical seawall subjected to both pulsating and impulsive wave conditions. It was noted that the distribution fitted the data well except for low values of $V/\overline{V}$ where some divergence was noted. In most engineering applications, where the extreme response is of primary interest, accurately describing these low volume events is of limited importance. The approach taken for the EA-Manual was to choose the shape of

distribution based upon overtopping volumes greater than the mean ($V/\overline{V} > 0$)[7].

The non-exceedance probability of a ranked data point (i) is strictly defined as:

$$P(V_i < v) = \frac{i}{N_{ow}}. \tag{34}$$

This definition is troublesome, however, when defining the probabilities for Weibull distribution fitting. It is clear, by inspection, that the highest ranked volume (i.e. V_{max}) will correspond to P = 1. This is not achievable with Weibull distribution, as the maximum value is infinite (i.e. P < 1).

In order to produce meaningful ranked probability values for a dataset it is necessary to rescale (and/or shift) the distribution. A commonly applied solution is the "Weibull formula":

$$P(V_i < v) = \frac{i}{N_{ow} + 1}. \tag{35}$$

It has been noted (e.g. Goda, 2000) that this position formula underestimates the non-exceedance probability when handling small datasets. It is therefore suggested that the Bernard position (e.g. Zhang *et al.*, 2006) plotting formula is used:

$$P(V_i < v) = \frac{i - 0.3}{N_{ow} + 0.4}. \tag{36}$$

The Bernard position formula shifts and rescales the distribution, through the numerator and denominator respectively. It should be noted that several plotting position formulae are available, and their usage is a subject of considerable debate. A more complex formula is outlined by Goda (2000). Goda's method, however, may only be applied where there is *a priori* knowledge of the Weibull shape parameter.

[7] This Weibull fitting methodology and its reasoning is not explicitly explained in the EA-Manual (Besley *et al.*, 1999). Full details are given in the accompanying project record (Besley *et al.*, 1999b).

Plotting against a Weibull scale (e.g. Figure 4.1) allows the agreement with the Weibull distribution to be assessed qualitatively. Weibull distributed data will be displayed as a straight line, allowing a simple visual check of the quality of fit. Quantification of the Weibull parameters (scale and shape) is achieved through a linear fit to the data (as displayed on the Weibull axes). The scale (a) and shape parameters are given by the formulae,

$$a = \exp\left(-\frac{m}{y_0}\right) \tag{37}$$

$$b = m \tag{38}$$

where m and y_o represent the gradient and y-axis intercept of the linear fit.

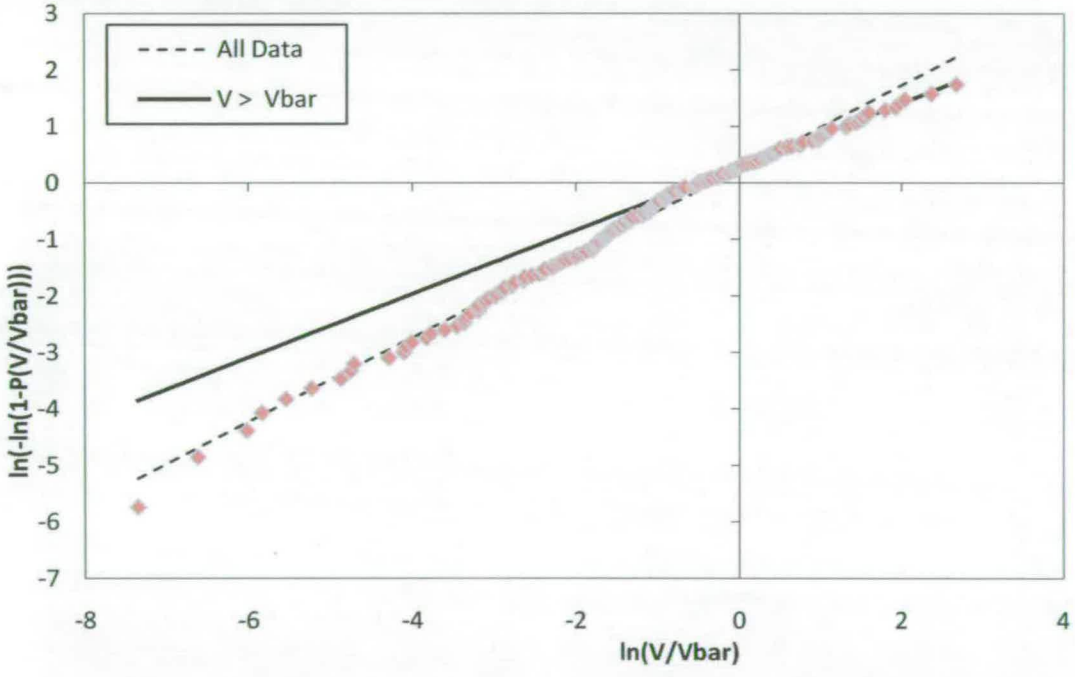

Figure 4.1 Measured overtopping volumes (s_{op} = 0.02, Series 2AY) plotted on Weibull axes. A Weibull distribution has been fitted to all data points, with a second distribution fitted only to volumes > V_{bar}.

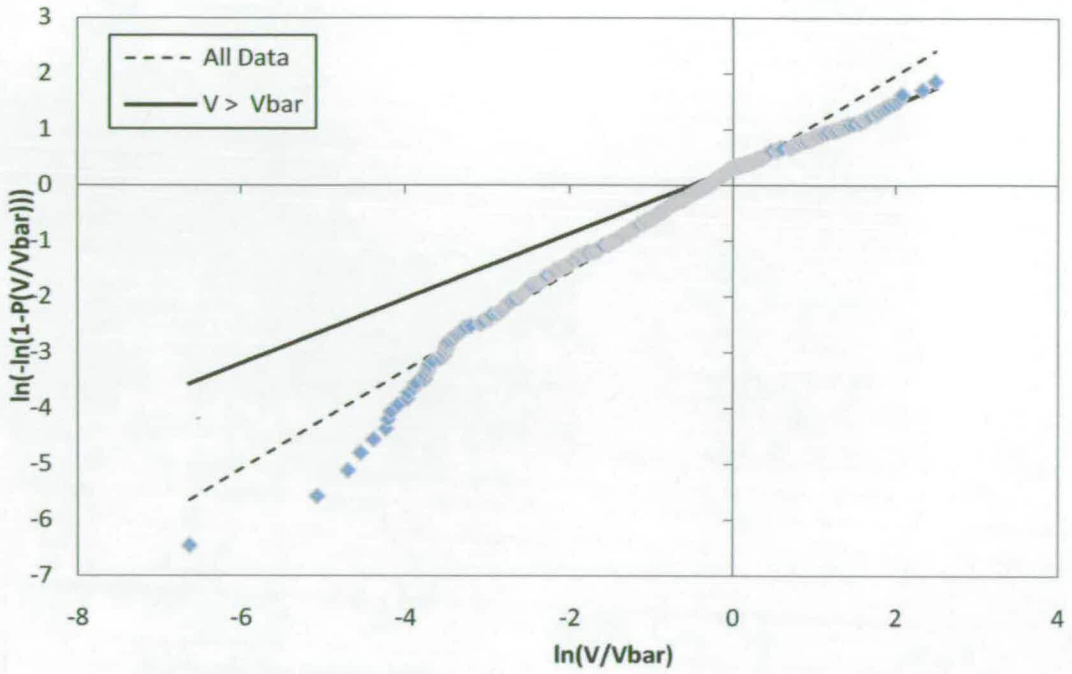

Figure 4.2 Measured overtopping volumes (s_{op} = 0.04, Series 4AY) plotted on Weibull axes with fitted distributions. A Weibull distribution has been fitted to all data points, with a second distribution fitted only to volumes > V_{bar}.

Deviations at the lower "extreme", similar to those observed Besley *et al.* (1999b), are apparent in both the s_{op} = 0.02 (Figure 4.1) and the s_{op} = 0.04 (Figure 4.2) datasets.

Besley *et al.* (1999b) do not attempt to explain the difficulty in accurately describing the smallest overtopping volumes with the Weibull distribution. The non-linear response observed at vertical seawalls (i.e. transition from non-impulsive to impulsive - §2.2.3) may explain why all events in the dataset do not fit the same parametric distribution. Indeed, the EA-Manual gives different shape parameters based upon the dominant overtopping mode (§2.4.1).

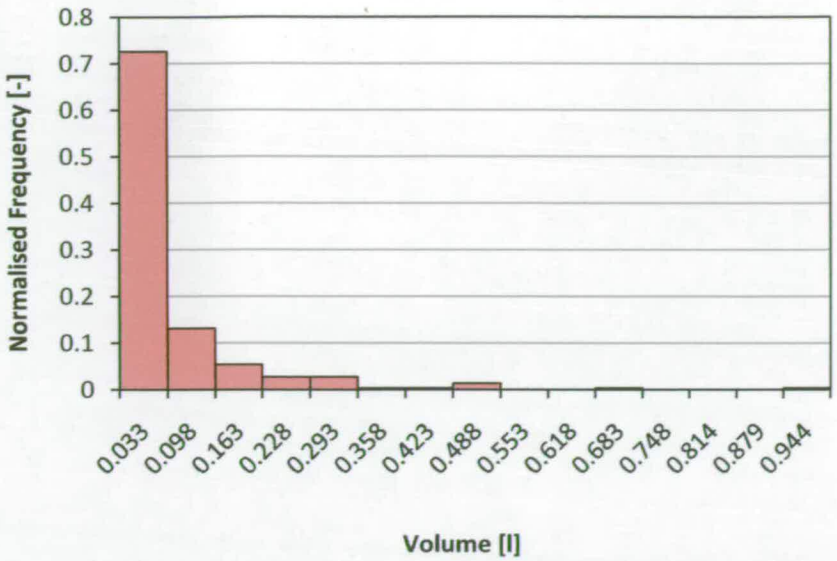

Figure 4.3 Typical histogram of measured overtopping volumes (s_{op} = 0.02).

When examining distributions of overtopping volumes it is worth considering the level of uncertainty associated with very small overtopping volumes. The detection and measurement of these events, which may only be a few millilitres, is difficult to achieve in practice. Careful attention was paid to accurately quantifying these small volumes (§3.3) obtained from the experimental programme. Nevertheless, the confidence in the measurements of these very small volumes is naturally less than the larger, more easily detected, events. It is suspected that some of these very small events are "false-positives". An inspection of the histogram in Figure 4.3 illustrates the large number of small volume events typically observed in a sample of overtopping measurements.

Given that very small events are difficult to quantify and are of significantly less interest than more extreme events, the approach taken by Besley *et al.* (1999b) would appear to be justified. The methodology of choosing the Weibull shape parameter (b) based upon $V/\overline{V} > 0$ has therefore been adopted in this research.

4.3 Extreme Value Distribution

4.3.1 Extreme Value Distribution Theory

The maximum individual overtopping volume (V_{max}) is conceptually a very simple parameter to define. It simply represents the largest individual overtopping measurement taken over a chosen time period (or number of waves) for a particular sea. This may not, however, always be the most appropriate definition. Empirical prediction equations (§2.4) do not, and cannot, produce a set of individual overtopping volumes, but instead take a probabilistic approach. The most probable value of V_{max} may be determined from distribution produced by the prediction formula.

The use of a single measurement to define V_{max} for a particular sea state clearly introduces the possibility of significant sampling error. Indeed, the reduction of this sampling error is a major motivation for the research presented in this thesis. This sampling error potentially may be reduced by defining V_{max} probabilistically, using the approach taken with the empirical prediction formulae. In this case, the distribution is fitted to the data collected from a particular test. This approach requires that there is sufficient confidence in the fit of the distribution to the data.

The use of a probabilistic method will typically reduce the variance of V_{max} when compared to the raw measurements, with the mean of V_{max} ideally unchanged. The desirability of this trait is debatable. It could be argued that the choice of technique is dependent on the number of tests to be conducted. If data is available from a large number of repeat tests the use of the raw V_{max} values may be more appropriate as the sampling errors will be negated. Financial and time pressures, however, mean that numerous tests for the quantification of V_{max} are rarely feasible. If it is believed that the variability of the probability distribution parameters is less than that of V_{max}, the probabilistic approach may offer greater confidence.

Probabilistic methods base the prediction of V_{max} on the number of overtopping waves (N_{ow}). The EA-Manual (Besley, 1999) and the European Overtopping Manual (Pullen *et al.*, 2007) describe the probability of an individual volume as the inverse of N_{ow}. Applying this to the widely used Weibull distribution gives the relationship,

$$P(V_i \geq V_{max}) = \frac{1}{N_{ow}} = \exp\left(-\frac{V_{max} - c}{a}\right)^b. \tag{39}$$

Rearranging for V_{max}:

$$V_{max} = a \cdot (\ln(N_{ow}))^{1/b}. \tag{40}$$

This definition may not be the most appropriate for the prediction of the extreme value (V_{max}) and is not widely used outside of the coastal engineering field. A more conventional statistical definition as described by Coles (2001)[8] is outlined below. $V_1,\ldots,V_{Now}$ are independent, unsorted variables.

$$\begin{aligned} P(V_{max} \leq v) &= P(V_1 \leq v, \ldots, V_{N_{ow}} \leq v) \\ &= P(V_1 \leq v) \times, \ldots, \times P(V_{N_{ow}} \leq v) = (F(v))^{N_{ow}} \end{aligned} \tag{41}$$

The function F(v) is the non-exceedance probability (Cumulative Distribution Function (CDF)) of the overtopping volume. Rather than estimate V_{max} directly from this function, the maximum values are predicted using the extreme value distribution derived above. Rewriting to state this distribution explicitly:

$$F_{V_{max}}(v) = G(v) = (F(v))^{N_{ow}} \tag{42}$$

where

$$F_{V_{max}}(v) = P(V_{max} \leq v) \tag{43}$$

The probability density function (g(v)) is the differential of the CDF (G(v)):

[8] Coles (2001) describes this technique in general terms, not as a tool for this specific application.

$$g(v) = G'(v) \tag{44}$$

It is straightforward to calculate the expected (i.e. mean) value of V_{max} using the following relationship:

$$E(V_{max}) = \int_0^\infty v \cdot g(v)dv. \tag{45}$$

The variance of V_{max}, and by implication the standard deviation (σ) may also be determined:

$$Var(V_{max}) = \sigma^2 = \int_0^\infty \{v - E(V_{max})\}^2 \cdot g(v)dv \tag{46}$$

Determining the value of V_{max} using this method potentially allows for a more complete understanding of errors associated with the extreme values. Rather than simply returning a single value of V_{max}, a measure of the uncertainty associated with the prediction may be incorporated into the result.

4.3.2 Extreme Value Distribution vs. EA-Manual/EurOtop

The difference between these V_{max} estimation methods may be demonstrated for different values of N_{ow}. Predicted V_{max} values were calculated using a shape parameter of 0.75, as given by the EurOtop manual. A nominal value of 1.0 was used for the scale parameter. Values of 5, 10, 50, 100 were chosen for N_{ow}. This relates to overtopping rates of 0.5% to 10% for a typical 1000 wave test. In real terms, this range covers low to fairly extreme rates of overtopping. Results are given in Table 4.1.

N_{ow}	$V_{max,a}$ [m³/m] EA-Manual, EurOtop	$V_{max,b}$ [m³/m] Extreme Value Distribution	$V_{max,b}$/ $V_{max,a}$	$\sigma(V_{max,b})$ [m³/m]
5	1.88	3.18	1.69	2.31
10	3.05	4.35	1.43	2.53
50	6.16	7.55	1.23	2.93
100	7.66	9.10	1.19	3.07

Table 4.1 Predicted V_{max} values and standard deviation based upon Weibull distribution with a shape parameter (b) of 0.75 and a nominal scale parameter (a) value of 1.0.

Examination of the predicted V_{max} results shows significant variation between the two methods, particularly for low values of N_{ow}. In the case of N_{ow} = 5, the extreme value distribution gives an expected value of V_{max} that is almost a factor of 1.7 larger than the current recommended formulae. The more extreme tests show smaller, but still notable, increases of the order of ~1.2 to ~1.4. The standard deviations obtained from the extreme value distribution are also of interest. The N_{ow} = 5 example shows a standard deviation that is greater than 70% of V_{max}, suggesting a high level of uncertainty when working with these small datasets. It is interesting to note that the value of the standard deviation increases only marginally with N_{ow}. This agrees with physical model data published by Pearson *et al.* (2001) showing little or no change in standard deviation with increasing test-length/dataset-size.

The example in Table 4.1 relates to a single Weibull shape parameter as given by the EurOtop manual. While this is convenient to analyse, distributions fitted to test results show significant scatter in terms of the shape parameter (Napp, 2004). The EA-Manual also includes a range of values in its empirical prediction formulae (§2.4.1). Figure 4.4 to Figure 4.7 illustrate predicted V_{max} values for the two definitions over a range of shape parameters. A nominal value of 1.0 is used for the scale parameter.

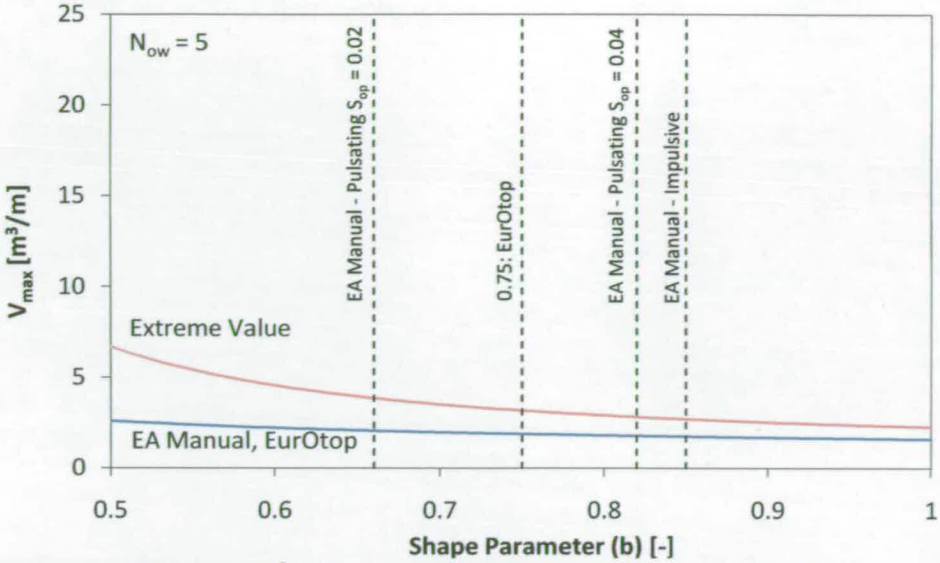

Figure 4.4 EA-Manual/EurOtop and Extreme Value Distribution V_{max} predictions for varying Weibull shape parameters. N_{ow} = 5.

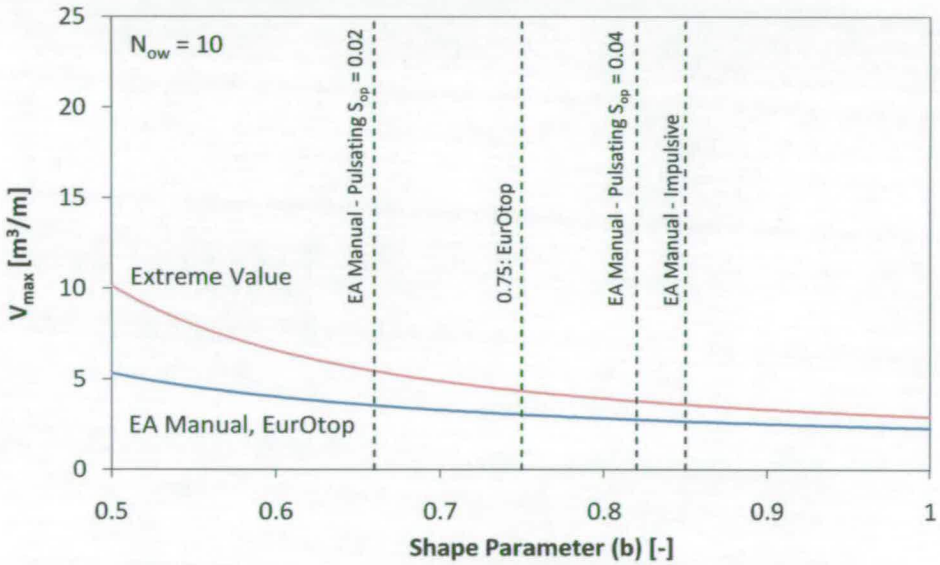

Figure 4.5 EA-Manual/EurOtop and Extreme Value Distribution V_{max} predictions for varying Weibull shape parameters. N_{ow} = 10.

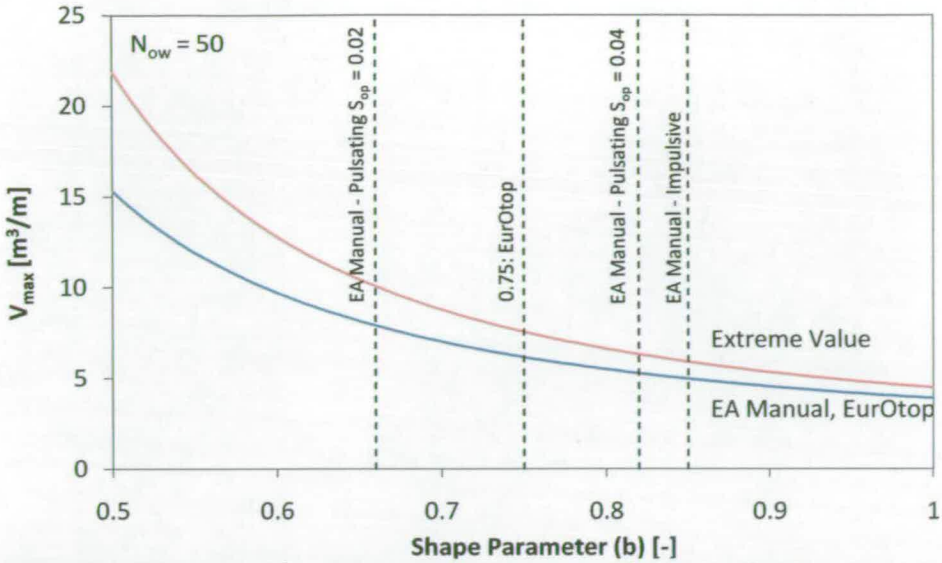

Figure 4.6 EA-Manual/EurOtop and Extreme Value Distribution V_{max} predictions for varying Weibull shape parameters. N_{ow} = 50.

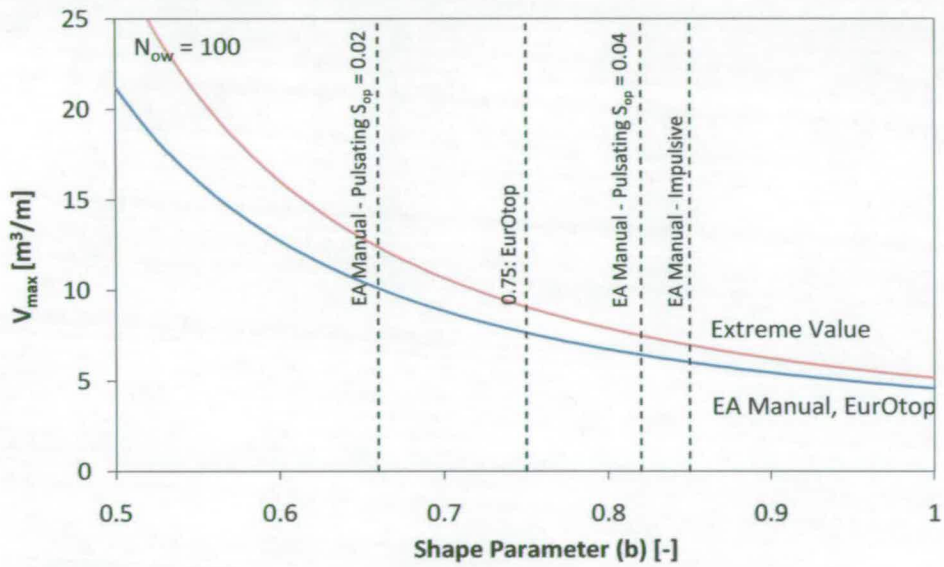

Figure 4.7 EA-Manual/EurOtop and Extreme Value Distribution V_{max} predictions for varying Weibull shape parameters. N_{ow} = 100.

The increase in V_{max} as predicted by the extreme value distribution is most evident in the cases where the datasets are small. In all cases the gap between the methods narrows as the value of the shape parameter increases.

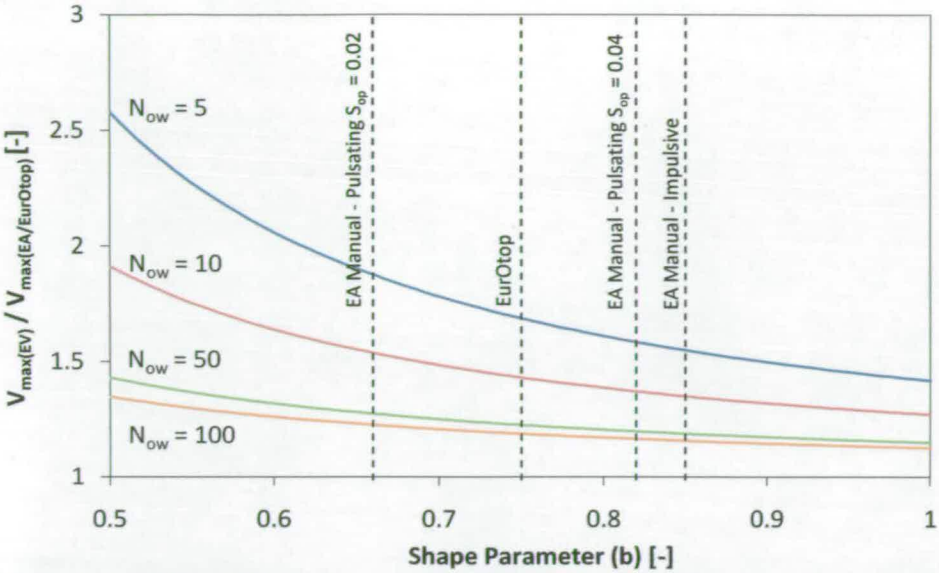

Figure 4.8 Ratio between V_{max} as predicted by the extreme value distribution to EA-Manual/EurOtop.

The relationship between the V_{max} methods is illustrated in Figure 4.8. In the case of N_{ow} = 5 the increase in V_{max} is approximately 2.0 for low values of the shape parameter (b ≈ 0.6). In the range of the prediction formulae the increase is between ~15% to ~ 100%. It is interesting to re-examine the results obtained by Napp (2004). It was noted that V_{max} was under predicted by a factor of approximately 1.25, even after attempts were made to improve the estimation of the scale and shape parameters. It is expected that this disagreement may be reduced, at least in part, if the extreme value distribution is used to estimate the value V_{max}. The tests carried out by Napp had shape parameters that generally agreed, on average, with the EA-Manual impulsive guidance. These overtopping tests resulted in the order of ~100 events per test. The values illustrated in Figure 4.8 suggest that the results obtained by Napp are under predicted by a factor of 1.5 to 1.2, accounting for the majority of the error. On this basis it would appear that Equation (45) will provide a more accurate estimate of the average value of V_{max} as estimated from the Weibull distribution.

4.3.3 V_{max} - Estimation from Extreme Value Distribution

A single overtopping test will give a single sample for V_{max}. All but one of the measurements are disregarded. It may, however, be useful to include these

measurements in the quantification of V_{max} through use of a fitted distribution. Current practice (e.g. EA-Manual / EurOtop) is to use a Weibull distribution for individual volumes and analysis of the tests conducted in this research would appear to support this method (§4.1). Weibull distributions were fitted to measurements from 52 tests corresponding to test programmes 2Y and 4Y as outlined in §3.6.2. The overtopping ratios of these tests (N_{ow}/N_w) cover a range of approximately 2%-20%. The expected maximum overtopping volume ($E(V_{max})$) was calculated for each test distribution using both the extreme value distribution (Equation (45)) and the method of the EA-Manual/EurOtop (Equation (40)).

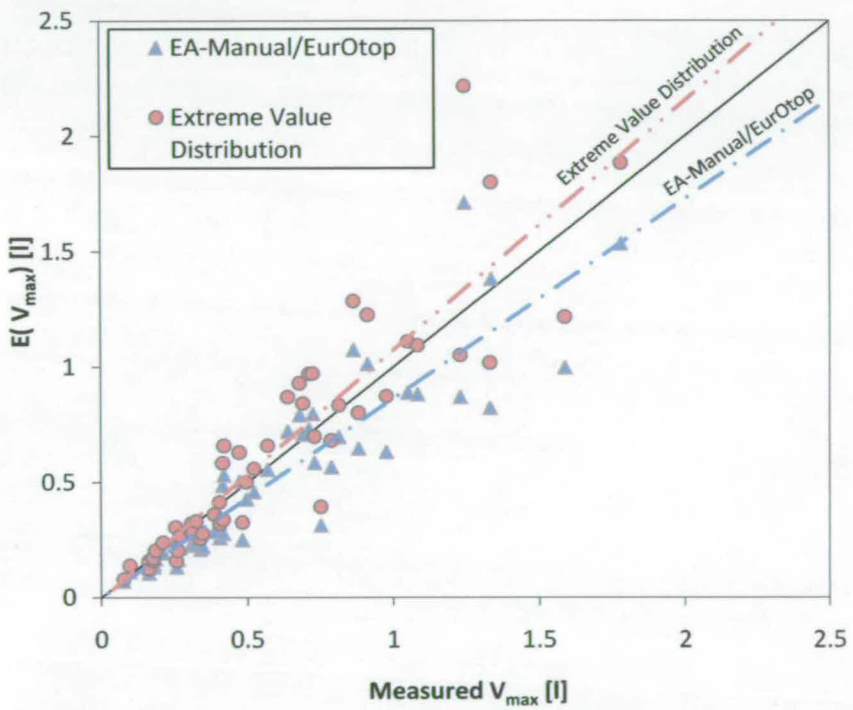

Figure 4.9 Measured V_{max} compared to probabilistic V_{max} obtained from fitted Weibull distributions.

Figure 4.9 illustrates the fitted maximum volumes ($E(V_{max})$) to the measured volumes obtained from the individual tests. The fitted and measured volumes show fairly good correlation for both the EV and EA-Manual/EurOtop distributions. Visual examination of the results suggests that there is a tendency for the EA-Manual/EurOtop equation to underestimate the value of V_{max}, a relationship not obviously apparent in the EV estimates.

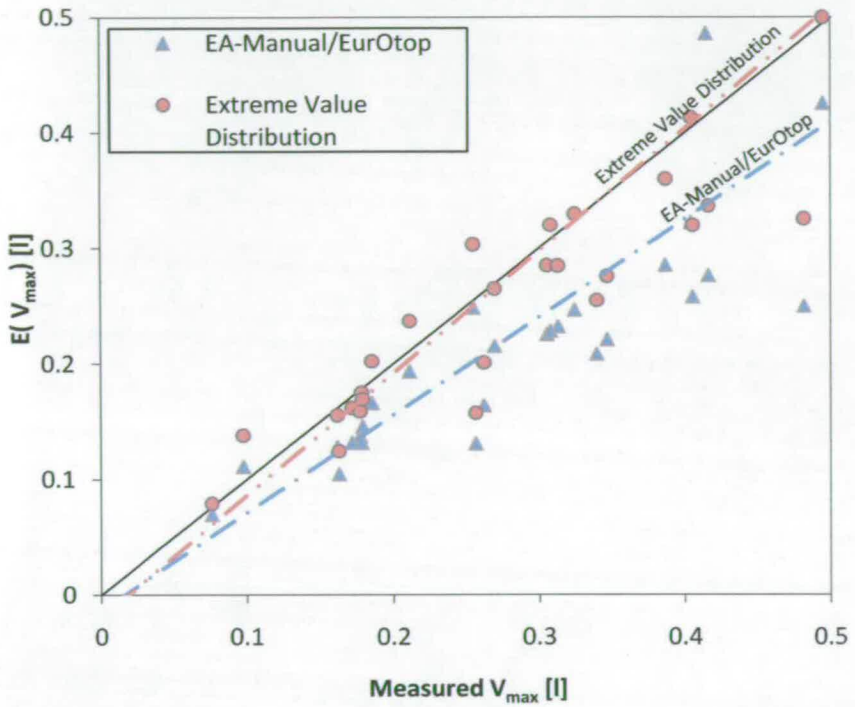

Figure 4.10 Measured V_{max} compared to probabilistic V_{max} obtained from fitted Weibull distributions – V_{max} < 0.5 litres.

The cluster of smaller overtopping measurements (V_{max} < 0.5 litres in the model) observed in Figure 4.9 is illustrated in Figure 4.10. The underestimation of V_{max} by the EA-Manual/EurOtop equation is clear, with the EV equation apparently showing the closest agreement.

While the $E(V_{max})$ values obtained from the EV distribution appear, on average, to show good agreement with the measured volume, there is clearly a high level of scatter present. An advantage of the EV distribution is that it allows for an estimation of the uncertainty through use of the theoretical variance and standard deviation (§4.3).

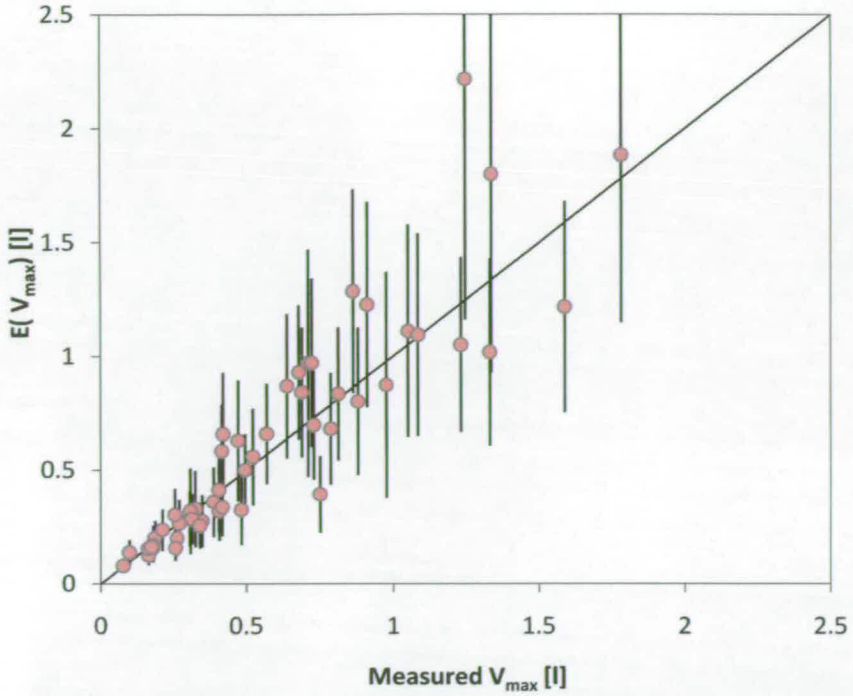

Figure 4.11 Measured V_{max} compared to probabilistic V_{max} (Extreme Value Distribution) obtained from fitted Weibull distributions. Error bars represent 1 standard deviation, as defined by the Extreme Value Distribution.

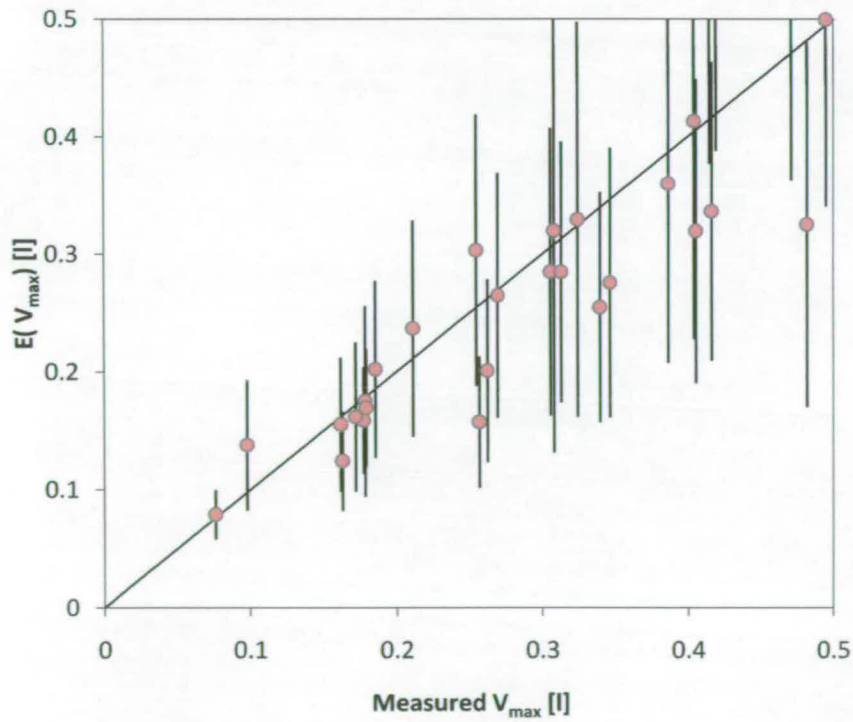

Figure 4.12 Plot as Figure 4.11, but showing $V_{max} < 0.5$ litres enlarged.

Figure 4.11 and Figure 4.12 illustrate the $E(V_{max})$ values from the fitted EV distributions, plotted here with error bars corresponding to ± 1 standard deviation as calculated from Equation (46). In the vast majority of cases the measured value of V_{max} lies within this range.

It is difficult to quantify the effectiveness of the extreme value distribution based upon a single test. In order to examine the method's effectiveness the average agreement across the dataset must be assessed. The ratio of the fitted to measured V_{max} values will be denoted as α in the following discussion:

$$\alpha = \frac{E(V_{max})}{V_{max}} \tag{47}$$

where $\alpha > 1$: overestimation by fitted distribution

$\alpha < 1$: underestimation by fitted distribution

Test Programme	EA-Manual/EurOtop		Extreme Value Distribution	
	Mean (α)	σ(α) / α	Mean (α)	σ(α) / α
2Y	0.846	0.240	1.063	0.240
4Y	0.847	0.262	1.024	0.260
2Y & 4Y	0.847	0.249	1.044	0.248

Table 4.2 Fitted V_{max} compared to measured V_{max}

The average agreement between the EA-Manual/EurOtop equation and the EV distribution is outlined in Table 4.2. There is no significant variation between the two datasets (s_{op} = 0.02 & 0.04). Taking the results from the two datasets the EurOtop method under-predicts the measured V_{max} by an average of ~25%. The EV distribution shows a significantly improved estimation, with V_{max} over-predicted by only 4-5%. The standard deviation of α appears to suggest the uncertainty associated with the two methods is virtually identical, with α values 25% from the mean not uncommon.

On the basis of the results outlined above it would appear that the extreme value distribution offers the best estimation of V_{max} for a Weibull distribution fitted to a individual test.

4.3.4 Estimated V_{max} Variation

The value of V_{max}, as estimated from a parametric distribution, is usually given as a single value with no reference to the associated uncertainty. This is the case with the formulae given in the EA and EurOtop manuals (§2.4.1). Using the extreme value distribution, as detailed above (§4.3.1), allows for the calculation of the expected standard deviation of V_{max}. (Equation (46)). The standard deviation, when compared to the expected (mean) value of V_{max}, may be used as a measure of the relative error in V_{max}. The ratio of the standard deviation to the expected value is defined as the "coefficient of variation" (C_v):

$$C_v = \frac{\sigma(V_{max})}{E(V_{max})}. \tag{48}$$

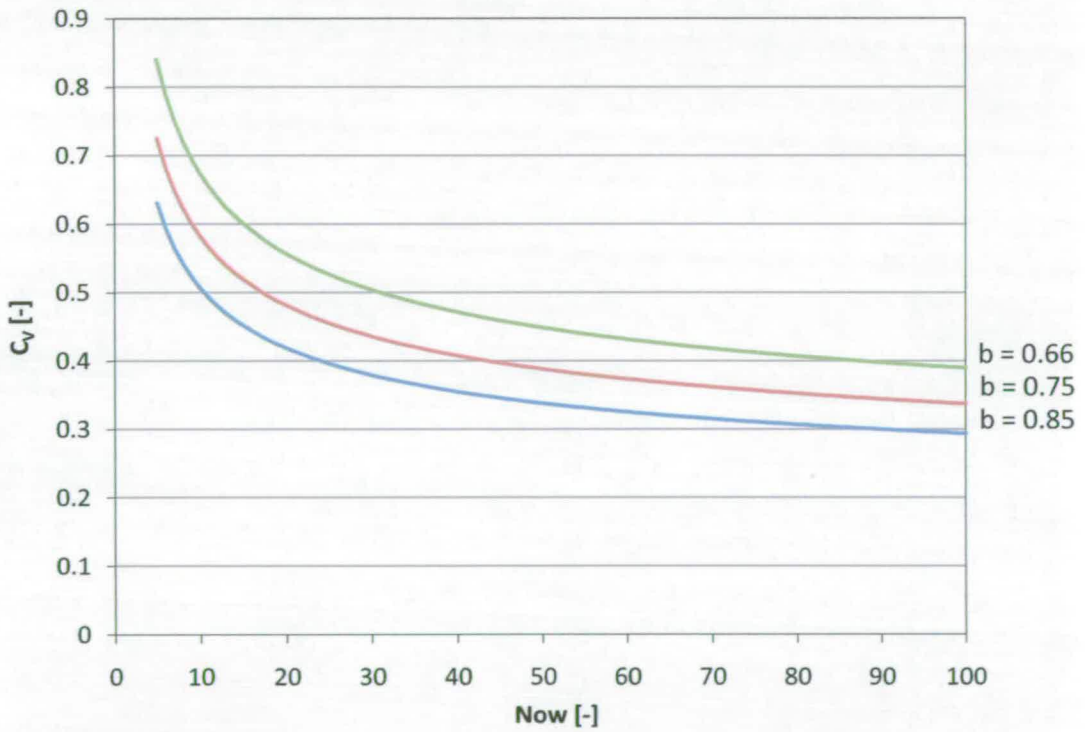

Figure 4.13 Expected Coefficient of Variation (C_v) dependency on N_{ow} for selected Weibull shape parameters (b)

The relationship between the expected coefficient of variation and the number of overtopping waves (N_{ow}) is illustrated in Figure 4.13. Plots are given for Weibull shape (b) parameters corresponding to a selection of the recommendations given by the EA-Manual & EurOtop (see Table 2.3). The value

of C_V is not given for $N_{ow} < 5$, where the EA-Manual deems the use of the Weibull distribution to be invalid.

It is observed in Figure 4.13 that C_V increases inversely with shape parameter (b), with the three distributions showing broadly similar behaviour. The variation increases as the value of N_{ow} reduces. This characteristic is significant to the assessment of low admissible overtopping scenarios. Confidence in the measured value of V_{max} will be comparatively low for low N_{ow} tests.

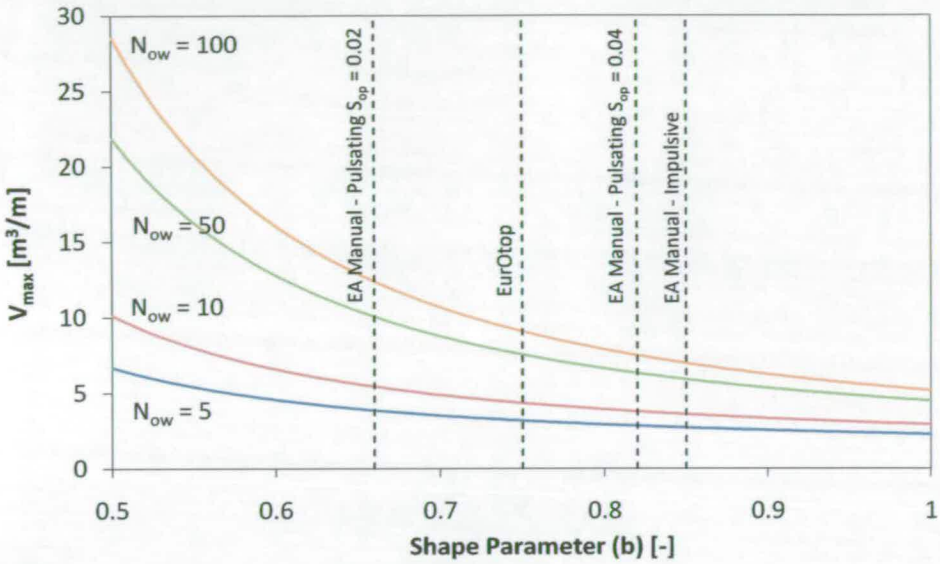

Figure 4.14 Extreme Value Distribution V_{max} predictions for varying Weibull shape parameters (nominal scale parameter: a = 1).

Further insight is gained by examining the expected value of V_{max} for selected values of N_{ow}. Figure 4.14 illustrates the expected values of V_{max} described in detail in §4.3.2. It is noted that the dependence on the shape parameter is reduced for low values of N_{ow}. The variation in V_{max} over the range of shape parameters given by the EA-Manual and EurOtop is less than 40% for the 5 event case, whereas the variation is approximately 75% for the N_{ow} = 100 scenario. It is suggested that for low N_{ow} predictions that it is more important to consider the inherent variation in V_{max} rather than the uncertainty in the shape parameter. This observation would tend to support, at least in low admissible overtopping situations, the approach of EurOtop in selecting a single shape parameter, rather than the multiple values given by the EA-Manual.

4.4 Individual Volume Exceedance Probability

The expected value of V_{max} is effectively a function of time (or more correctly N_{ow}). This is clearly useful when attempting to quantify the maximum value over a certain length of time, such as for a particular storm or wave tank test. It may be more useful, however, to be able to apply a measure of the largest overtopping volumes independently of the measurement duration. This may be achieved by examining the individual volume exceeded by a certain proportion of measured events. The value $V_{x\%}$ refers to volume exceeded by x % of the overtopping waves in a sequence. In a large dataset this may be inferred directly from the data through analysis of the ranked data. In overtopping work, however, the datasets are unlikely to be large enough (in the hundreds) for the accurate quantification of the lowest probability events. It is more normal, therefore, to calculate exceedance probabilities based upon some parametric probability distribution. In the case of the commonly used Weibull distribution the value of $V_{x\%}$ is calculated thus,

$$V_{x\%} = a \cdot (-\ln(1 - x\%))^{1/b}, \tag{49}$$

where a and b represent the scale and shape parameters respectively.

It should be noted that the convention used here is to describe the exceedance probability in terms of overtopping events (N_{ow}) rather than the number of waves (N_w) measured at the structure. This choice of definition may be a point of contention with some of those working in the coastal and marine engineering field, although it is the convention used in the majority of publications. In many cases the value of N_w is nominal, introducing an element of uncertainty into the calculation. It also confusing, in terms of statistical convention, to base the exceedance values on the total number of waves. The non-overtopping waves, having a null value, are not incorporated into the dataset represented by the fitted distribution.

4.5 Repeat Test Uncertainty

4.5.1 Methodology and Outline Results

The standard distribution as predicted by the extreme value distribution (§4.3.2) gives a measure of the uncertainty expected in the value of V_{max} obtained from a set of N_{ow} measurements. If the distribution (g(v)) is known the variance (and the standard deviation) may be calculated using Equation (46). In the analysis above (§4.3.3) distributions of the Weibull family were fitted to results obtained from each individual test. These distributions may be based upon a relatively small number of measurements. In the case of 1% of the waves overtopping, only 10 measurements will be produced from a typical 1000 wave test. Repeat tests carried out with the same input spectrum would be expected to produce identical overtopping volume distributions if the test length is sufficiently long.

The two "baseline" test series 2AY and 4AY are examined here in order to establish a reliable estimation of V_{max} for their respective input spectra. Both these test series consist of 10 unique time-series realisations produced with different seed numbers used to generate the pseudo-random distribution of phase angles. The datasets contain 219 and 448 overtopping events in total for the 2AY and 4AY test series respectively. Fitting a Weibull distribution to this complete dataset rather than the individual tests will give a more accurate description of the individual volume distribution f(v) for the two sea states. Calculating the average value of N_{ow} for each test allows the calculation of the extreme value distribution (g(v)) and the expected value of V_{max} ($E(V_{max})$). It is also possible, given that the total number of overtopping events is known, to calculate the expected value of V_{max} for the entire dataset. These test series baseline values will be notated as $V_{max,base}$ here and are described in Table 4.3.

	2AY	4AY
# Tests	10	10
All Data		
N_{ow}	219	448
V_{max} [l]	0.976	0.405
$E(V_{max})$ [l]	0.960	0.5323
Individual Test Run		
Mean N_{ow}[9]	21.9	44.8
Mean V_{max} [l]	0.344	0.229
$E(V_{max})$ [l] $\{V_{max,base}\}$	0.432	0.268

Table 4.3 Measured and expected V_{max} values for 2AY and 4AY datasets

The value of $E(V_{max})$ for a single "average test" (1000 waves) shows good agreement with the mean of the measured V_{max} values. The agreement is within ~25% and ~20% for the 2AY and 4AY datasets respectively.

4.5.2 Observed Variation in Weibull Parameters

The uncertainty of probabilistically obtained overtopping measures ($E(V_{max})$ and exceedance levels) will be dependent on variations in the Weibull distribution parameters. The Weibull scale and shape parameters obtained from distributions fitted to individual tests from the s_{op} = 0.02 & 0.04 test series are presented here. These results are compared to published values given by the EA-Manual and EurOtop (§2.4.1 and Table 2.3).

[9] The average value of N_{ow} is expressed as a non-integer value here for extreme value distribution calculation purposes.

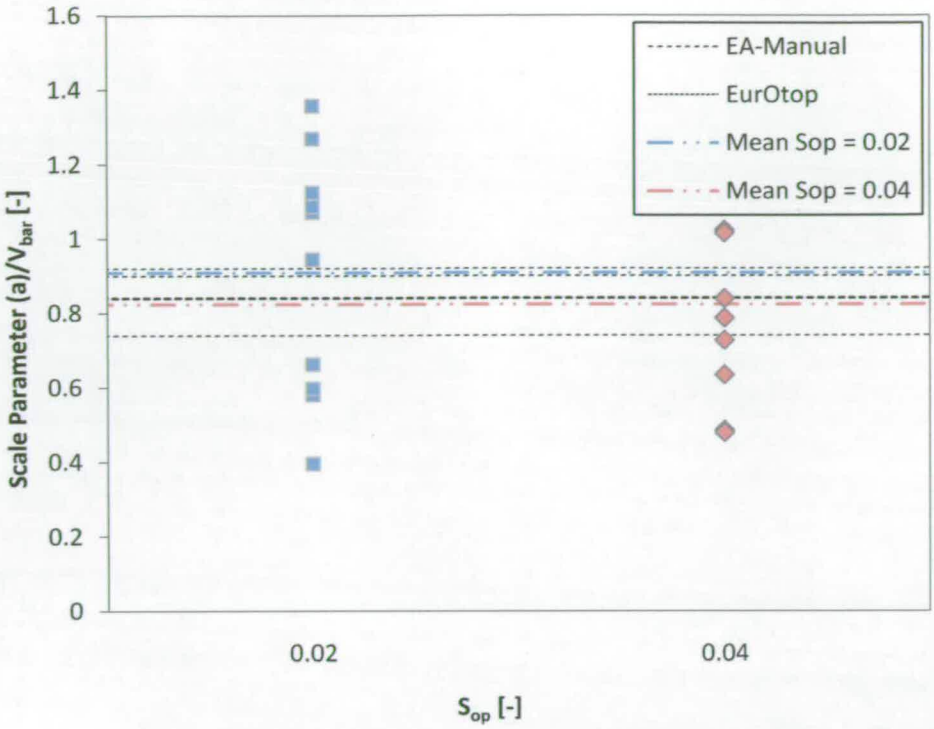

Figure 4.15 Weibull scale parameter(a) normalised by $\overline{V}$ for s_{op} = 0.02 & 0.04 test series

The Weibull scale parameter (a) values obtained from the individual test distributions, normalised against that test's $\overline{V}$ measurement, are illustrated in Figure 4.15. A large degree of scatter is apparent for both test series, although this is more prevalent in the s_{op} = 0.02 series. Many scale parameter values disagree significantly with the published scale parameters (EA-Manual and EurOtop).

The mean values of the scale parameter are also illustrated in Figure 4.15. The s_{op} = 0.02 dataset produced a mean normalised scale parameter of 0.91. Under pulsating conditions the EA-Manual predicts a normalised *a* value of 0.74 where s_{op} = 0.02. If impulsive events dominate, a value of 0.92 is recommended. The figure obtained is clearly closer to the impulsive value, despite pulsating events being the observed dominant response (§5.3.3).

The s_{op} = 0.04 dataset produced a mean normalised scale parameter of 0.82, with the EA-Manual recommended a value of 0.90 for pulsating conditions. The

EurOtop recommendation is a fixed value of 0.84, as originally given by Franco *et al.* (1994).

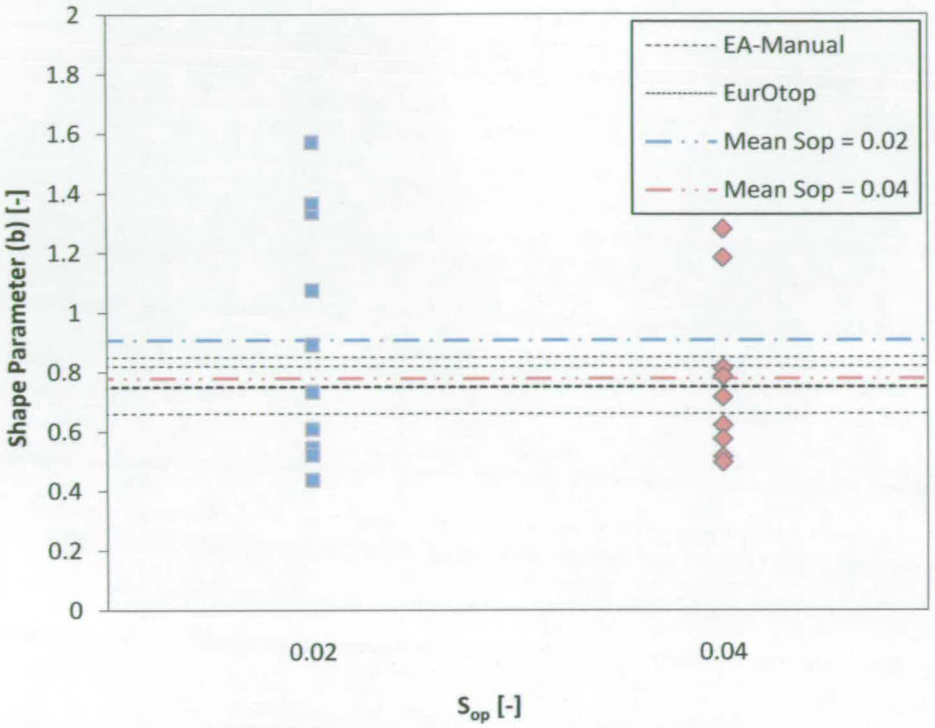

Figure 4.16 Weibull shape parameter (b) for s_{op} = 0.02 & 0.04 test series

The Weibull shape parameter (b) values obtained from the individual test distributions are illustrated in Figure 4.16. The values are highly scattered, particularly the s_{op} = 0.02 measurements. The mean of the s_{op} = 0.02 tests was 0.91. This is significantly higher than the expected value (0.66) given by the EA-Manual for pulsating conditions. The impulsive shape parameter, given by the EA-Manual, is 0.85 with EurOtop recommending a value of 0.75. The s_{op} = 0.04 dataset produces a mean shape parameter of 0.78. This shows close agreement with both the Eur0top value (0.75) and the EA-Manual recommendation for pulsating conditions (0.82).

The scale and shape parameters from the s_{op} = 0.02 tests show closer agreement with the EA-Manual's impulsive regime guidance than the pulsating overtopping values. This is at odds with the observed behaviour, which suggested pulsating events were dominant.

The scale and shape parameters from the s_{op} = 0.04 tests were close to those given by the EA-Manual for pulsating conditions (as observed during testing). The parameters also showed close agreement with the values given by the EurOtop manual.

It is not possible, nor was it intended, to validate the Weibull parameters of the published guidance (EA-Manual and EurOtop). This could only be achieved through a test matrix examining a wide range of sea states and structure configurations, whereas this testing was intended to investigate the variability associated with repeat tests. It is of interest to note, however, that the parameter means are largely within the range of values found in the published guidance.

The difficulty in characterising a particular test through its Weibull distribution is apparent through the level of variation in both the scale and shape parameters. Certainly, it would not be possible to make an informed comparison of the two test series illustrated here based only upon single test runs. This level of uncertainty present in the distributions may support and justify the less complex approach of EurOtop (compared to the EA-Manual), where single values are given for the scale and shape parameters.

4.5.3 Observed Variation in V_{max}

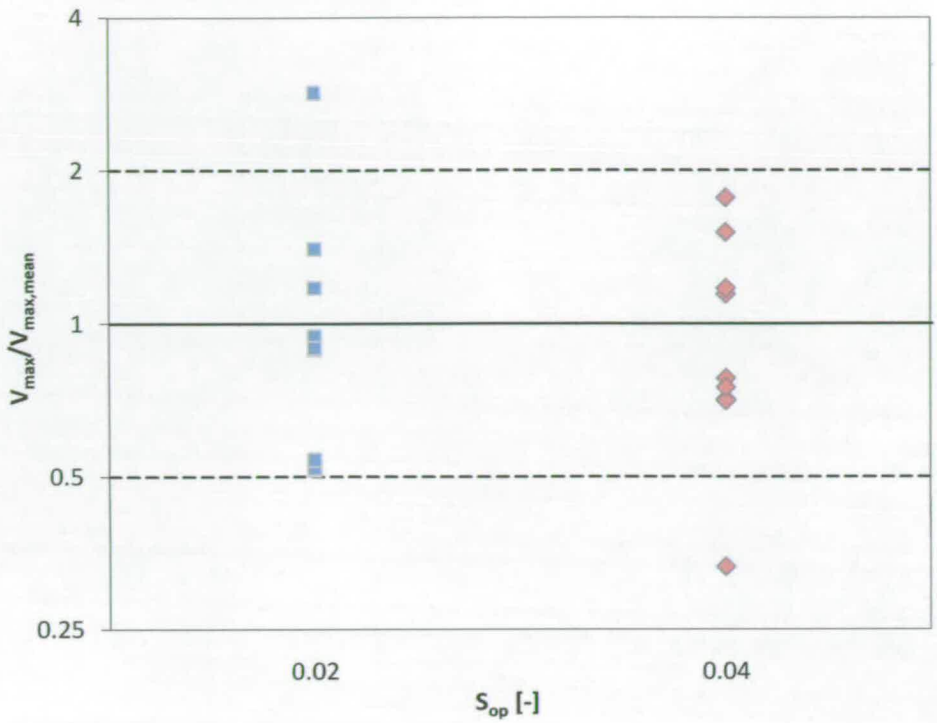

Figure 4.17 Measured values of V_{max} for s_{op} = 0.02 and s_{op} = 0.04 test series. Values normalised against the test series mean. The dashed lines represent a deviation of ×/÷ 2 from the mean. Note Y-axis log scale.

The individual V_{max} values measured from the s_{op} = 0.02 and 0.04 test series are illustrated in Figure 4.17 with the values normalised against the mean (for that particular test series). It is clear that there is inherent scatter in the values obtained for these repeat tests, with both the s_{op} = 0.02 and 0.04 test series showing broadly similar behaviour. The majority of the measurements fall within a factor of ×/÷ 2.0 from the mean of their test series. This variation appears to be slightly higher than the expected coefficient of variation (§4.3.4) would suggest.

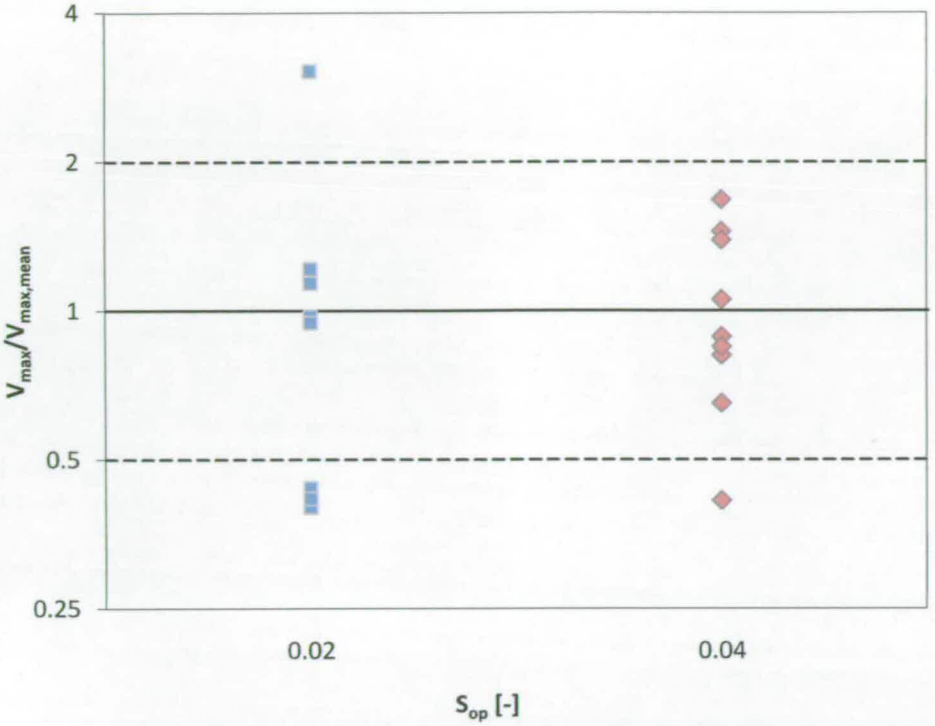

Figure 4.18 Expected values of V_{max} obtained from individually fitted Weibull distributions for s_{op} = 0.02 and s_{op} = 0.04 series. Values normalised against the test series mean. The dashed lines represent a deviation of ×/÷ 2 from the mean.

The expected values of V_{max} as calculated from individually fitted Weibull distributions are illustrated in Figure 4.18. The scatter is broadly similar to that observed for the directly measured V_{max} values (Figure 4.17). This is at odds with the expected observation if the underlying distribution and N_{ow}-per-test were consistent (in which case there would be no observed scatter).

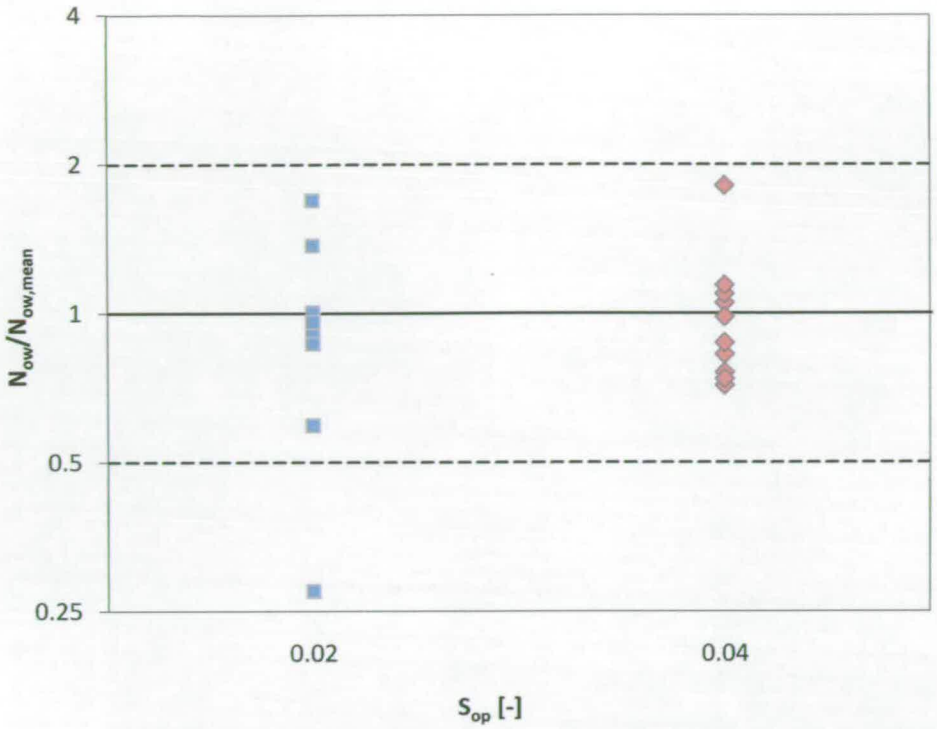

Figure 4.19 Measured values of N_{ow} for s_{op} = 0.02 and s_{op} = 0.04 test series. Values normalised against the test series mean. The dashed lines represent a deviation of ×/÷ 2 from the mean.

The variation in measured N_{ow} falls approximately within the range of ×/÷ 2 from the mean, as illustrated in Figure 4.19. The large magnitude of these variations, only marginally smaller than observed for the measured V_{max} values, may partially explain the behaviour in the expected V_{max} predictions. The variation in the Weibull shape and scale parameters is discussed below (§4.5.2). The high level of scatter in N_{ow} qualitatively agrees with the observations of Napp (2004), although Napp's measurements were not based on repeat tests with the same spectrum.

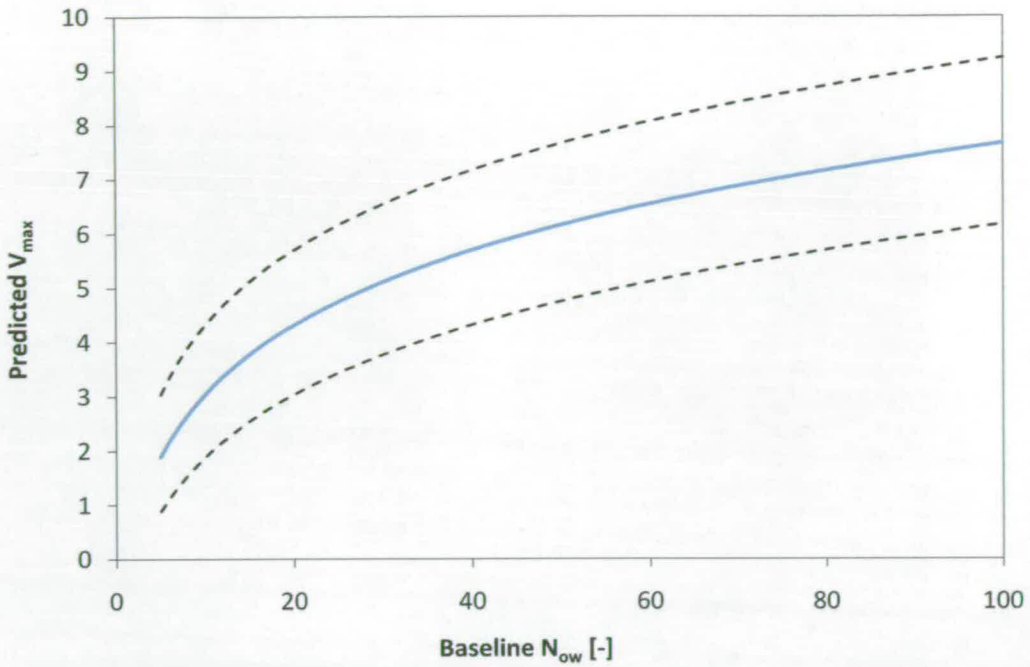

Figure 4.20 EA-Manual/EurOtop method predicted V_{max} values for a range of baseline N_{ow}. The dashed lines represent calculations for values of ×/÷ a factor of 2 in N_{ow} from the baseline N_{ow}. Weibull shape parameters are a =1, b = 0.75.

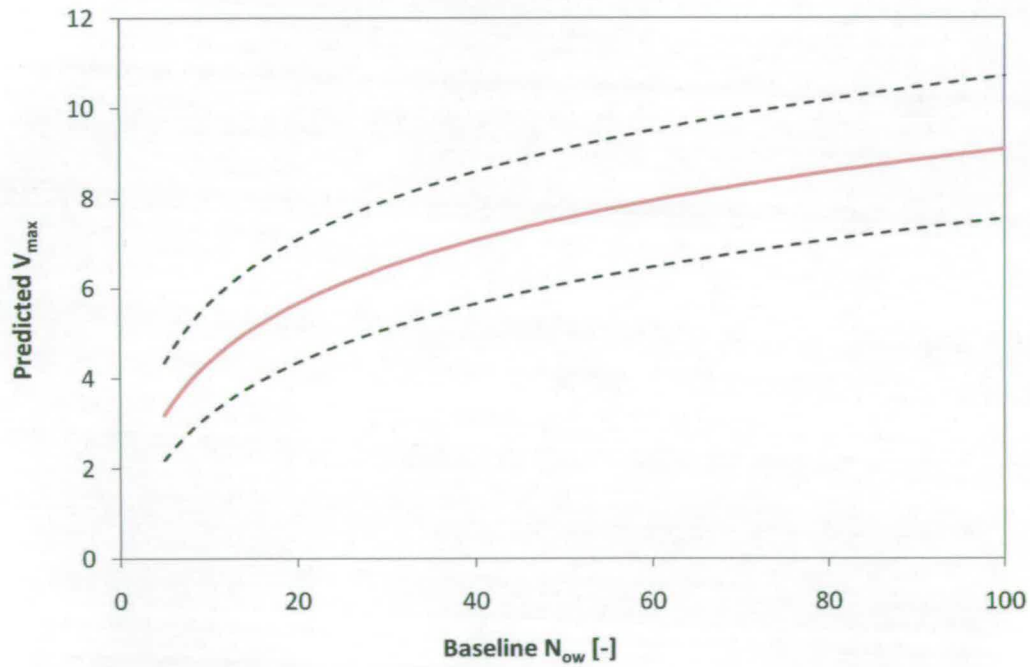

Figure 4.21 Extreme Value method predicted V_{max} values for a range of baseline N_{ow}. The dashed lines represent calculations for values of ×/÷ a factor of 2 in N_{ow} from the baseline N_{ow}. Weibull shape parameters are a =1, b = 0.75.

The variation in N_{ow} is significant as it used as an input in both the prediction formulae of the EA-Manual and EurOtop (§2.4.1) and the Extreme Value method

(§4.3.1). Figure 4.20 illustrates the predicted V_{max} over a range of N_{ow} values for fixed values of the Weibull scale and shape parameters (a =1, b =0.75). V_{max} is calculated using the method of the EA-Manual and EurOtop (§2.4.1). The influence of ×/÷ 2 factor variation in the "baseline" value of N_{ow} is also indicated. This process is repeated using the Extreme Value formula (§4.3.1) as illustrated in Figure 4.21.

The influence of the uncertainty in N_{ow} is similar for both the EurOtop and Extreme Value predicted V_{max}. The uncertainty in the EurOtop curve relates to approximately V_{max} ± 30%. The variation reduces slightly for the Extreme Value prediction to approximately ± 25%. The relative uncertainty is greatest at the lower values of N_{ow}: ± ~85% for EurOtop, ± ~40% for Extreme Value Theory. This level of uncertainty is significant, but is lower than the relative uncertainty in N_{ow} (×/÷ factor 2 in this example).

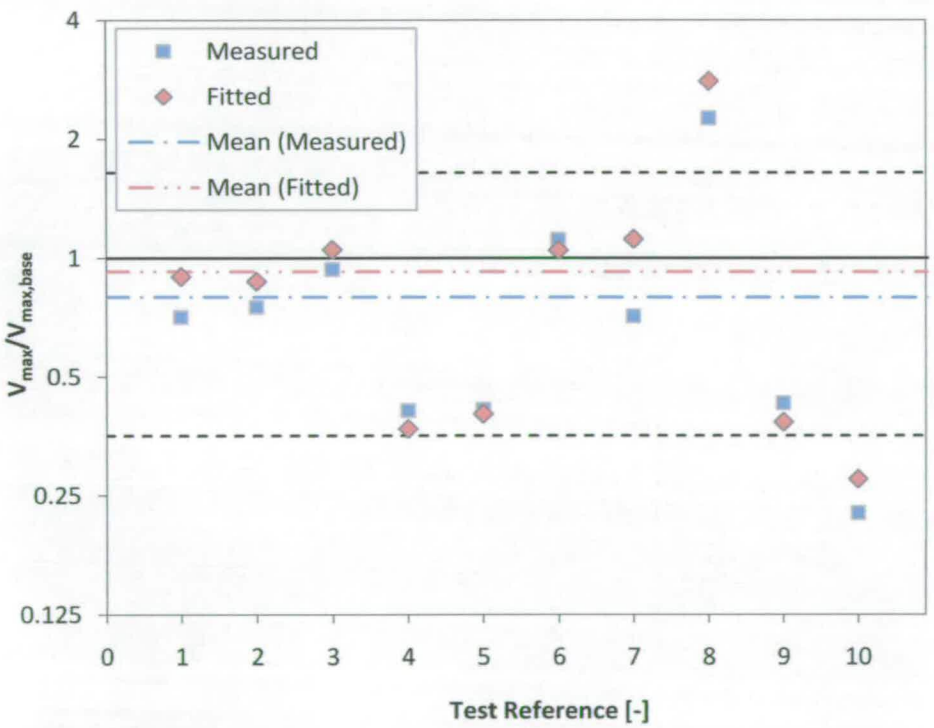

Figure 4.22 Measured and fitted Weibull derived V_{max} values compared to $V_{max,base}$. s_{op} = 0.02. The dashed lines represent a deviation of ±1 σ from the baseline value.

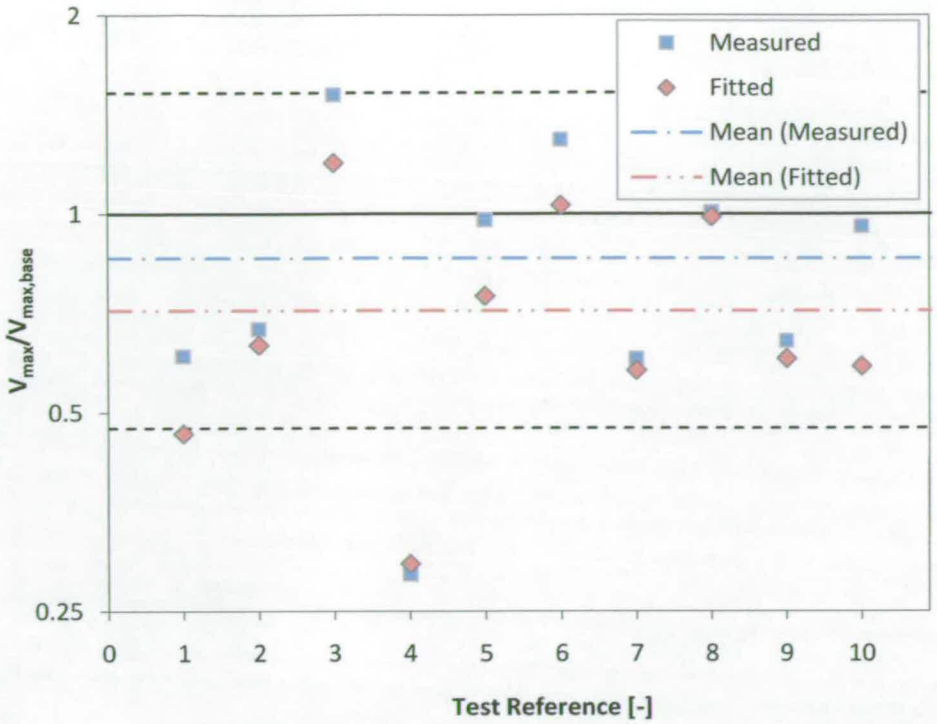

Figure 4.23 Measured and fitted Weibull derived V_{max} values compared to $V_{max,base}$. s_{op} = 0.04. The dashed lines represent a deviation of ±1 σ from the baseline value.

The measured (V_{max}) and fitted Weibull ($E(V_{max})$) extreme values for each individual test are plotted in Figure 4.22 (s_{op} = 0.02) and Figure 4.23 (s_{op} = 0.04). The value of V_{max} is normalised against $V_{max,base}$, representing the expected "baseline" value of V_{max} for the complete datasets (§4.5.1). The standard deviation (σ), as calculated from the Extreme Value Distribution, is also illustrated. It is observed that the majority of measurements (V_{max} and $E(V_{max})$) fall within the bounds of ± 1 σ. It is interesting to note that the mean of $E(V_{max})$ falls below $V_{max,base}$ (§4.5.1) in both test series. This phenomena is discussed in detail below (§4.5.2).

The perceived benefit of working with probabilistically derived value of V_{max} is that the extreme value is inferred from many measurements (in the form of the fitted distribution) rather than a single value (the measured V_{max}). In doing so it is hoped that the inherent variability in V_{max} will be reduced. It is clear from Figure 4.22 and Figure 4.23, however, that the values of V_{max} and $E(V_{max})$ are closely correlated.

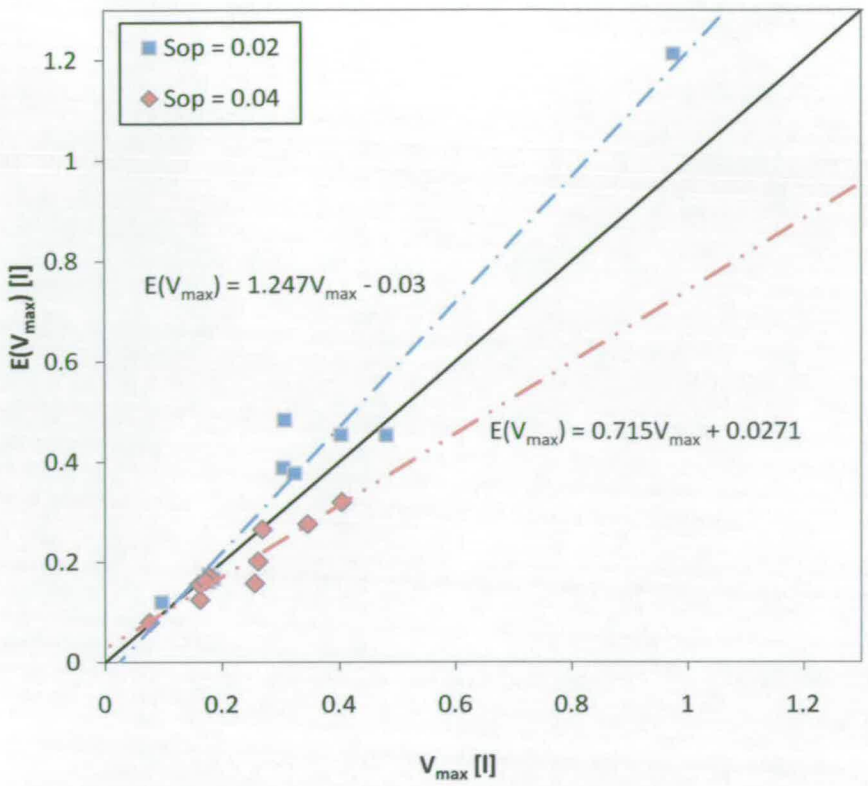

Figure 4.24 Relationship between measured V_{max} and fitted Weibull derived V_{max} ($E(V_{max})$) for s_{op} = 0.02 & 0.04 test series.

The relationship between V_{max} and $E(V_{max})$ is illustrated clearly in Figure 4.24. Both test series present a high degree of correlation between the measured and expected values of V_{max}. The values are close to equivalent (1:1) in each case (1:1.25 and 1:0.72 respectively). It is clear that the individual values V_{max} and $E(V_{max})$ are closely coupled.

In the fitting of distributions to small samples the largest value (V_{max}) will have a proportionally larger influence in the fitting process, producing the high interdependence between V_{max} and $E(V_{max})$ observed here. It should be recalled that the procedure used by the EA-Manual (Besley *et al.*, 1999b) is followed here, by which only values exceeding $\overline{V}$ are used to assess the goodness-of-fit (§4.2.2). This typically results in a distribution determined by less than 50% of the collected sample. In the case of the s_{op} = 0.02 tests this relates to approximately 10 overtopping events. On this basis there would appear to be little advantage in evaluating the extreme response (V_{max}) based upon

individually fitted Weibull distributions. The use of fitted distributions also introduces the disadvantage that the estimation of V_{max} is potentially influenced by measurements from a different response regime to the maximum value (§2.2.3).

4.5.4 Observed Variation in Exceedance Probability

The value of a given exceedance probability is dependent on the Weibull parameters (scale and shape). The observed uncertainty in these parameters is discussed in §4.5.2 and §4.5.3.

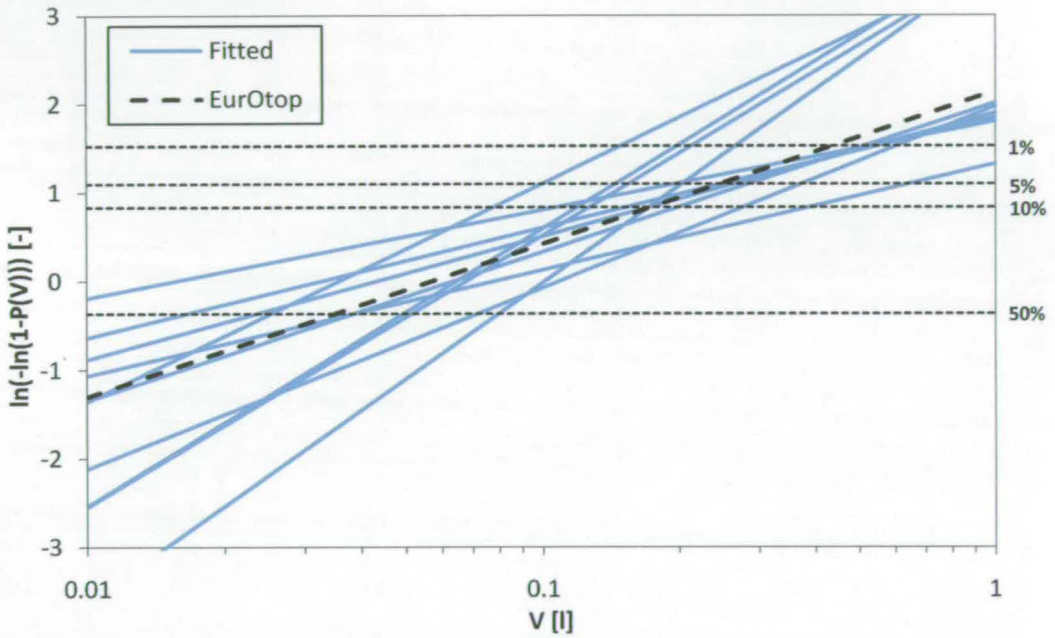

Figure 4.25 Weibull cumulative density functions for individual s_{op} = 0.02 test series. Selected exceedance probabilities are indicated.

The Cumulative Density Functions (CDF) obtained from the s_{op} = 0.02 tests are illustrated in Figure 4.25. The EurOtop distribution is also plotted for comparison. A selection of exceedance levels (50%, 10%, 5%, 1%) are also indicated. The scattered scale and shape parameters observed in §4.5.2 produce a highly variable set of distributions. Examination of the exceedance levels suggests a high level of scatter in the associated volumes.

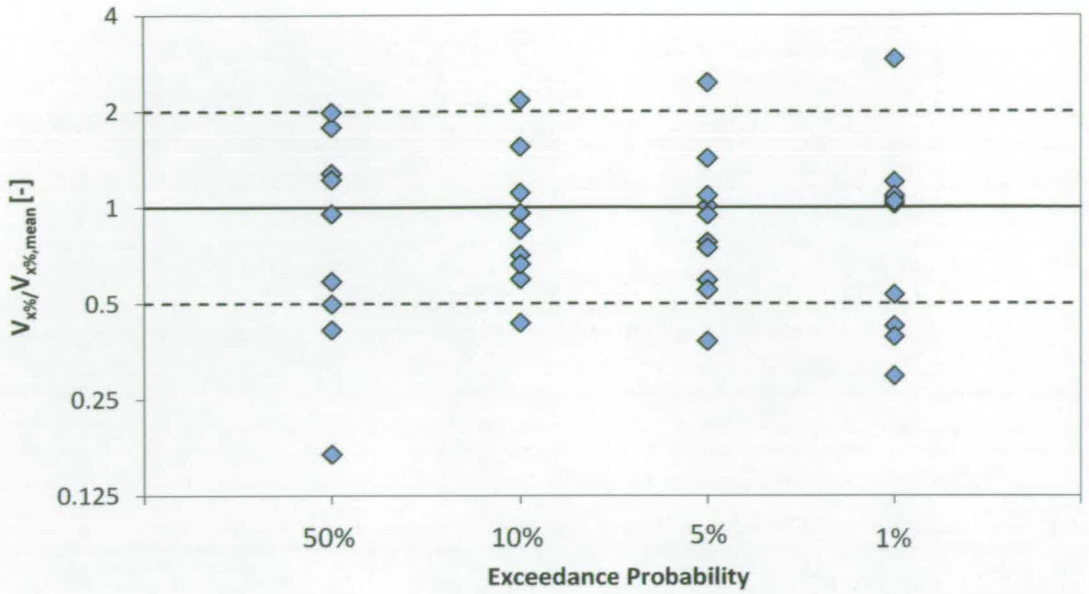

Figure 4.26 Normalised overtopping volumes for selected exceedance probabilities. Individual tests – s_{op} = 0.02.

The overtopping volumes associated with the exceedance levels illustrated in Figure 4.25 are reproduced in Figure 4.26. The volumes have been normalised against the mean volume (for the given exceedance level) for the purposes of clarity. Variations from the mean in excess of a factor of two are apparent for all illustrated exceedance levels. There is some indication that the scatter increases for lower exceedance values, with the exception of the 50% (median) quantile.

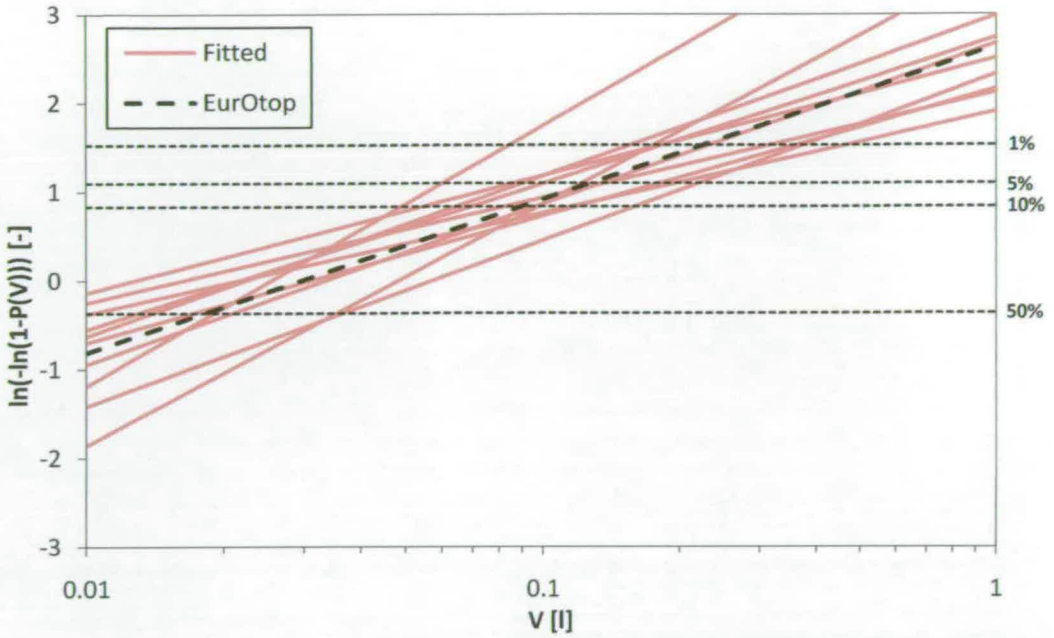

Figure 4.27 Weibull cumulative density functions for individual s_{op} = 0.04 test series. Selected exceedance probabilities are indicated.

The Weibull CDF distributions for the s_{op} = 0.04 dataset are illustrated in Figure 4.27. The distributions are highly variable, but show greater coherence than the s_{op} = 0.02 tests (Figure 4.25). In particular the less variable nature of the shape parameter observed in §4.5.2 results in a fairly consistent gradient in the CDF plots. A high level of scatter is still apparent, however, for the selected exceedance levels.

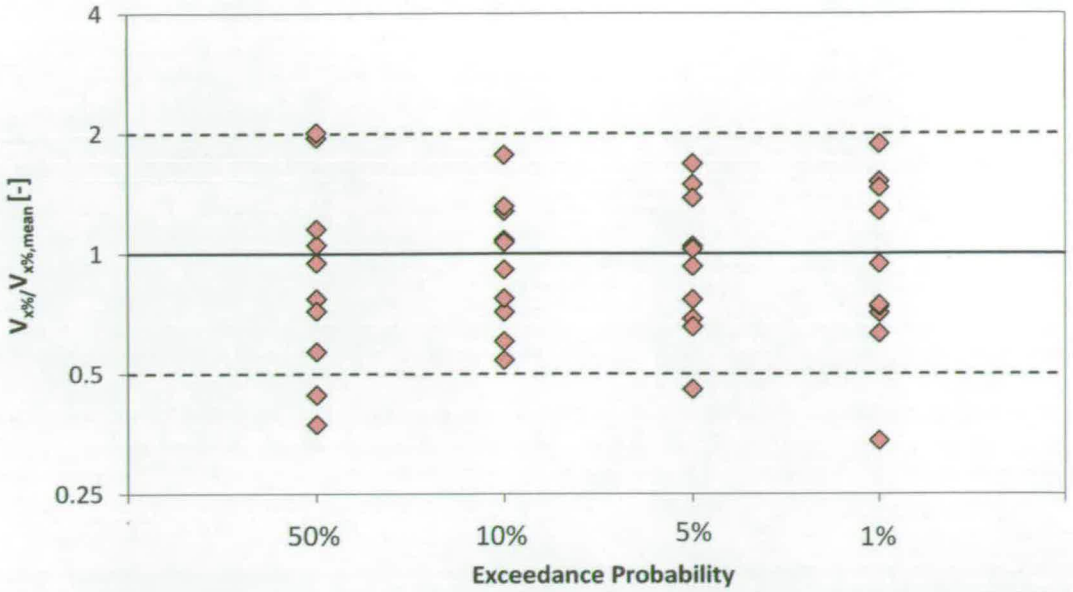

Figure 4.28 Normalised overtopping volumes for selected exceedance probabilities. Individual tests – s_{op} = 0.04.

While the distributions for the s_{op}= 0.04 tests appear less diverse than the s_{op} = 0.02 plots, the volume exceedance values remain highly scattered, as illustrated in Figure 4.28. The volumes vary by approximately a factor of two from the mean, although the variation is slightly smaller than observed for the s_{op} = 0.02 tests. The scatter increases as the exceedance probability reduces with the exception of the $V_{50\%}$ values.

The quantile value ($V_{x\%}$) scatter present in both test series is broadly similar in magnitude to the variation observed in the V_{max} measurements (§4.5.3). There is some evidence that the lowest probability events are associated with the greatest degree of uncertainty in both datasets. The exception to this observation in both cases is the $V_{50\%}$ values, representing the median of the distribution. This is counterintuitive, as it would usually be expected that the distribution is better defined for these relatively high probability events. It should be recalled, however, that Weibull fitting methodology applied here selects the shape parameter based upon the volumes exceeding the mean (§4.2.2). In the case of the long-tailed, positively-skewed distributions present in overtopping studies, the median value ($V_{50\%}$) will fall below the mean ($\overline{V}$). The distribution may not, therefore, be considered valid for this probability

region ($V < \overline{V}$). The optimisation of distributions for low probability events is not always explicitly explained in the published guidance (e.g. EA-Manual and EurOtop). Care must therefore be exercised if these parameters are to be used for the quantification of values below $\overline{V}$.

4.6 Summary

The baseline (Design Sea) datasets from the experimental programme (§3) were examined to quantify the uncertainty in individual overtopping parameters. It is noted that significant uncertainty is present in most individual overtopping measures (e.g. V_{max}, $V_{x\%}$, N_{ow} etc.). Typically parameters varied from their relevant mean value by a factor of two. The fitted Weibull distributions also showed significant scatter (in terms of their scale and shape parameters) for the individual 1000 wave tests. The results obtained here are used as a benchmark for the application of the Importance Sampling technique, as described in §5 and §6.

In addition to examining overtopping uncertainties the estimation of V_{max} from a fitted probability distribution was also explored. In particular, the use of an extreme value method was examined. This method produced a slightly higher estimate, under most circumstances, of the maximum individual overtopping volume (V_{max}) relative to the estimation procedure used in the currently used published guidance. The use of an extreme value method also allows for an estimate of the uncertainty associated with V_{max} through the calculation of the standard deviation.

The significance of these findings is discussed further in §7.

5 Improved Methods for Wave Modelling

5.1 Introduction

Physical model tests using random waves are inefficient when characterising the extreme response. In this chapter a technique known as "Importance Sampling" is described. This technique aims to reduce the length of random wave tests while maintaining the advantages of random wave testing, namely the absence of the need for *a priori* knowledge of a functional relationship (or relationships) describing the nature and magnitude of the response.

The conceptual development of the "Importance Sampling" technique is explained. The elements required for applying the technique in practice are described along with the techniques required to analyse the output data.

5.2 Importance Sampling

5.2.1 Importance Sampling Basis and Philosophy

The sampling errors inherent with the quantification of the maximum individual overtopping volume are difficult to reduce while maintaining the advantages of random wave modelling. Random wave testing has several strengths when examining complex wave interactions in shallow water. Perhaps most importantly, few (if any) assumptions need be made regarding the relationship between individual wave characteristics and the measured discrete response. Providing that a significantly long test is conducted, the response distribution should be representative of that particular sea state, with the important proviso that the extremes of the distribution are likely to be poorly defined. In most practical cases the modeller need not be concerned with the actual processes

that have produced the response. The lack of an accurate description of the relationship between the response and the wave parameters is an obstacle to reducing the sampling error associated with the maximum response. This is one of the major barriers to the application of deterministic wave groups to vertical seawall overtopping (§2.5).

The lack of a requirement to understand the exact relationship between individual waves and the response reveals another strength of random wave modelling. Coastal engineering models very often involve transforming offshore wave climates to shallower inshore regions. In cases where a representative model has been constructed the transformations of individual waves and groups should be accurately reproduced, resulting in a representative sea state at the structure.

These random wave model strengths also represent the barriers to reducing the sampling error. Deterministic modelling attempts to improve the sampling efficiency by creating a particular wave at some point in time and space. This is clearly the antithesis of a random wave model. The Importance Sampling techniques described here attempt to maintain the advantages of random wave modelling as much as is practically possible and thereby sidestep the obstacles present in a purely deterministic approach.

Two variations on the Importance Sampling method are outlined below (§5.2.2 and §5.2.3). The basic philosophy for both is the same. It is first assumed that a more energetic sea will produce more large events at the structure. The distribution of responses will be shifted both in terms of the mean of the responses and the extreme region. This assumption is likely to be valid for the vast majority of marine engineering applications, although what constitutes a "more extreme" sea is debatable and is covered in this research.

If the assumption stated above holds true, model tests carried out using a sea more extreme than the design sea will produce more instances of the maximum response. This, of course, is a fairly obvious statement. The challenge is to

analyse meaningfully these "extreme sea" test results. It is the process of testing with an extreme sea and the associated statistical analysis that forms the basis of the Importance Sampling method.

The potential strength of using Importance Sampling is that it relies almost entirely on measurements taken at, or near, the structure. It maintains the strength of conventional random modelling in that wave transformations due to the sea bathymetry need not be modelled in detail. The technique is based upon the measurement of the waves as they naturally occur, with no need to generate deterministic waves or groups.

In this research two distinct Importance Sampling methods were investigated. The basic theory and differences between these methods is explained and examined below. The descriptions below are intended to illustrate the thought processes involved in formulating the foundations of the Importance Sampling method.

5.2.2 Importance Sampling – Wave Identification

Importance Sampling is a variance reduction technique most commonly used in the field of structural failure analysis (see e.g., Melchers, 1999). It is a technique applied to the modelling of systems where the probability of failure is low. This is clearly a situation analogous to the low frequency occurrence of large overtopping events.

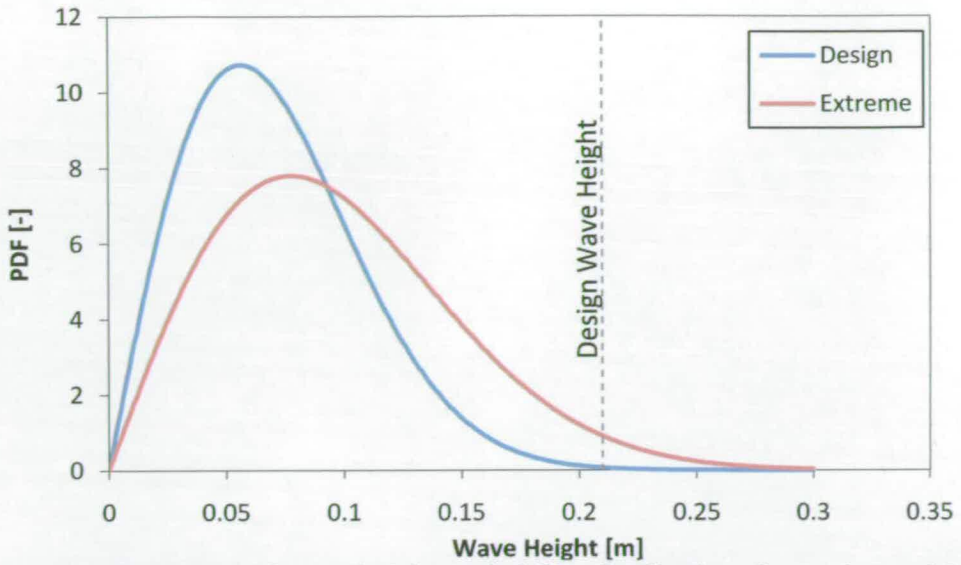

Figure 5.1 Hypothetical wave height probability distributions for Design and Extreme Seas showing the maximum wave height (from an original sketch by Prof. Julian Wolfram (Wolfram *et al.*, 2004)).

Importance Sampling examines the largest events in one distribution (the "Design Sea") through the use of a second, more extreme distribution (the "Extreme Sea"). The use of this technique is perhaps best explained by simple, one-dimensional, example. Figure 5.1 illustrates two wave height distributions at tank scale representing the Design and Extreme Seas. In this example the magnitude of the hypothetical response is assumed to be directly related to the wave height. The design wave associated with the largest response is therefore simply the wave with the largest wave height (H_{max}). This wave, by definition, is at the extreme of the distribution with only a single occurrence in any particular test.

The use of the Extreme Sea moves the point of interest away from the extremity of the wave height distribution. The expected frequency (f) of occurrence of the design wave height in the Extreme Sea is described by the ratio of the probability densities:

$$\frac{f_{Design}}{f_{Extreme}} = \frac{P_{Design}(H)}{P_{Extreme}(H)}. \tag{50}$$

This "wave identification" technique is an elegant method for reducing the sampling error associated with low frequency events. A further advantage is that waves larger than the maximum design wave height will be included in the test run. This allows for the extreme region of the response to be better understood. In the wave overtopping application, the responses associated with these larger-than-design waves may indicate a change in overtopping regime (§2.2.3). Given the inherent uncertainty associated with defining the Design Sea state, the knowledge that a change in response behaviour is imminent may be valuable when producing conservative design/assessment guidance.

The Importance Sampling technique also allows for a number of different Design Seas to be analysed using a single Extreme Sea distribution. Marine studies are often carried out on the basis of return periods. The distributions in Figure 5.1 may be considered as having return periods of, say, 100 years (Design Sea) and 10 000 years (Extreme Sea). The Importance Sampling technique in this example will return a value for the maximum response in the 100 year Design Sea with improved confidence. It is possible though to replace this particular Design Sea with distributions representing different return periods as necessary (e.g. 50 years, 200 years etc.). The Design distribution will tend towards the Extreme distribution as the return period increases, with the sampling frequency reducing and the confidence intervals expanding.

The example outlined above is based upon one parameter (wave height). In the case of wave overtopping it is not likely that any single wave parameter is directly related to the individual overtopping volume. Precious little research has been conducted associating overtopping volume with the contemporaneous characteristics of the elevation time series. Some indication, however, of the joint relationship of the overtopping behaviour may be found in the empirical prediction formulae for the individual volume distribution (§2.4). The method described by Besley (1999) indicates a dependence on both significant wave height and mean/peak period. This does not necessarily indicate that individual volumes will be related to the height and period of individual waves but it does

suggest that a simple one-dimensional application of the Importance Sampling method may be insufficient.

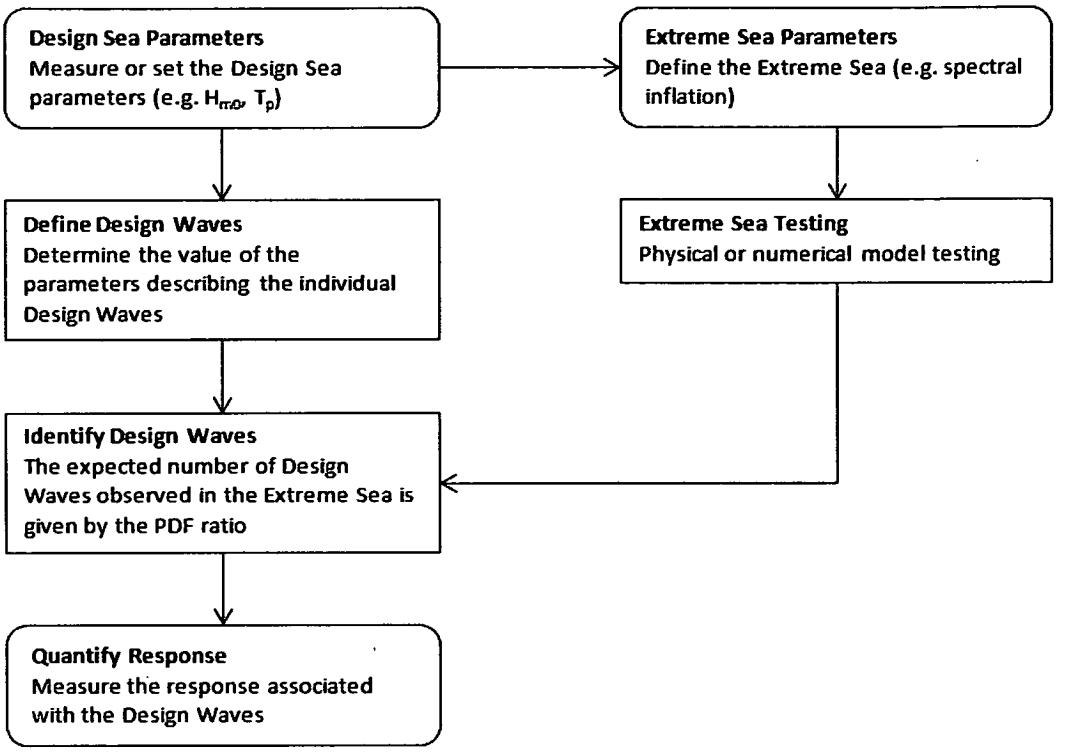

Figure 5.2 Importance Sampling methodology – wave identification

Figure 5.2 illustrates how the Importance Sampling method may be applied to a modelling situation where there is a clear understanding of the qualitative relationship between the relevant individual wave parameters and the response. Defining these relationships may be relatively straightforward in some applications. A possible application may be situations with a significant "air-gap problem". An example of this would be wave loading on the underside of a bridge or jetty. Few waves will make contact with the structure, giving the characteristic problem of a very small sample size. The magnitude of the load exerted on the structure will be closely related to the wave crest elevation (Allsop *et al.*, 2006) in this example.

The "wave identification" Importance Sampling example appears to be a powerful technique but the need to define the nature of the relationship between the wave parameters and the individual overtopping presents a

formidable challenge. It may also rather defeat the purpose of the applying the Importance Sampling technique to a particular problem at all. The technique becomes limited to situations where the response is well characterised, suggesting that the uncertainty associated with the measurements is already low. Given that this technique is ideally not limited only to vertical seawall overtopping applications a new approach is desirable. This requirement led to the formulation of the "wave exclusion" method outlined in the following section.

5.2.3 Importance Sampling – Wave Exclusion

The method outlined above involves identifying the design waves within an Extreme Sea. In cases where these parameters are difficult to define the practicality of this approach becomes severely limited. The "wave exclusion" method detailed here attempts to sidestep this limitation by removing irrelevant data, rather than attempting to identify the design waves.

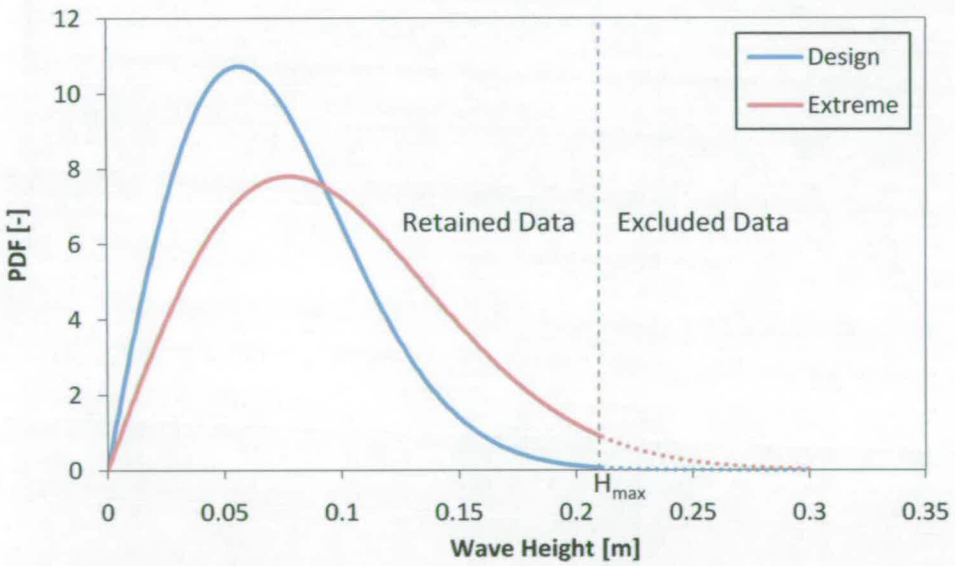

Figure 5.3 Hypothetical wave height probability distributions for Design and Extreme Seas showing the maximum wave height and excluded data.

The philosophy behind the wave exclusion method remains broadly similar to the conventional Importance Sampling method (§5.2.2). The extreme events in the Design Sea are examined using a second, more Extreme Sea. Taking the same one-dimensional example from above, the wave height distributions of

these seas are illustrated in Figure 5.3. The maximum wave height is marked on the axis as before. The key difference here is that this maximum wave height is no longer considered to be the design wave height. It is not assumed that the largest response is associated with H_{max}. Instead, the overly-extreme waves ($H > H_{max}$) are excluded from the Extreme Sea dataset along with their associated responses. The result is a dataset containing waves representative of the Design Sea, but with the distribution shifted to give more of the largest waves. The responses will be similarly representative of the Design Sea, but will also be shifted to better describe the extreme region of their distribution.

The wave exclusion method relies on some knowledge on the relationship between individual wave parameters and the associated response. In the example above it is assumed that increasing the wave height will produce more extreme responses. The relationship may, however, be relatively weak. It is not assumed that the response is strictly proportional to the wave height. Rather, the working principle is that an increase in average wave height will result in a shift in the distribution towards the extreme region.

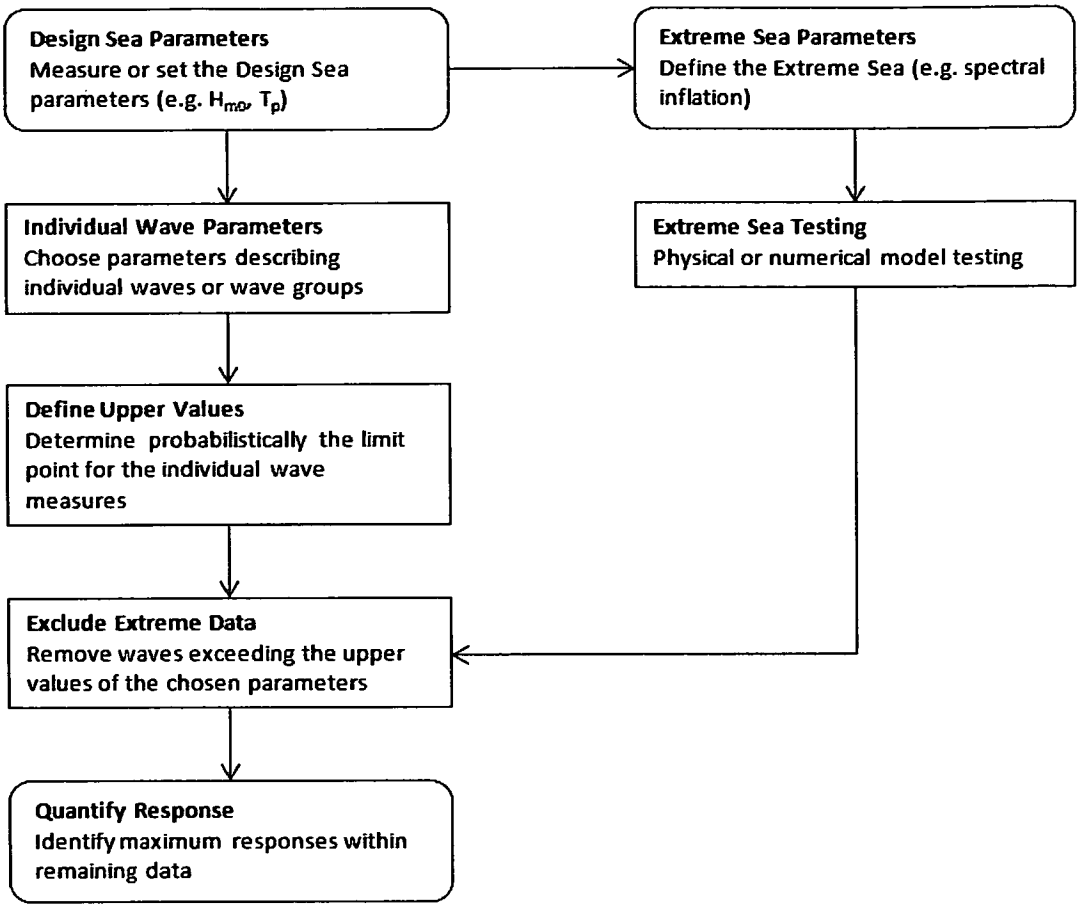

Figure 5.4 Importance Sampling methodology – wave exclusion

The flowchart in Figure 5.4 illustrates how the wave exclusion method may be applied to a modelling problem using univariate distributions. The Extreme Sea dataset is filtered such that no single parameter (as included in the univariate distributions) is outside the limits of the Design Sea. These waves in the filtered dataset are considered to be representative of the Design Sea, with the distribution shifted to produce a greater number of extreme events. This method is illustrated by example in §6.

5.3 Design and Extreme Seas

5.3.1 Spectral Inflation

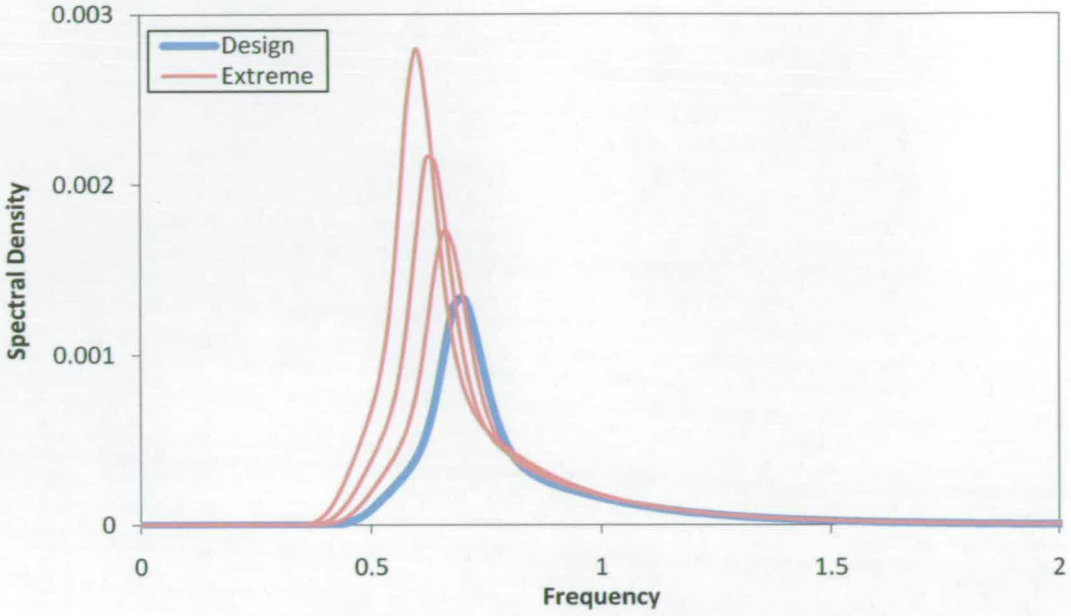

Figure 5.5 Design and Extreme Sea JONSWAP spectra for nominal H_{m0} and T_p with $\gamma = 3.3$. Extreme Sea spectra correspond to spectral inflation values of 1.1, 1.2 and 1.3.

The Importance Sampling technique requires testing be carried out with a sea more extreme than the conventionally used design sea (§5.2). The scaling of the Design Sea to produce the Extreme Sea is carried out through manipulation of the spectral parameters. The most intuitive measure for moving between the Design and Extreme Sea conditions is through scaling of the surface elevation, the most obvious measure being the significant wave height (H_{m0}). The surface elevation is measured in both space and time. In order to correctly move to the Extreme Sea distribution a spectral "inflation" method which accounts for wave period should be used.

The technique employed here is to maintain the peak offshore steepness (s_{op}) between the Design and Extreme Seas. The scaling in therefore applied in both elevation and time (i.e. the wave period). The "shape" of the waves in terms of the individual wave steepnesses are thereby maintained (ignoring, at this stage, non linear effects). The use of offshore spectral measures is intended to avoid the need to account for the spectral transformations as the waves propagate

from deep to shallow water. A major objective of Importance Sampling technique is to avoid the requirement for detailed descriptions of these transformation processes (§5.2.1). The "Spectral Inflation Factor" I_s is defined simply as the ratio of Design to Extreme Sea H_{m0} values:

$$I_s = \frac{H_{m0,Extreme}}{H_{m0,Design}}. \tag{51}$$

The peak period (T_p) of the spectrally inflated sea is back-calculated based upon maintained steepness:

$$T_p = \left[\frac{2\pi}{g} \cdot \frac{H_{m0}}{S_{op}}\right]^{\frac{1}{2}}. \tag{52}$$

The definition of the spectrum in terms H_{m0} and T_p (or f_p) is useful as most spectra (JONSWAP, Pearson Moskowitz etc.) are parameterised in these terms[10]. JONSWAP spectra with inflation factors of 1.1, 1.2 and 1.3 are illustrated in Figure 5.5.

The elevation-time histories produced for this research were based upon the JONSWAP spectrum with a peak amplification factor (γ) of 3.3. In experimental applications these spectra were produced using Edinburgh Design's *Wave* software (§3.2.1). This software allows the peak frequency (f_p) to be directly input, while the target value of H_{m0} must be achieved through measurement and calibration based upon wave gauge measurements. In practice, determining the correct gain value was not onerous, requiring iteration using a small number of short (~250 wave) tests. Applying the spectral inflation process is therefore achievable with little difficulty in an experimental setting[11]. Spectra produced

[10] The original spectral equations are often defined by fetch distance (JONSWAP) and the wind speed defined at a given height above sea level (JONSWAP and PM). The "parameterised" versions of these spectral equations may be given in terms of $H_{1/3}$ rather than H_{m0} (e.g. Goda, 2000). This reflects common practice at the time of derivation. To maintain clarity, and because the difference between $H_{1/3}$ and H_{m0} tends to be small, the significant wave height is defined exclusively in terms of H_{m0} in this instance.

[11] The application of the spectral inflation process was further simplified in this research by a useful quirk of the spectral formulae implementation in the *Wave* software. A particular "gain" value in the spectral function corresponds to a constant value of s_{op}. Thus once the calibration

for synthesising seas for numerical modelling purposes are easily produced using the parameterised spectral equations. Where required in this research these spectra were produced using the equations given by Goda (2000).

5.3.2 Non-Linearity and Wave Transformations

In a situation where the sea is adequately described by linear theory, the move from the Design Sea to the Extreme Sea may be visualised as a simple scaling exercise in both space (wave elevation) and time (wave period). The shapes of the individual waves in terms of asymmetry and crest front steepness will, on average, be unchanged. In a linear sea application the distributions of the relevant parameters for Wave Identification (§5.2.2) or Wave Exclusion (§5.2.3) may be readily produced from the spectrum. The simplest method for achieving this is to fit distributions to measurements from synthesised elevation-time histories. While fairly crude, this is computationally inexpensive and readily implemented. Alternatively, more sophisticated parametric methods are available for producing distributions directly from the spectrum (e.g. joint-distribution of wave height and period, see Goda (2000)).

The use of the Importance Sampling method in linear seas has some attractive applications for deep-water modelling situations. An example may be the exploration of the "air-gap" problem whereby only infrequently large waves surpass the threshold at which they impact the underside of a structure (e.g. a fixed oil platform, bridge or jetty). Dynamic responses of floating structures such as wave energy converters or floating oil platforms (as explored by Cassidy *et al.*(2001) using the "Constrained NewWave" theory) may also be of interest. The use of the technique in linear seas also lends itself well to the proposed Importance Sampling "pre-filtering" method (§7.3)

While linear wave theory greatly simplifies the implementation of the Importance Sampling technique, the sea states involved in coastal engineering research are likely to be significantly non-linear. This manifests itself in

---

has been completed for the Design Sea, the spectral inflation process may applied simply by calculating the correct value of f_p for the Extreme Sea and holding the gain parameter constant.

asymmetry in the wave profiles. This asymmetry may be observed around the still water line, with the individual wave crest elevations being greater, on average, than the corresponding trough elevation. Goda (2000) showed that crest elevation of laboratory generated regular waves may account for up to 80% of the wave height. Asymmetry is also observed as the front of the wave profile becomes steeper than the rear.

The effectiveness of the Importance Sampling method is potentially affected by increased non-linearity in the Extreme Sea. Goda (2000) proposes the following formula (with notation updated here) for describing the index of non-linearity (Π):

$$\Pi_{m0} = \frac{H_{m0}}{L_p} \coth^3(k_p \cdot h) \tag{53}$$

The spectral inflation method involves maintaining a constant value of s_{op} (§5.3.1). Inspection of above formula shows that the H/L term will remain constant. The water depth (h) is also constant. The increase in non-linearity is therefore related to the wavenumber (k), which is directly calculated from the wavelength (L).

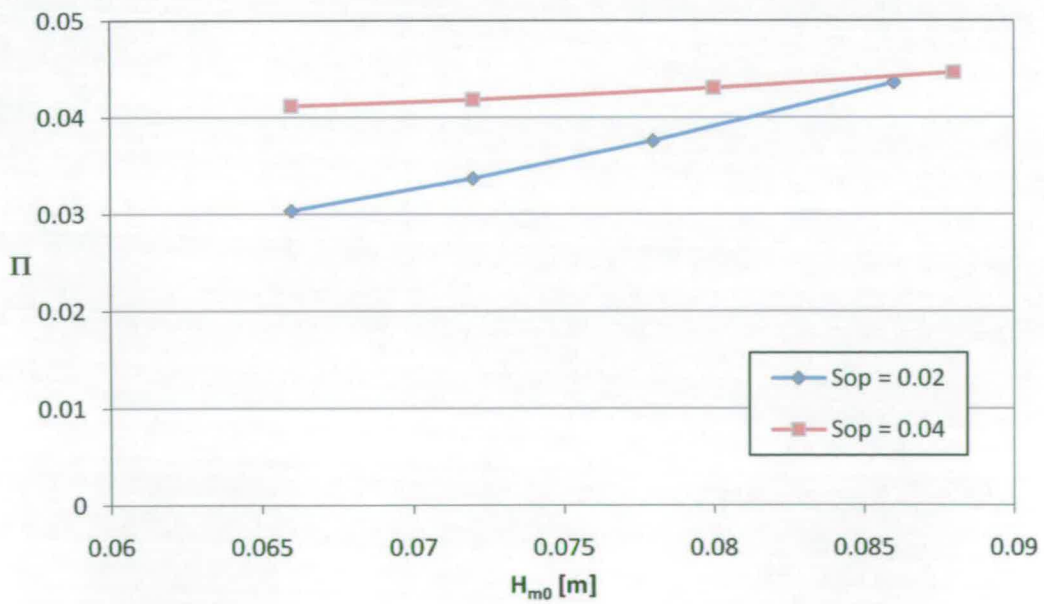

Figure 5.6 Non-linearity index for deep water laboratory measurements.

The value of the non-linearity index ($\prod$) was calculated for deep-water measurements taken from the laboratory tests detailed in §3.6.2 (Figure 5.6). It is observed that the non-linearity index remains fairly constant for the $s_{op} = 0.04$ test series. There is a more marked increase in the $s_{op} = 0.02$ test series, with an increase in H_{m0} of 30% relating to an increase of approximately 40% in the value of $\prod$. Nevertheless, all the deep-water values of $\prod$ illustrated in Figure 5.6 correspond to relatively mild non-linearity. Charts produced by Goda (2000) illustrate strong surface-elevation non-linearity for values of $\prod$ over 0.05, outwith the range of these measurements.

The above analysis is encouraging in terms of suggesting only mild increase in overall non-linearity of the sea state in the Importance Sampling application. This gives confidence that the mechanisms acting upon the incident wave train will be similar in both the Design and Extreme Seas. It should be recalled, however, that the Importance Sampling method is based upon measurements from individual waves and/or short wave groups (§5.2.1). The Importance Sampling method is expected to be effective if a hypothetical design wave from the design sea is reproduced and identified accurately in the Extreme Sea. It is desirable, for practical reasons, to describe this design wave in the simplest terms possible, for example wave height and period. In a laboratory situation it is postulated that this design wave will be subject to approximately the same degree of non-linearity in both the Design and Extreme Seas, regardless of the value of $\prod$.

5.3.3 Overtopping Regime Changes

Wave overtopping at vertical seawalls is a non-linear process. Overtopping waves may be broadly characterised as pulsating (green-water), impulsive (violent) or broken. The overtopping regime is commonly predicted using either the relative wave height (H_{m0}/h_s), as recommended by PROVERBS (Oumeraci *et al.*, 2001) or the h_* parameter (Equation (2)) as used by the EA and EurOtop manuals (§2.2.3). In both cases these methods describe the predominant regime for a particular sea state. They do not predict the behaviour of individual waves.

Ideally the Spectral Inflation process (§5.3.1) would not involve a change of overtopping regime. In practice this may be difficult to achieve, particularly as the conditions which bring about the onset of a change in regime may be unknown or poorly defined.

The Design Sea tests carried out as part of the experimental programme were formulated to produce predominately pulsating overtopping events. The h_* parameter for the $s_{op} = 0.02$ tests, however, falls below the threshold at which impulsive events would be expected to be predominant[12]. In practice, qualitative observation of the Design Sea tests showed little evidence of impulsive overtopping.

Figure 5.7 and Figure 5.8 illustrate the values of the mean discharge obtained from the $s_{op} = 0.02$ and $s_{op} = 0.04$ test series respectively. These values have been plotted against the h_* parameter to give a measure of the expected overtopping regime. Plotted alongside the measured results are the predicted discharge values obtained from the empirical equations given by the EA-Manual. While this research does not examine mean discharge, this comparison gives a useful indication of the change in predominant regime in moving from the Design Sea to the Extreme Sea. It should be noted that the leftmost values (lower h_*) represent the more extreme seas in these plots.

[12] The target parameters were chosen to give an h_* parameter relating to pulsating overtopping. The average value of H_{m0} obtained from the repeated test runs was slightly larger than that measured from the calibration sea, resulting in the lower value of h_*.

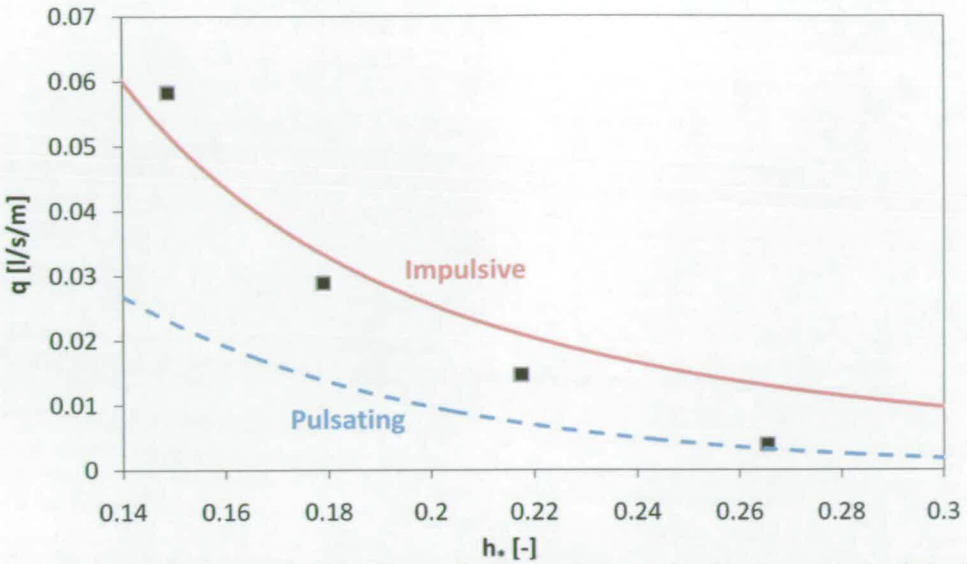

Figure 5.7 Theoretical (EA-Manual) overtopping discharge values (q) for breaking (impulsive) and non-breaking (pulsating) conditions. Data points represent measured values for the s_{op} = 0.02 test series (§3.6.2)

The values of h_* obtained for the s_{op} = 0.02 test series all fall below the threshold (h_* < 0.3) where the predominant behaviour is expected to be impulsive. The least extreme sea, however, shows very close agreement with the prediction with the pulsating prediction formulae, as illustrated in Figure 5.7. This agrees with the observed overtopping behaviour, where few impulsive overtopping events were evident. The trend observed with increased Spectral Inflation (reduced h_*) is for the tests to show closer agreement with impulsive overtopping formulae.

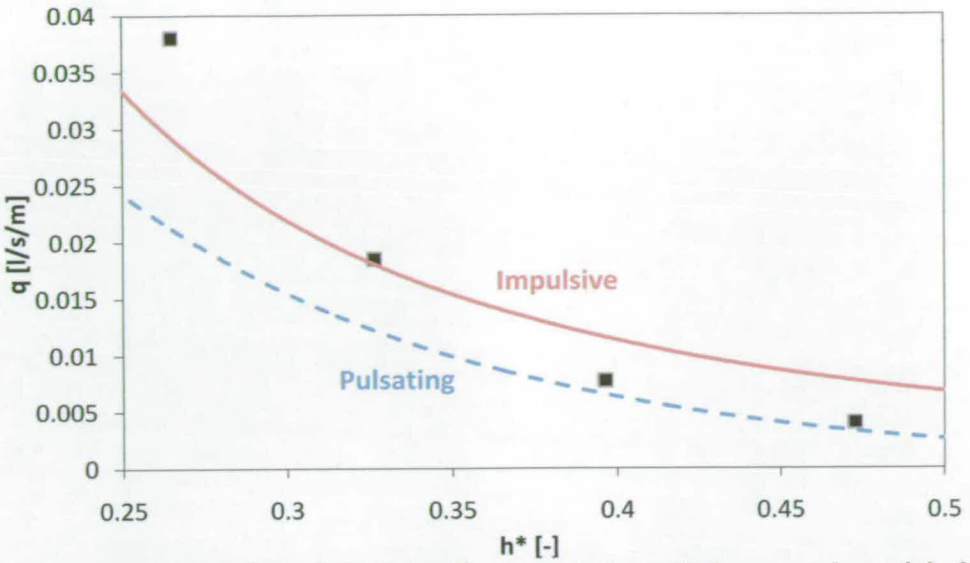

Figure 5.8 Theoretical (EA-Manual) overtopping discharge values (q) for breaking (impulsive) and non-breaking (pulsating) conditions. Data points represent measured values for the s_{op} = 0.04 test series (§3.6.2)

The trend observed for the s_{op} = 0.04 test series (Figure 5.8) is similar to that observed for the s_{op} = 0.02 results (Figure 5.7). The least extreme seas appear to correspond to the pulsating prediction with the more extreme seas agreeing with the impulsive formulae. The results illustrated in Figure 5.8 appear to suggest that the two largest seas are predominately impulsive. It is worth considering that these are empirical equations based upon datasets with considerable scatter. It is not, therefore, unreasonable that a sea with an h^* value of little over 0.3 should exhibit impulsive overtopping behaviour. It is also feasible that all these seas were primarily pulsating at the structure, and have simply resulted in larger than predicted discharge values for that sea. The values obtained are all within a factor of two of the pulsating prediction, which represents fairly typical scatter for this type of prediction. This explanation would agree with the qualitative observations of the tests, which suggested a fairly limited number of impulsive overtopping events. The discrepancy with the s_{op} = 0.02 dataset may conceivably be caused by steeper waves in the s_{op} = 0.04 dataset creating more impulsive-like events as they impact the seawall. Further investigation of this phenomenon would likely require more data than was collected during the course of this research. In particular, video recording

at the structure would be of interest to establish the overtopping mechanism of individual waves.

The issue of greatest significance to the Importance Sampling method is to establish whether moving from one predominant response regime to another adversely affects the effectiveness of the technique. *In extremis*, this will clearly be the case. It would not be feasible to infer the behaviour of a Design Sea containing solely pulsating waves from an Extreme Sea containing solely impulsive waves. In reality, this would represent a very large inflation of the Design Sea spectrum. The nature of the overtopping response is, at present, defined by the predominant behaviour. If the Extreme Sea produces design wave group(s) at a greater frequency than the Design Sea, even if the response of this wave group differs from the predominant behaviour, then the principles of the Importance Sampling method remain true. It is also worth noting that the most extreme response from a particular sea exhibit different behaviour than the predominant behaviour. In a pulsating sea it is possible that the extreme response will relate to a violent overtopping event. The Importance Sampling method will produce more of these rare impulsive events. The projected benefits of the Importance Sampling method in describing non-linear behaviour are discussed in §5.2.1.

5.4 Multivariate Data Filtering

5.4.1 Data Filtering Methodology

The Wave-Exclusion Importance Sampling method outlined in §5.2.3 is illustrated using univariate distributions. This was the method originally considered as the basis of technique. Based upon a chosen upper quantile the Extreme data would be filtered based upon the distributions of the chosen parameters. Based upon these individual parameters, the measurements taken within this filtered Extreme Sea dataset would be within the limits of the Design Sea. Recalling that the purpose of the wave-exclusion method is to produce a dataset containing only waves representative of the Design Sea, but with a greater number of extreme waves (and events), suggests that this technique

would initially appear to be valid. Examining the bivariate distributions, however, highlights the limitation of this technique.

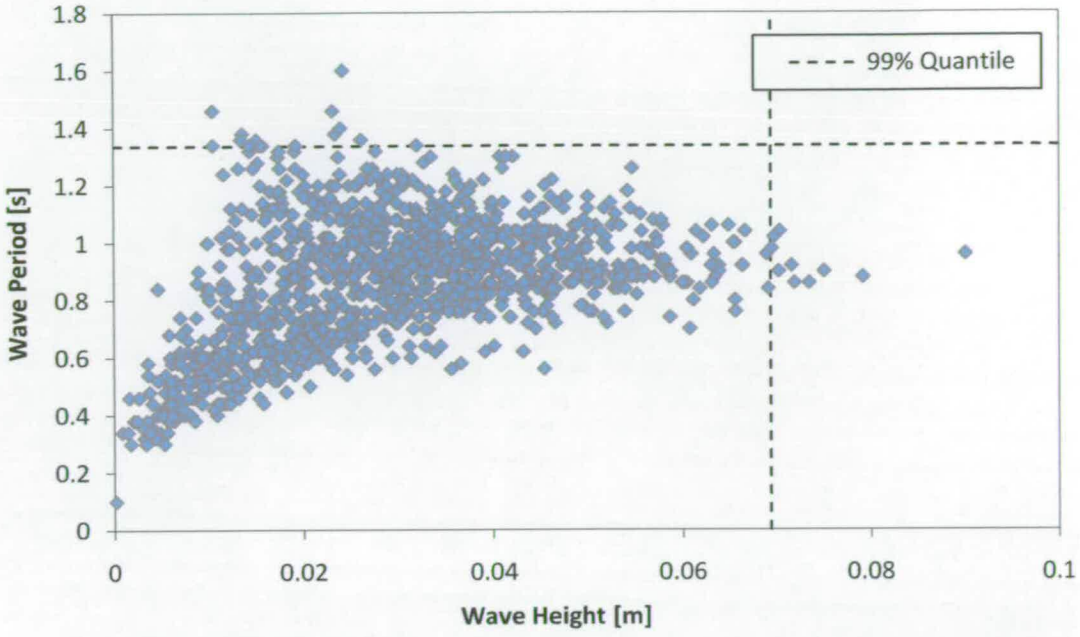

Figure 5.9 Joint-Distribution of Height and Period. (s_{op} = 0.04. Test Reference: 4AYcal1).

The bivariate distribution in Figure 5.9 illustrates a typical theoretical joint distribution of wave height and period. The data in this example is measured in the wave flume in shallow water (test reference 4AYcal1). The upper limits of the individual parameters are shown, as determined from their respective univariate distributions. It is clear that serial filtering by single parameters will produce a "square-edged" distribution, as illustrated by the 99% quantiles in Figure 5.9, which does correspond to the shape of the data "cloud". The obvious solution to this univariate data-exclusion problem is to instead use joint-probability distributions for the filtering process which account for the relationships between the multiple parameters. These distributions may be produced from theory or from empirical fitting, as discussed below (§5.5).

The filtering process for single joint-probability distribution is identical to that applied to the single univariate case. That is, the data lying outwith a particular quantile level are removed from the dataset.

5.4.2 Bivariate Filtering

Multivariate (joint) probability distributions may, in theory, describe the relationship between many variables. In reality, it is usually impractical to describe the relationship between large numbers of variables with a single probability distribution. This so called "curse of dimensionality" is particularly damaging to estimates at the extreme of a distribution (Wand & Jones, 1995). In the context of the Importance Sampling technique, it is unlikely that the end user will be satisfied with a limit of only 2-3 variables. It is also clear, however, that a univariate approach cannot account for any interaction between variables, as discussed above.

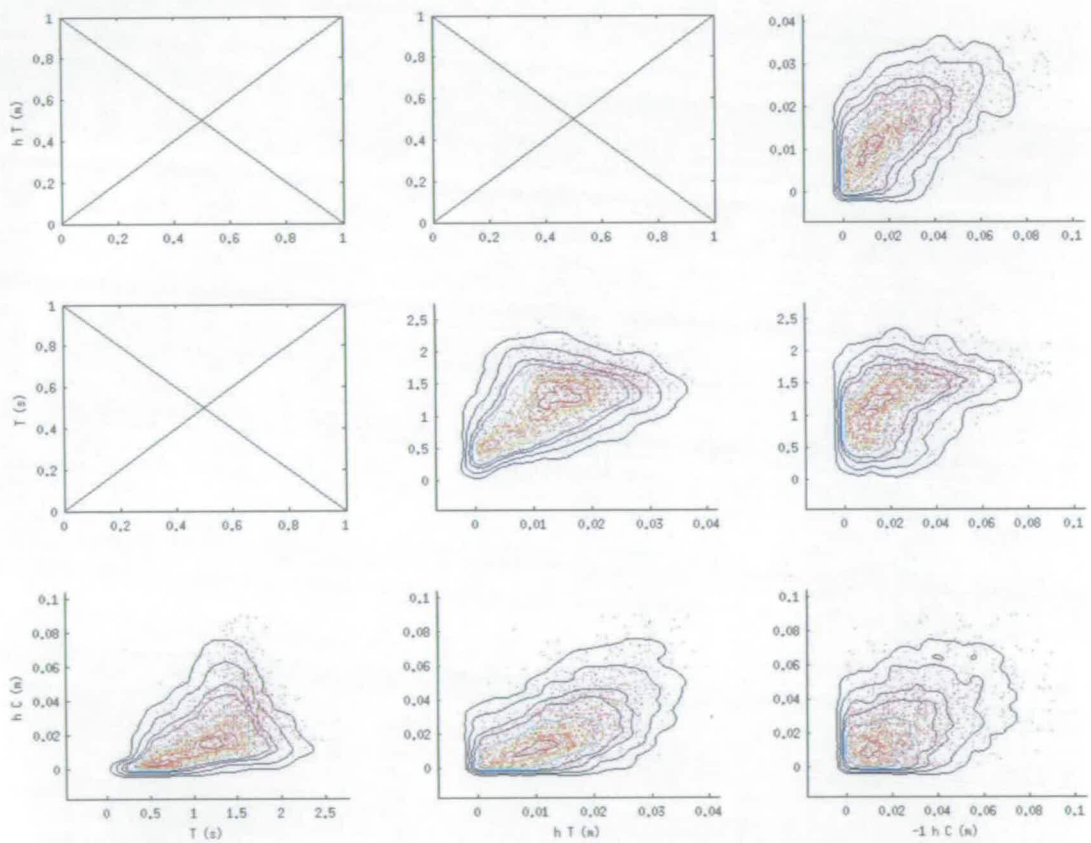

Figure 5.10 KDE bivariate probability matrix for four parameters. Outer contours represent 99.9% non-exceedance.

The approach taken is to conduct the filtering process based upon a matrix of bivariate distributions, accounting for joint relationships on a "parameter-pair" basis. An example of a bivariate distribution matrix is illustrated in Figure 5.10

for four variables. The total number of distributions in the matrix is derived from the binomial coefficient:

$$N_{distributions} = \frac{N_{parameters}!}{2 \cdot (N_{parameters} - 2)!} \tag{54}$$

The use of bivariate distributions retains the flexibility of the Importance Sampling method (by allowing the use of non-parametric techniques) while accounting for the interaction between the measured wave parameters. More complex multivariate methods are difficult, if not effectively impractical, to implement and are unlikely to be suited to the Kernel Density Estimation method (KDE - §5.5) utilised here.

The final filtering consideration is the choice of quantile at which the filtering process should be applied. Ideally the non-exceedance level should be set at 100% to prevent a non-conservative output from the filtering process. The often asymptotic nature of the probability distributions, however, makes this impractical. The upper filtering bound was, therefore, set at 99.9%, deemed to be the highest practical limit for the KDE method (see §5.5).

5.5 Kernel Density Estimation

5.5.1 Kernel Density Estimation Basics

Kernel Density Estimation (KDE) is a non-parametric technique for fitting distributions to a set of data. The Importance Sampling technique, as implemented here, is heavily reliant on this technique for fitting distributions to Design Sea measurements. This section aims to give an outline of the KDE method as implemented in this research. The formulae and methods outlined below have been implemented either in custom MATLAB functions or in functions incorporated in the WAFO toolbox. Where not otherwise referenced, the formulae detailed below are as given by Wand & Jones (1995).

The simplest non-parametric fitting technique is probably the histogram. While useful for visualising data, histograms have the disadvantage that the centre

position and size of each bin may strongly influence the resulting shape of the distribution. A further disadvantage is that the resulting distribution consists of a series of step changes, rather than a smoothed continually varying curve.

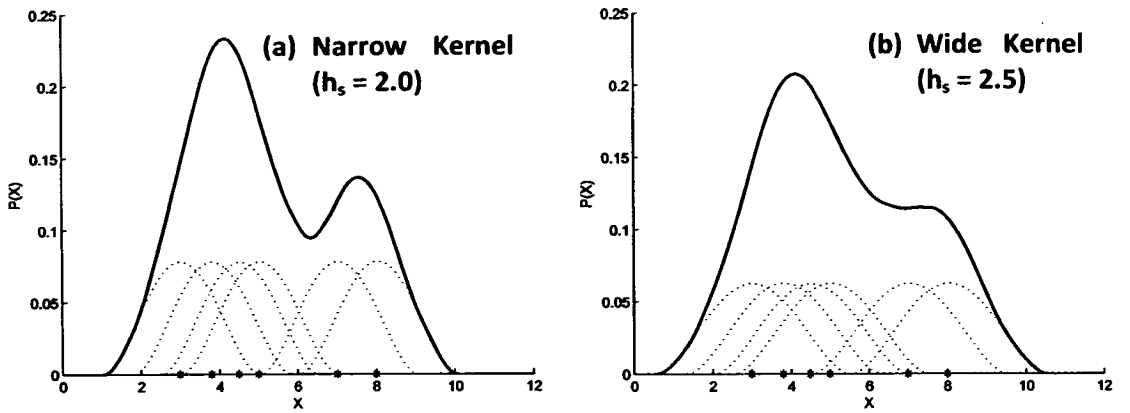

Figure 5.11 Univariate kernel density estimates for a small dataset. Examples a given for two kernel sizes ("bandwidths").

KDE methods are similar in concept to the histogram, but crucially avoid the requirement to bin the data. Instead an individual "kernel" is placed at the location of each data point. Superposition of these kernels produces an estimate of the shape of the probability distribution. A simple example of this technique using six data points is illustrated in Figure 5.11. The size of the individual kernel is determined by its "bandwidth" (h). It may be observed that increasing the bandwidth (Figure 5.11(b) over Figure 5.11(a)) results in increased smoothing of the distribution, as well as slightly extending the extreme tails of the curve. Care must be taken that the chosen bandwidth neither over nor under-smoothes the estimated probability density distribution, as discussed in detail below.

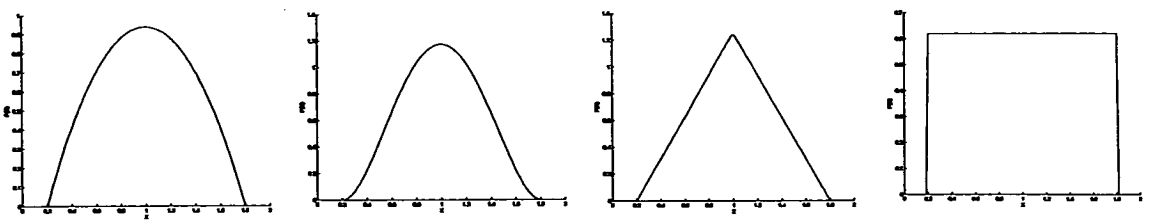

(a) Epanechnikov **(b) Biweight** **(c) Triangular** **(d) Rectangular**

Figure 5.12 Commonly used kernel shapes

In addition to the kernel bandwidth, a variety of shapes are available to describe the individual kernels. Four common kernel shapes (Epanechnikov, Biweight, Triangular and Rectangular) are illustrated in Figure 5.12. The Gaussian (normal) kernel is also commonly used. It is noted by Wand & Jones (1995) that kernel shape is of considerably less importance than the kernel width (bandwidth) in influencing the estimated distribution. Wand & Jones (1995) suggest that the Epanechnikov kernel is optimal. It is noted, however, that other kernels are only marginally less effective. The Epanechnikov kernel has, therefore, been used throughout this research, with investigations concentrating on the selection of the bandwidth parameter.

The examples illustrated above (Figure 5.11 and Figure 5.12) outline the approach in producing univariate density estimations. The extension of the technique to multivariate estimation, as required for this research, is conceptually straightforward. In the bivariate case a two dimensional kernel is applied. The bandwidth may vary for the two dimensions and the axes of the kernel may be rotated from the coordinate axes. This process may be applied to higher dimensions, but easy visualisation is not possible above three dimensions.

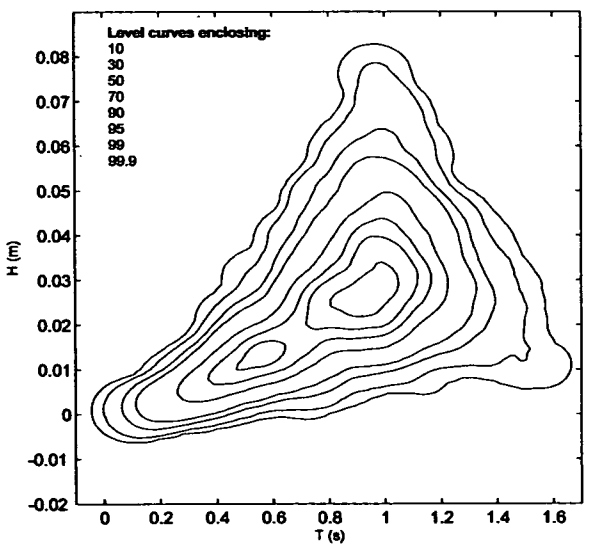

Figure 5.13 Contour plot illustrating quantile levels for joint-distribution of wave height and period

Once the probability density has been estimated for the dataset, it is straightforward to calculate the quantile levels, as illustrated in Figure 5.13. This is most easily applied by numerical integration of the probability distribution surface, which is returned by the software (custom MATLAB and WAFO toolbox functions) as a matrix map.

5.5.2 Multivariate Kernel Density Estimation

A univariate kernel density estimate is made up of individual kernels (k) summed to describe a vector (z) representing a particular parameter (e.g. wave height). These individual kernels have the property:

$$\int k(z)dz = 1. \tag{55}$$

The fact that the integral of these individual kernels is defined and finite allows for these kernels to be easily scaled such that the resulting formulation correctly represents a probability density distribution, as is described in detail below. This research utilises the Epanechnikov kernel (Epanechnikov, 1969), described in univariate form as

$$k(z) = \frac{3}{4}(1 - z^2) \cdot 1_{\{|z|<1\}}. \tag{56}$$

In order to describe a d-variate, n-length, dataset $(\mathbf{X}_1,\ldots,\mathbf{X}_n)$ a multivariate version of the kernel is required. Each data will contain d-number of values, with the components notated as:

$$\mathbf{X}_i = [X_{i1}, \ldots, X_{id}]^T. \tag{57}$$

Similarly, the vector (x) of d-number parameters is represented thus:

$$\mathbf{x} = [x_1, \ldots, x_d]^T. \tag{58}$$

The multivariate kernel is derived from the univariate formula to produce a radially symmetric kernel in d dimensions. In the case of Epanechnikov formula the kernel will take the form (Silverman, 1986):

$$K(\mathbf{x}) = \frac{1}{2 \cdot c_d}(d+2)(1-\mathbf{x}^T\mathbf{x}) \cdot 1_{\{\mathbf{x}^T \cdot \mathbf{x}<1\}} \tag{59}$$

where c_d represents the unit volume of a d-dimensional sphere:

$$c_d = \frac{\pi^{d/2}}{\Gamma\left(\frac{n}{2}+1\right)}. \tag{60}$$

It may be shown by inspection that the multivariate Epanechnikov kernel with d = 1 is identical to univariate version described in Equation (56). Similar to the univariate case (Equation (55)), the multivariate kernel satisfies the condition:

$$\int K(\mathbf{x})d\mathbf{x} = 1. \tag{61}$$

In order to apply the KDE method effectively it is usually necessary to rescale, and possibly rotate, the kernel. This is achieved through the application of a bandwidth matrix to produce a rescaled kernel formula ($K_{\mathbf{H}}$):

$$K_{\mathbf{H}}(\mathbf{x};\mathbf{H}) = |\mathbf{H}|^{-1/2} \cdot K\left(\mathbf{H}^{-1/2} \cdot \mathbf{x}\right). \tag{62}$$

The bandwidth values ($h_1,\ldots,h_{1/2d(d+1)}$) are described in a symmetric "bandwidth matrix" (**H**). In the bivariate case this matrix takes the form:

$$\mathbf{H} = \begin{bmatrix} h_1^2 & h_3^2 \\ h_3^2 & h_2^2 \end{bmatrix}. \tag{63}$$

If there is no rotation applied to the kernel the value of h_3 will be zero, with the bandwidth matrix taking the form

$$\mathbf{H} = \mathbf{I} \cdot \left[h_1^2, \ldots, h_d^2\right]^T, \tag{64}$$

where **I** is the identity matrix.

Finally, the estimated probability density function ($\hat{f}(\mathbf{x})$) may be calculated through summation of the scaled kernels:

$$\hat{f}(\mathbf{x}) = n^{-1} \sum_{i-1}^{n} K_{\mathrm{H}}(\mathbf{x} - \mathbf{X}_i). \tag{65}$$

5.5.3 Kernel Rotation

The rotated and scaled kernel is easily visualised in two-dimensional space, as illustrated later in this chapter. In the case of identical scaling (constant bandwidth) and no rotation, the kernel will be symmetrical around the axes. In reality, it is noted by Wand & Jones (1995) that it is rarely practical to apply identical smoothing in all dimensions. This is intuitively true when dealing with joint-distributions describing variables of differing scale and magnitude, such as wave-height and wave-period. The benefits of using rotated kernels are less clear. In a bivariate distribution Wand & Jones (1995) suggest that the benefits of kernel rotation are marginal when both variables are normally distributed. This is not the case, however, when the dataset is non-Gaussian. The efficiency[13] of the density estimation fell to a low of approximately 25% when using non-optimally rotated kernels in the presented study. Given the non-Gaussian nature of many of the parameters measured in coastal waters it was deemed that the use of rotated kernels should be explored in the application of the Importance Sampling method.

The two bandwidths (for the bivariate case) and the rotation angle are a function of all three bandwidth parameters ($h_{1...3}$) contained with the bandwidth matrix **H** described in Equation (63). A simple "blind" optimisation may not require knowledge of the actual rotation angle and smoothing along the rotated axes. If, however, it is desirable to exert constraints, or a fixed rotation angle, the bandwidth matrix must be translated to a more manageable form. The three parameters required are:

---

[13] Wand & Jones (1995) measured efficiency using the Asymptotic Relative Efficiency (ARE) criterion. In simple terms this technique compares the quality-of-fit of one distribution (e.g. rotated kernel estimation) with the quality-of-fit of another distribution (e.g. non-rotated kernel estimation). The "quality-of-fit" is determined through comparison of the estimated distribution (KDE) with the parent distribution from which the dataset was generated. The disagreement between these distributions was calculated by Wand & Jones using the Asymptotic Mean Integrated Square Error (AMISE).

h_X : The bandwidth along the rotated X axis,

h_Y: The bandwidth along the rotated Y axis,

Θ: The angle of rotation [rads].

Neither Wand & Jones (1995) nor Silverman (1986) detail this relationship. It may, however, be deduced through comparison to the standard rotation matrix. In the bivariate case this will take the form:

$$\mathbf{H}^{-1/2} = \begin{bmatrix} {h_X}^2 & 0 \\ 0 & {h_Y}^2 \end{bmatrix}^{-1/2} \cdot \begin{bmatrix} \cos\theta & \sin\theta \\ -\sin\theta & \cos\theta \end{bmatrix} = \begin{bmatrix} h_X \cdot \cos\theta & h_X \cdot \sin\theta \\ -h_Y \cdot \sin\theta & h_Y \cdot \cos\theta \end{bmatrix} \tag{66}$$

Rewriting the bandwidth matrix in the same form ($\mathbf{H}^{-1/2}$):

$$\mathbf{H}^{-1/2} = \begin{bmatrix} h_1^2 & h_3^2 \\ h_3^2 & h_2^2 \end{bmatrix}^{-1/2} = \begin{bmatrix} a & c \\ c & b \end{bmatrix} \tag{67}$$

The matrix inverse square root calculation required in Equation (67) is not necessarily trivial. It is, however, easily carried out in software packages such as MATLAB. The following formulae will therefore refer to the three resultant parameters (a, b ,c).

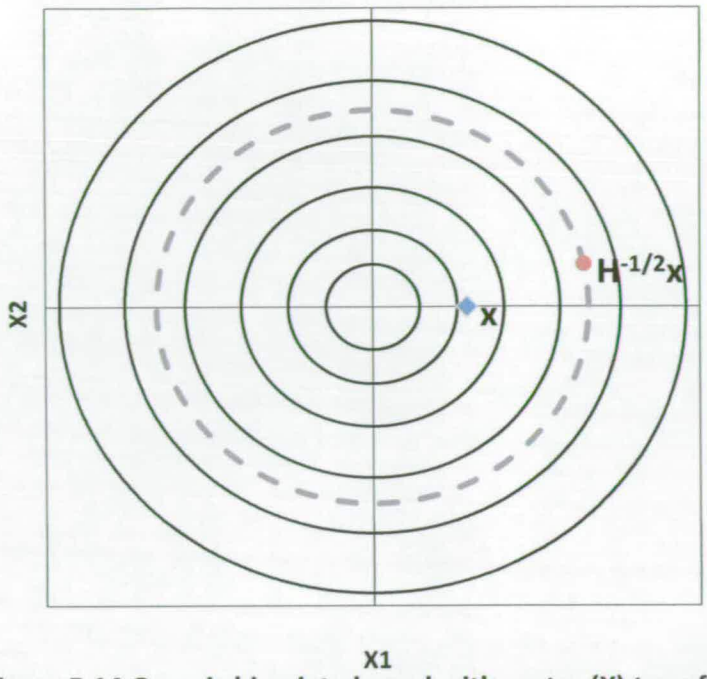

Figure 5.14 Generic bivariate kernel with vector (X) transformed by the bandwidth matrix (H).

Inspection of Equations (66) and (67) reveal that these bandwidth matrices cannot be directly equivalent, as the matrix in Equation (66) is not necessarily symmetrical, unlike the standard bandwidth matrix. Indeed, Equation (66) will only be symmetrical in the case where there is no applied rotation. In order to understand how these two forms of the bandwidth matrix can produce equivalent results it is important to note the radially symmetrical nature of the bivariate kernel, a generic example of which is illustrated in Figure 5.14. A vector ($\mathbf{x}$) is transformed by the bandwidth matrix ($\mathbf{H}$) to affect the rotation and smoothing. This transformed vector has the value $\mathbf{H}^{-1/2}\mathbf{x}$ (see Equation (62)). Inspection of the kernel in Figure 5.14 illustrates that any vector lying the same distance from the origin as $\mathbf{H}^{-1/2}\mathbf{x}$ will produce the same kernel density value. In other words, the two forms of the bandwidth matrix will give identical results if the magnitude of $\mathbf{H}^{-1/2}\mathbf{x}$ is identical for given values of h_X, h_Y and Θ. It is also noted from Equation (62) that both forms of the bandwidth matrix must have equal determinants. This relationship gives rise to the following four equations:

$$a^2 + c^2 = (h_X \cdot \cos\theta)^2 + (h_Y \cdot \sin\theta)^2 \qquad (68)$$

$$b^2 + c^2 = (h_X \cdot \sin\theta)^2 + (h_Y \cdot \cos\theta)^2 \tag{69}$$

$$c \cdot (a + b) = \sin\theta \cdot \cos\theta \cdot (h_X^2 - h_Y^2) \tag{70}$$

$$a \cdot b - c^2 = h_X \cdot h_Y \tag{71}$$

Combining these formulae allows transformation of the standard three parameter bivariate bandwidth matrix (Equation (63)) to the form h_X, h_Y and Θ.

$$h_X = \frac{1}{4} \cdot \left[\frac{a^2 - b^2}{\cos 2\theta} + a^2 + b^2 + 2 \cdot c^2\right]^{-1/2} \tag{72}$$

$$h_Y = \frac{1}{4} \cdot \left[\frac{b^2 - a^2}{\cos 2\theta} + a^2 + b^2 + 2 \cdot c^2\right]^{-1/2} \tag{73}$$

$$\theta = \frac{1}{2} \cdot \arctan\frac{2 \cdot c}{a - b} \tag{74}$$

The reverse transformation is given by the formulae:

$$a = [(h_X \cdot \cos\theta)^2 + (h_Y \cdot \sin\theta)^2 - c^2]^{-1/2} \tag{75}$$

$$b = [(h_X \cdot \sin\theta)^2 + (h_Y \cdot \cos\theta)^2 - c^2]^{-1/2} \tag{76}$$

where

$$c = \frac{h_X - h_Y}{2} \cdot \sin 2\theta \tag{77}$$

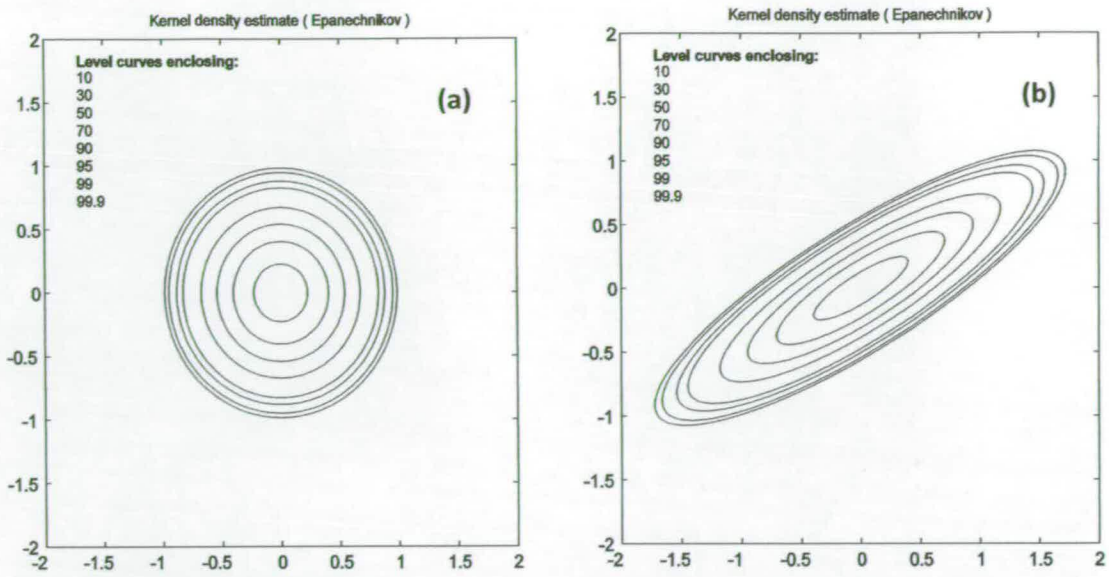

Figure 5.15 Radially symmetrical kernel (a) and reshaped and rotated kernel (b) with h_X = 2, h_Y = 0.5 and $\Theta = \pi/6$.

The result of the **x** vector transformation process illustrated in Figure 5.14 is that the radially symmetric kernel (K) is transformed into a rescaled and rotated kernel (K_H). This process is illustrated by the kernels plotted in Figure 5.15. The bandwidth matrix **H** was produced using Equations (75) to (77) to give a rotation angle of $\pi/6$ radians. The bandwidth parameters for the rotated axes were set to $h_X = 2$ and $h_Y = 0.5$. The kernel shapes were produced using the WAFO MATLAB toolbox, which has the capacity to take an externally calculated bandwidth matrix as an input.

The method outlined above for calculating the kernel reshaping properties allows for more intuitive and transparent investigation of the KDE method when compared to the standard three-parameter bivariate bandwidth matrix (Equation (63)). A particular strength is the ability to prescribe a particular rotation angle, leaving only two bandwidth parameters to be optimised. This is not possible with the standard matrix as the rotation angle is a property of all three parameters ($h_{1...3}$).

5.5.4 Bandwidth Estimation – Normal Scale Rule

The value of the kernel bandwidth is extremely important for optimising the estimated probability distribution for a set of data. A variety of methods are available for estimating the bandwidth values. Only a fairly small subset is appropriate, however, for the purposes of this research. The main requirement for the density methods in the Importance Sampling method is that they are entirely data-driven. That is, they are estimated based only upon the information garnered from the input dataset. This allows the greatest degree of flexibility in applying the Importance Sampling method, as the kernel density estimates need not be "tuned" as new or drastically altered parameters are selected for inclusion in the analysis.

A commonly applied method as described by Silverman (1986) and Wand & Jones (1995) is the "normal scale rule". This technique optimises the bandwidth parameter for a normally distributed dataset. The bandwidth value (h_s) is given as

$$h_s = \left[\frac{8 \cdot \pi^{1/2} \cdot R(k)}{3 \cdot \mu_2(k)^2 \cdot n}\right]^{1/5} \cdot \sigma \tag{78}$$

where

$$R(k) = \int k(x)dx, \tag{79}$$

$$\mu_2(k) = \int z^2 \cdot k(z)dz \tag{80}$$

and n is the total number of samples. The example above describes a univariate case. In order to calculate the bandwidth matrix (**H**) for a multivariate dataset the above equations are applied to each dimension in turn.

The primary advantage of the normal scale method is that it is easily applied with minimum of computational effort. The clear disadvantage is that it will give sub-optimal performance where the dataset is not normally distributed. This

tends to manifest itself in over-smoothing of distribution (Wand & Jones 1995). This is potentially significant as many wave parameter distributions show significant bias away from Normal distributions. It also does not allow for easy calculation of kernels with rotated axes, or for estimation of the smoothing parameter (§5.5.2).

The limitations of the normal scale rule are not necessarily fatal to the application of the technique. This research is primarily concerned with accurately describing the behaviour near the boundaries of the dataset. In the case of the wave-exclusion method (§5.2.3) the main requirement is to produce a filtering "window" through which the most extreme data is removed from the dataset. If over-smoothing has little influence on the extremes of the distribution the filtering process will be relatively unaffected.

5.5.5 Bandwidth Estimation – Least Squares Cross Validation (LSCV)

The second method explored for estimation of the bandwidth is the technique of Least Squares Cross-Validation (LSCV) as described by Silverman (1986) and Wand & Jones (1995). This method, as with the normal scale rule (§5.5.4), is fully automatic, being reliant only on the inputted dataset.

The LSCV estimator operates by examining the sensitivity of removing a single data sample on the estimate of the distribution. In essence, the distribution is calculated using the complete dataset (n samples) and then recalculated using the dataset with a single datum removed (n-1 samples). The error between these distributions is calculated for each sample in turn to give a measure of the "averaged" error. This process is repeated as required in order to iterate an optimal values of the bandwidth matrix (**H**).

The LSCV value is calculated from

$$\mathrm{LSCV}(\mathbf{H},K_{\mathbf{H}}) = \int \hat{f}(\mathbf{x};\mathbf{H},K_{\mathbf{H}})^2 d\mathbf{x} - 2\cdot n^{-1}\sum_{i=1}^{n}\hat{f}_{-1}(\mathbf{X}_i;\mathbf{H},K_{\mathbf{H}}) \qquad (81)$$

where the "leave-one out" density estimator is given by

$$\hat{f}_{-1}(\mathbf{X}_i; \mathbf{H}, K_{\mathbf{H}}) = (n-1)^{-1} \sum_{j \neq i}^{n} K_{\mathbf{H}} \cdot (\mathbf{x} - \mathbf{X}_j). \tag{82}$$

The minima of LSCV(**H**) will correspond to the estimated optimal bandwidth matrix (**H**). Unlike the normal scale rule (§5.5.4) this method allows the inclusion of rotated kernels as the bandwidth matrix may be optimised in its entirety. The normal scale rule only allows for estimates of individual variants.

In order to apply the LSCV technique of the bandwidth matrix it is necessary to select a range of bandwidth values over which to conduct the optimisation. The approach suggested by Wand & Jones (1995) is to select an upper bound for the bandwidth parameters using the "oversmoothed" bandwidth (h_{os}):

$$h_{os} = \left[\frac{243 \cdot R(k)}{35 \cdot \mu_2(k)^2 \cdot n}\right]^{1/5} \cdot \sigma \tag{83}$$

where σ is the standard deviation of the sample, n is the number of samples and $R(k)$ and $\mu_2(k)$ are described in Equations (79) and (80). As the name suggests, the oversmoothed bandwidth parameter describes a bandwidth with a bandwidth known to be larger than the optimal value. It is also observed, through comparison with Equation (78), that the relationship with the normal scale bandwidth (h_s) may be shown to be:

$$\frac{h_s}{h_{os}} = 0.93 \tag{84}$$

The attractiveness of the LSCV technique lies in the lack of assumptions required in selecting the values of KDE parameters (**H**, α etc.). This is in line with the philosophy and requirements of the Importance Sampling method (§5.2.1). The major disadvantage is the increased computational effort required.

5.6 Filtered Dataset Analysis

5.6.1 Definition of Extreme Values

The Importance Sampling method, as detailed above (§5.2), delivers a filtered dataset of waves and their associated measured responses. This filtered extreme sea dataset is intended to contain waves representative of the design sea condition, but with the response distribution shifted to produce proportionally more of the largest magnitude events. A major challenge in applying the Importance Sampling technique is the analysis and interpretation of this extreme sea dataset.

The simplest value for characterising the extreme overtopping response is V_{max}, the largest single value obtained from a given record. The average value of V_{max} will increase with the length of the test, due to its probabilistic nature. V_{max} is a function of the test length. Straightforward comparisons of V_{max} values can therefore only be made for tests of the same length[14].

If the Importance Sampling method has been applied effectively all the results contained within the filtered extreme sea dataset should be representative of the design sea conditions. The largest results obtained from the filtered dataset should therefore represent design sea overtopping volumes. It is difficult, however, to put these measurements in context in terms of V_{max}. The filtered dataset is effectively equivalent to a certain number of repeat tests with the design sea. If a functional relationship between the overtopping response (i.e. its magnitude) and the contemporaneous wave climate could be known it would be possible to relate the value of N_w in the extreme sea to an equivalent N_w for the design sea conditions. Given this information it would be possible to identify *N* maximum overtopping events in the filtered extreme sea dataset for a given design N_w. Indeed, this is the approach originally considered as the basis of the Importance Sampling method (Wave Identification - §5.2.2).

[14] Test length is defined here as the total number of waves (N_w).

The Importance Sampling method applied here assumes there is no known functional relationship between the measured individual wave parameters and their associated overtopping volume (Wave Exclusion – §5.2.3). While this presents advantages in terms of flexibility, it also prevents easy analysis of the V_{max} values. The alternative that has been explored has been to calculate the maximum overtopping values in terms of exceedance probabilities.

The exceedance value (e.g. $V_{1\%}$) is not strictly dependent on test length, although confidence in the calculated results will decrease for shorter tests (§4.5.4). Characterising the extreme behaviour in terms of a certain exceedance probability sidesteps the problem of defining a particular "Design Sea equivalent test length" for the filtered Extreme Sea dataset.

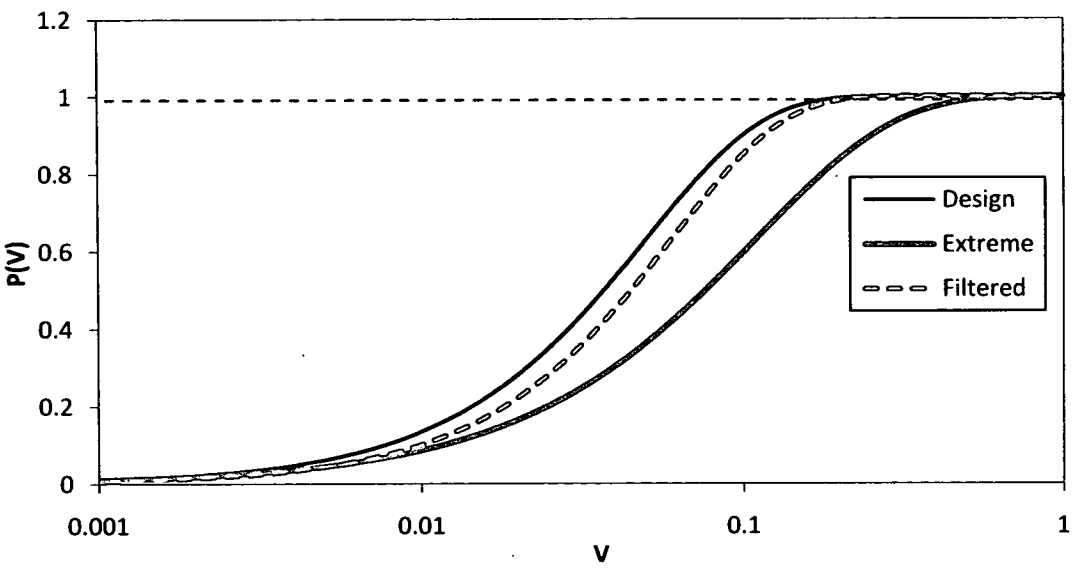

Figure 5.16 Idealised overtopping volume CDF distributions (Weibull) for Design, Extreme and Filtered seas.

The nature of the Importance Sampling technique produces different probability distributions for the design sea and the filtered extreme sea datasets. The filtered extreme sea is shifted to produce more occurrences of the largest events. This behaviour is observed clearly in the example data presented in Figure 5.16. If the Importance Sampling technique has been applied successfully, the Design Sea and filtered Extreme Sea distributions should converge to produce similar tails. Low exceedance overtopping volumes are

therefore expected to converge for the design and filtered extreme seas, as illustrated in the example in Figure 5.16.

5.6.2 Block Value Analysis

The Importance Sampling method is proposed as a tool for improving the "efficiency" of random wave model testing. In essence the goal is to shorten the test length without impairing the accuracy of the obtained results. It is proposed, therefore, that changes in efficiency brought about by the Importance Sampling method are simply defined by the reduction in test length achieved. This term will be referred to as the Filtering Coefficient defined as:

$$Filtering\ Coefficient = \frac{N_{w\_Extreme}}{N_{w\_Design}} \tag{85}$$

Thus a lower value of the filtering coefficient indicates the need for a shorter Extreme Sea. It should be noted that test length has been defined in terms of the total number of waves (N_w). This is useful when comparing results from laboratory testing conducted at different scales. It would be equally correct to refer to test length in terms of time, assuming the test scale remains constant.

The move from the Design Sea to Extreme Seas of increasing Spectral Inflation Factors (I_s) will produce more overtopping results for a given test length. The test series conducted for assessing the Importance Sampling technique (§3.6.2) involved multiple repeat Design Sea tests, each of a nominal 1000 waves. The Extreme Sea test series were designed to produce approximately the same total number of overtopping events (N_{ow}) as the Design Sea dataset.

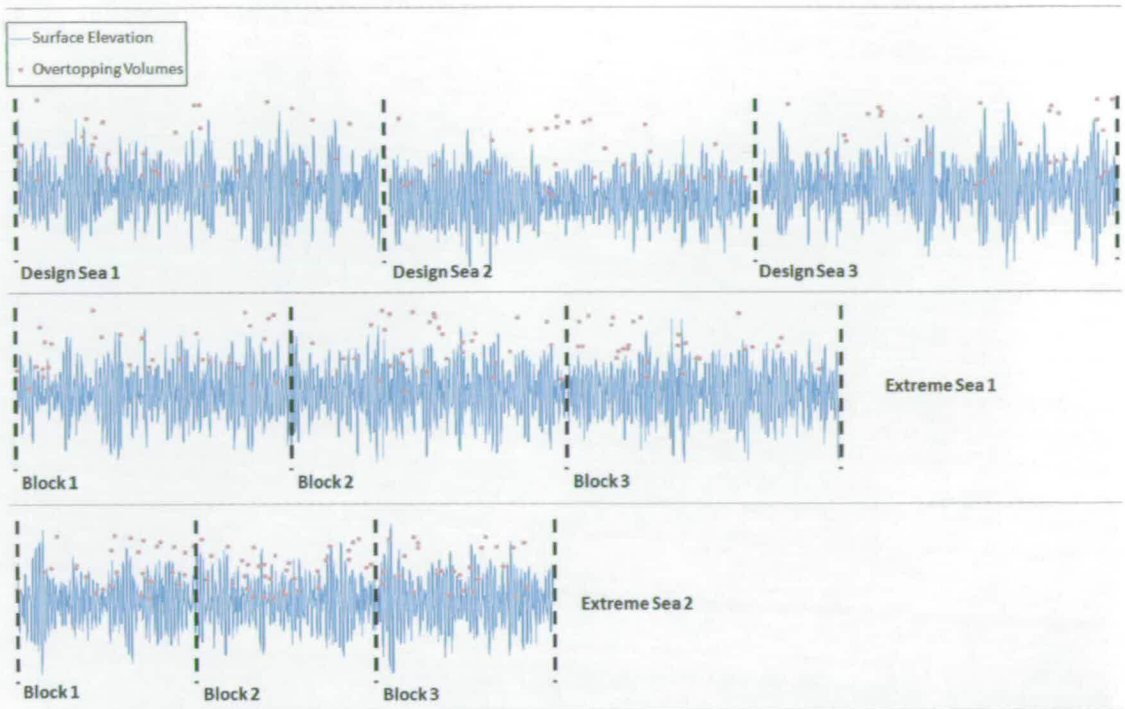

Figure 5.17 Hypothetical block analysis example (plots for illustration purposes only). Three Design Sea tests are replicated by two shorter Extreme Seas, each divided into three blocks. Each Extreme Sea block contains the same number of overtopping events as a single Design Sea test.

The analysis of a given Extreme Sea dataset involves combining the wave measurements, with associated overtopping values where appropriate, into a single long record. This record is then divided into equal length segments, with the number of segments equalling the number of Design Sea tests, as represented graphically in Figure 5.17. The average number of overtopping events within each "block" will be similar to the average number of overtopping events for each Design Sea test. Each of these blocks effectively represents a short duration test with the Design Sea. The Importance Sampling technique may then be applied to each of these blocks to produce a number of filtered Extreme Sea datasets.

The data within the filtered Extreme Sea blocks may then analysed in the same manner as outlined in §4.5. This analysis technique effectively holds the average value of N_{ow} constant, rather than working with a fixed test length (N_w). It would also be possible to vary the test length within the laboratory. The practicalities of this will depend of the facility. In the case of the wave flume used in this

experimental programme (§3.2.1) the test lengths are not infinitely adjustable and the record from a particular test would require trimming to adjust it to the predetermined length.

Setting the length of each block to produce the same N_{ow}, on average, as the Design Sea requires some *a priori* knowledge of the process (i.e. the value of N_{ow}). A practical application of the technique may be free from this constraint as the value of $V_{x\%}$ is independent of the test length, although confidence may be low for short tests. The block analysis approach would therefore be abandoned and $V_{x\%}$ calculated from the entire filtered Extreme Sea dataset. In the example outlined in §6 the block analysis approach is used to cross compare the Extreme Sea output with the baseline Design Sea values.

The combination of the tests into a single record assumes that the elevation time series may be treated as a stationary process. Given that each Extreme Sea test in a given series is produced from the same spectrum this assumption is valid. It should be noted the combined record was produced in such a way that the "breaks" between the tests were identified. This was to prevent anomalies when examining the influence of wave groups (e.g. the effect of the preceding waves on overtopping behaviour).

5.7 Summary

Two distinct, but related, versions of the Importance Sampling technique were proposed for detailed examination. The method selected (Wave Exclusion) is intended to avoid the requirement for a detailed functional relationship between individual wave parameters and the overtopping response. This methodology potentially offers significant flexibility in the application of the technique to overtopping modelling and other relatively poorly understood phenomena.

A non-parametric method (Kernel Density Estimation) was explored for the estimation of the Design Sea probability distributions required for the application of Importance Sampling. Kernel Density Estimation requires

relatively few assumptions regarding the underlying nature of the distribution and is therefore in keeping with the aim of producing a flexible methodology. The basis of the technique is explained along with several options for optimisation of the resulting probability distributions.

6 Importance Sampling Results and Analysis

6.1 Introduction

This chapter details the results obtained from the application of the previously described Importance Sampling technique (§5) to experimental vertical seawall overtopping measurements conducted at small scale (§3). The input wave parameters required to implement the technique are selected based on observations of the overtopping behaviour. The method is then implemented using these input conditions to produce estimates of V_{max} and $V_{1\%}$ for two different Design Seas.

The optimisation of the probability estimation procedure is examined and the effect on the Importance Sampling output presented

6.2 Importance Sampling Wave Parameters

6.2.1 Design Wave Groups

The Importance Sampling technique, in both Wave-Identification (§5.2.2) and Wave-Exclusion (§5.2.3) forms, requires a definition of the design wave group[15]. The requirement of this definition varies considerably between the two methods.

Wave Identification

The Wave-Identification method relies on a known functional relationship describing the expected response associated with a given wave group. This

[15] The term "wave group" is used loosely here. It may refer to a single wave, or even potentially a small portion of a single wave.

functional relationship need not precisely quantify the expected response associated with the wave group, but rather identify the most extreme wave groups within a given record. This is a non-trivial procedure given the potentially complex nature of the hydrodynamic response at a fixed or floating structure. In the case of wave overtopping the response has been observed to be non-linear, giving rise to the likelihood of multiple functional relationships. The response may also be non-monotonic when measured against certain parameters (e.g. wave height), further complicating attempts to identify the design wave group. The Wave-Identification Importance Sampling technique requires accurate identification of these design wave groups in order to be effective. It may be quite feasible to identify a subset of wave groups likely to produce large overtopping responses. This information is not sufficient, however, to identify the ratio of design wave group occurrence frequencies between the Design and Extreme Seas (Equation (50)).

Wave Exclusion

The definition of the design wave group required for the Wave-Exclusion technique is somewhat different. A detailed functional relationship between the wave group and the overtopping volume is not necessary. Instead, a subset of parameters describing the design wave group is required (§5.2.3). For example, in a simple scenario it may be sufficient to describe a wave only by its height. The Importance Sampling technique produces an upper bound for this parameter, but it is not necessarily the wave with the greatest height that produces the largest magnitude response. A more complex modelling scenario may, for example, require the inclusion of the wave period. The Wave-Exclusion process will now also exclude non-representative wave periods. Associated parameters, such as wave steepness, will also be filtered from the Extreme Sea dataset.

It is important to distil down the available range of wave group describing parameters to a small subset of significant measurements. A large number of parameters increases computational effort and also risks unnecessary "over-

filtering" of the dataset. Perhaps counter-intuitively, the conservative approach is to use a smaller number of filtering parameters. The selection of these parameters for use in the Wave-Exclusion Importance Sampling technique is outlined below.

6.2.2 Wave Parameters

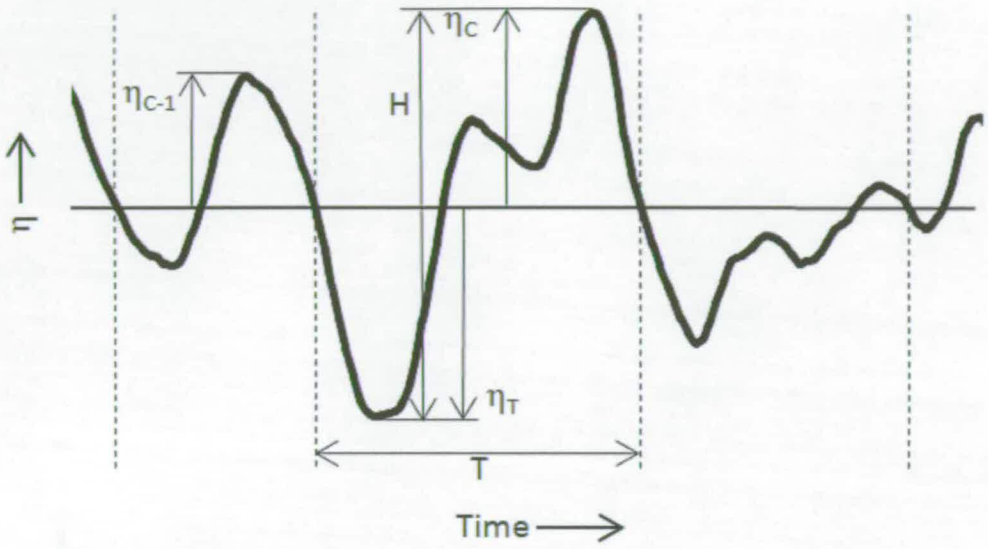

Figure 6.1 Generic wave group with labelled measurement parameters

The simplest wave parameters can be defined as being measured in space or time. Parameters produced from a point measurement (e.g. wave gauge) will produce measurements in terms of elevation (e.g. wave height) and period (e.g. down-crossing period, crest period etc.). These measurements may be considered to be "primary" parameters. All other "secondary" parameters (e.g. steepness, wavelength) are produced using these measurements.

The Wave-Exclusion Importance Sampling technique may be applied using only these primary parameters, and that is the approach taken here. This is consistent with the relatively scant knowledge describing the relationship between the individual wave form and the overtopping response. In modelling situations where a response function is better defined, more sophisticated parameters (e.g. crest front steepness) may be substituted into the filtering process. This approach may potentially improve the efficiency of the filtering

process by reducing the number of variates included in the KDE estimation stage.

Wave Elevation Parameters

An obvious parameter for characterising the vertical displacements of a wave is the wave height. This is simply defined as the difference between the maximum and minimum elevation between successive zero-crossings. In this research the convention is to use the zero-downcrossing method (e.g. Figure 6.1) unless otherwise stated. The wave height has the drawback, however, of not being measured against a fixed reference plane. The alternative approach is to define the waves using the crest (η_C) and trough (η_T) elevations directly. These measurements are taken from the still water level, providing a fixed frame of reference to the seawall structure.

Wave Period Parameters

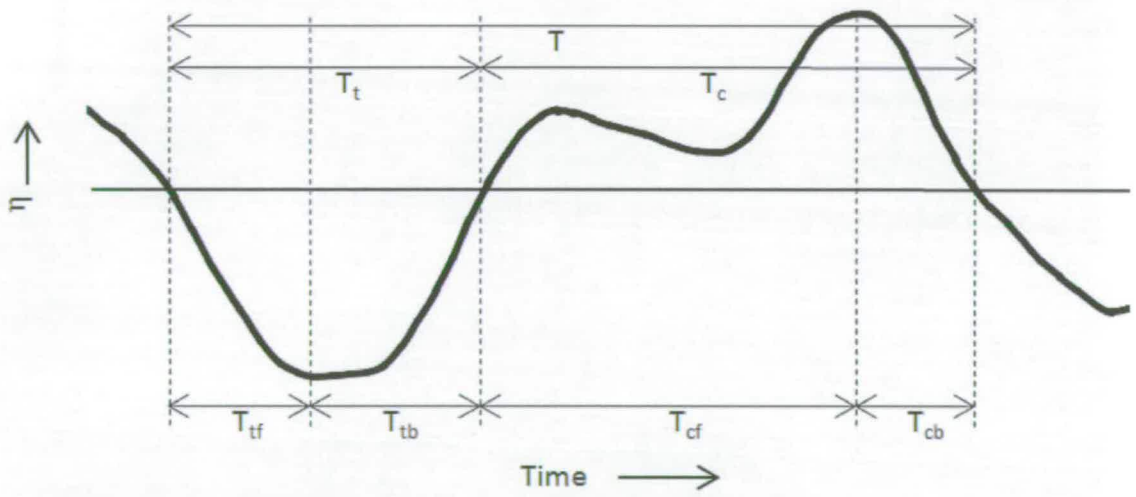

Figure 6.2 Generic wave with labelled period measurements

A variety of parameters are available for characterising the zero-crossing behaviour of an individual wave. The wave period (T) was measured using zero downcrossing analysis, as illustrated in Figure 6.2. The zero downcrossing method is intuitively appropriate for overtopping analysis as it defines an individual wave with the trough prior to the crest. This allows a steep crested wave to be logically defined in terms of its period and height.

Further parameters are available to characterise the wave in the time-domain (see e.g. Guedes Soares *et al.,* 2004). These include the crest and trough period (T_c and T_t respectively). The wave may be further subdivided into four constituent periods describing the front and back of the crest and trough. The notation in Figure 6.2 has been formulated for consistency, but it should be noted that there appears to be no convention for the naming of these parameters. The application of these wave period measurements has not been explored in this research, but it is suggested that they may be of relevance to future research. Several "steepness coefficients", as described by Guedes Soares *et al.* (2004) may be formulated using these measures. These may possibly provide future tools for the characterisation of wave-by-wave overtopping.

6.2.3 Wave Group Definition

The datasets from the X test series (§3.6.2) were examined to establish any dependence between the parameters discussed and the measured individual overtopping volumes. This analysis is not intended to produce a full functional relationship, but rather qualitatively highlight any relevant interactions between the wave group and the structure.

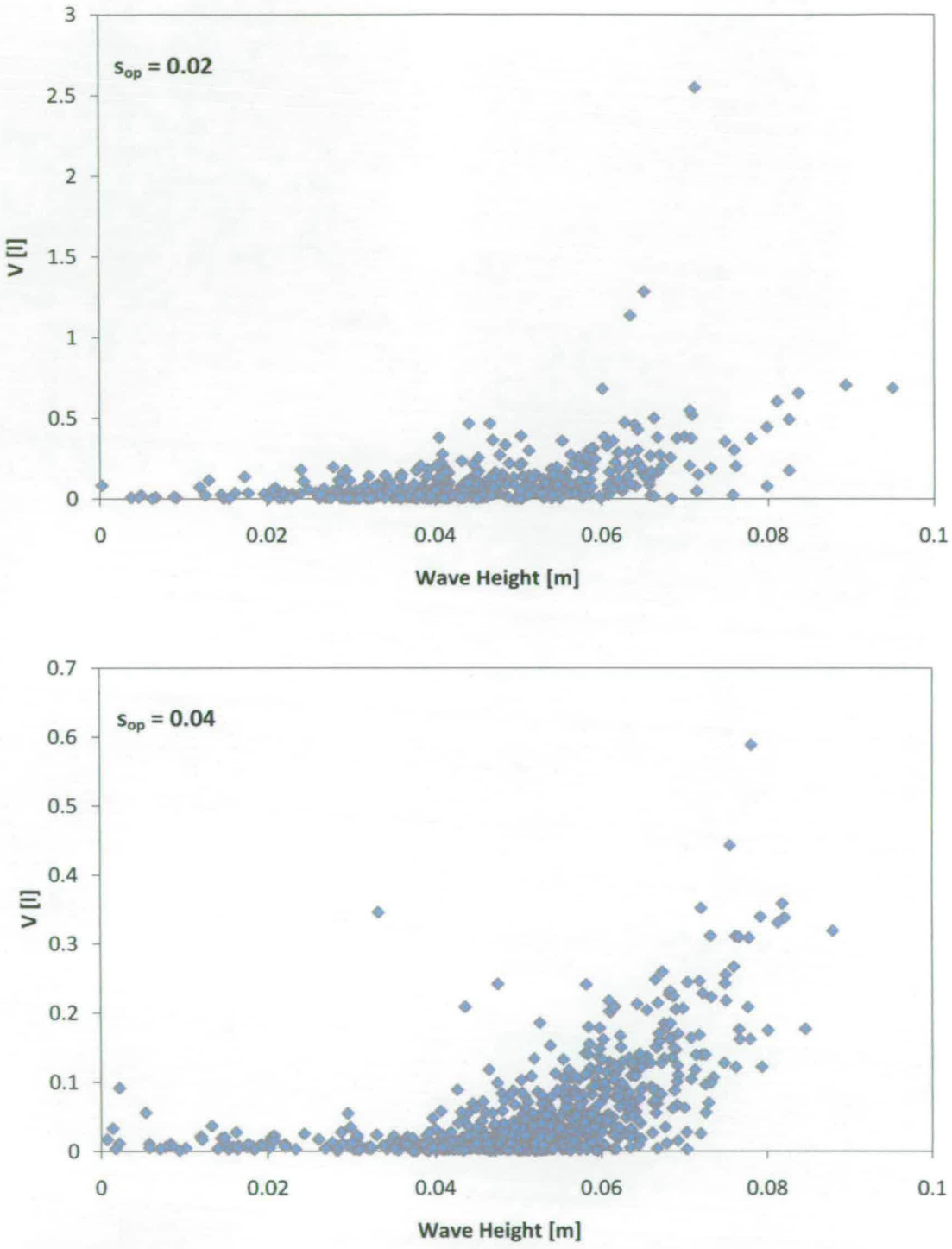

Figure 6.3 Individual overtopping volumes plotted against individual wave height. XA Test series.

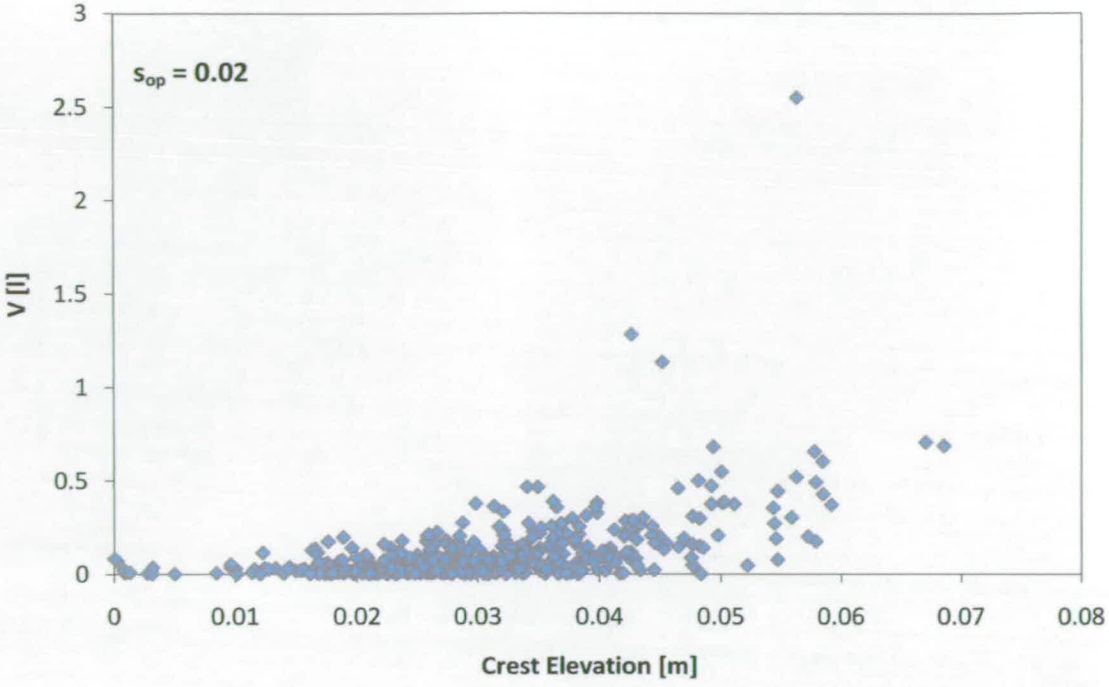

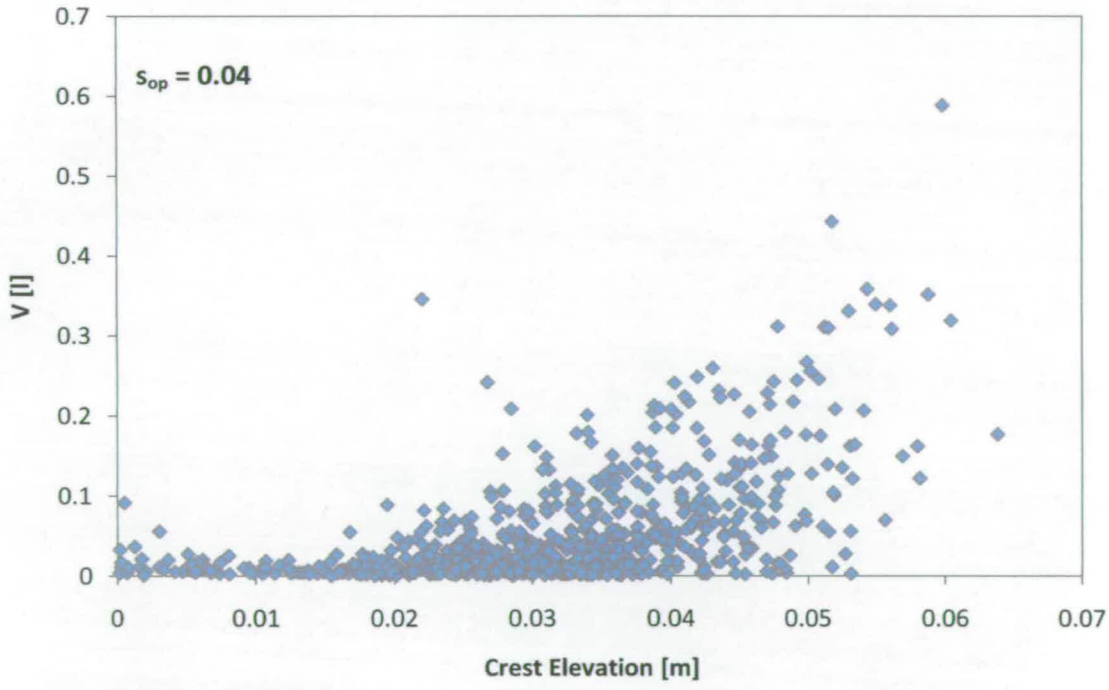

Figure 6.4 Individual overtopping volumes plotted against individual wave crest elevation. s_{op} = 0.02 & s_{op} = 0.04. AX Test series.

The relationships between the overtopping volume and individual wave height and crest elevation are illustrated in Figure 6.3 and Figure 6.4 respectively for the AX test series. The distribution of data points would appear to be broadly similar for both the wave height and crest elevation plots.

It is clear that the largest waves (in terms of crest elevation or wave height) tend to produce the largest overtopping volume. It is also apparent, however, that many large waves also produce a rather small overtopping response. There are also a number of relatively large events associated with waves significantly smaller than the maximum (e.g. less than half the height/crest-elevation). A large wave does not necessarily result in a large overtopping volume, nor is a large overtopping volume necessarily indicative of a large wave.

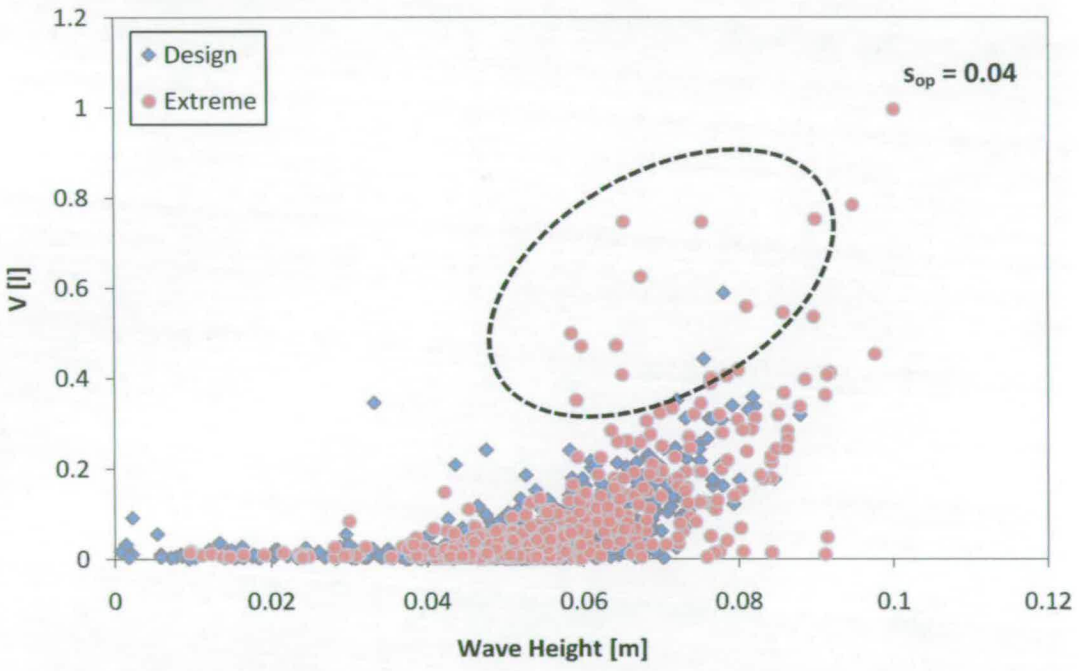

Figure 6.5 Individual overtopping volumes plotted against individual wave height. Design and Extreme Seas illustrated.

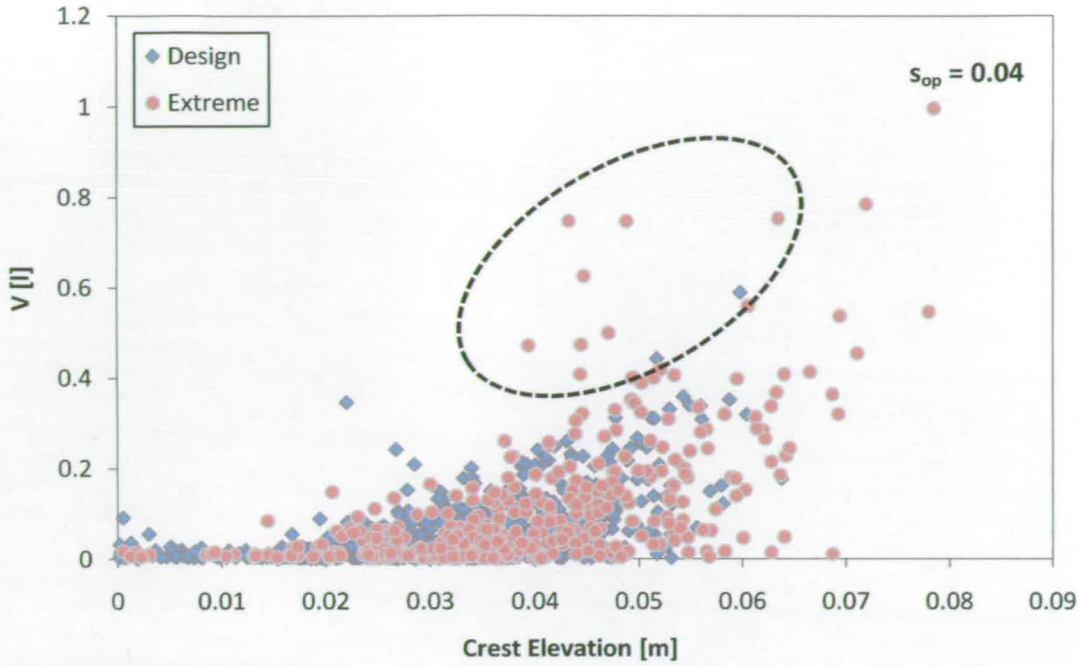

Figure 6.6 Individual overtopping volumes plotted against individual wave crest elevation. Design and Extreme Seas illustrated.

Further evidence that a univariate approach is unlikely to be sufficient is presented when examining results taken from an Extreme Sea (4BX test series). This data is available for the s_{op} = 0.04 sea state and the measurements are overlaid against the Design Sea data in Figure 6.5 (wave height) and Figure 6.6 (crest elevation). It is noted that the overtopping volume "upper limit" for a given wave height or crest elevation is often higher in the Extreme Sea. A cluster of measurements exhibiting this behaviour is highlighted in the above plots. The bulk of the measurements in the Extreme Sea do lie within, or close, to the boundary of the Design Sea data cloud. The highlighted data points are sufficient, however, to give a spurious output in the case of a univariate data filtering process.

Binned Overtopping Volume Analysis

While the wave-height/crest-elevation appears to exert a strong influence on the magnitude of the overtopping response, there are clearly other factors that must be explored.

It has been noted above that there has been no formal attempt to produce a detailed functional overtopping relationship. Rather, the bivariate relationship between the crest elevation and other selected parameters has been explored. The aim here is to identify useful trends that may be incorporated into the Importance Sampling filtering process. The analysis has taken the two datasets from the AX test series. Each overtopping wave in assigned a "bin" defined by the two parameters, and the mean volume for each bin expressed in the three-dimensional column plots presented below.

Crest & Trough Elevation

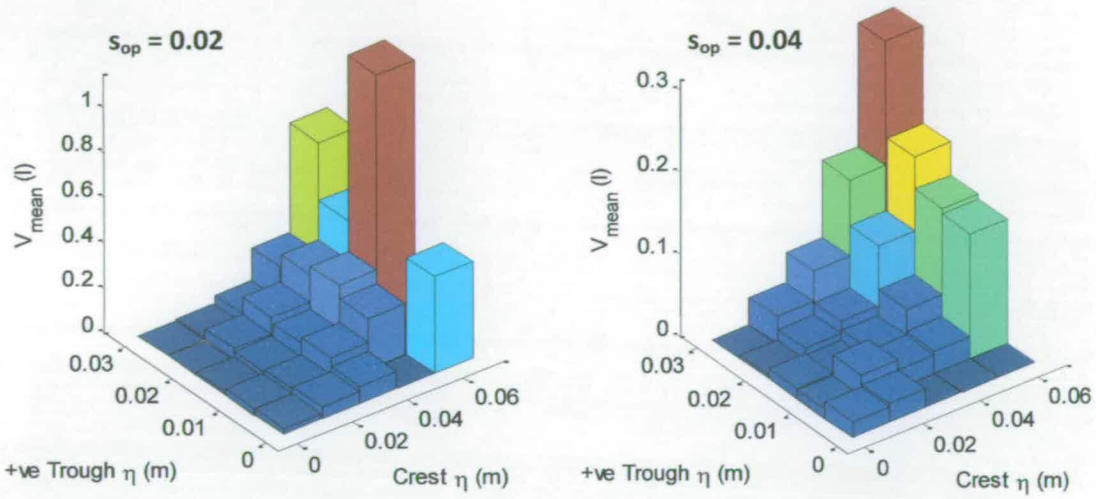

Figure 6.7 Binned mean overtopping volumes by crest and trough elevation

It is observed in Figure 6.7 for both test series that the overtopping volume increases with crest elevation, as previously illustrated in Figure 6.4. The joint relationship with trough elevation differs between the test series. The measurements from the s_{op} = 0.02 test series show little correlation with the trough elevation. In the case of the steeper test series (s_{op} = 0.04) the relationship is markedly different. The joint relationship suggests that the largest events are associated with waves with deep preceding troughs for a given crest elevation bin. This effectively indicates that waves with a large zero-downcrossing wave height are the most likely to be associated with the largest overtopping volumes. This wave height relationship is less strong for the s_{op} = 0.02 sea state.

Crest Elevation and Wave Period

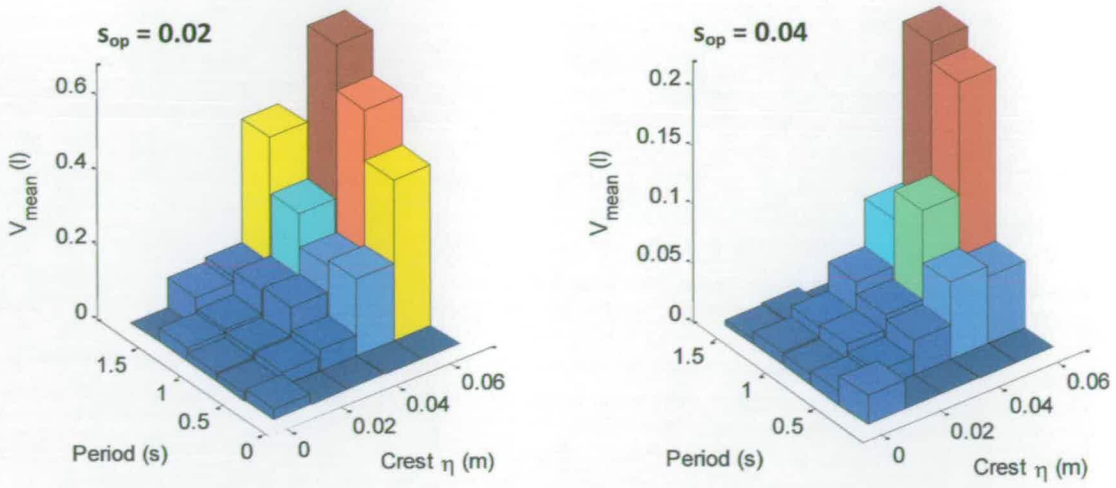

Figure 6.8 Binned mean overtopping volumes by crest elevation and wave period

The overtopping volume joint-relationship with crest elevation and zero-downcrossing period is illustrated in Figure 6.8. The s_{op} = 0.02 test series shows a general trend for overtopping volumes to increase with period, with this being more apparent for the larger crest elevations. This is intuitively reasonable due to the greater "elevated" mass of water per wave. The largest volumes in the s_{op} = 0.04 test series are associated with the longer period waves. There is not, however, a definitive trend across the crest elevation bins.

It would be intuitively expected that the joint relationship would be similar for the both test series. These plots effectively examine the dependency on wave steepness, with the same crest/period bin in each plot corresponding to the same individual wave steepness. It is clear from examination of the plots that both the distribution and particularly the magnitude of the volumes differ significantly. This lends support to the hypothesis that several parameters must be included in Importance Sampling filtering process.

Crest Elevation and Preceding Crest Elevation

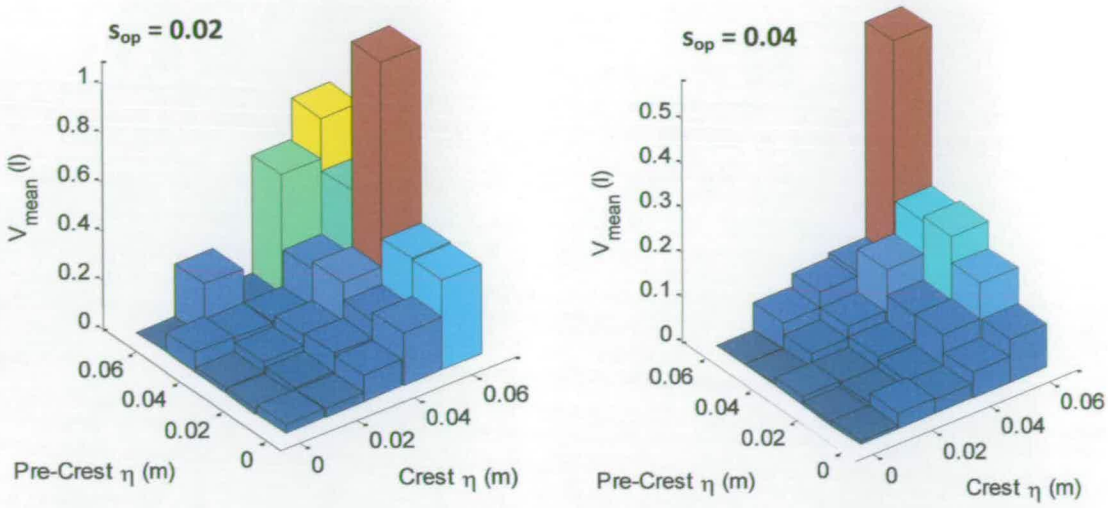

Figure 6.9 Binned mean overtopping volumes by crest elevation and preceding crest elevation

The vertical seawalls used in this research are expected to produce few "hysteresis" effects. The overtopping wave is expected to be primarily influenced by the properties of a single wave, rather than long wave groups. Vertical seawalls are, however, highly reflective structures. The wave preceding the overtopping wave will interact in some manner with the overtopping wave immediately prior to its impact with the seawall. This may conceivably be in the form of wave setup, or a non-linear action which may "trip" the wave into breaking.

The overtopping volumes binned by the overtopping wave crest elevation and the crest elevation of the preceding wave are illustrated in Figure 6.9. It is noted that the largest distributions tend to be associated with the larger preceding crest elevations. This relationship is quite clear for the steeper (s_{op} = 0.04) test series, even if the very large measurement in the extreme bin (largest crest elevations) is excluded. This relationship is less apparent for the s_{op} = 0.02 data, although several of the largest measurements are contained within the large preceding crest bins.

6.3 KDE Parameters

6.3.1 Optimisation of KDE Parameters

Kernel Density Estimation (KDE – §5.5) is used to produce Probability Density Functions (PDF) describing the Design Sea states for use in the Importance Sampling filtering process (§5.2.3). KDE is a non-parametric technique in which few assumptions need to be made regarding the underlying properties of the sample data.

The properties of the KDE distribution are determined by the size and shape of the kernels forming the distribution (§5.5.1). In the case of a bivariate distribution the size is altered in two dimensions by the bandwidth matrix (§5.5.2). The kernel may be resized over axes coincident with the data axes, or the axes may be rotated (§5.5.3). The bandwidth matrix controls the level of smoothing applied to the KDE distributions. Oversmoothing the distribution will tend to obscure the detail of the underlying distribution (e.g. bimodal properties may be masked). Undersmoothing the distribution will exaggerate the influence of individual data points, making the distribution less representative of the system as a whole.

The dimensionless kernel shape (i.e. ignoring the resizing due to the bandwidth matrix) is determined by an underlying kernel density function (§5.5.1 and Figure 5.12). It is noted by Wand & Jones (1995) that the choice of kernel density function is relatively unimportant in influencing the KDE distribution. The Epanechnikov kernel (§5.5.2 – Equation (56)) is therefore used throughout this research, with optimisation techniques concentrating on selection of the bandwidth parameters.

The optimisation technique employed here is Least Squares Cross Validation (LSCV – §5.5.5). This is a data driven method requiring no subjective decisions on behalf of the user. A disadvantage is that the convergence can be somewhat unreliable for different data samples drawn from the same parent distribution

(Silverman, 1986; Wand & Jones, 1995). Two broad approaches are therefore suggested: -

1. Direct estimation from LSCV, noting possible problems with convergence of the optimisation algorithm.
2. Pre-selection of the bandwidth matrix using guidance inferred from LSCV optimisation of synthesised (or previously measured) datasets.

Method 2 has the advantage that the bandwidth matrix parameters can be averaged over a number of tests, minimising the uncertainty involved with direct application of the LSCV method. The obvious obstacle is obtaining the datasets with which the LSCV optimisation can be applied. In cases where a large Design Sea dataset in available this is feasible by simply averaging the results obtained for each sample using Method 1. In practice this is unlikely to be feasible as, by design, the Importance Sampling method is intended to reduce the length of Design Sea testing required for an experimental programme. The alternative is to use synthesised data. Two synthesised data approaches are detailed below. It is important to remember at this stage that LSCV procedure is only concerned with the selection of the bandwidth matrix, not the distributions themselves. The KDE method always uses the Design Sea data to produce the probability density distributions, regardless of applied bandwidth optimisation procedure.

Another noted limitation of the LSCV procedure is the considerable computational effort required. A single bivariate KDE probability distribution takes of the order of a few seconds to calculate for a typical ~1000 sample dataset. The LSCV technique, however, requires N+1 iterations of the KDE estimation (recall the "leave one out" basis of the technique – §5.5.5) for each set of input conditions (i.e. the bandwidth matrix). This must then be repeated multiple times to conduct the optimisation. A single bivariate optimisation takes several hours, even when utilising a powerful computing facility.

Parametric Spectrum – Synthesised Sea

The simplest solution available to produce datasets for LSCV optimisation is to describe the sea state using a standard parametric spectrum (e.g. JONSWAP). Different realisations of the elevation time series may then be synthesised using linear wave theory. In the examples illustrated below (§6.3.2 & §6.3.3) 10 unique elevation time series were produced, each consisting of ~1000 waves. The elevation time series were produced from a JONSWAP spectrum (γ = 3.3) with a nominal H_{m0} and T_p[16]. This method does not account for any shallow water transformation of the spectrum (if the model input spectrum is used) or wave train. It is, however, easily applied without any requirement for model test data.

Measured Spectrum – Synthesised Sea

The second approach explored is to synthesise the elevation time series based upon a measured spectra. In the examples explored below (§6.3.2) the spectra are measured from the Design Sea (2AY & 4AY). The elevation time series are synthesised using linear wave theory in the same manner as described above.

Measured Sea (Design Sea dataset)

The most realistic elevation time series information is obtained from physical model testing without recourse to synthesised data. Thus all wave transformation processes are correctly accounted for. It is, however, unrealistic to expect this data to be available when applying the IS method. Indeed, where large design sea datasets available the advantages of IS method (primarily improved efficiency) are largely moot. In this case, this design sea data (test series 2AY and 4AY – §3.6.2) are available and may be used for cross-comparison with the synthesised optimisation approaches explored above.

[16] The linear nature of this method (with constant γ = 3.3) effectively renders the process dimensionless. The analysis has, therefore, only been conducted for single value of H_{m0} (= 1) and T_p (= 1).

6.3.2 Bivariate Bandwidth

LSCV Methodology

The LSCV optimisation technique minimises the value of the LSCV over a range of bandwidth values. In order to keep the computational requirements manageable the optimisation was conducted over a 7 x 7 grid for each bivariate distribution. The optimisation was conducted over the range $0.5 \cdot h_{os}$ - $1.0 \cdot h_{os}$, where h_{os} is the oversmoothed bandwidth estimator (§5.5.5).

The bandwidth minimum was calculated, to a value of 3 significant figures, through cubic spline interpolation of the LSCV values. This process significantly reduced the computational requirements of the optimisation. A final cross check was made comparing the interpolated LSCV minima with the calculated LSCV value for this optimised bandwidth. This error was shown to be less the 1% in all cases.

The LSCV results are illustrated below for the various scenarios described in §6.3.1. The mean value of the normal scale rule bandwidth estimator (h_s - §5.5.4) is also plotted. It should be recalled that the value of h_s has a constant ratio with overscaled bandwidth used as the upper bound of the optimisation (h_s / h_{os} = 0.93). In each optimisation scenario 10 different realisations (or measurements) of the elevation time series were used to produce the inputs to the optimisation. Where a measured spectrum was used this was taken from a wave gauge measurement in shallow water from a single ~1000 wave test (YA dataset - §3.6.2). This spectral measurement was taken from the first numbered test in each test series (i.e. 2AYcal1 and 4AYcal1).

The LSCV optimisation process was carried out for the four parameters identified in §6.2.3, namely:

- Wave period (T)
- Trough elevation (η_T)
- Crest elevation (η_C)
- Preceding-wave crest elevation (η_{C-1})

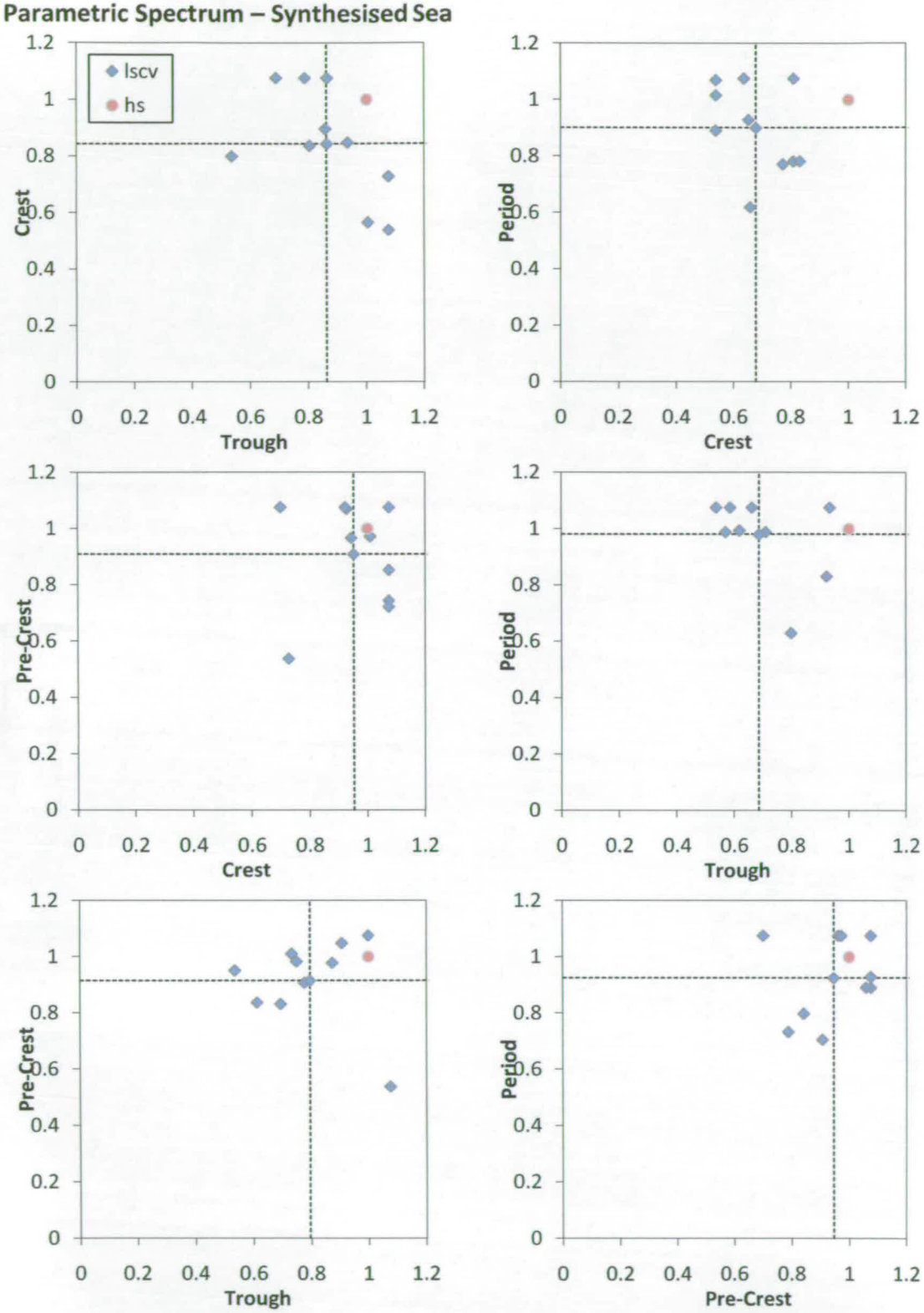

Figure 6.10 LSCV bandwidth values relative to normal scale rule bandwidth – JONSWAP spectrum (γ = 3.3) with synthesised seas. Dashed lines represent mean.

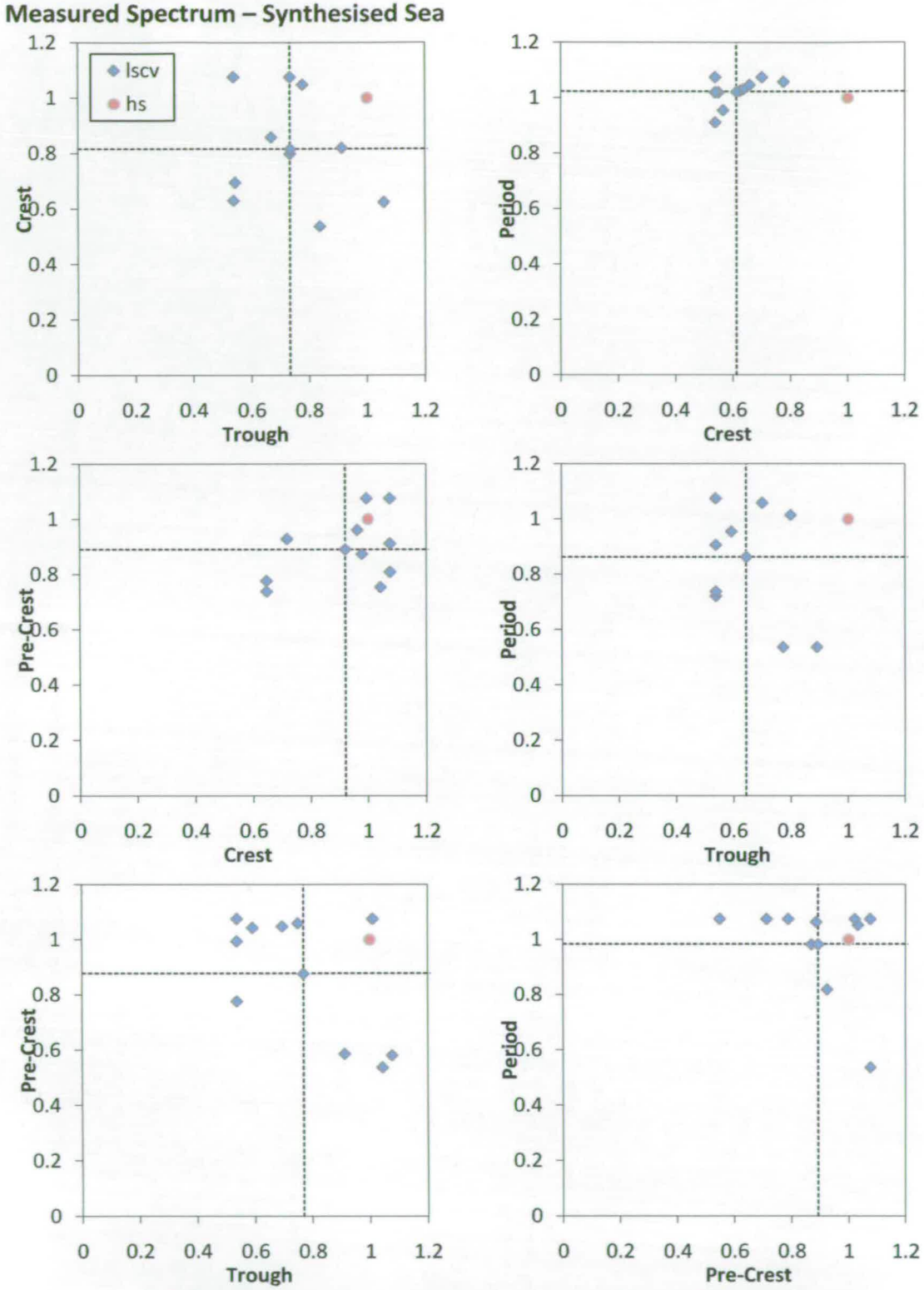

Figure 6.11 LSCV bandwidth values relative to normal scale rule bandwidth – Measured Spectrum (Reference: 2AYcal1) with synthesised seas. Dashed lines represent mean. s_{op} = 0.02.

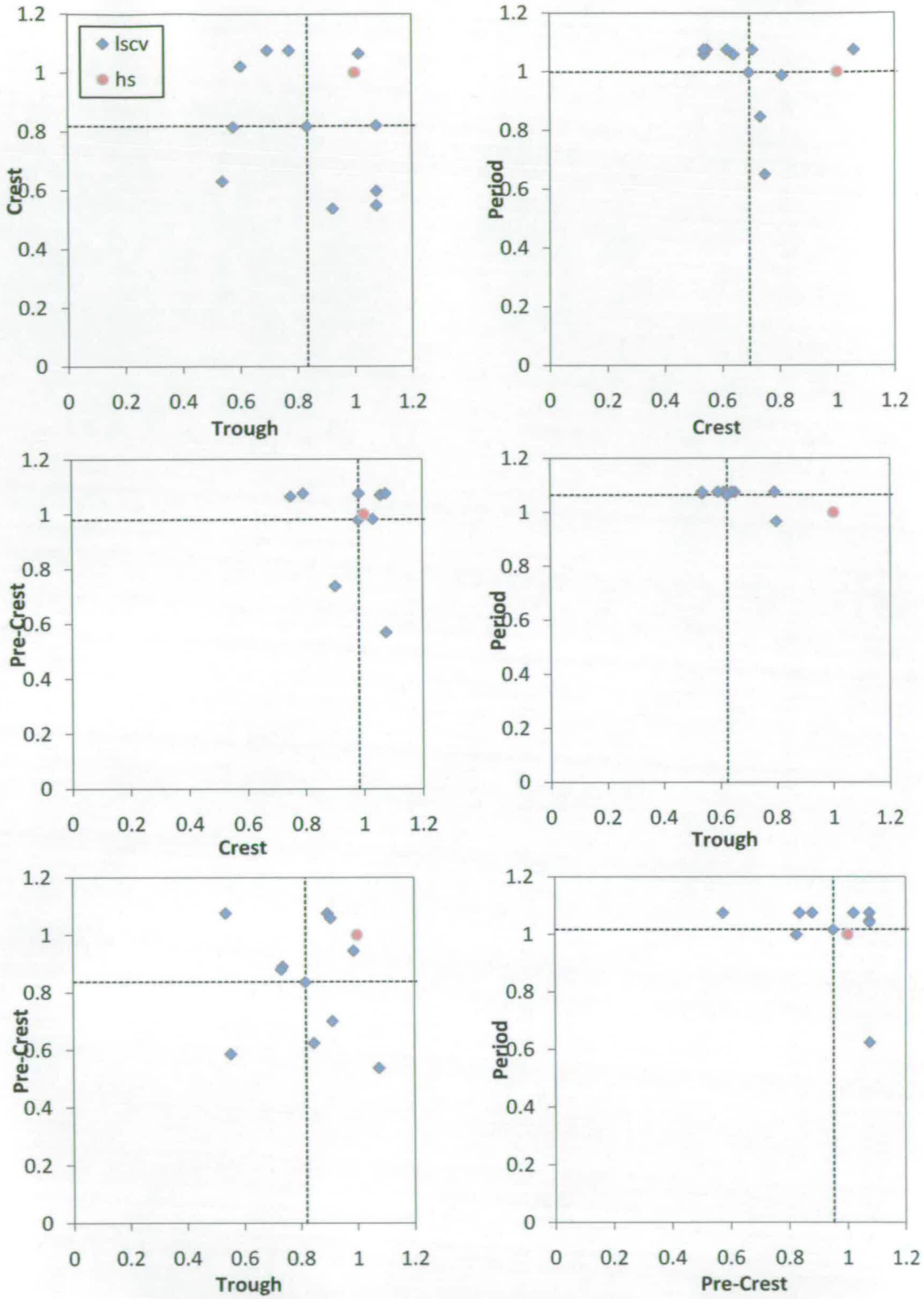

Figure 6.12 LSCV bandwidth values relative to normal scale rule bandwidth – Measured Spectrum (Reference: 4AYcal1) with synthesised seas. Dashed lines represent mean. s_{op} = 0.04

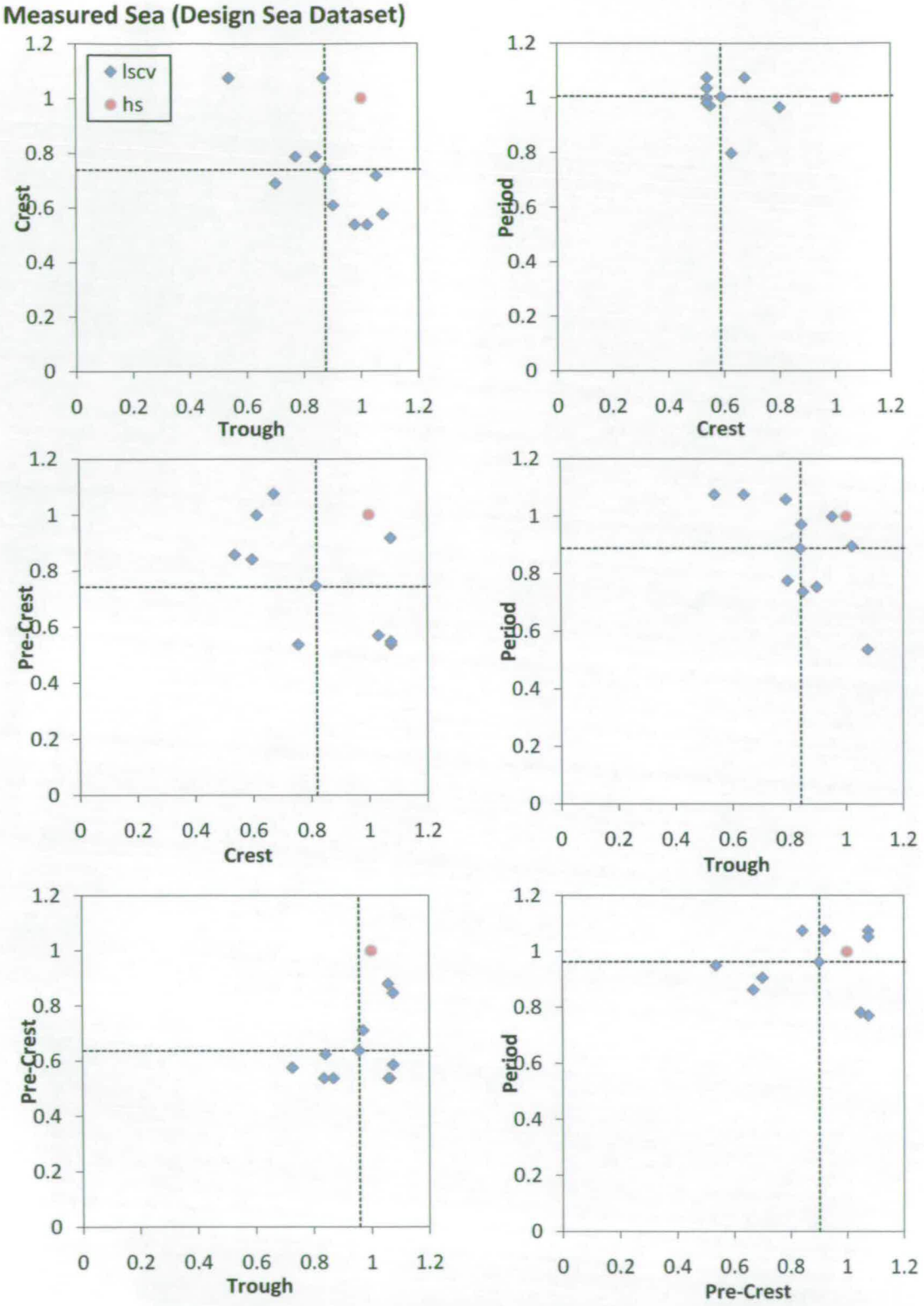

Figure 6.13 LSCV bandwidth values relative to normal scale rule bandwidth – Measured elevation time series (Test Series: 2AY) with synthesised seas. Dashed lines represent mean. s_{op} = 0.02

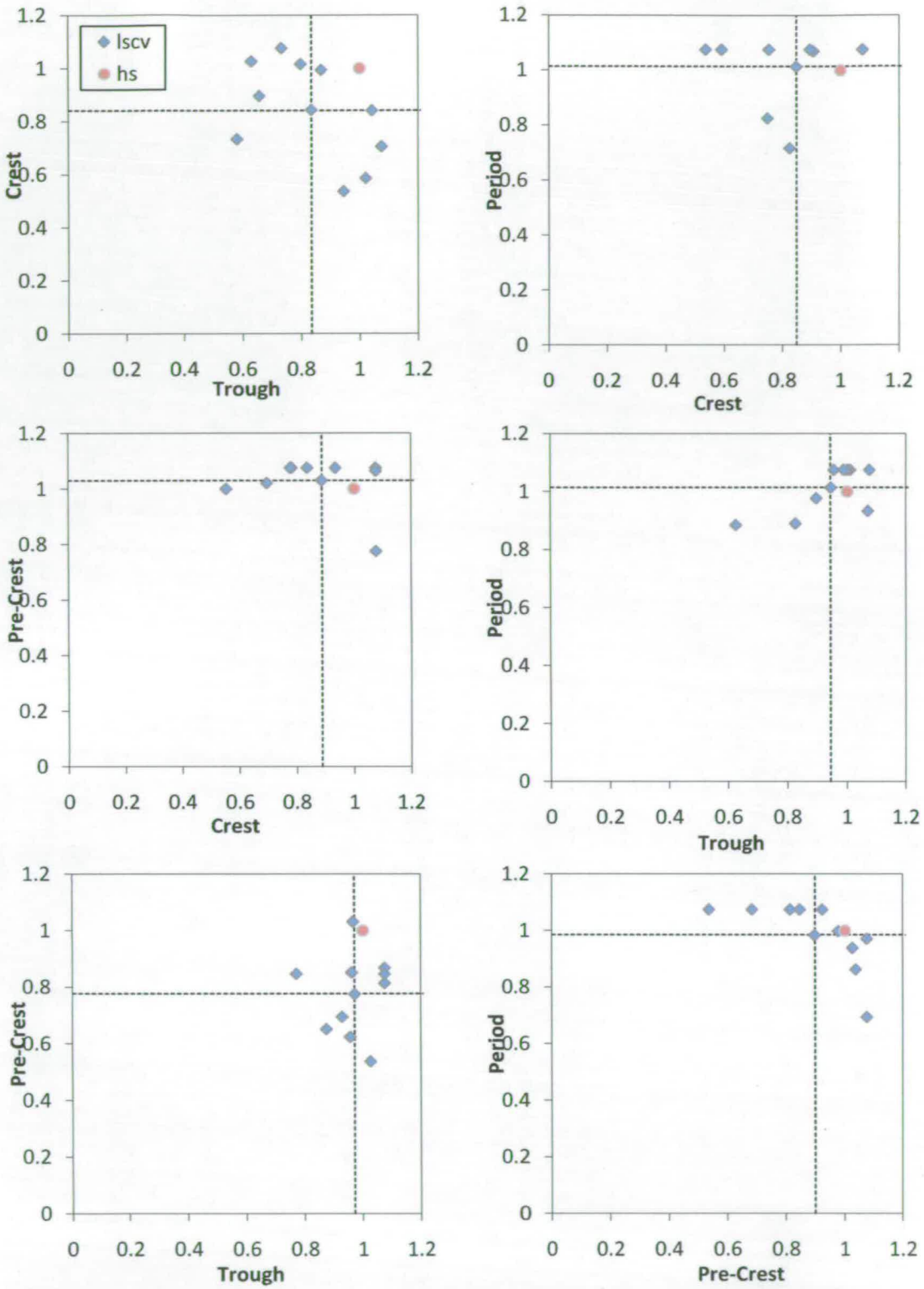

Figure 6.14 LSCV bandwidth values relative to normal scale rule bandwidth – Measured elevation time series (Test Series: 4AY) with synthesised seas. Dashed lines represent mean. s_{op} = 0.04

Bandwidth Analysis Summary

The LSCV bandwidth values illustrated in Figure 6.11 to Figure 6.14 show significant levels of scatter for all bivariate data pairs. While some plots show reduced scatter there are no clear patterns between similar bivariate pairs. In some cases it is noted that the LSCV bandwidth value is at the upper boundary of the optimisation range. This result is somewhat unexpected as this boundary represents the bandwidth produced by the oversmoothing criterion (§5.5.5). This represents a bandwidth for which the KDE is known to be sub-optimal (hence the term "oversmoothed"). It was therefore decided not to redefine the upper boundary as it was felt unwise to use bandwidth estimates which are known to be greater than the theoretical upper limit. None of the bandwidth values were on the lower boundary (half the oversmoothed bandwidth), although in some cases the minima were close to this lower boundary.

The mean LSCV bandwidth values relative to the normal scale bandwidth (represented by the dashed lines in the above plots) are examined below for each analysis method (as described in §6.3.1).

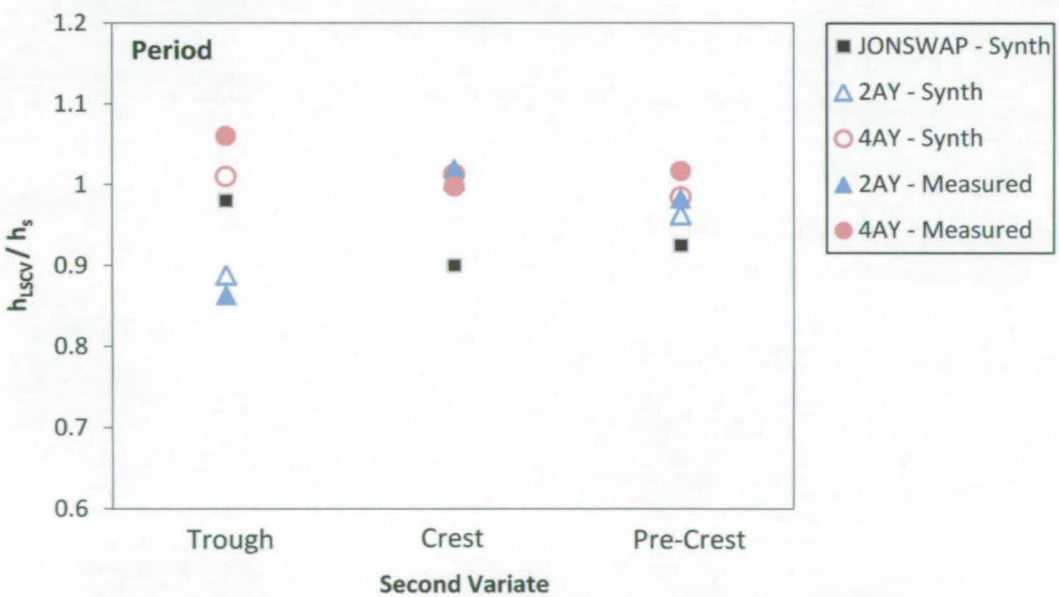

Figure 6.15 Wave Period mean h_{LSCV} bandwidth for various bivariate distributions

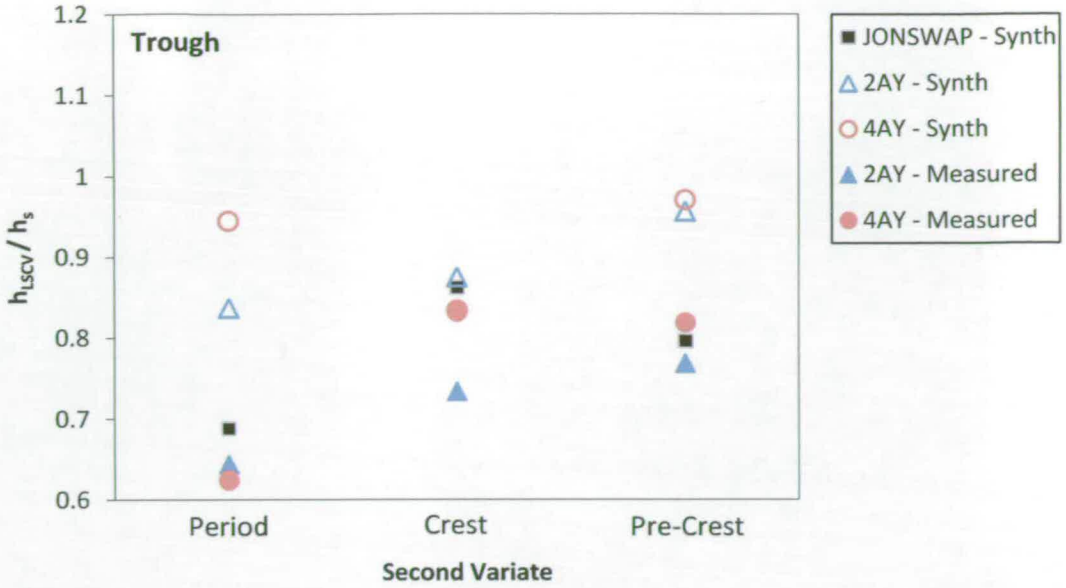

Figure 6.16 Trough Elevation mean h_{LSCV} bandwidth for various bivariate distributions

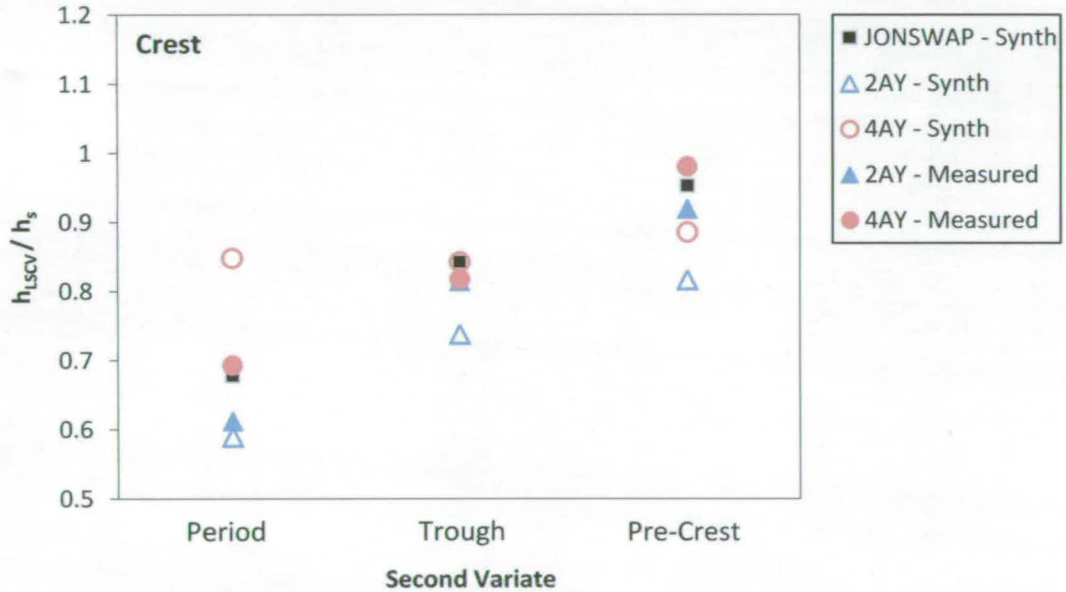

Figure 6.17 Crest Elevation mean h_{LSCV} bandwidth for various bivariate distributions

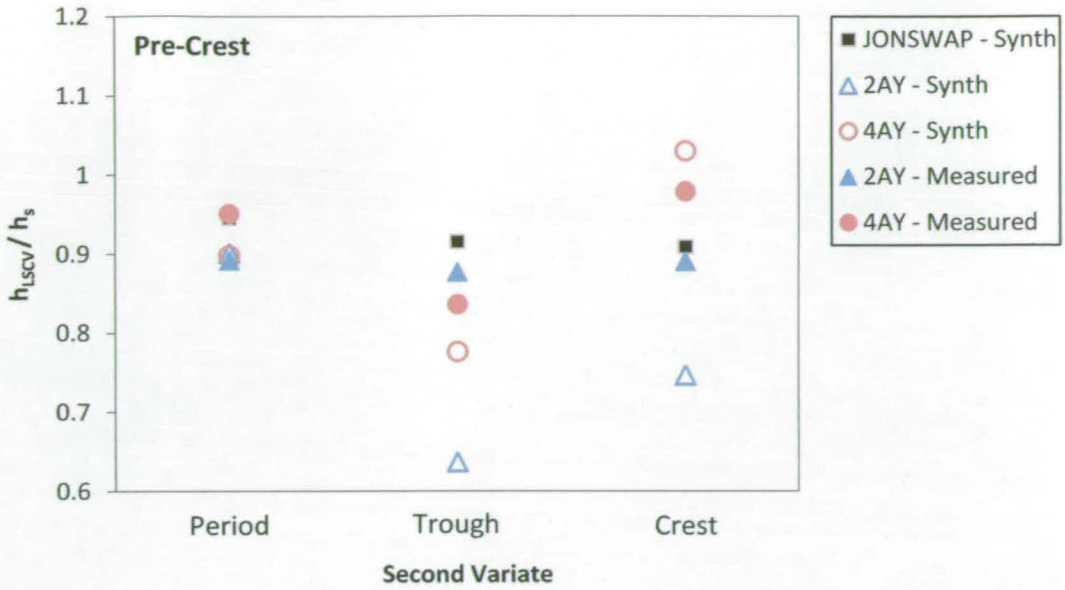

Figure 6.18 Preceding-Crest Elevation mean h_{LSCV} bandwidth for various bivariate distributions

The wave period bandwidth value for three different bivariate distributions are described in Figure 6.15. The agreement between the measured spectrum-synthesised data (2AY – Synth & 4AY – Synth) and the measured data is quite good. The bandwidth obtained with the fully synthesised data shows the greatest disagreement with the measured data.

This pattern is repeated to a lesser extent across the bandwidth values obtained for the trough elevation (Figure 6.16), crest elevation (Figure 6.17) and preceding crest elevation (Figure 6.18). The scatter in the results appears to be quite significant.

6.3.3 Kernel Rotation

The theory describing kernel rotation is described in §5.5.3. In simple terms, kernel rotation is equivalent to rotating the axes of the bivariate distribution. In doing so the kernels may be resized along these rotated axes, producing a more natural fit to the underlying data structure.

The datasets obtained from the 2AY and 4AY datasets are examined here using the LSCV optimisation method. The kernels are rotated over the range $-\pi/4 \leq \theta \leq \pi/4$. 101 linearly spaced rotation angles (θ) were examined over this range.

The analysis was conducted for each of the ten ~1000 wave seas in each dataset. It should be noted that this procedure was time-consuming, with each dataset (with 6 bivariate distributions) taking approximately 36 hours to analyse using a powerful remote computing facility[17]. This limitation made it impractical to optimise the bandwidth values using the LSCV method, as this procedure would be required for each value of Θ. Instead, the bandwidth was estimated for the rotated axes using the Normal Scale Rule (§5.5.4).

[17] The computing time required is likely to approximately double for a standard desktop computer

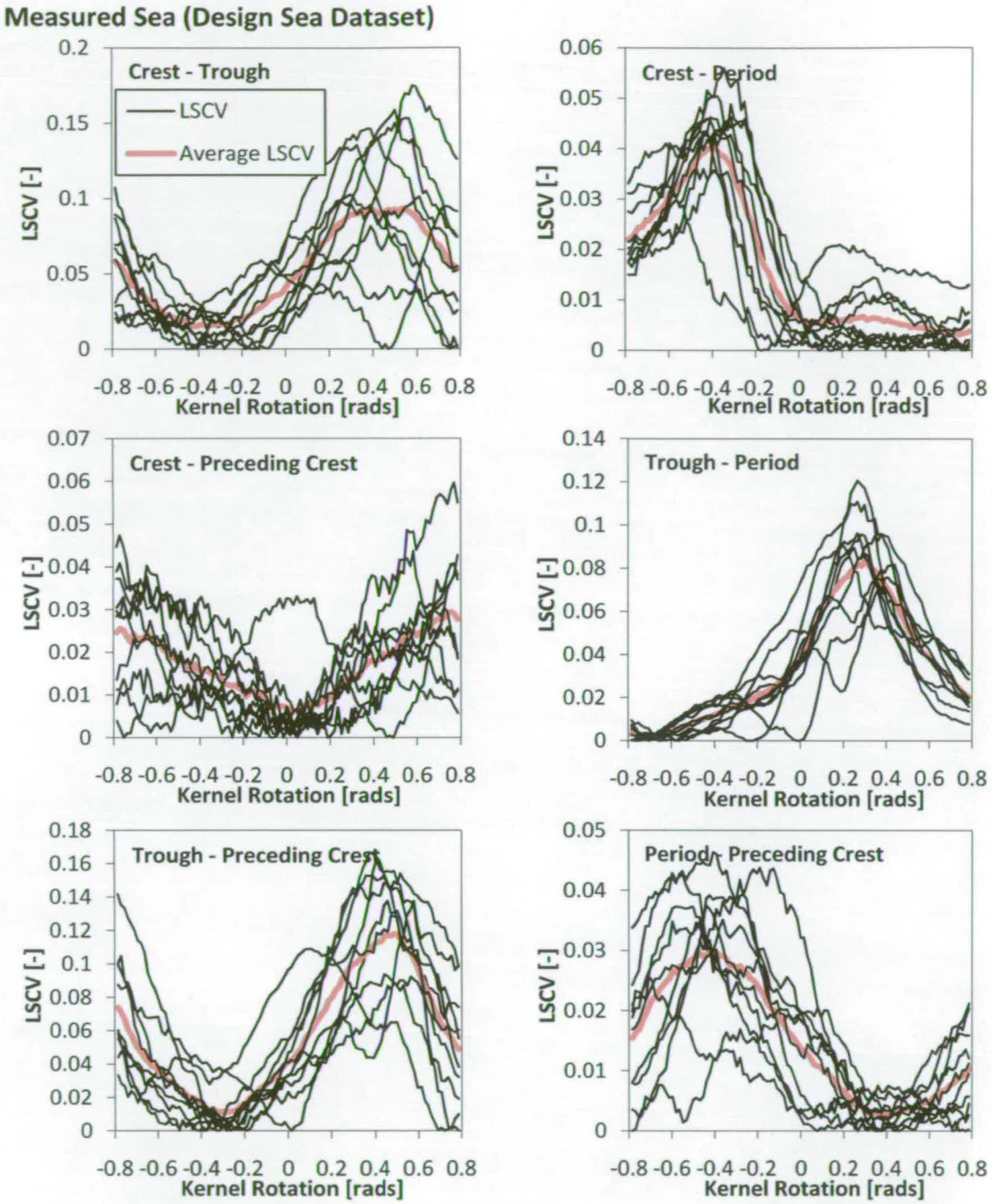

Figure 6.19 LSCV analysis of kernel rotation angle for bivariate joint distributions. 2AY dataset (s_{op} = 0.02).

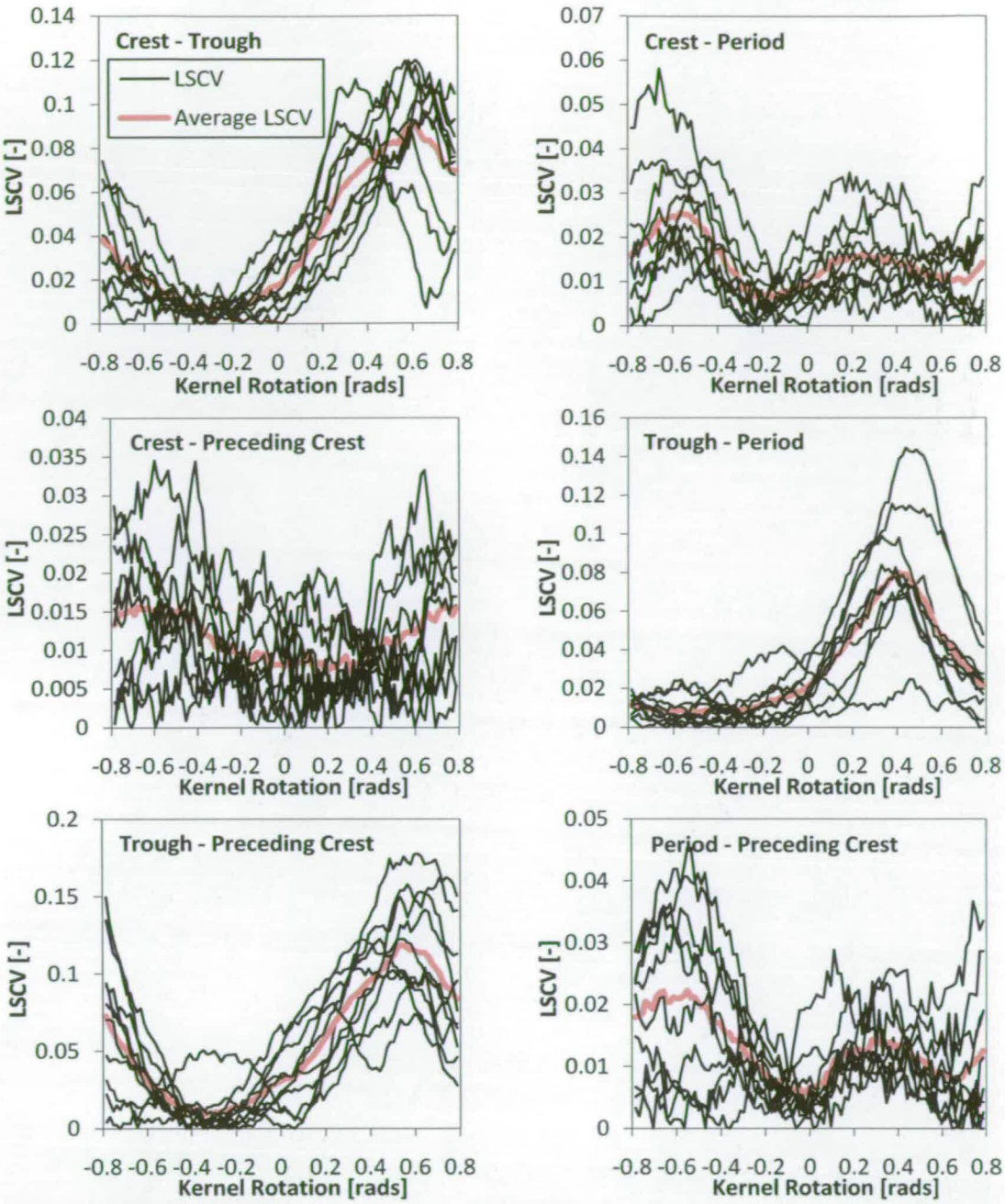

Figure 6.20 LSCV analysis of kernel rotation angle for bivariate joint distributions. 4AY dataset (s_{op} = 0.04).

The results of the LSCV optimisation are illustrated above for the 2AY (Figure 6.19) and 4AY (Figure 6.20) datasets. It is observed that there are significant differences in the LSCV values obtained for each individual sea, although in most cases the trends are similar. In some cases very clear optimums are identified (e.g. Trough – Preceding Crest). In other parameter-pairs, however, the minimum (indicating the optimum LSCV value) is not particularly well defined.

This is observed in the Crest – Preceding Crest plots for both datasets, where the individual sea results show considerable variability. This behaviour is also noted in the Crest – Period results obtained for the 2AY dataset. In this case the average LSCV value suggests the optimum value of Θ is close to $\pi/4$ (the upper boundary of the optimisation), while examination of Figure 6.19 suggests this optimised value is only very slightly preferable to a zero rotation angle.

The optimised rotation angles are given below for the 2AY (Table 6.1) and 4AY (Table 6.2) datasets. These are the angles used in the application of the Importance Sampling method outlined in §6.4.3.

s_{op} = 0.02	Trough	Crest	Pre-Crest
Period	-0.707	0.738	0.361
Trough	-	-0.361	-0.283
Crest	-	-	0.047

Table 6.1 LSCV optimised rotation angles measured in radians. 2AY dataset (s_{op} = 0.02).

s_{op} = 0.04	Trough	Crest	Pre-Crest
Period	-0.615	-0.141	-0.110
Trough	-	-0.298	-0.330
Crest	-	-	0.314

Table 6.2 LSCV optimised rotation angles measured in radians. 4AY dataset (s_{op} = 0.04).

6.4 Importance Sampling Results

6.4.1 Extreme Sea Filtering

The 2Y and 4Y test series (§3.6.2) were used to analyse the effectiveness of the Importance Sampling technique. It should be recalled that each test series consists of a "baseline" dataset (2AY & 4AY) consisting of ten ~1000-wave Design Sea tests each produced from the same spectrum but with a different realisation of the elevation time series (i.e. with a different set of random phase angles). In addition to these Design datasets there are three sets of Extreme Seas for the two test series. These conform to Spectral Inflation Factors (§5.3.1) of 1.1, 1.2 and 1.3. This relates to an increase in H_{m0} of 10%, 20% and 30% with

the steepness held constant at 0.02 and 0.04 for the 2Y and 4Y test series respectively. The lengths of these Extreme datasets was chosen to produce approximately similar numbers of overtopping waves (N_{ow}) as measured in the combined Design Sea dataset. It should be noted that the Extreme Sea tests are treated here as single continuous test, although for practical purposes they were measured as a number of shorter tests (of ~500 or ~1000 waves). The MATLAB software used to conduct the analysis takes account of discontinuities in the combined record to prevent incorrect analysis of "wave groups" that actually comprise measurements from two separate test records.

The filtering process was carried out based upon the four parameters discussed in §6.2.3. The resulting bivariate KDE probability matrix (illustrated previously in Figure 5.10) produces a filtered Extreme Sea dataset using the process described in §5.4. The KDE distributions are produced from a single measured Design Sea test (~1000 waves), reflecting the methodology required for a "real life" application of the Importance Sampling application where only limited Design Sea data is likely to be available. The KDE bandwidth matrix is selected as a factor of the normal scale bandwidth, as described above (§6.3.2). Three bandwidth estimation methods were used:

1. Normal Scale Rule
2. LSCV optimised parametric spectrum – synthesised sea ("*LSCV – Synth*")
3. LSCV optimised measured spectrum – synthesised sea ("*LSCV - Meas/Synth*").

These methods are all available to the engineer applying the Importance Sampling technique with only limited Design Sea data. The influence of kernel rotation (§6.4.3) was examined using elevation time series measured in the flume ("*LSCV - Meas*").

6.4.2 Extreme Sea Block Analysis (Optimised Bandwidth)

The output of the filtered Extreme Seas was analysed using the "block analysis" approach outlined in §5.6.2. This involves dividing the filtered Extreme Sea

record into ten equal length segments (measured in terms of N_w). The outputs of these segments (i.e. the individual overtopping volumes) are then examined as if they are measured outputs from a number of discrete tests. It should be recalled that the length of the Extreme Sea datasets were chosen such that the total number of overtopping waves (N_{ow}) is similar to the measurements taken from the Design Sea dataset (see §3.6.2 for further information).

The output from the blocks is examined in terms of V_{max} and $V_{1\%}$ (the overtopping volume exceeded by 1% of overtopping waves). It is noted that the definition of V_{max} obtained from the filtered Extreme Sea output is problematic (§5.6.2). The expected value of V_{max} will increase with test length due to the increased sample size (N_{ow}). The blocks comprising each filtered Extreme Sea output represent, in theory, the output from a longer Design Sea test, with the distribution shifted to produce more extreme events. Recalling, however, that each block is intended to approximate a ~1000 wave Design Sea test, and that the upper bounds of the overtopping volumes are intended to be similar, it may be appropriate to examine the value of V_{max} in the conventional manner. The V_{max} values for each block are therefore presented below for comparison with the Design Sea output.

In both cases (V_{max} and $V_{1\%}$) the filtered Extreme Sea block analysis output is expressed as a factor of the mean Design Sea output (i.e. the mean of V_{max} or $V_{1\%}$). Results are presented for both 2Y and 4Y test series (s_{op} = 0.02 and 0.04 respectively). Results using the three bandwidth estimator approaches described above (§6.4.1) are discussed.

Extreme Sea Filtering Level

The filtering process was applied using each of the ten Design Sea tests (for both the 2AY and 4AY datasets). The level of filtering for each Extreme Sea dataset may be expressed by the proportion of waves remaining after the filtering process ($N_{Filtered}$ / N). This ratio may describe either the full dataset (N_w) or the overtopping waves only (N_{ow}). These "filtering coefficients" are illustrated in the plots below. In each case the data points represent the average filtering

coefficient for each dataset with the error bars describing the range of values obtained (representing the spread across the ten Design Sea tests used as the input to the filtering process).

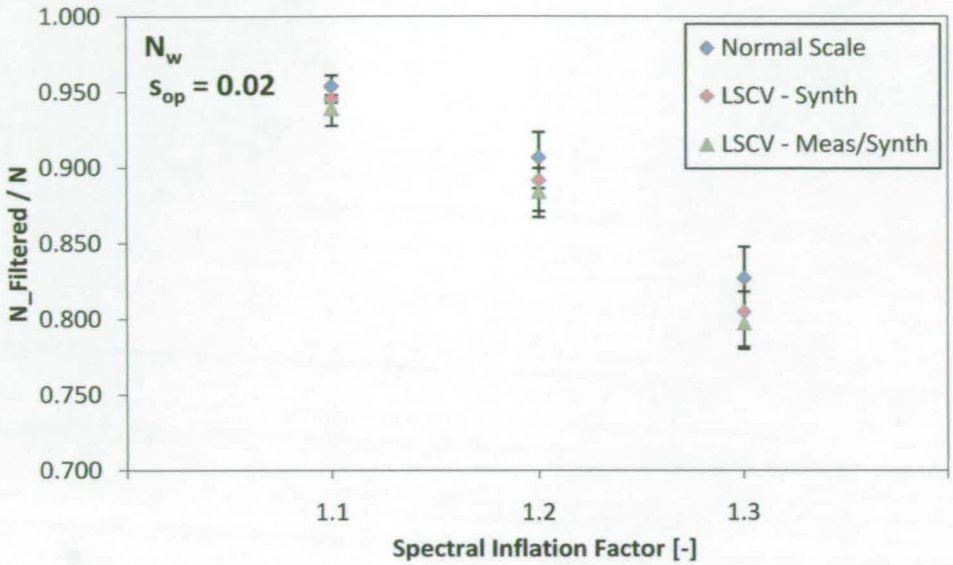

Figure 6.21 Filtering level for all measured waves (N_w) for Extreme Seas in the 2Y dataset

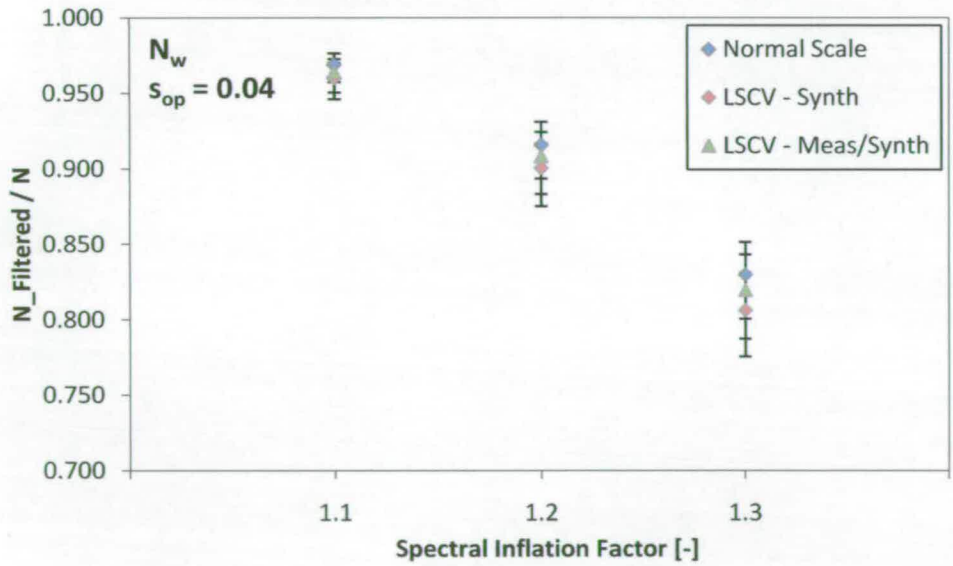

Figure 6.22 Filtering level for all measured waves (N_w) for Extreme Seas in the 4Y dataset

The level of filtering for the complete datasets (N_w) is described in Figure 6.21 (2Y: s_{op} = 0.02) and Figure 6.22 (4Y: s_{op} = 0.04). The level of filtering appears to be broadly similar for the two datasets. The lowest level of spectral inflation (1.1) shows approximately 95% of the waves retained. Increasing the spectral inflation value to 1.2 gives a filtering coefficient of ~90%. The strongest filtering

occurs, as expected, in the 1.3 spectral inflation dataset with approximately 80% of the dataset retained after filtering. These filtering coefficients are expressed more precisely in Table 6.3.

Dataset	Bandwidth Method	Spectral Inflation Factor		
		1.1	1.2	1.3
2Y	Normal Scale	0.954	0.907	0.824
	LSCV – Synth	0.945	0.892	0.805
	LSCV – Meas/Synth	0.939	0.884	0.797
4Y	Normal Scale	0.969	0.916	0.830
	LSCV – Synth	0.960	0.901	0.806
	LSCV – Meas/Synth	0.964	0.909	0.820

Table 6.3 Average N_w filtering coefficient for 2Y and 4Y test series.

The filtering coefficients obtained for the three bandwidth selection methods are broadly similar. The normal scale rule KDE distributions give rise to the least severe filtering. This is due to the LSCV estimated bandwidths having values below that of the normal scale rule (see § 6.3.2). The smaller bandwidths will produce probability distributions which are less "spread" at the extreme, therefore resulting in slightly fewer events passing through the filter.

The variation between the size of the filtered Extreme Sea outputs (using different Design Sea inputs) is typically of the order of 1-2%, with the largest variation seen for the most Extreme Sea (spectral inflation factor of 1.3).

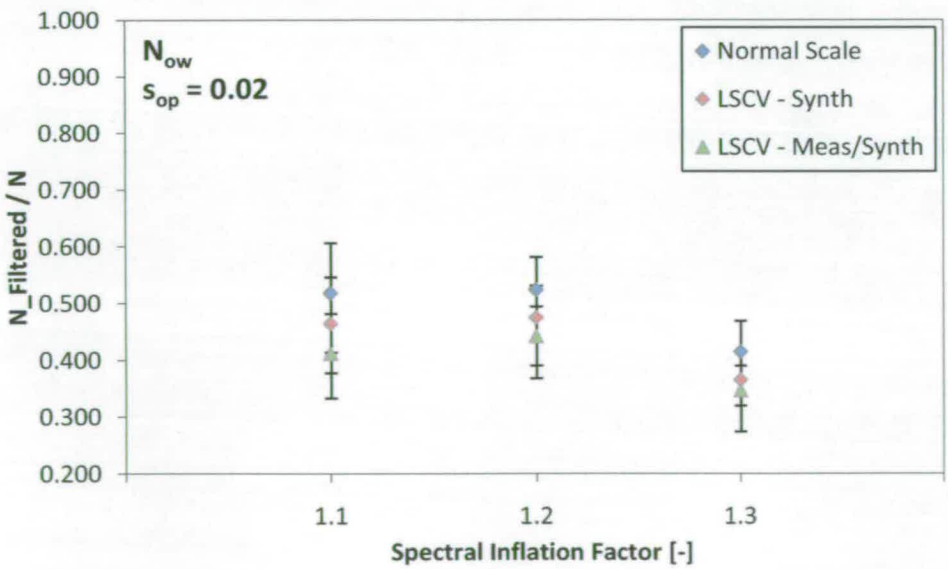

Figure 6.23 Filtering level for overtopping waves (N_{ow}) for Extreme Seas in the 2Y dataset

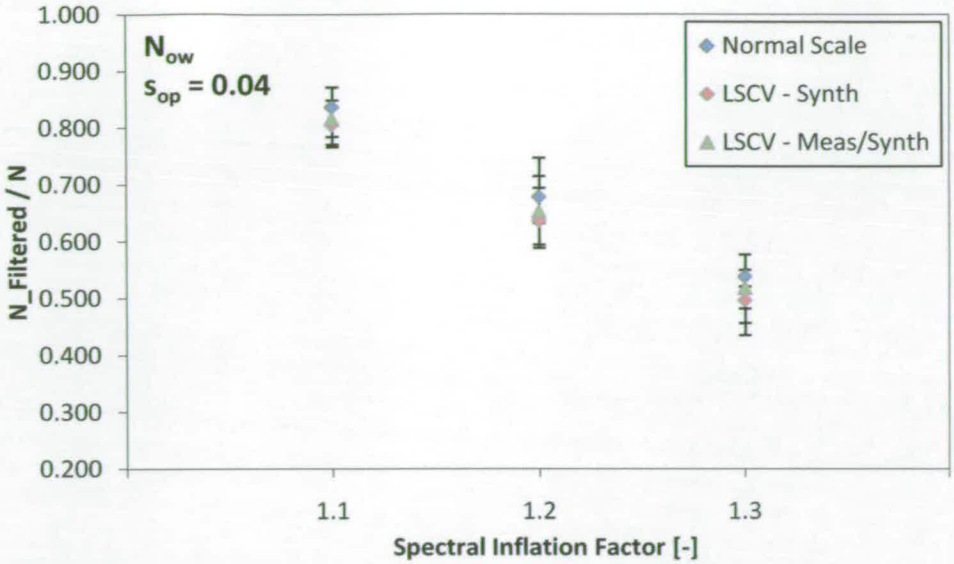

Figure 6.24 Filtering level for overtopping waves (N_{ow}) for Extreme Seas in the 4Y dataset

The level of filtering for the overtopping wave datasets (N_{ow}) is described in Figure 6.23 (2Y: s_{op} = 0.02) and Figure 6.24 (4Y: s_{op} = 0.04). In this case the level of filtering varies considerably between the 2Y and 4Y test series, contrasting with the agreement observed for the N_w filtering measure. In the case of the s_{op} = 0.02 measurements, between 40% and 50% of the overtopping waves are retained. It is intuitive that the filtering for the overtopping waves (N_{ow}) be more severe than for the entire dataset (N_w) as the majority of overtopping events will be found at the extremes of the distributions where the filtering is applied. Nevertheless, the level of filtering observed here is very high. The filtering is more moderate for the steeper test series (s_{op} = 0.04) with 50% - 80% of the overtopping waves retained. The filtering coefficient is also more linear in relation to the spectral inflation factor. The average filtering coefficients for both test series are given in Table 6.4.

Dataset	Bandwidth Method	Spectral Inflation Factor		
Dataset		**1.1**	**1.2**	**1.3**
2Y	Normal Scale	0.518	0.524	0.415
	LSCV – Synth	0.464	0.475	0.365
	LSCV – Meas/Synth	0.412	0.442	0.347
4Y	Normal Scale	0.836	0.678	0.539
	LSCV – Synth	0.805	0.636	0.497
	LSCV – Meas/Synth	0.816	0.653	0.519

Table 6.4 Average N_w filtering coefficient for 2Y and 4Y test series.

The sensitivity of the filtering coefficient to the input Design Sea is greater for N_{ow} data than observed with N_w coefficients. The N_{ow} filtering coefficient varies by 7% - 10% in the case of the 2Y test series, compared to a maximum of ~2% for the N_w data. The variability is smaller for the 4Y test series with a disagreement of 3 % - 6% from the mean.

V_{max} Results

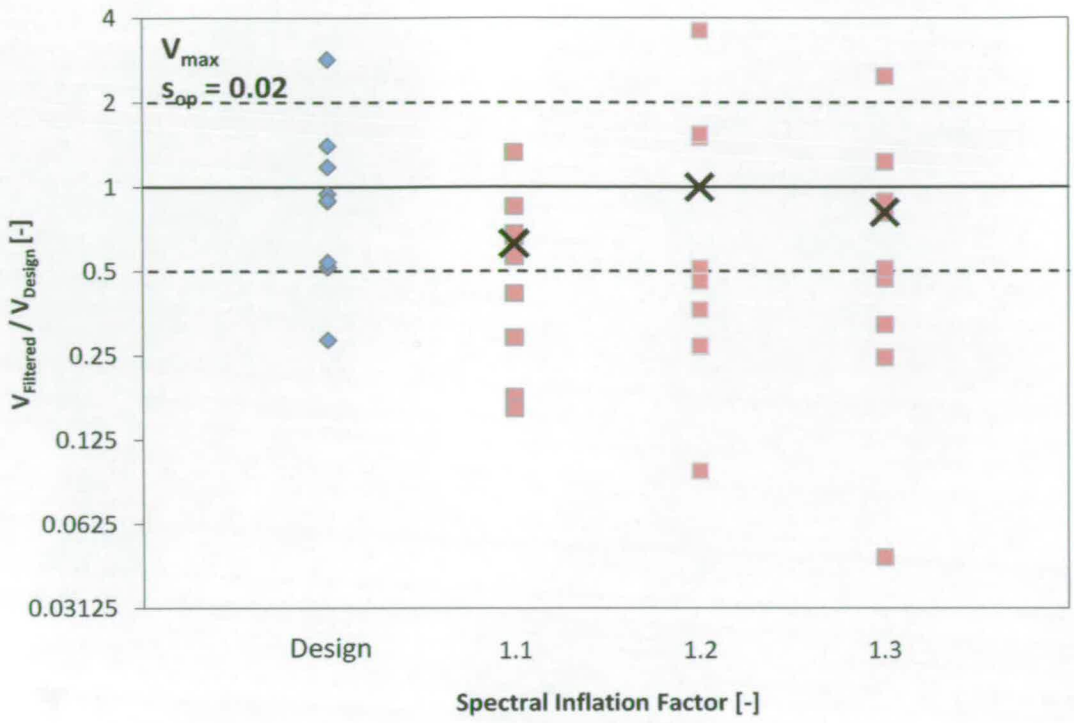

Figure 6.25 V_{max} block analysis (LSCV – Meas/Synth Method). 2Y test series. "X" denotes mean values for each Extreme Sea Dataset.

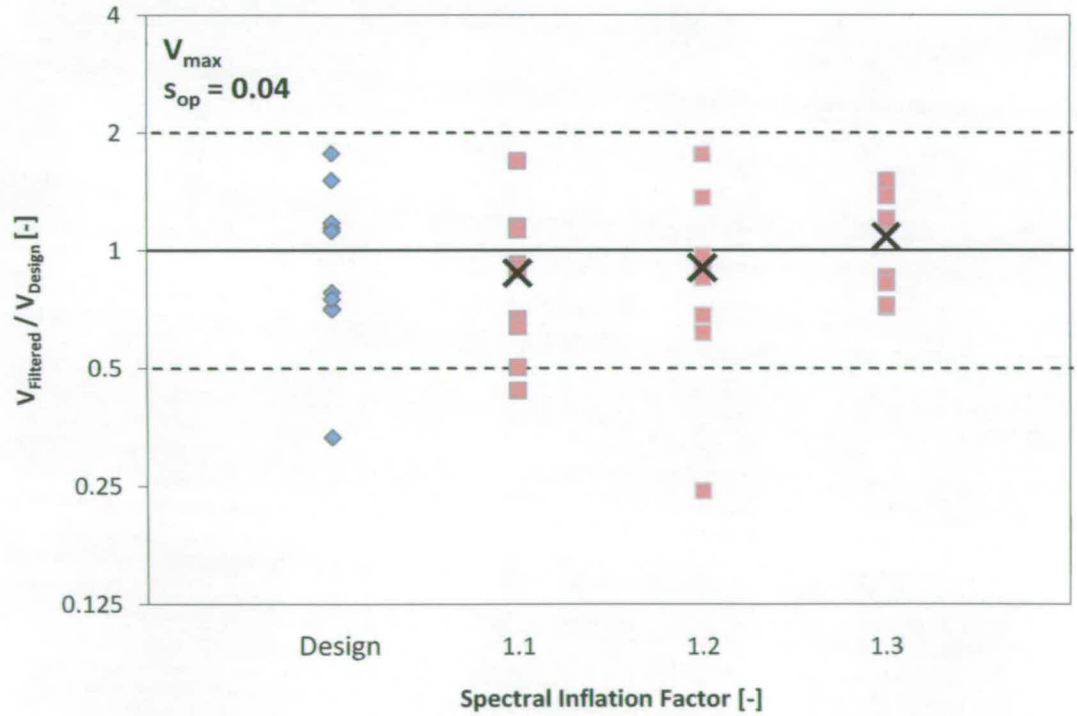

Figure 6.26 V_{max} block analysis (LSCV – Meas/Synth Method). 4Y test series. "X" denotes mean values for each Extreme Sea Dataset.

Examples of filtered Extreme Sea V_{max} outputs are illustrated above for the two test series (2Y: Figure 6.25; 4Y: Figure 6.26). These results only illustrate the output obtained using the "LSCV - Meas/Synth" bandwidth estimator method for clarity. It should be recalled that a single Design Sea measurement is used as an input to the filtering process. The results expressed here use the same input sea in all cases[18]. The sensitivity to the Design Sea input is examined below (§6.4.4).

The results obtained from the Extreme Seas show broad agreement with the Design Sea output for both test series. The agreement in the 2Y test series (s_{op} = 0.02) shows the poorest agreement, particularly for the 1.1 spectral inflation dataset (2BY). The output obtained here is non-conservative, although it remains within a factor of two of the mean Design Sea output. It is noted above (Figure 6.23) that the level of filtering applied to this dataset is more severe than would intuitively be expected and stands apart from the approximately linear filtering coefficient trend seen in the 4Y dataset (Figure 6.24). The mean results obtained for the 1.2 and 1.3 spectral inflation datasets (2CY and 4DY) show good agreement with the Design Sea data, particularly in the case of the 1.2 spectral inflation factor. It is observed that the variability of the results obtained from the Extreme Sea datasets tends to rise for the larger spectral inflation factors.

The mean V_{max} values obtained for the 4Y test series (Figure 6.26) show good agreement with the Design Sea dataset. The level of uncertainty observed in the Extreme Seas is broadly similar to Design Sea dataset.

[18] Test references 2AYcal8 and 4AYcal7 for the 2Y and 4Y test series respectively.

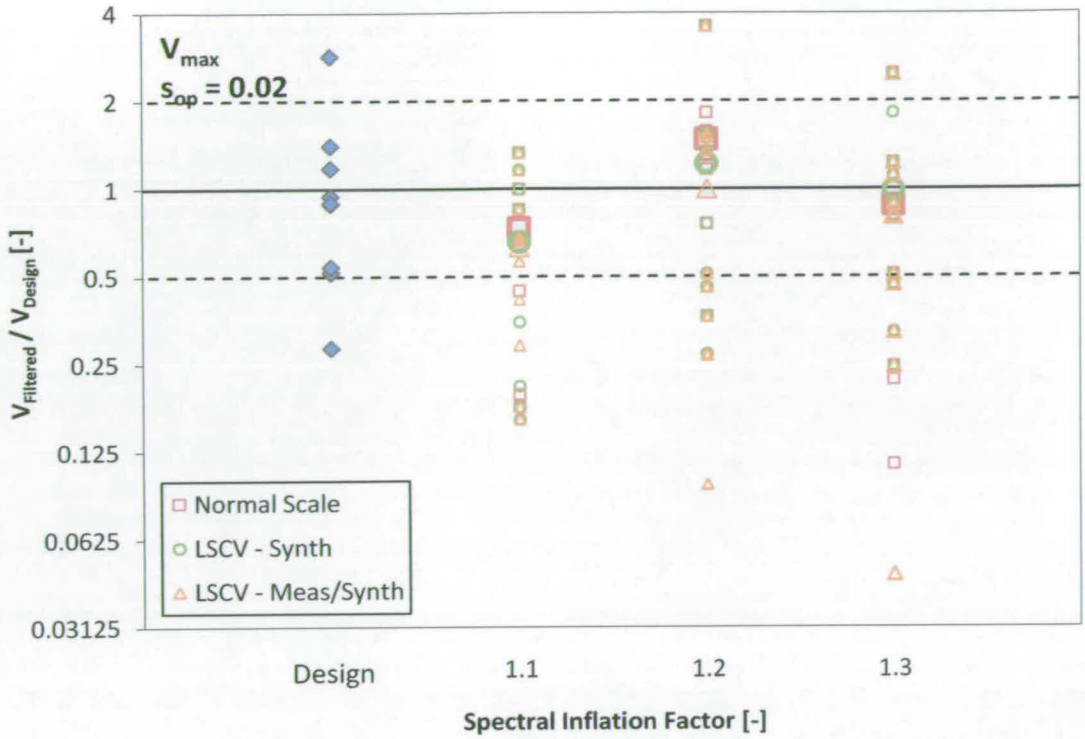

Figure 6.27 V_{max} block analysis (multiple bandwidth methods). 2Y test series. Emphasised data points denotes mean for each Extreme Sea dataset.

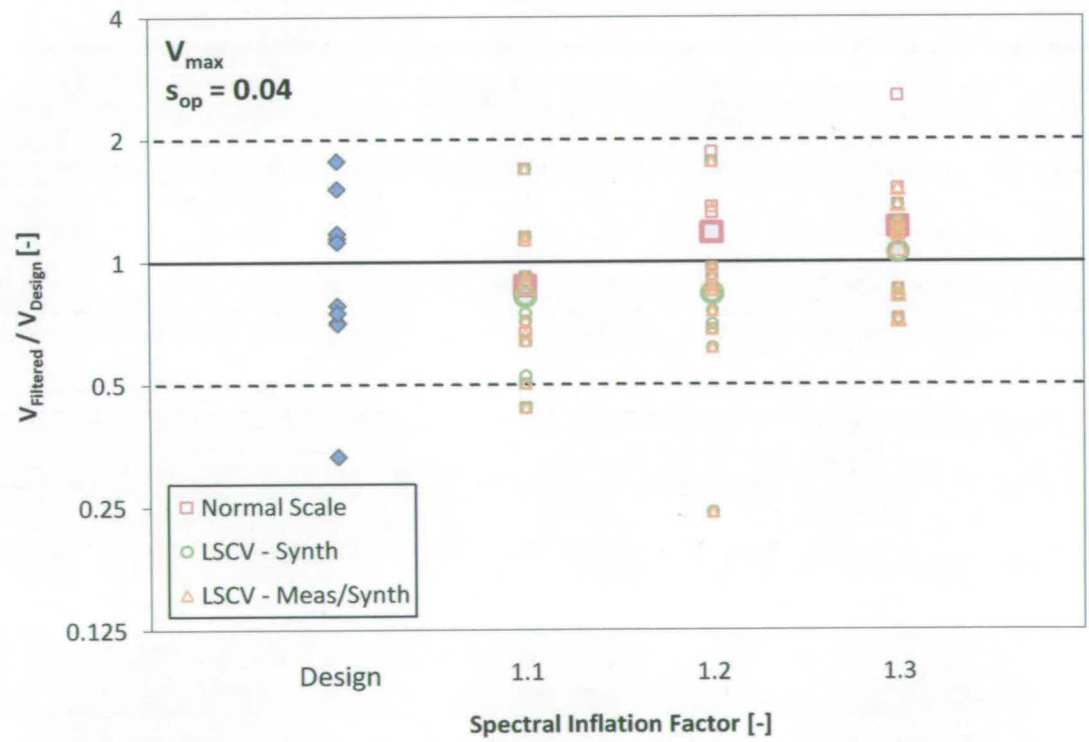

Figure 6.28 V_{max} block analysis (multiple bandwidth methods). 4Y test series. Emphasised data points denotes mean for each Extreme Sea dataset.

The results illustrated for the two datasets (Figure 6.25 and Figure 6.26) are reproduced above with additional data representing the output from the two other bandwidth estimation methods ("Normal Scale Rule" and "LSCV-Synth"). The emphasised, enlarged, data points represent the mean value for each filtered Extreme Sea dataset.

It is observed that the outputs from the different filtering methods are in close agreement for both the 2Y test series (Figure 6.27) and the 4Y test series (Figure 6.28). In both cases the mean V_{max} value obtained with the Normal Scale Rule is slightly higher than the LSCV bandwidth methods. This is likely related to the less severe filtering applied by the "smoother" probability distributions obtained from these Normal Scale probability distributions (§6.4.1). The results obtained from both LSCV estimation methods show very close agreement.

$V_{1\%}$ Results

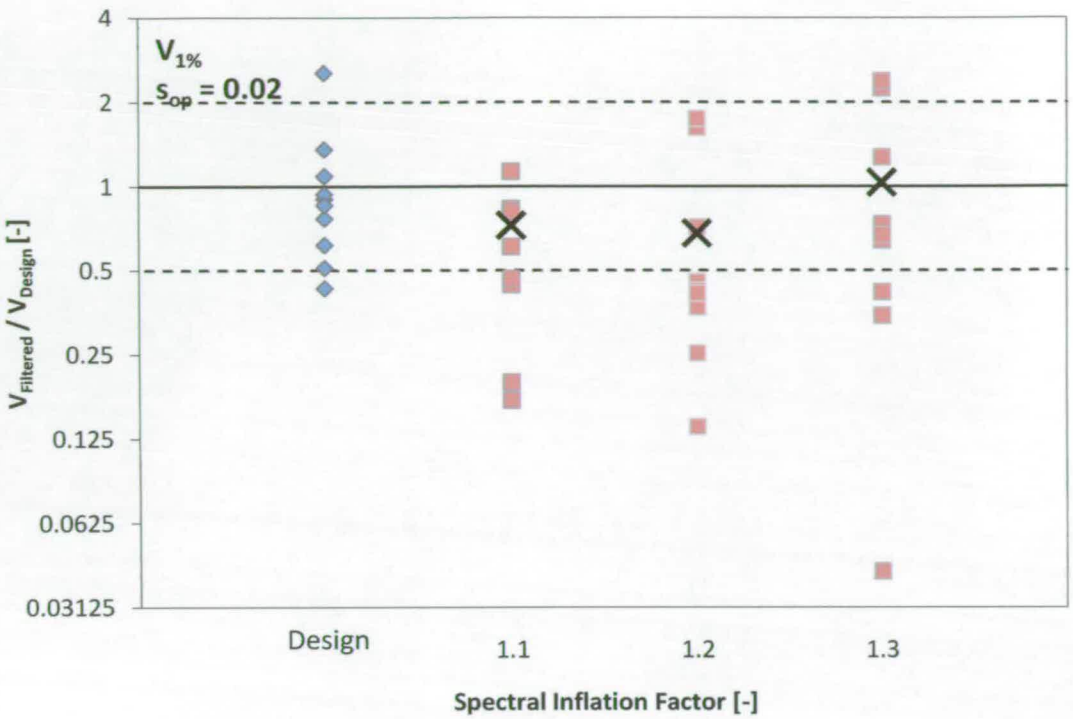

Figure 6.29 $V_{1\%}$ block analysis (LSCV – Meas/Synth Method). 2Y test series. "X" denotes mean values for each Extreme Sea Dataset.

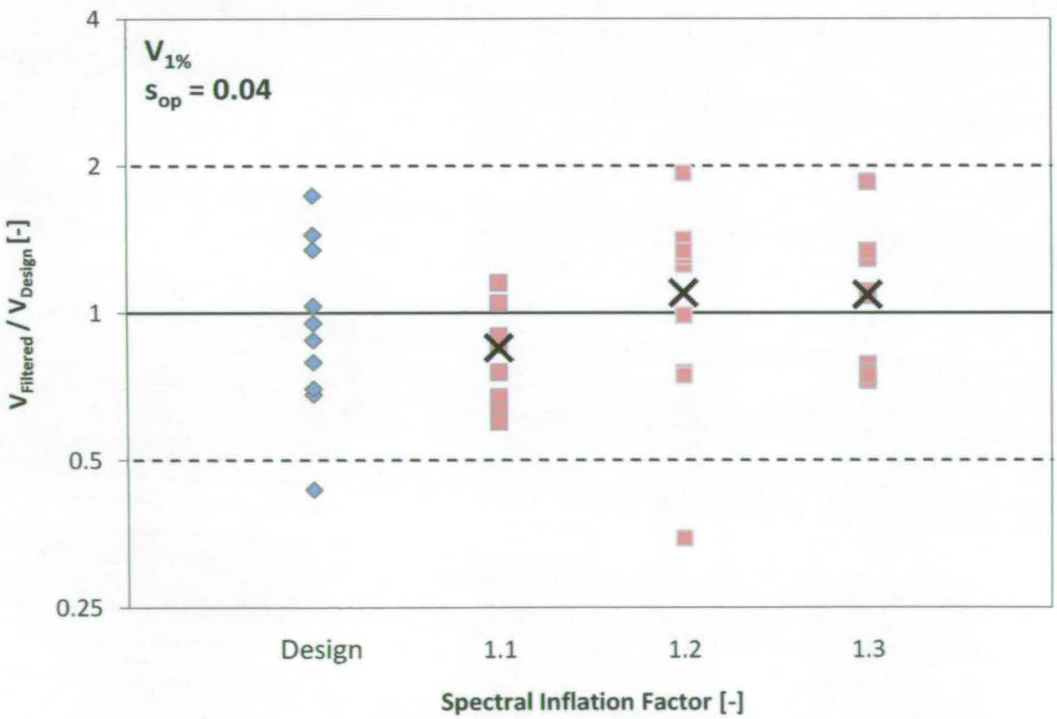

Figure 6.30 $V_{1\%}$ block analysis (LSCV – Meas/Synth Method). 4Y test series. "X" denotes mean values for each Extreme Sea Dataset.

Examples of filtered Extreme Sea $V_{1\%}$ outputs are illustrated above for the two test series (2Y: Figure 6.29; 4Y: Figure 6.30). These results only illustrate the output obtained using the "LSCV - Meas/Synth" bandwidth estimator method for clarity.

The results obtained for the 2Y test series (Figure 6.29) underestimate the overtopping volume for both 1.1 and 1.2 spectral inflation factor datasets (2BY and 2CY) respectively. The results obtained for the most extreme dataset (2DY, spectral inflation factor of 1.3) show close agreement with the Design Sea values. This differs somewhat from the trend observed in V_{max} data illustrated previously, where the largest volumes were associated with 1.2 spectral inflation factor. In all cases the mean value of $V_{1\%}$ is within a factor of two of the Design Sea data, although it is non-conservative in this example. The variability associated with the Extreme Sea dataset is somewhat larger than observed in the Design Sea.

The results for the 4Y test series (Figure 6.30) show closer agreement with the mean value of $V_{1\%}$ within 10 - 15% of the mean Design Sea value. The variability of the measurements is similar to those observed in the Design Sea tests.

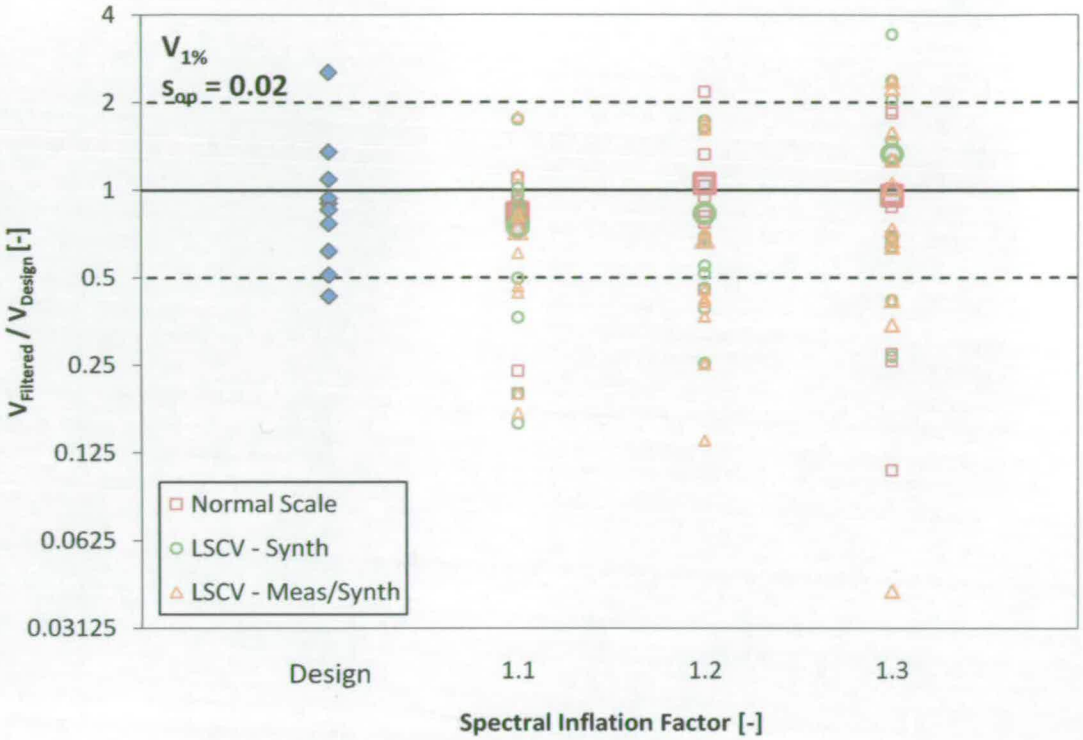

Figure 6.31 $V_{1\%}$ block analysis (multiple bandwidth methods). 2Y test series. Emphasised data points denotes mean for each Extreme Sea dataset.

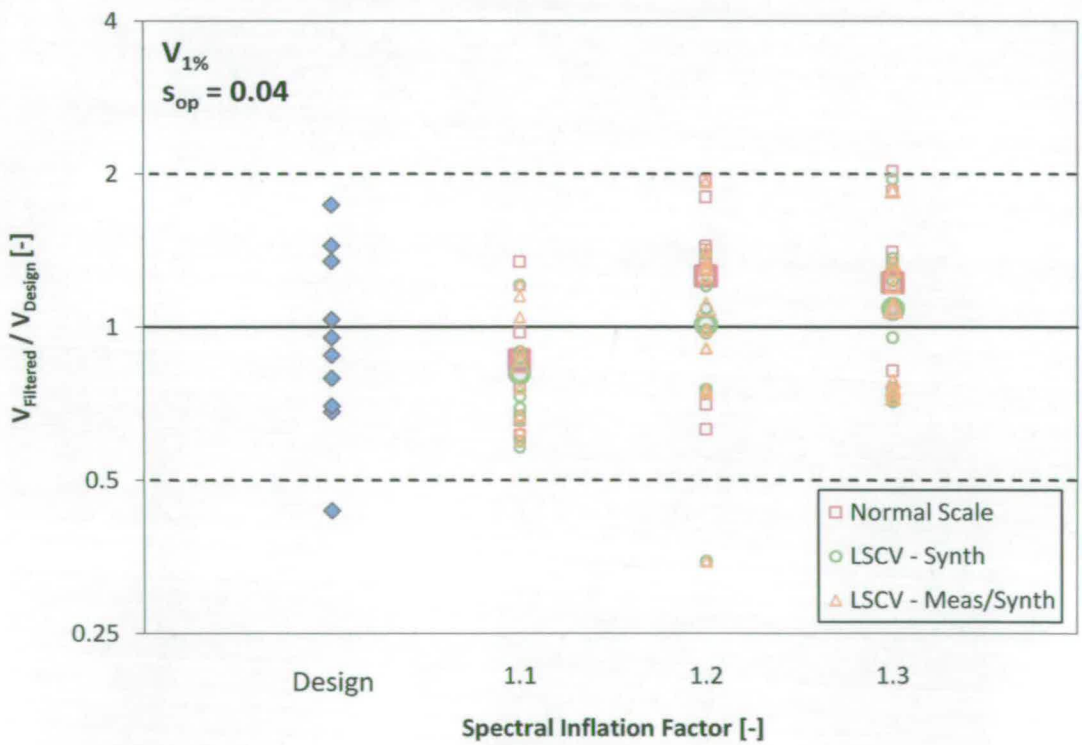

Figure 6.32 $V_{1\%}$ block analysis (multiple bandwidth methods). 4Y test series. Emphasised data points denotes mean for each Extreme Sea dataset.

The three bandwidth estimation methods are compared in Figure 6.31 (2Y test series) and Figure 6.32 (4Y test series). The methods produce broadly similar outputs, as observed with the V_{max} results discussed above. The Normal Scale Rule method gives the most conservative estimate of $V_{1\%}$ in all cases except the most Extreme Sea in the s_{op} = 0.02 dataset (2DY). There is minimal disagreement between the LSCV estimation methods.

6.4.3 Extreme Sea Block Analysis (Optimised Kernel Rotation)

The kernel rotation angles detailed in §6.3.3 are compared here to results obtained using the Normal Scale Rule bandwidth estimator.

Extreme Sea Filtering Level

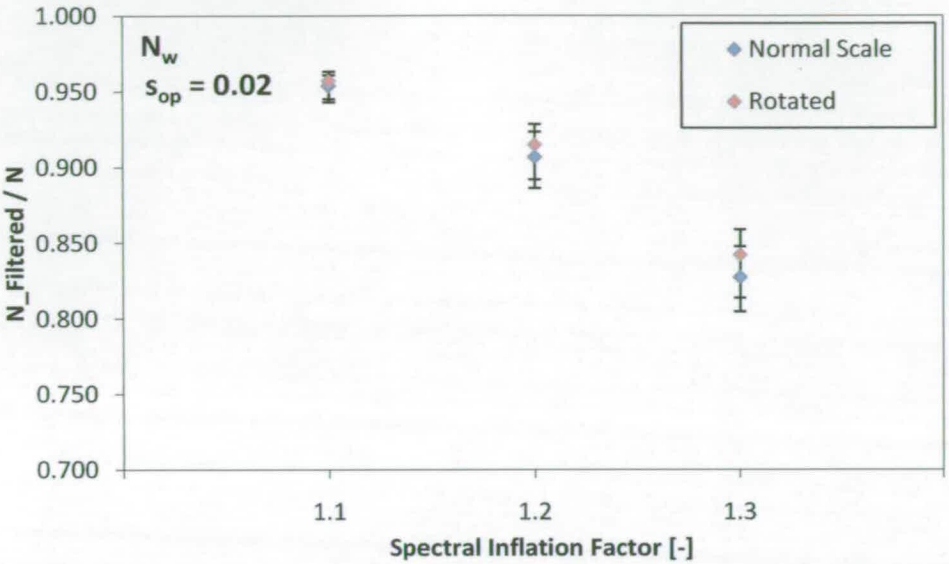

Figure 6.33 Filtering level for all measured waves (N_w) for Extreme Seas in the 2Y dataset

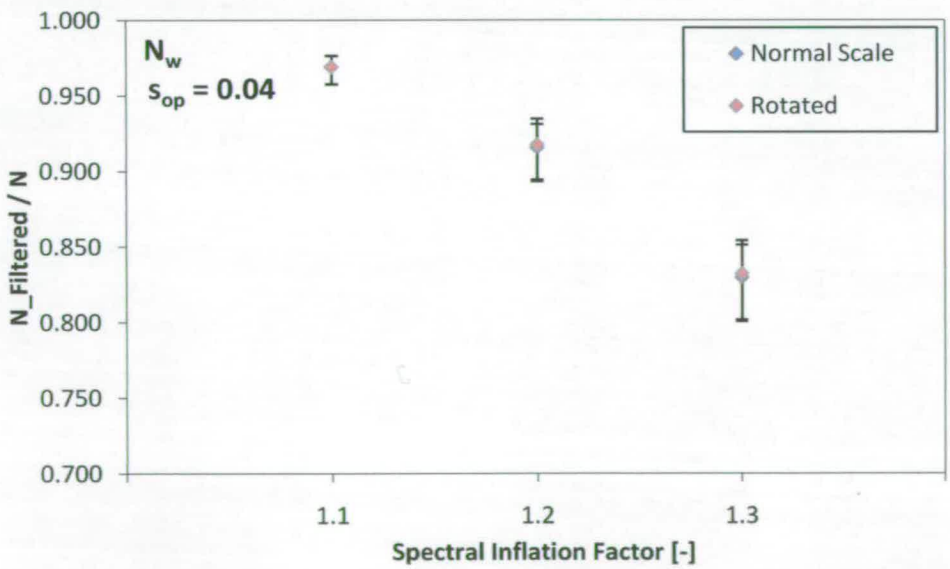

Figure 6.34 Filtering level for all measured waves (N_w) for Extreme Seas in the 4Y dataset

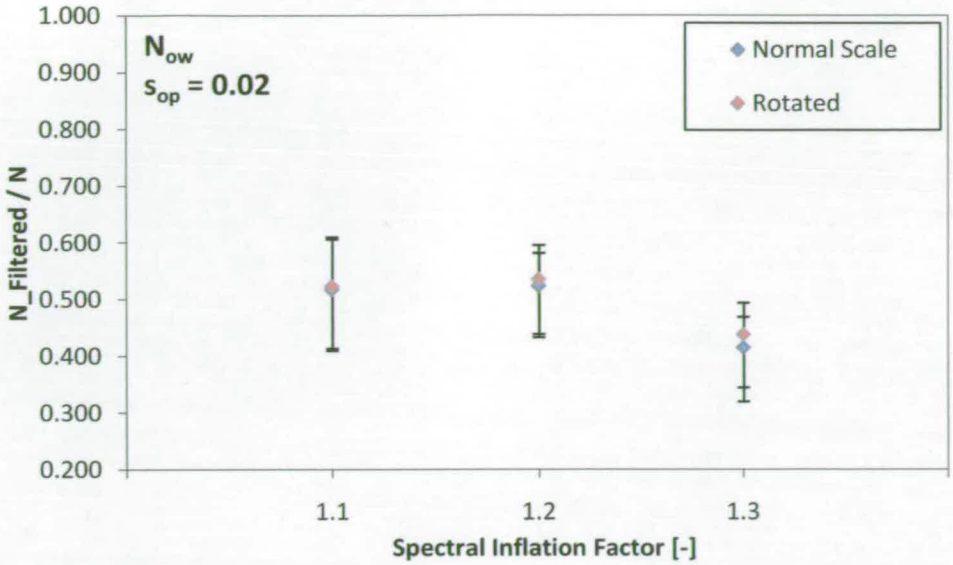

Figure 6.35 Filtering level for overtopping waves (N_{ow}) for Extreme Seas in the 2Y dataset

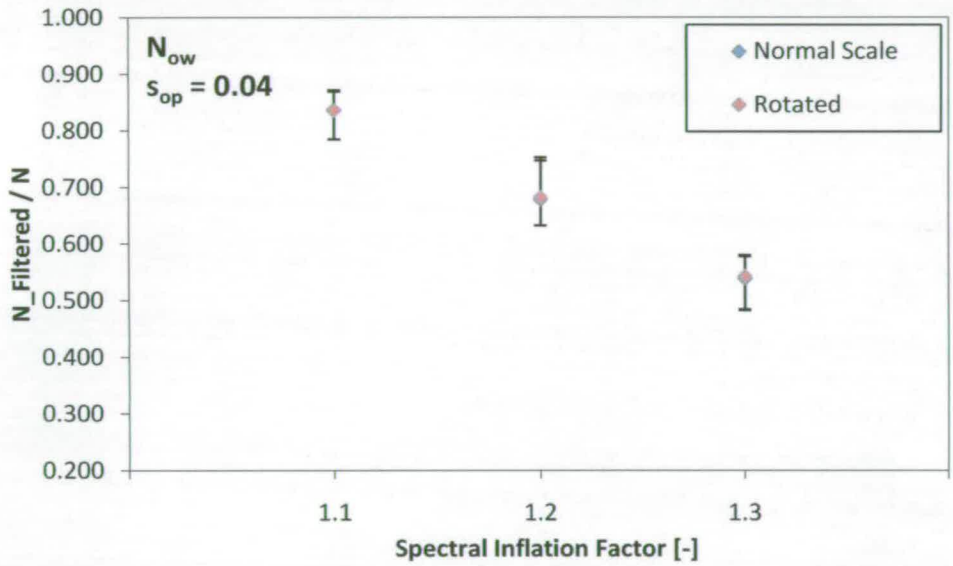

Figure 6.36 Filtering level for overtopping waves (N_{ow}) for Extreme Seas in the 4Y dataset

It is observed in the plots above that the results obtained using the kernel rotation angle are very similar to those obtained using the conventional Normal Scale Rule. This is particularly true for the results obtained from the 4Y test series (s_{op} = 0.04). Where there is an observable difference the filtering process is slightly less severe in the rotated kernel case.

V_{max} Results

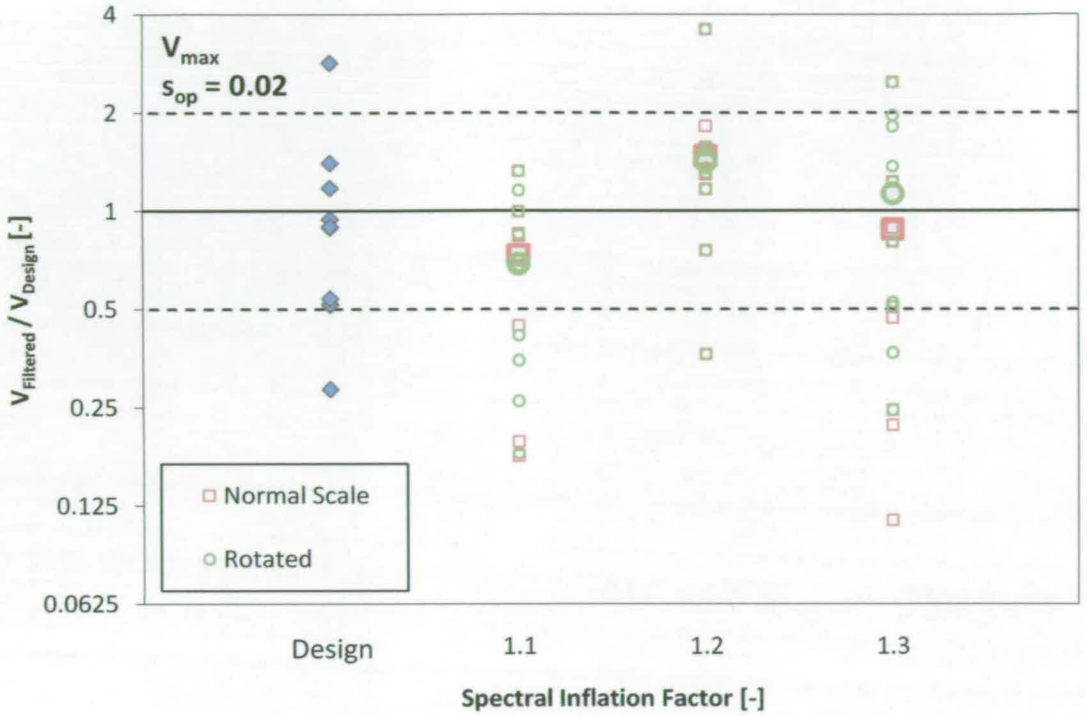

Figure 6.37 V_{max} block analysis (rotated bandwidth method). 2Y test series. Emphasised data points denotes mean for each Extreme Sea dataset.

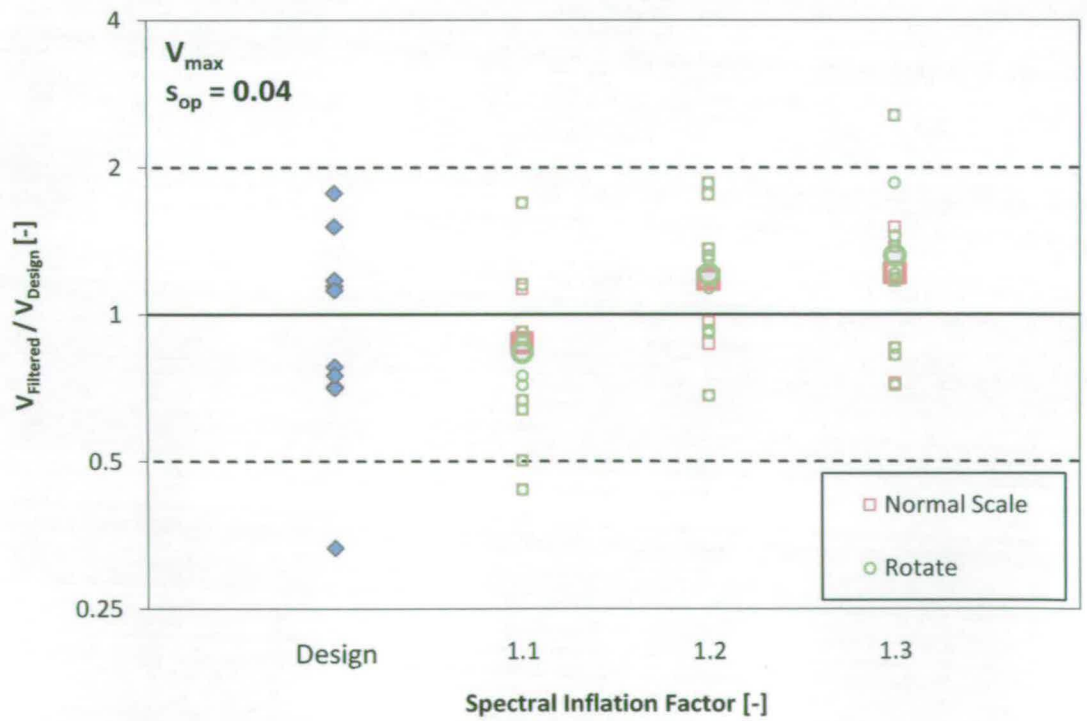

Figure 6.38 V_{max} block analysis (rotated bandwidth method). 4Y test series. Emphasised data points denotes mean for each Extreme Sea dataset.

$V_{1\%}$ Results

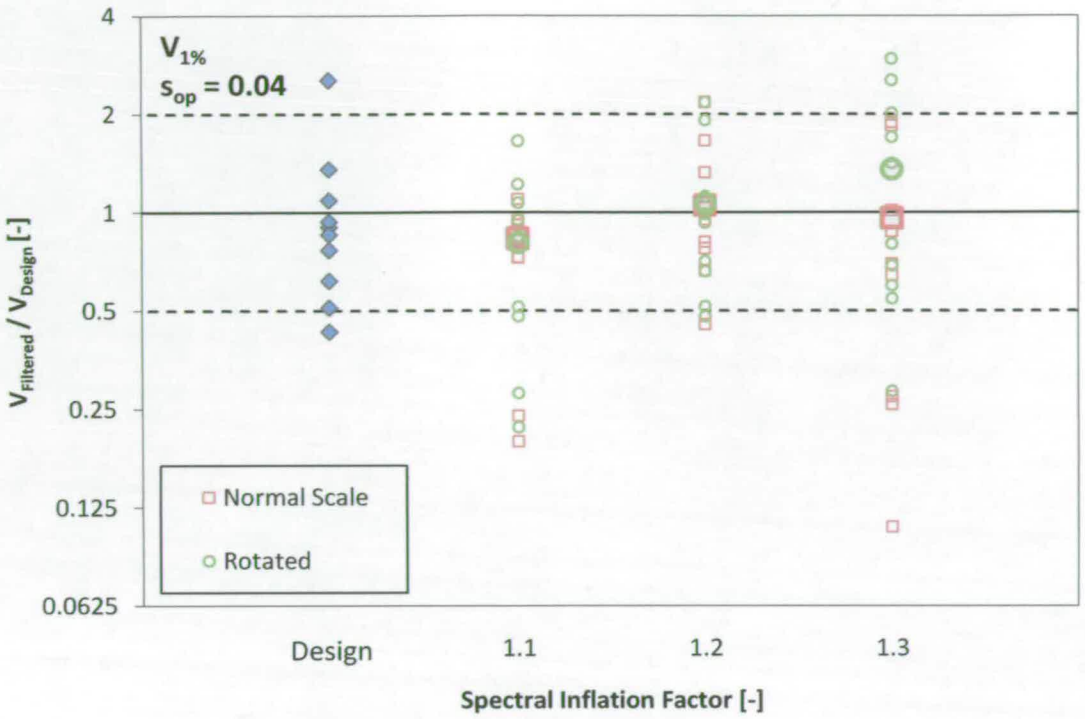

Figure 6.39 $V_{1\%}$ block analysis (rotated bandwidth method). 2Y test series. Emphasised data points denotes mean for each Extreme Sea dataset.

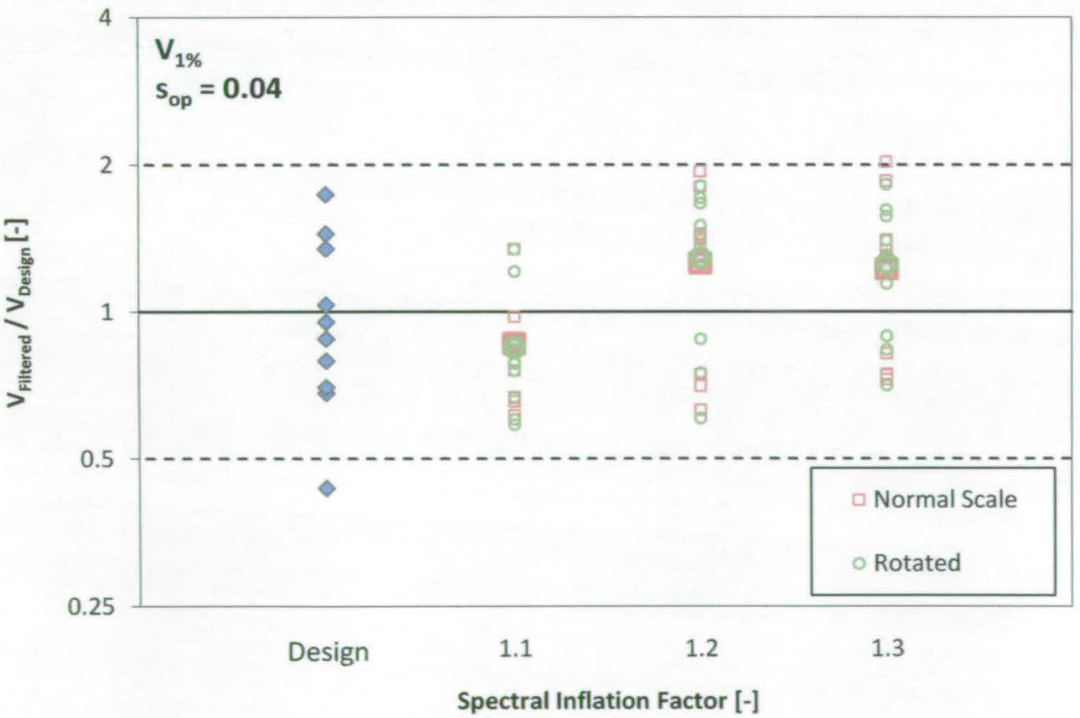

Figure 6.40 $V_{1\%}$ block analysis (rotated bandwidth method). 4Y test series. Emphasised data points denotes mean for each Extreme Sea dataset.

The V_{max} block analysis results are detailed above for 2Y (Figure 6.37) and the 4Y (Figure 6.38) test series. There is little observable difference between the results, mirroring the behaviour of the filtering coefficient results outlined above.

This behaviour is repeated for the $V_{1\%}$ results (2Y: Figure 6.39; 4Y: Figure 6.40). The results obtained from the rotated kernel filtering process are, to all intents and purposes, identical to those obtained with the Normal Scale Rule.

6.4.4 Sensitivity to Design Sea Input

The results presented above are based upon a single Design Sea test selected from each dataset (2AY and 4AY). The mean extreme value (V_{max} or $V_{1\%}$) is presented for each filtered Extreme Sea. The sensitivity of this "mean - extreme" value to the Design Sea input (used to produce the filtering probability distributions) is examined here.

The sensitivity to the Design Sea is presented below as the "Variation from the Baseline". The "baseline" value is simply the mean V_{max} or $V_{1\%}$ value obtained for that particular filtered Extreme Sea taken across all ten Design Sea inputs.

V_{max} Sensitivity

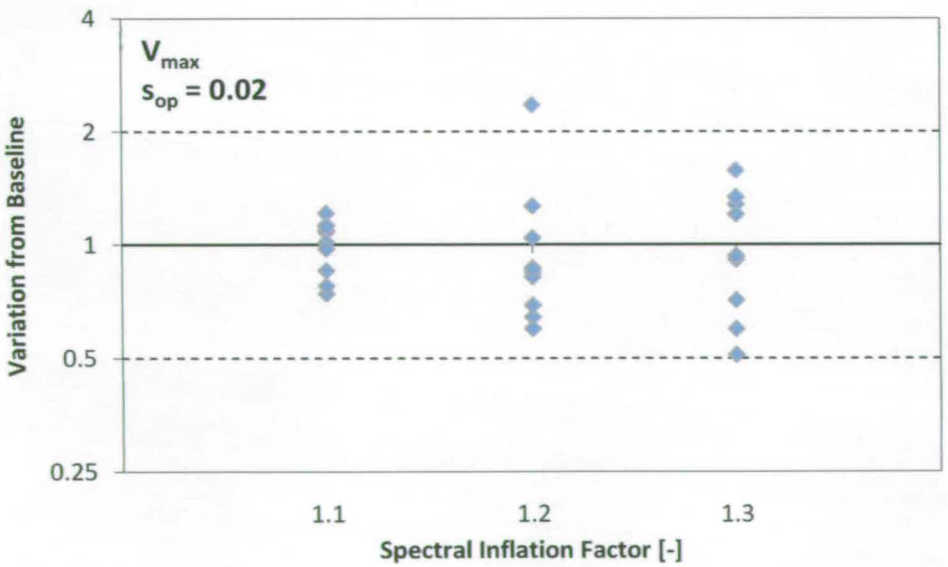

Figure 6.41 Variation in mean V_{max} with changing Design Sea Input. 2Y test series.

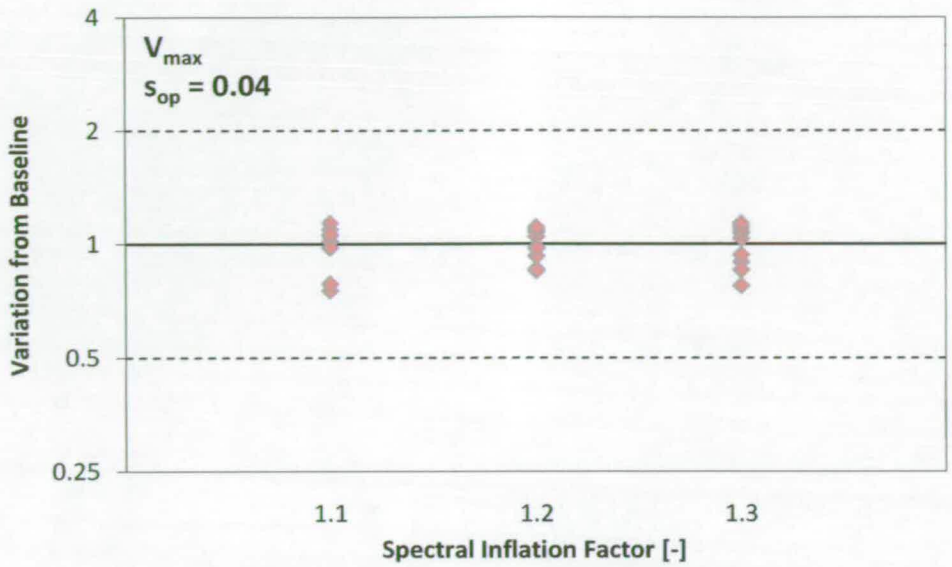

Figure 6.42 Variation in mean V_{max} with changing Design Sea Input. 4Y test series.

The variation in V_{max} is illustrated above for the s_{op} = 0.02 (Figure 6.41) and s_{op} = 0.04 (Figure 6.42) test series. The results show markedly different behaviour. The 2Y test series show variations of a factor of 1.5 -2 from the baseline for the larger spectral inflation factors. The variation is considerably smaller for the lowest spectral inflation factor, with a variation of a factor of approximately 1.2.

The sensitivity to the Design Sea input is considerably smaller for all results in the 4Y test series. In this case the results are spread by a factor of 1.10 – 1.15 from the baseline.

$V_{1\%}$ Sensitivity

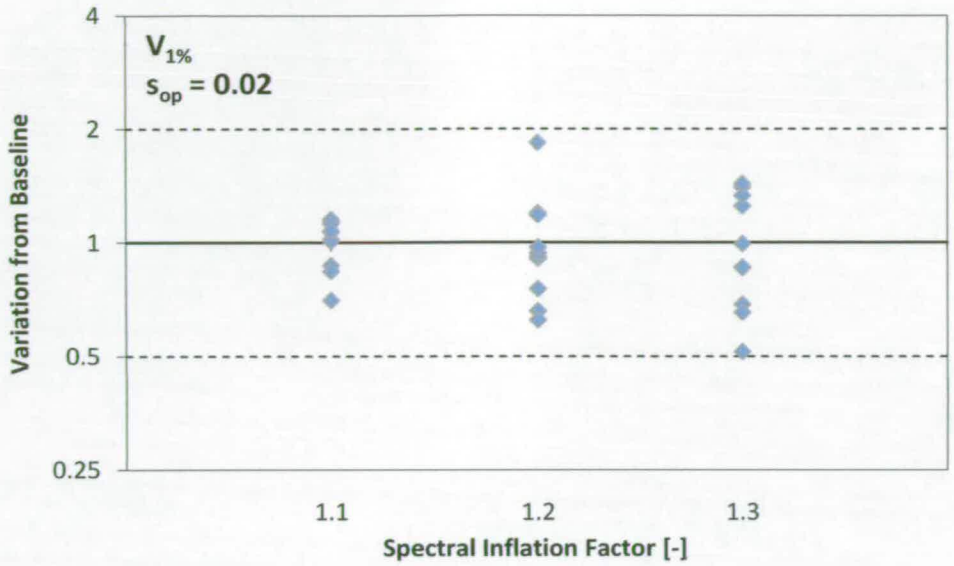

Figure 6.43 Variation in mean $V_{1\%}$ with changing Design Sea Input. 2Y test series.

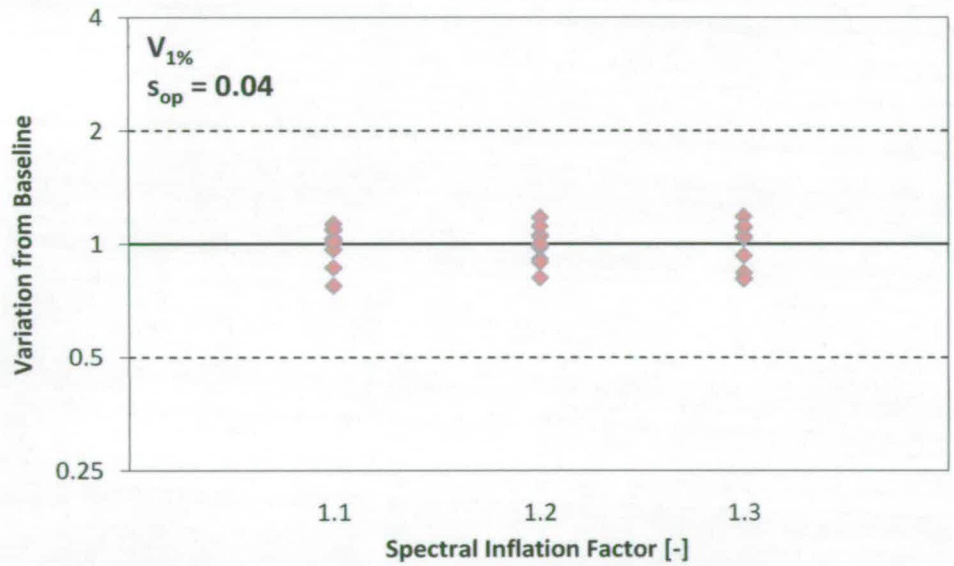

Figure 6.44 Variation in mean $V_{1\%}$ with changing Design Sea Input. 4Y test series.

The sensitivity of the $V_{1\%}$ to the input sea condition is very much the same as those observed in the V_{max} results. Given the close correlation of $V_{1\%}$ to V_{max} this outcome is expected.

6.4.5 Efficiency Gains

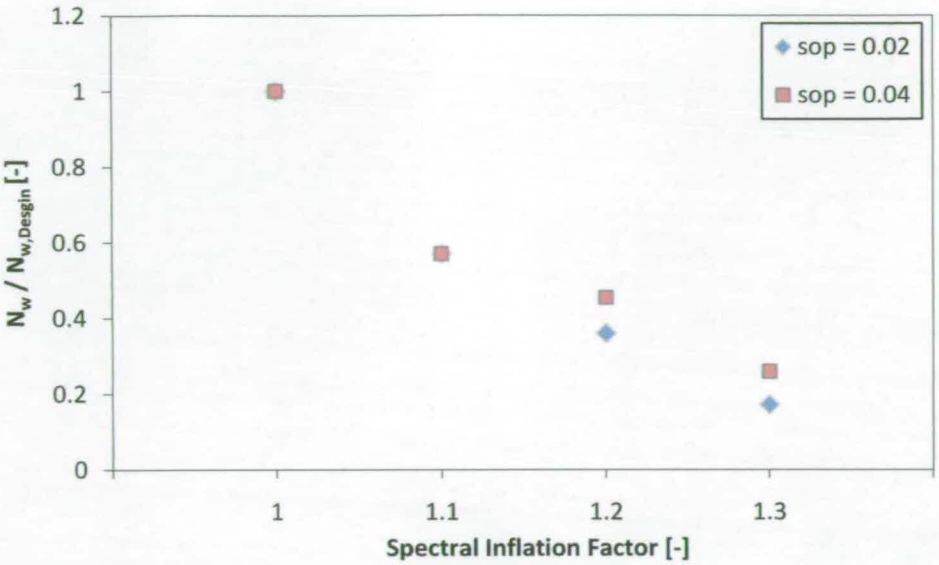

Figure 6.45 Extreme Sea dataset test lengths relative to the Design Sea dataset.

The overreaching aim of the Importance Sampling technique is to increase the efficiency of random wave modelling. In real terms this is measured by the reduction in test length. The relative test lengths (in terms of N_w) of the Extreme Seas (prior to filtering) are illustrated in Figure 6.45. It should be recalled that these test lengths were chosen such that the Extreme Sea datasets would contain a similar number of overtopping events as the Design Sea dataset.

If the results outlined in this chapter are deemed acceptable it is seen that the Importance Sampling technique potentially offers very significant saving in modelling time. The use of modest spectral inflation (I_s = 1.1) almost halves the test length. In the largest Spectral Inflation scenario the test length is reduced below 30% of its original length.

6.5 Summary

The Importance Sampling method outlined in §5 is applied here using small scale overtopping measurements (§3). This includes an analysis of the Kernel Density Estimation (KDE) optimisation techniques also described in the previous chapter. The efficiency gains achievable with the Importance Sampling technique are quantified primarily using the baseline values detailed in §4. The

influence of certain assumptions and parameters (e.g. spectral inflation factor) are examined along with the sensitivity to the choice of Design Sea. The obtained results suggest it is viable to utilise Extreme Sea tests with durations of 25% - 60% of the parent Design Sea, depending on the level of spectral inflation. The significance of these findings are discussed in §7.

7 Discussion

7.1 Overtopping Measurement and Behaviour

The uncertainty inherent in overtopping measurements was examined based upon experimental results. In contrast to earlier studies these experimental results involved repeat tests using the same input spectrum and experimental setup. A detailed analysis of these results is outlined in §4.5.

7.1.1 Measured N_{ow} and V_{max} Uncertainty

The number of overtopping waves (N_{ow}) and the peak individual overtopping volume (V_{max}) are parameters that may be determined directly from overtopping measurements (i.e. they are not inferred from fitted probability distributions). The value of N_{ow} is of interest as it is used in the calculation of a number of other overtopping parameters. The value of N_{ow} is relevant here if the value of V_{max} is to be inferred from a particular probability distribution (e.g. EurOtop guidance). The probabilistic nature of the overtopping response gives rise to larger expected values of V_{max} as N_{ow} increases.

The published guidance (EA-Manual and EurOtop) uses the two-parameter Weibull distribution to describe individual overtopping volumes. The impact of the error in N_{ow} is twofold. Firstly, the probability associated with V_{max} is defined by N_{ow}. If, for example, $N_{ow} = 100$, then $V_{max} = V_{1\%}$. Secondly, the Weibull scale parameter is a function of $\overline{V}$, which is, in turn, a function of N_{ow} and V_{total} (the total overtopping volume collected over the measurement period).

The variability in V_{max} and N_{ow} was examined in §4. The analysis was based on two datasets with s_{op} values of 0.02 and 0.04 (datasets 2AY and 4AY respectively, see §3.6.2). Ten repeat tests were conducted for each dataset, each conforming to the same spectrum but with a different realisation of the elevation time series (i.e. with a different set of random phase angles). The tests were designed to produce overtopping ratios (N_{ow}/N_w) of approximately 5% under conditions which were predominately pulsating, but with overtopping regimes close to where impulsive conditions would be expected. Qualitative observations of the experiments appeared to confirm this behaviour. These tests also form the Design Sea datasets used in exploring the Importance Sampling technique (§7.2).

There is little published literature on the uncertainties associated with overtopping measurements. The magnitudes of these uncertainties are often informally referred to within the coastal engineering community as being with a "factor of two" from the mean. This belief would appear to well justified based upon the results collected here. The value of N_{ow} varied by slightly less than a factor of two from the mean for both datasets. While significant in its own right, the influence of this uncertainty is reduced when calculating the expected peak individual overtopping volume from the EurOtop Weibull distribution, relating to an error of approximately ±30% in V_{max}.

The "factor of two" rule also stands up well when examining the variability in V_{max} for the two datasets. All but one test result in each dataset was within a factor of two of the mean V_{max} value.

7.1.2 Weibull Distribution and $E(V_{max})$ / $V_{x\%}$ Uncertainty

The two-parameter Weibull distribution is well established for the description of individual overtopping volumes, as noted above. The EA and EurOtop manuals give empirical guidance on the selection of these Weibull parameters for engineering design purposes. While it is not the purpose of this research to validate this guidance some limited comparisons can be made with the established approaches, as discussed below.

The use of fitted parametric distributions (e.g. Weibull) can be useful in the analysis of collected datasets. Whilst exceedance probabilities ($V_{x\%}$) can be inferred directly from the data, this process is unreliable, or impossible, with small datasets. In a dataset, for example, with 20 data it would not be possible to directly determine an exceedance probability below $V_{5\%}$, and this result would be subject to uncertainty borne by being determined from a single sample. The use of fitted distributions potentially negates this effect. This same approach may also be applied to the estimation of V_{max}. If determined from a fitted distribution the expected value of V_{max} ($E(V_{max})$) is no longer based upon a single measurement, but is determined by sample size taken as a whole.

Weibull distributions were fitted to ten seas in the two datasets (2AY and 4AY). These datasets typically consisted of 20 - 40 samples. Examination of the Weibull parameters (scale (a) and shape (b)) show significant scatter with variations of up 40-60% from the mean. The scatter is slightly greater for the shape parameter values. The significance of this scatter is apparent when examining the resulting individual volume parameters. The values of $E(V_{max})$ show no reduced scatter when compared to the measured V_{max} values, and are actually more widely distributed for the $s_{op} = 0.02$ dataset.

The scatter observed in V_{max} results is also present in the fitted exceedance levels. The scatter in $V_{1\%}$ is of the order of a factor of 2 - 3 from the mean. This scatter is not restricted to low exceedance probabilities, with similar behaviour observed at the 50% quantile (median) level.

There appears to be no appreciable advantage in using fitted Weibull distributions to calculate V_{max} in the datasets measured here. It is also noted that the values of V_{max} (as measured) and $E(V_{max})$ are closely correlated. This is likely due to the small sample sizes employed. This increases the influence that single data points (i.e. V_{max}) will have on the Weibull fitting procedure. These small sample sizes are, however, typical of a challenging coastal engineering scenario. Structures with high permissible discharge rates (i.e. large value of N_{ow}) are less likely to require accurate quantification of the extreme individual

overtopping volumes. Seawalls and breakwaters protecting, for example, important infrastructure or areas with public access will be designed for low discharge rates. The small sample sizes employed here are not, therefore, atypical.

7.1.3 Application of the Extreme Value Distribution

While the use of fitted Weibull distributions appear to offer no advantage in terms of reducing uncertainty, they do present some useful opportunities to examine the sensitivity of the overtopping response to certain input parameters (e.g. N_{ow}).

The expected value of V_{max} was examined for a number of Weibull distribution shape parameters with varying values of N_{ow}. It is important at this stage to recall the definition of the V_{max}, as calculated from the Weibull distribution. The EA and EurOtop manuals define the probability of an individual overtopping volume exceeding V_{max} as:

$$P(V_i \geq V_{max}) = \frac{1}{N_{ow}}. \tag{86}$$

The volume associated with this probability is calculated from a given Weibull distribution using the formula:

$$V_{max} = a \cdot (\ln(N_{ow}))^{1/b}. \tag{87}$$

This definition of the extreme value is, however, somewhat unconventional. The relationship actually describes the exceedance probability associated with the largest event in the record, not the most probable value of the largest event.

The expected value of V_{max} is described better by employing an extreme value distribution. As the name suggests, this method produces a probability distribution of V_{max} values. If the Cumulative Probability Distribution (CDF) of the individual overtopping volumes (F(V)) is known, the CDF of V_{max} (G(V)) may be calculated using the relationship:

$$G(v) = \left(F(v)\right)^{N_{ow}}. \tag{88}$$

Calculating the Probability Density Function (g(v)) from the CDF allows the expected value of V_{max} to be expressed thus:

$$E(V_{max}) = \int_0^{\infty} v \cdot g(v)dv. \tag{89}$$

This approach also has the advantage that the variance, and therefore the standard deviation (σ), may be extracted from the extreme value distribution:

$$Var(V_{max}) = \sigma^2 = \int_0^{\infty} \{v - E(V_{max})\}^2 \cdot g(v)dv. \tag{90}$$

The estimates of V_{max} obtained from the extreme value distribution are higher than those using the EA-Manual/EurOtop methodology. In small datasets (N_{ow} < 10) the extreme value may increase $E(V_{max})$ by a factor of two for Weibull distributions with a small shape parameter (< 0.6). It is more typical, however, for the increase to be of the order of a factor of 1.2 – 1.5 for samples of ~50 measurements. In tank testing terms this corresponds to a 1000 wave test with 5% of the waves overtopping. This is typical of the tests conducted in this research.

The ability to estimate the standard deviation for a particular distribution allows a quantitative estimation of the expected uncertainty associated with various shape parameter values and levels of N_{ow}. It was observed that the magnitude of the standard deviation relative to V_{max} (i.e. the coefficient of variation (C_v)) increased considerably for low values of N_{ow}. The value of C_v was greater than 0.7 for N_{ow} < 10 compared to C_v < 0.4 for N_{ow} > 50. The sensitivity to the shape parameter was shown to be comparatively small with a difference in C_V of approximately 0.1 across the range of shape parameters given the EA-Manual. The large predicted standard deviations are corroborated by the scattered V_{max} results recorded in the physical model programme.

7.1.4 Comparison to Existing Guidance

Two engineering guidance manuals have been referred to frequently in this research: the EA-Manual (1999) and EurOtop (2007). These publications use the Weibull distribution to estimate the value of V_{max}, using the prediction formula described above (Equation (88)). The guidance is given in the form of the Weibull scale and shape parameters. A methodology is also outlined for estimation of N_{ow} (see §2.4.1 for more information).

Although the methodology is broadly similar in both manuals, the EA-Manual gives a matrix of scale and shape parameters with the appropriate value dependent upon the predominant overtopping regime (i.e. breaking or non-breaking) and the offshore peak steepness (s_{op}). The EurOtop manual takes a simpler approach by defining only a single shape parameter, with the scale parameter described as a function of $\overline{V}$. The dependence on the overtopping regime is therefore removed. While this approach may appear less advanced than the EA-Manual guidance the data collected in this research would appear to support this approach. The shape parameters recorded in the repeat tests (datasets 2AY an 4AY) show considerable variability, as discussed above. Shape parameters over the range 0.4 – 1.6 were recorded. This is considerably greater than the range of shape parameters given in the EA – Manual (0.66 – 0.85). Given the level of uncertainty in the Weibull distributions the pragmatic approach would appear to be to adopt a single shape parameter, as taken by the EurOtop guidance. This value (b = 0.75) appears to offer good agreement with the datasets recorded here.

It should be noted that it was not the intention of this research to validate the EA-Manual or EurOtop guidance. It is possible that more extensive testing would suggest that the approach of the EA-Manual, with its dependence on the overtopping regime and s_{op}, is preferable. This testing would, however, have to take account of the variability inherent in the measurement of overtopping data. Repeated or long duration, tests would be required to ensure sufficient confidence in the fitted distributions. It would not be satisfactory to quantify the

scale or shape parameter based upon a single iteration of a particular test setup, except possibly in cases where the dataset is large (high N_{ow}).

7.2 Importance Sampling

7.2.1 Method Overview

Modelling Inefficiency

The analysis outlined above details the high level of uncertainty associated with the prediction and measurement of extreme overtopping volumes, both in terms of the peak individual volume (V_{max}) and low exceedance volumes (e.g. $V_{1\%}$). In addition to this uncertainty, the physical and numerical modeller must also contend with the inefficiency of the modelling process when testing using random seas. Standard practice is to use elevation time series' consisting of a nominal 1000 waves. Only a small number of waves will be significant for the quantification of the extreme response. In the case of the measured V_{max} only one wave, by definition, will be of interest.

This inefficiency is potentially costly. In the relatively small scale wave flume facility used in this research (§3.2.1) 1000 waves equates to a test length of approximately 20 minutes. In a large experimental facility the durations may be much longer. At the GWK facility in Hanover, Germany, a 1000 wave test with a mean wave period of ~8 seconds will take ~2 hours to complete. A more typical test will take ~1 hour. Large test matrices may therefore be costly in terms of facility hire and personnel cost. Regardless of the financial considerations (which may not be particularly relevant in an academic environment), it is attractive to increase the proportion of useful data obtained for a test programme.

Deterministic Modelling

If a functional relationship can be established between the incident waves and the overtopping response then deterministic approaches become attractive. A deterministic approach involves generating a particular wave (or wave group) rather than the long random elevation time series used in conventional testing.

The difficulty with this approach is twofold. Firstly, the generation of the functional relationships is likely to require considerable research into the wave interaction with the structure or device in question. This may reduce the flexibility of the technique when applied to new applications. Secondly, for coastal applications the transformation of the wave group as it propagates into shallow (or intermediate depth) water must be taken into account. At present no established deterministic modelling procedure exists, although recent research is promising (Jayaratne *et al.*, 2008).

While deterministic modelling is likely to come to further prominence in the future, random wave modelling still offers many important features for the modelling of coastal structures. The strongest advantage of random wave modelling is the non-requirement for a functional relationship describing the response. It is instead assumed that within a long enough test series the response will be adequately characterised. Indeed, the development of functional relationships for deterministic modelling purposes is likely to be dependent on random wave modelling.

The development of functional relationships may be complicated by the potentially non-linear response at the structure. Waves may overtop the structure in a non-breaking or breaking (violent) manner. The "sudden switch" which may be observed as waves change regime will require different wave groups to reproduce the appropriate response. This non-linear behaviour may impair the quality of fit of the parametric distributions (e.g. Weibull) to the measured data. If the prime reason for the physical modelling programme is to quantify the extreme behaviour it is not particularly desirable to have a fitted distribution which is dominated by events corresponding to a different response mode.

Importance Sampling Philosophy

These considerations led to the development of the Importance Sampling technique outlined in this thesis. The challenge here is to increase the proportion of "extreme" events occurring within a random sea. This was to be

achieved without recourse to detailed functional relationships. The aim was to produce a robust, flexible technique which retains the most useful features of conventional random wave testing while reducing its inherent inefficiency.

In order to produce more extreme events it is necessary to use a more Extreme Sea. The Extreme Sea is produced from the Design Sea (used in conventional testing) based on the Spectral Inflation process (§5.3.1). This process "scales" the Design Sea spectrum in both space (in terms of H_{m0}) and time (in terms of T_p). This Extreme Sea will clearly produce events more extreme than found in the Design Sea. The challenge of the Importance Sampling technique is to remove these overly extreme events. The result is a "filtered" Extreme Sea dataset containing waves/events representative of the Design Sea, but with the distribution shifted to produce more of the largest events.

The filtering technique is a probabilistic process which identifies waves (rather than events) that are outwith the expected conditions for the Design Sea. This requires the following:

- A method for describing individual waves and wave groups.
- Input data describing the Design Sea conditions.
- A method for estimating probability distributions based on the Design Sea data.

The Importance Sampling technique does not require that the shallow water transformation processes be understood in detail. The Spectral Inflation process is applied offshore (e.g. as input to the wavemaker). The filtering process is then based upon measurements taken in shallow water. In doing so the method retains the strengths of a conventional stochastic approach (i.e. random wave modelling). Deterministic modelling (e.g. NewWave) requires a more complete understanding of these transformation processes.

7.2.2 Method Application

Design Wave Group

The Importance Sampling technique takes as an input a subset of individual-wave characterisation parameters defining the "Design Wave Group". Unlike the conventional definition of a "Design Wave" these parameters are not quantified at this stage. Rather, the upper limits are determined based upon a series of bivariate probability distributions produced from Design Sea data measured in shallow water.

In the absence of a well-described functional relationship there is some difficulty in determining the parameters to be used to characterise these Design Wave groups. It is also desirable to minimise the number of parameters to prevent the Importance Sampling technique from becoming unwieldy and computationally expensive. In its simplest form a wave may be defined in terms of elevation and time by its zero-downcrossing wave-height and wave-period. The wave-height has the drawback, however, that it is not measured from a fixed reference plane. The definition may be further refined, therefore, by substituting the maximum crest elevation and trough elevation for the wave-height. These measures are taken from the still water level and will therefore remain fixed relative to the seawall structure.

A final parameter used in the definition of the Design Wave group is the maximum crest elevation of the preceding wave. The influence of wave groupiness on wave overtopping is not a well understood (or studied) phenomenon. There is some evidence observed here that large preceding wave crests tend to result in larger individual overtopping volumes, particularly in steeper seas. It is thought that this behaviour may be related to the interaction of the reflected preceding wave with the overtopping wave, perhaps "tripping" the wave into breaking. This phenomenon would perhaps form an interesting topic for future research.

The final Design Wave group was therefore defined by the following parameters:

- Wave period (T)
- Trough elevation (η_T)
- Crest elevation (η_C)
- Preceding-wave crest elevation (η_{C-1})

Importance Sampling Filtering

The Design Wave Group parameters form the input to the Importance Sampling filtering technique. An array of six bivariate joint distributions (in the case of four input parameters) describes the interactions between each parameter pair. These distributions are produced based upon Design Sea measurements collected in shallow water. The solution used to formulate these distributions is Kernel Density Estimation (KDE), a non-parametric technique that is driven solely by the collected dataset. This is attractive as it retains the flexibility of the technique should different a different set of Design Wave parameters be selected.

The mathematics of KDE are described in detail in §5.5. In simple terms a KDE probability estimation is produced by the summation of many individual kernels, one for each sample in the dataset. The size and shape of these kernels will influence the form of the final probability distribution. In this research two elements were examined:

- The "bandwidth" parameters, describing the size of the individual kernels along the x and y axes of the bivariate distributions.
- The orientation of the kernel. The kernel is resized along a rotated set of axes.

These elements were optimised using a technique known as Least Squares Cross Validation (LSCV – §5.5.5). This technique was found to be computationally highly expensive and the optimised bandwidth parameters

appeared to show poor convergence. This convergence was lessened when determining the optimum rotation angle.

The Importance Sampling technique was applied using the optimised bandwidth parameters and rotation angles. The bandwidth parameters were also calculated using the "Normal Scale Rule" method. The normal scale rule is quickly and simply determined from the data (without the need for costly optimisation) but is based upon the assumption that the sample is normally distributed. This assumption may not be justified here.

After estimation of the bivariate distributions the low probability events (> 99.9% non-exceedance) are removed from the Extreme Sea dataset. The results of the experimental programmed are discussed below. These results showed little sensitivity to the different bandwidth optimisation methods. Changes in kernel rotation angle also produced little difference in the outcome. Measurements taken with the Normal Scale bandwidth and zero - rotation angle showed a variation of only a few percent from the optimised values. This result is somewhat surprising as kernel density estimation is known to be highly sensitive to the kernel shape. The explanation may lie in the relative level relative of filtering applied to the Extreme Sea datasets. It is noted that the number of overly-extreme waves removed the Extreme Sea dataset is broadly similar for the different KDE optimisation techniques. The definition of the extreme of the distribution appears to be fairly insensitive to the range of bandwidth parameters used in this research.

It is suggested, based upon the above observations, that the Normal Scale rule is adequate for the estimation of the bandwidth parameters and that there is little benefit in applying kernel rotation. This solution avoids the need for costly, and perhaps ultimately impractical, use of the LSCV optimisation technique.

7.2.3 Achievable Gains

Importance Sampling Test Programme

The Importance Sampling technique was examined using two test series with peak offshore steepnesses (s_{op}) of 0.02 and 0.04. Each test series consisted of ten baseline Design Sea tests of ~1000 waves and three sets of Extreme Sea tests.

The Design Sea tests were conducted under predominately non-breaking conditions, although violent breaking events were observed for both test series. This suggests the largest overtopping volumes may not be associated with non-breaking waves.

Spectral Inflation values of 1.1, 1.2 and 1.3 were applied to produce the Extreme Seas. The lengths of the Extreme Sea datasets (in terms of N_w) were chosen to produce similar number of overtopping events (N_{ow}) to the Design Sea dataset.

The Importance Sampling technique was applied to the Extreme Sea dataset using various KDE optimisation methodologies. As the outputs obtained from these methods were broadly similar no distinction will be made between the results in the discussion below.

The analysis of the Extreme Sea datasets was conducted by dividing the wave record into 10 equal length blocks, effectively creating the equivalent of 10 short random seas. The overtopping outputs in these blocks were then compared to the overtopping measurements from the 10 long Design Sea tests. This analysis was conducted for both V_{max} and $V_{1\%}$ measurements.

The outputs from the Importance Sampling method (V_{max} and $V_{1\%}$) are broadly similar to the results obtained from the conventional Design Sea tests. The scatter in the results is typically of the order of factor of two from the mean. The overall agreement with the Design Sea is within a factor of 1.5 from the mean. It is noted, however, that the results are not necessarily conservative. The Importance Sampling technique may potentially underestimate (or

overestimate) the extreme overtopping volumes. This uncertainty is, based upon the results collected here, within the range typically accepted for overtopping quantification.

The Spectral Inflation factors used here produced Extreme Sea datasets significantly shorter than the Design Sea case. A fairly modest spectral inflation factor of 1.1 approximately halved the test length, while the largest spectral inflation level produced a test length approximately a quarter of the length of the conventional tests. This equates to a 10,000 wave test series being replicated using only 2500 waves, plus the 1000 waves required to define the Design Sea state. Further efficiency gains could be achieved if the requirement to measure the Design Sea was removed. The possibility of achieving this is discussed briefly below.

7.2.4 Noted Limitations

The Importance Sampling technique, in its current form, requires measured data describing the Design Sea. This takes the form of an elevation time series measured in shallow water thereby describing the incident wave climate at the structure.

If the Importance Sampling technique is to offer significant efficiency savings it is required that these Design Sea test are kept relatively short. It was decided that a single Design Sea test (~1000 waves) be used as the input to the Importance Sampling analysis. If this technique is applied in a "real world" scenario this may represent the test used to characterise the mean response.

In this case, ten realisations of the Design Sea were available for the two datasets (s_{op} = 0.02 and 0.04). Examining the sensitivity of the Importance Sampling technique to the input Design Sea revealed differing behaviour between the two test series. In the s_{op} = 0.02 test series, varying the choice of Design Sea altered the mean V_{max} and $V_{1\%}$ values by a factor of 1.5 - 2.0. This is clearly significant, although it is within the "factor of two" uncertainty commonly quoted for overtopping measurements.

The sensitivity of the s_{op} = 0.04 datasets to the Design Sea input condition is somewhat smaller. The variation in the mean V_{max} and $V_{1\%}$ values is typically of the order of 1.10-1.15 from the mean.

7.3 Further Work and Development

The Importance Sampling technique, as outlined here, is intended as a first iteration of the method. In effect, it is a feasibility study examining its suitability for deployment in commercial and academic research fields.

One recognised drawback is the requirement for a measured Design Sea dataset for the production of the filtering probability distributions. Removing this element would improve efficiency (less testing) and flexibility. Extreme Sea datasets could be reanalysed using different Design Sea test conditions without recourse to tank testing. A time-domain numerical modelling approach (e.g. Boussinesq) may offer a solution for the production of the shallow water Design Sea elevation time series.

The Importance Sampling technique, as described, removes overly-extreme waves and their associated responses from a measured sequence of waves (§5.2.3) in a spectral-inflated sea (§5.3.1). While this brings about an improvement in efficiency compared to conventional modelling, a certain proportion of the waves are disregarded with no useful information having been extracted. A suggested method, referred to as "pre-filtering", involves removing these overly-extreme waves prior to generation. There are several challenges presented by this technique. The filtered waves and wave groups would require "re-stitching" to assemble a continuous elevation time series. Some understanding of the wave transformation effects would also be required to translate the elevation time series, measured at the structure, to an input to the wavemaker (or numerical model). The absence of a requirement to model wave transformations is a feature of the "conventional" Importance Sampling method developed in this research. The pre-filtering technique is effectively deterministic in this regard and loses this key advantage of the conventional

method. In deep and intermediate water applications, however, this element of the method becomes less important. The pre-filtering technique has applications for modelling scenarios where the structure (or device) cannot withstand the overly extreme events produced during conventional Importance Sampling. For example, a study into the stability of rubble breakwaters would not be feasible using the Importance Sampling technique in its current form due to the damage inflicted on the structure.

8 Conclusions

This research investigated the feasibility of adapting and applying a statistical technique (Importance Sampling) to the measurement of individual overtopping volumes at vertical seawalls. While the basis of this technique originates from the field of Monte Carlo modelling the methodology developed here is novel and differs significantly from the original application. The aim of Importance Sampling is to improve the efficiency of random wave modelling for the purposes of quantifying the largest overtopping volumes. This technique was developed during the course of this research with consideration to future maritime engineering applications. Care was taken to ensure the developed technique would not be limited to seawall modelling applications.

Examination of the published literature identified little information regarding the level of uncertainty associated with the prediction and measurement of maximum individual overtopping values (e.g. V_{max}). In order to address this knowledge gap the uncertainty associated with maximum overtopping values in two large overtopping datasets was quantified. This data also provides a benchmark by which the effectiveness of the Importance Sampling technique may be measured. Conclusions relating to this study are presented below alongside the conclusions relating to the Importance Sampling technique.

8.1 Individual Overtopping Volume Uncertainty

- Little previous work was identified into the uncertainty associated with quantification of maximum individual overtopping volumes. A physical modelling programme was developed to collect data for study of this

uncertainty. Repeat vertical seawall overtopping tests using the same deep water spectrum but with different realisations of the elevation time series were successfully conducted. Measured values of V_{max}, $V_{1\%}$ and N_{ow} showed considerable variability for these repeat tests. Variations of a factor of two from the "baseline" value should be expected for these parameters.

- Weibull distributions fitted to the repeat tests show considerable uncertainty. Examining the scale and shape parameters reveals variability from the mean by a factor of two. The uncertainty is manifested in considerable variability in the exceedance volumes ($V_{x\%}$). Again, a variation of a factor of two is expected in $V_{x\%}$. This variation is not limited to the least probable (extreme) events.
- Small sample sizes (e.g. 50 samples in a typical N_{ow} / N_w = 5% test) results in a high correlation between V_{max} and $E(V_{max})$ (i.e. the value of V_{max} determined probabilistically from the distribution). The use of fitted Weibull distributions should not be considered as a viable technique for reducing uncertainty in the quantification of extreme overtopping volumes.
- The value of $V_{1\%}$ is closely correlated with V_{max} for small sample sizes. There is no reduction in uncertainty by characterising the extreme overtopping volume using $V_{1\%}$ rather than V_{max}.
- The use of an extreme value distribution was identified as an alternative to the V_{max} estimation procedure employed in the EA-Manual and EurOtop. This approach provides a theoretical basis for the estimation of the V_{max} uncertainty.
- The use of an extreme value distribution was explored through the examination of two large overtopping datasets. The resulting V_{max} estimate was higher by up to a factor of two in small datasets ($N_{ow} < 10$). Larger datasets show a more typical increase of 20 – 50%. It is recommended that consideration be given by the EurOtop authors to shifting to this method in any future version of the manual

- The use of a single scale and shape parameter in the EurOtop guidance appears to be justified. The average of the distributions fitted to the measured data shows good agreement with the EurOtop guidance. The scattered nature of the individual fitted distributions suggests that a more complex characterisation is likely to be difficult to achieve.

8.2 Importance Sampling

- A novel Importance Sampling methodology was developed and applied to vertical seawall overtopping measurements obtained from the experimental programme. The aim of providing an efficiency improvement over the conventional random wave modelling approach was achieved for the modelled examples. The Importance Sampling technique produced datasets between 25% - 60% of the Design Sea dataset depending on the level of spectral inflation.
- The Importance Sampling technique physical measurement programme was conducted successfully for three Extreme Sea datasets. This related to increases in H_{m0} of 10%, 20% and 30% (Spectral Inflation factors of 1.1, 1.2 and 1.3). These test lengths were, respectively, ~60%, ~40% and ~25% of the length of the original Design Sea test series.
- Kernel Density Estimation (KDE) presented a practical technique for non-parametric estimation of probability distributions based upon measured Design Sea data. The technique was successfully implemented for the filtering of the Extreme Sea dataset.
- The Least Squares Cross Validation (LSCV) KDE optimisation technique proved to be unwieldy and inefficient in practice. The resulting V_{max} and $V_{1\%}$ outputs were relatively insensitive to the optimisation technique. It is recommended, therefore, that the LSCV technique is not applied to the estimation of the KDE parameters. The simpler Normal Scale Rule is sufficient.
- The use of "kernel rotation" for the production of the KDE distributions is not recommended. The V_{max} and $V_{1\%}$ values showed little sensitivity to

the optimised rotation angle. The LSCV optimisation process is also computationally expensive, further reducing the attractiveness of this refinement.

- V_{max} and $V_{1\%}$ values obtained using the Importance Sampling technique showed broad agreement with the baseline measurements obtained from the Design Sea tests. The uncertainty in the measurements was typically of the order of a factor of two from the mean.
- The sensitivity of the process to the Design Sea input was not conclusively ascertained. A conservative estimate suggests the mean V_{max} or $V_{1\%}$ may vary by a factor of two. The uncertainty observed in the s_{op} = 0.04 dataset was considerably smaller than this result, with typical variations of a factor of 1.10 – 1.15.

References

Allsop, N.W.H., Besley, P. & Madurini, L. (1995) "Overtopping performance of vertical and composite breakwaters, seawalls and low reflection alternatives." Paper to the final MCS Project Workshop, Alderney, May 1995

Allsop, N.W.H., Bruce T., Pearson, J., Alderson, J. & Pullen, T. (2003) "Violent wave overtopping at the coast, when are we safe?" Int. Conf. on Coastal Management 2003, pp 54-69, ISBN 0 7277 3255 2, Thomas Telford, London.

Allsop, N.W.H, Cuomo, G. & Tirindelli, M. (2006) "New Prediction Method of Wave-in-Deck Loads on Exposed Piers / Jetties / Bridges" Proc. 30th Int. Conf. Coastal Engineering, San Diego, 5, pp 4482-4493, ASCE

Allsop, N.W.H., Bruce, T., Pearson, J. & Besley, P. (2005) "Wave overtopping at vertical and steep seawalls" Jour. Maritime Engineering, 158, pp 103-114, ICE

Besley, P., Stewart, T. & Allsop, N.W.H. (1998) "Overtopping of vertical structures: new prediction methods to account for shallow water conditions", Proc. ICE Conf. Coastlines, Structures and Breakwaters, 2001, pp 245-255, ICE, London

Besley P. (1999) "Overtopping of Seawalls" HR Wallingford, R & D Project Record W5/006/5

Brodtkorb, P.A., Johannesson, P., Lindgren, G., Rychlik, I. & Sjo, E. (2000). "WAFO – A Matlab Toolbox for Analysis of Random Waves and Loads" Proc. ISOPE 2000, pp 343-350

Bruce, T., Allsop, N. W. H. & Pearson, J. (2001) "Violent overtopping of seawalls—extended prediction methods." Proc. of the ICE Conference on Shorelines, Structures and Breakwaters, September 2001. Thomas Telford, London, pp 245–255.

Cassidy, M.J., Eatock Taylor, R. & Houlsby, G.T. (2001) "Analysis of jack-up units using a Constrained NewWave methodology" Jour. Applied Ocean Research, 23, pp. 221-234

Coles, S. (2001) "An Introduction to Statistical Modeling of Extreme Values" Springer-Verlag London Ltd. ISBN 1-85233-459-2

EA-Manual (1999) "Overtopping of Seawalls. Design and Assessment Manual" HR Wallingford, R & D Technical Report W 178, Author: Besley, P., ISBN 1 85705 069X

Endoh, K. & Takahashi, S. (1994) "Numerically Modelling Personnel Danger on a Promenade Breakwater due to Overtopping Waves" Proc. 24th Int. Conf. Coastal Engineering, Kobe, 5, pp 1016-1029, ASCE

Epanechnikov, V.A. (1969) "Non-parametric estimation of a multi-variate probability density" Jour. Theory of Probability and its Applications, 14, pp 153-158

EurOtop. (2007) "Wave Overtopping of Sea Defences and Related Structures: Assessment Manual", Authors: Pullen, T., Allsop, N.W.H., Bruce, T., Kortenhaus, A., Schüttrumpf, H. & van der Meer, J.W., www.overtopping-manual.com

Franco, C., Franco, L., Restano, C. & van der Meer J.W. (1994) "Wave overtopping on vertical and composite breakwaters" Proc. 24th Int. Conf. Coastal Engineering, Kobe, 5, pp 1030-1045, ASCE

Goda, Y. (2000) "Random seas and design of maritime structures (2nd Edition)", World Scientific Publishing. ISBN 981-02-3256-X

Guedes Soares, C., Cherneva, Z. & Antão, E.M. (2004) "Steepness and asymmetry of the largest waves in storm sea states" Jour. Ocean Engineering, 31, pp 1147-1167

Hunt, A., Taylor, P. H., Borthwick, A. G. L., Stansby, P. K., & Feng, T. (2003). "Kinematics of Focused Waves on a Plane Beach in the U.K. Coastal Research Facility", Proc. Coastal Structures Conference 2003, ASCE, pp 740-750

Ingram, D., Bruce, T., & Allsop, N.W.H. (2008) "Post-Overtopping Loads Behind Vertical Structures" Proc. 31th Int. Conf. Coastal Engineering, Hamburg, Germany, 4, pp 3144-3156, ASCE

Jayaratne, R., Hunt A., Bullock, G. & Bredmose, H. (2008) "Individual Violent Overtopping Events: New Insights" Proc. 31th Int. Conf. Coastal Engineering, Hamburg, Germany, 4, pp 2983-2995, ASCE

Krogstad, H.E. & Arntsen, Ø.A. (2000) "Linear Wave Theory – Part B" Norwegian University of Science and Technology, Trondheim, Norway

Mansard, E.P.D. & Funke, E.R. (1987) "On the reflection analysis of irregular waves" National Research Council, Canadian Hydraulic Laboratory Technical Report, TR-HY-017

Melchers, R.E. (1989), "Importance sampling in structural Systems", Jour. Structural Safety, 6, pp 3-10, Elsevier Scientific

Melchers, R.E. (1999) "Structural Reliability Analysis and Prediction – 2nd Edition" John Wiley & Sons Ltd., Chichester, ISBN 0-4719-8771-9

Napp, N. (2004) "Impulsive Overtopping of Vertical Seawalls under Oblique Wave Conditions" Doctoral Thesis, University of Edinburgh

Oumeraci, H., Kortenhaus, A., Allsop, N.W.H., de Groot, M. Crouch, R., Vrijling, H. & Voortman, H. (2001) "Probabalistic Design Tools for Vertical Breakwaters" PROVERBS Workshop, ISBN 90-5809-249-6

Pearson, J., Bruce, T. & Allsop, N.W.H. "Prediction of Wave Overtopping at Steep Seawalls – Variabilities and Uncertainties" Proc. "Waves '01", San Francisco, USA, ASCE

Rozario, J.B., Tromans, P.S., Taylor, P.H. & Efthymiou M. (1993) "Comparison of Loads Predicted using 'NewWave' and other Wave Models with Measurements on the Tern Structure" Jour. Underwater Technology, Summer 1993, pp. 24-29

Silverman, B.W. (1986) "Density Estimation for Statistics and Data Analysis" Chapman and Hall Ltd., London, ISBN 0-412-24520-1

Shuto, N. (1974) "Nonlinear long waves in a channel of variable section" Jour. Coastal Engineering in Japan, 18, pp 1-12

Smith, G.M., Seijffert J.W.W. & van der Meer, J.W. (1994) "Erosion and Overtopping of Grass Dike Large Scale Model Tests", Proc. 24th Int. Conf. Coastal Engineering, Kobe, ASCE

Tedd, J. (2007) "Testing, Analysis and Control of the Wave Dragon Wave Energy Converter" Doctoral Thesis, Aalborg University

Tromans, P.S., Anaturk, A.R. & Hagemeijer, P. (1991) "A New Model for the Kinematics of Large Ocean Waves - Application as a Design Wave", Proc. First International Offshore and Polar Engineering Conference, ISOPE, 3, 64-71 ISBN 0 9626104 8 8

Wolfram, J., Allsop, N.W.H. & Bruce, T. (2004) "Importance Sampling in Coastal Hydraulics & Offshore Experiments". EPSRC Case For Support – incomplete draft (not submitted).

Wand, M.P. & Jones, M.C. (1995) "Kernel Smoothing" Chapman & Hall / CRC, Boca Raton, FL, USA, ISBN 978-0-412-55270-0

Zhang, L.F., Xie, M. & Tang, L.C. (2006) "Bias correction for the least squares estimator of Weibull shape parameter with complete and censored data" Jour. Reliability Engineering and System Safety, 91, pp. 930-939

Acknowledgements

This PhD research would not have been possible without the support of my supervisors Dr Tom Bruce and Prof William Allsop. Their help and guidance is very much appreciated. The advice of Prof David Ingram was welcomed throughout this research. In particular I thank him for his support when presenting this work at two international conferences.

This research topic was borne from an idea originally suggested by Prof Julian Wolfram. His contribution is gratefully recognised.

The research outlined in this thesis was supported by the Supergen Marine Energy Consortium (EPSRC GR/S26958/01). The support of the Scottish Funding Council for the Joint Research Institute with Heriot-Watt University (part of the Edinburgh Research Partnership) is gratefully acknowledged.

Undertaking this research would have been a very much more daunting project without the support network of my fellow PhD students. Particular gratitude is due to Brian Sellar, Alasdair McDonald, Jake Parkpoom and Paul Stott.

My family and friends have been incredibly supportive over the course of this research. I hope I can repay their encouragement and good humour.

Tom Davey

August 2009

Glossary

Notation	Units	Definition
a	[-]	Weibull scale parameter
b	[-]	Weibull shape parameter
c	[-]	Weibull location parameter
f_p	[Hz]	Peak spectral frequency
H	[m]	Individual wave height (crest to trough)
$H_{1/3}$	[m]	Significant wave height defined as the average of the third largest waves
H_{m0}	[m]	Significant wave height measured from the spectrum. $H_{m0} = 4.0m_0^{1/2}$
H_0'	[m]	Equivalent deepwater wave height. Defined as significant wave height after refraction and diffraction effects but before transformation due to shoaling and breaking
h_s	[m]	Depth at the toe of the structure
L	[m]	Wavelength from zero-downcrossing analysis (unless otherwise stated)
L_m	[m]	Wavelength associated with the mean wave period
L_{op}	[m]	Peak offshore wavelength calculated from the spectrum
m_n	[-]	n^{th} spectral moment
N_w	[-]	Number of waves
N_{ow}	[-]	Number of overtopping waves

Notation	Units	Definition
q	[m³/s/m] or [l/s/m]	Mean overtopping discharge
Q_h	[-]	Dimensionless mean overtopping discharge for impulsive seas
R_c	[m]	Seawall (or breakwater) crest freeboard as measured from the still water line
R_h	[-]	Dimensionless crest freeboard for impulsive seas
s	[-]	Wave steepness ($s = H / L$)
s_{op}	[-]	Peak offshore wave steepness. $s_{op} = H_{m0} / L_{op}$
T	[s]	Wave period from zero-downcrossing analysis (unless otherwise stated)
T_m	[s]	Mean wave period
T_p	[s]	Peak wave period measured from the spectrum
V	[m³] or [l]	Individual overtopping volume
$V_{x\%}$	[m³] or [l]	Individual overtopping volume exceeded by x% of overtopping waves
$\overline{V}$ (V_{bar})	[m³] or [l]	Mean individual overtopping volume
V_{max}	[m³] or [l]	Maximum individual overtopping volume
V_{total}	[m³] or [l]	Total cumulative overtopping volume collected over a defined period of time
η_C	[m]	Wave crest elevation
η_T	[m]	Wave trough elevation (positive downwards)

Appendix 1 – Physical Model Parameters

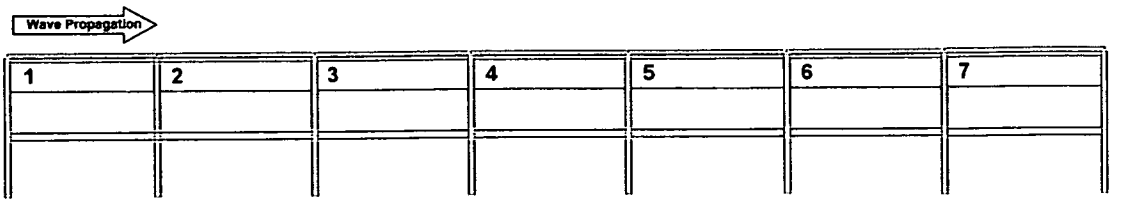

Figure A1.1 Schematic representation of the wave flume with numbered sections

Configuration Code	Wave flume gradient by section						
	1	2	3	4	5	6	7
X	-	-	1:20	1:30	1:30	1:30	1:30
Y	-	-	1:17	1:30	1:30	1:30	1:30

Table A1.1 Wave flume beach gradients

Reference	Wave Gauge Positions measured from the wavemaker [m]					
	1	2	3	4	5	6
2A	3.75	10.49	13.45	13.55	13.80	-
4AX	3.75	10.49	13.45	13.55	13.80	-
4BX	3.75	10.49	13.45	13.55	13.80	-
2AY	5.5	5.825	6.313	14.062	14.233	14.49
2BY	5.5	5.858	6.394	14.039	14.219	14.49
2CY	5.5	5.893	6.483	14.014	14.205	14.49
2DY	5.5	5.933	6.582	13.989	14.189	14.49
4AY	5.5	5.655	5.888	14.212	14.323	14.49
4BY	5.5	5.671	5.926	14.195	14.313	14.49
4CY	5.5	5.688	5.969	14.178	14.303	14.49
4DY	5.5	5.706	6.016	14.159	14.292	14.49

Table A1.2 Wave Gauge Positions

Variable Name	Legacy	New	Notes
graddect1	40	25	Detection strip gradient threshold [V/s]
graddect2	-	5	Detection strip gradient threshold ("Possible" event) [V/s]
vlow1	3.5	0.5	Detection strip voltage threshold [V]
vlow2	-	0	Detection strip voltage threshold ("Possible" event) [V]
gradamp	-	0.5	Loadcell envelope gradient threshold [V/s]
spread	0.5	0.6	Minimum gap between events [s]
lagMx	-	0.5	Maximum collection lag (§3.3.3) [s]
lagMn	-	0.25	Minimum collection lag (§3.3.3) [s]

Table A1.3 Overtopping detection and measurement parameters

Note: The legacy and new implementations use different overtopping detection apparatus (the detection strips on the crest of the seawall). Although identical in concept the two sets of apparatus differed in their detection characteristics. The values voltage gradient and threshold values detailed in Table A1.3 are therefore not directly comparable between the two systems.

Appendix 2 – Physical Model Test Results

The results obtained from the physical modelling programme are outlined in the table below. Each test reference refers to two separate tests: a calibration test with the beach extended to pierce the still water line and a second overtopping test with the seawall apparatus installed.

		Deep Water Measurements (Calibration Test)				Shallow Water Measurements (Calibration Test)					Overtopping Measurements (Overtopping Test)				
Reference	Duration [s]	H_{m0} [m]	T_p [s]	T_m [s]	s_{op}	H_{m0} [m]	T_p [s]	T_m [s]	h_*	H_{m0}/h_s	N_{ow}	N_w	q [l/m/s]	V_{bar} [l]	V_{max} [l]
2AX1	500	0.062	1.321	0.981	0.023	0.033	1.412	0.953	0.419	0.236	78	570	0.0378	0.0908	0.6818
2AX2	500	0.062	1.388	0.997	0.021	0.033	1.365	0.936	0.433	0.236	30	561	0.0224	0.1399	1.1356
2AX3	500	0.064	1.321	0.977	0.023	0.034	1.321	0.951	0.404	0.246	56	573	0.0444	0.1485	2.5517
2AX4	500	0.064	1.321	1.036	0.023	0.034	1.321	0.927	0.425	0.246	82	540	0.0441	0.1008	0.5011
2AX5	500	0.063	1.365	0.970	0.022	0.034	1.365	0.948	0.416	0.240	37	577	0.0202	0.1024	0.3601
2AX6	500	0.078	1.412	0.997	0.025	0.043	1.343	0.965	0.312	0.309	48	561	0.0184	0.0719	0.6560
2AX7	500	0.076	1.343	1.032	0.027	0.042	1.365	0.948	0.336	0.297	78	542	0.0452	0.1087	0.7056
2AX8	500	0.077	1.300	1.017	0.029	0.042	1.321	0.979	0.314	0.298	55	550	0.0339	0.1155	0.6039
Mean		**0.068**	**1.346**	**1.001**	**0.024**	**0.037**	**1.352**	**0.951**	**0.382**	**0.263**	**58.0**	**559.3**	**0.0333**	**0.1098**	**0.8995**
4AX1	1000	0.074	1.059	0.885	0.042	0.043	1.078	0.859	0.391	0.311	73	1197	0.0105	0.0538	0.3400
4AX2	1000	0.073	1.059	0.884	0.042	0.043	1.078	0.846	0.409	0.306	76	1198	0.0108	0.0535	0.3388
4AX3	1000	0.073	1.041	0.883	0.043	0.043	1.024	0.845	0.410	0.306	89	1200	0.0091	0.0382	0.1776
4AX4	1000	0.072	1.059	0.874	0.041	0.043	1.097	0.856	0.402	0.305	80	1213	0.0133	0.0623	0.3116
4AX5	1000	0.071	1.041	0.871	0.042	0.043	1.059	0.856	0.403	0.304	114	1217	0.0127	0.0418	0.2488
4AX6	1000	0.072	1.041	0.863	0.043	0.042	1.078	0.845	0.415	0.302	105	1228	0.0137	0.0491	0.5890
4AX7	1000	0.069	1.041	0.866	0.041	0.041	1.041	0.850	0.425	0.292	83	1223	0.0099	0.0446	0.3460
4AX8	1000	0.073	1.059	0.880	0.042	0.043	1.059	0.859	0.399	0.305	85	1204	0.0123	0.0542	0.4433
4AX9	1000	0.073	1.097	0.879	0.039	0.042	1.097	0.864	0.397	0.302	84	1206	0.0133	0.0594	0.3315
Mean		**0.072**	**1.055**	**0.876**	**0.042**	**0.043**	**1.068**	**0.853**	**0.406**	**0.304**	**87.7**	**1209.6**	**0.0117**	**0.0508**	**0.3474**
4BX1	1000	0.096	1.205	0.930	0.042	0.053	1.205	0.961	0.257	0.378	211	1138	0.0585	0.1040	0.9968
4BX2	1000	0.095	1.205	0.920	0.042	0.052	1.205	0.954	0.267	0.369	179	1152	0.0493	0.1032	0.7847
Mean		**0.096**	**1.205**	**0.925**	**0.042**	**0.052**	**1.205**	**0.957**	**0.262**	**0.373**	**195.0**	**1145.0**	**0.0539**	**0.1036**	**0.8908**

		Deep Water Measurements (Calibration Test)				Shallow Water Measurements (Calibration Test)					Overtopping Measurements (Overtopping Test)				
Reference	Duration [s]	H_{m0} [m]	T_p [s]	T_m [s]	s_{op}	H_{m0} [m]	T_p [s]	T_m [s]	h_*	H_{m0}/h_s	N_{ow}	N_w	q [l/m/s]	V_{bar} [l]	V_{max} [l]
2AY1	1000	0.065	1.489	1.171	0.019	0.044	1.437	1.159	0.274	0.278	21	861	0.0037	0.0654	0.3054
2AY2	1000	0.067	1.437	1.174	0.021	0.047	1.437	1.162	0.258	0.295	20	858	0.0036	0.0674	0.3241
2AY3	1000	0.066	1.437	1.176	0.020	0.046	1.437	1.151	0.270	0.286	19	867	0.0049	0.0966	0.4040
2AY4	1000	0.065	1.437	1.151	0.020	0.045	1.437	1.159	0.269	0.284	13	860	0.0022	0.0634	0.1772
2AY5	1000	0.066	1.437	1.21	0.020	0.046	1.437	1.193	0.252	0.286	6	835	0.0012	0.0745	0.1782
2AY6	1000	0.064	1.437	1.178	0.020	0.045	1.437	1.169	0.267	0.281	30	853	0.0045	0.0565	0.4815
2AY7	1000	0.067	1.437	1.169	0.021	0.046	1.437	1.170	0.258	0.290	37	851	0.0039	0.0398	0.3077
2AY8	1000	0.065	1.463	1.179	0.020	0.045	1.463	1.159	0.269	0.283	30	861	0.0105	0.1309	0.9763
2AY9	1000	0.065	1.437	1.178	0.020	0.045	1.437	1.159	0.272	0.280	22	861	0.0030	0.0508	0.1853
2AY10	1000	0.065	1.489	1.17	0.019	0.045	1.489	1.167	0.267	0.282	21	855	0.0018	0.0329	0.0975
Mean		**0.066**	**1.45**	**1.176**	**0.020**	**0.046**	**1.445**	**1.165**	**0.266**	**0.285**	**21.9**	**856.2**	**0.0039**	**0.0678**	**0.3437**
2BY1	1000	0.072	1.517	1.246	0.020	0.050	1.517	1.207	0.224	0.314	45	827	0.0157	0.1306	0.8800
2BY2	1000	0.073	1.517	1.225	0.020	0.051	1.546	1.229	0.212	0.320	45	812	0.0155	0.1291	0.5682
2BY3	1000	0.071	1.517	1.233	0.020	0.050	1.517	1.212	0.223	0.313	18	823	0.0043	0.0898	0.3864
2BY4	1000	0.072	1.546	1.221	0.019	0.050	1.575	1.244	0.213	0.311	49	802	0.0206	0.1578	1.3309
2BY5	1000	0.071	1.546	1.244	0.019	0.049	1.546	1.237	0.217	0.308	47	806	0.0148	0.1184	0.7100
2BY6	1000	0.071	1.575	1.281	0.018	0.050	1.517	1.230	0.216	0.313	52	811	0.0170	0.1226	0.7291
Mean		**0.071**	**1.536**	**1.242**	**0.019**	**0.050**	**1.536**	**1.227**	**0.218**	**0.313**	**42.7**	**813.5**	**0.0147**	**0.1247**	**0.7674**
2CY2	1000	0.078	1.606	1.295	0.019	0.055	1.606	1.292	0.179	0.343	76	772	0.0258	0.1272	0.7229
2CY3	1000	0.078	1.575	1.303	0.020	0.056	1.575	1.302	0.174	0.348	87	766	0.0205	0.0884	0.7871
2CY4	1000	0.076	1.638	1.309	0.018	0.054	1.638	1.281	0.185	0.338	97	779	0.0371	0.1435	1.5872
2CY5	1000	0.079	1.546	1.302	0.021	0.056	1.546	1.279	0.179	0.349	106	780	0.0322	0.1141	1.0502
Mean		**0.078**	**1.591**	**1.302**	**0.020**	**0.055**	**1.591**	**1.289**	**0.179**	**0.345**	**91.5**	**774.3**	**0.0289**	**0.1183**	**1.0368**

		Deep Water Measurements (Calibration Test)				Shallow Water Measurements (Calibration Test)					Overtopping Measurements (Overtopping Test)				
Reference	Duration [s]	H_{m0} [m]	T_p [s]	T_m [s]	s_{op}	H_{m0} [m]	T_p [s]	T_m [s]	h_*	H_{m0}/h_s	N_{ow}	N_w	q [l/m/s]	V_{bar} [l]	V_{max} [l]
2DY1	500	0.084	1.638	1.347	0.020	0.060	1.707	1.325	0.156	0.374	76.0	393.0	0.0546	0.1346	1.0840
2DY2	500	0.086	1.638	1.353	0.020	0.061	1.707	1.365	0.145	0.380	59.0	384.0	0.0653	0.2075	1.3360
2DY3	500	0.087	1.707	1.331	0.019	0.061	1.707	1.341	0.149	0.381	52.0	391.0	0.0619	0.2232	0.8630
2DY4	500	0.087	1.638	1.329	0.021	0.062	1.707	1.344	0.146	0.388	58.0	387.0	0.0514	0.1661	1.2311
Mean		**0.086**	**1.655**	**1.340**	**0.020**	**0.061**	**1.707**	**1.344**	**0.149**	**0.381**	**61.3**	**388.8**	**0.0583**	**0.1828**	**1.1102**
4AY1	1000	0.066	0.9526	0.8678	0.046	0.046	1.050	0.868	0.472	0.288	37.0	1150.0	0.0026	0.0266	0.1628
4AY2	1000	0.065	1.024	0.8718	0.039	0.045	1.024	0.868	0.485	0.280	32.0	1144.0	0.0038	0.0441	0.1789
4AY3	1000	0.065	1.011	0.8539	0.041	0.045	1.011	0.877	0.471	0.283	39	1169	0.0058	0.0560	0.4053
4AY4	1000	0.066	0.9752	0.8631	0.045	0.046	1.037	0.869	0.473	0.287	34	1156	0.0020	0.0223	0.0761
4AY5	1000	0.066	1.011	0.8702	0.041	0.046	1.024	0.880	0.459	0.288	47	1147	0.0042	0.0336	0.2619
4AY6	1000	0.066	0.999	0.8774	0.042	0.046	1.037	0.876	0.464	0.288	44	1137	0.0053	0.0449	0.3465
4AY7	1000	0.064	0.999	0.8633	0.041	0.044	1.064	0.871	0.487	0.277	33	1155	0.0029	0.0328	0.1616
4AY8	1000	0.066	0.9752	0.8835	0.044	0.046	0.964	0.882	0.455	0.290	49	1129	0.0056	0.0426	0.2691
4AY9	1000	0.065	1.011	0.8619	0.041	0.045	1.024	0.868	0.482	0.282	82	1157	0.0044	0.0200	0.1717
4AY10	1000	0.066	1.024	0.8696	0.040	0.046	1.024	0.860	0.481	0.288	51	1147	0.0038	0.0276	0.2563
Mean		**0.066**	**0.998**	**0.868**	**0.042**	**0.046**	**1.026**	**0.872**	**0.473**	**0.285**	**44.8**	**1149.1**	**0.0040**	**0.0350**	**0.2290**
4BY1	1000	0.072	1.05	0.9162	0.042	0.050	1.050	0.910	0.396	0.313	67	1089	0.0075	0.0421	0.2545
4BY2	1000	0.072	1.037	0.9029	0.043	0.049	1.037	0.919	0.393	0.309	72	1105	0.0089	0.0465	0.4160
4BY3	1000	0.071	1.024	0.913	0.043	0.050	1.037	0.917	0.392	0.310	56	1093	0.0063	0.0424	0.3127
4BY4	1000	0.071	1.05	0.9157	0.041	0.049	1.037	0.910	0.402	0.308	91	1090	0.0068	0.0282	0.2110
4BY5	1000	0.072	1.078	0.918	0.040	0.049	1.092	0.921	0.393	0.307	85	1087	0.0103	0.0454	0.7508
4BY6	1000	0.071	1.05	0.916	0.041	0.049	1.092	0.912	0.402	0.306	69	1089	0.0065	0.0352	0.3394
Mean		**0.072**	**1.048**	**0.914**	**0.042**	**0.049**	**1.058**	**0.915**	**0.396**	**0.309**	**73.3**	**1092.2**	**0.0077**	**0.0400**	**0.3807**

		Deep Water Measurements (Calibration Test)				Shallow Water Measurements (Calibration Test)					Overtopping Measurements (Overtopping Test)				
Reference	Duration [s]	H_{m0} [m]	T_p [s]	T_m [s]	s_{op}	H_{m0} [m]	T_p [s]	T_m [s]	h_*	H_{m0}/h_s	N_{ow}	N_w	q [l/m/s]	V_{bar} [l]	V_{max} [l]
4CY1	1000	0.081	1.064	0.9558	0.046	0.054	1.122	0.964	0.324	0.340	107	1044	0.0177	0.0619	0.5211
4CY2	1000	0.081	1.122	0.9487	0.041	0.055	1.154	0.959	0.324	0.344	115	1051	0.0190	0.0619	0.4191
4CY3	1000	0.080	1.107	0.9543	0.042	0.054	1.107	0.959	0.330	0.337	80	1045	0.0168	0.0788	0.4946
4CY4	1000	0.079	1.092	0.946	0.042	0.054	1.122	0.967	0.325	0.337	136	1054	0.0199	0.0548	0.4709
4CY5	1000	0.079	1.138	0.95	0.039	0.054	1.138	0.962	0.331	0.335	98	1050	0.0193	0.0738	0.4145
Mean		**0.080**	**1.105**	**0.9509**	**0.042**	**0.054**	**1.129**	**0.962**	**0.327**	**0.339**	**107.2**	**1048.8**	**0.0185**	**0.0662**	**0.4640**
4DY1	1000	0.090	1.17	1.004	0.042	0.061	1.170	1.025	0.256	0.381	177	994	0.0373	0.0790	0.6377
4DY2	1000	0.088	1.138	0.9935	0.043	0.060	1.138	1.013	0.268	0.372	180	1004	0.0399	0.0831	0.6891
4DY3	1000	0.088	1.187	0.9983	0.040	0.059	1.187	1.009	0.272	0.371	167	999	0.0369	0.0828	0.8131
Mean		**0.088**	**1.165**	**0.9986**	**0.042**	**0.060**	**1.165**	**1.016**	**0.265**	**0.375**	**174.7**	**999**	**0.0380**	**0.0816**	**0.7133**